GEOCHEMICAL AND FLUID INCLUSION STUDIES OF PEGMATITES FROM PARTS OF SOUTHWESTERN NIGERIA

BY

MATTHEW OYEDELE OYEDOKUN

B.Sc. (Benin), M.B.A., M.Sc. (Ibadan)

MATRIC N0:112817

A thesis in the department of Geology

Submitted to University of Ibadan, in partial fulfilment of the requirements for the award of the degree of

DOCTOR OF PHILOSOPHY

of the

UNIVERSITY OF IBADAN

JUNE, 2019

ABSTRACT

Geochemical assessment of fluid inclusions in minerals has been successfully used in the description of genesis and characteristics of different ore-forming fluids. However, there are few reported applications of fluid inclusions study in the delineation and characterisation of ore-forming fluids in pegmatites from southwestern Nigeria. This study was designed to determine the type, origin and characteristics of fluids involved in the genesis of pegmatites from parts of southwestern Nigeria.

Systematic geological mapping was carried out in the Olode, Komu and Idiyan areas. Forty-eight samples of pegmatite were subjected to petrographic studies. In addition, 16 whole rock samples of pegmatite and 32 mineral extracts (11 feldspar, 13 muscovite, 8 biotite) were analysed for major, trace and rare-earth elements using inductively coupled plasma optical emission spectrometry technique. Fluid inclusion study was carried out on pegmatitic quartz using microthermometry. Descriptive statistics and geochemical variation plots were used for data evaluation.

Identified lithological units were quartz muscovite schist, sillimanite quartzite, granite gneiss and amphibolite. The pegmatites contained mainly albite, microcline, quartz, biotite and muscovite. Major oxides concentration (%) for pegmatite and mineral extracts were: SiO_2 (35.22 – 82.17%), Al_2O_3 (0.73 – 34.81%), Fe_2O_3 (0.1 – 19.79%), MnO (0.004 – 1.693), MgO (0.01 – 8.55%), CaO (0.01 – 2.61), Na_2O (0.09 – 10.16%) and K_2O (0.08 – 12.66%), respectively. The concentration (ppm) for Be, Zn, Nb, Sn, Cs, W and Ta ranged as 1.00 – 384.00, 30.00 – 3800.00, 0.60 – 330.00, 1.00 – 319.00, 0.70 – 475.00, 17.20 – 933.00 and 0.32 – 107.00, respectively. Elevated concentrations of Sn were observed in muscovite extracts while elevated concentrations of W were observed in whole pegmatite. Plots of Ta vs K/Cs, K/Rb vs Rb, K/Rb vs Ba, Ta vs K/Cs, Rb vs Ba and Ta vs Cs + Rb showed that the pegmatites were unmineralised to mineralised muscovite class pegmatites. Three types (I, II and III) of aqueous primary to pseudo-secondary inclusions were observed. Type I were two-phase liquid (L)-vapor (V); (L+V; L>V); ~2-100 μm occurring as isolated inclusions, clusters and trails. Type II inclusion was three-phase: Liquid+ Vapor + Solid (L+V+S), ~2 – 15 μm and they occurred as isolated individuals and in trails. Type III were monophase (liquid) at room temperature and occurred as isolated inclusions, clusters and in trails that also

contained types I and II. Type I inclusion has salinity of 0.7-21.9wt% $NaCl_{eq.}$ All inclusions homogenised into the liquid phase at temperature of total homogenisation (Th) of 80.1-335.1°C. Temperature-pressure modelling revealed type II inclusion with Th of 350°C as the earliest fluid trapped and were associated with late magmatic-hydrothermal fluids and type II inclusion were trapped at 250°C. Type I inclusion was trapped at 160-250°C, indicating dilution and interaction of ore-forming fluid with meteoric water while Type III inclusion was trapped at a much lower temperature of <50 °C based on Th values.

The pegmatites of Southwestern Nigeria are characterised by aqueous fluid inclusions of primary and pseudo-secondary types and they are of magmatic to meteoric origins.

Keywords: Aqueous Primary inclusions, Ore-forming fluid, Magmatic origin
Word count: 479

DEDICATION

I dedicate this to the glory of God, my darling wife, Funmilayo and children.

ACKNOWLEDGEMENTS

I give thanks to God for His protection, guidance and wisdom in the course of this research work.

I extend my gratitude to my supervisor, Prof. O. A. Okunlola, for his patience and understanding. I would also like to appreciate all lecturers of the Department of Geology; Prof Elueze (of blessed memory), Prof. A.I. Olayinka (the Vice Chancellor, University of Ibadan), Prof. Adeyemi, Prof. Tijani, Prof. Ehinola (the Head of Department), Dr. Akaegbobi (of blessed memory), Dr Bolarinwa, Dr Nton, Dr Boboye, Dr Olatunji, Dr. Oyediran (research coordinator), Dr Adeigbe, Dr. Osinowo and all non-academic members of staff.

In addition, I would like to thank Prof. T.A. Ewemoje of the Department of Agriculture and Environmental Engineering, Dr. A.A. Ayoade of the Department of Zoology, Dr. M.O. Adeniyi of the Department of Physics for their support and Mrs Bisi Okuntoro Idowu; the secretary to the Vice Chancellor, University of Ibadan.

I will like to express my sincere appreciation to my darling wife, Mrs Funmilayo Oyedokun and children; Ayomide, Ajibola, Favour and Emmanuel, who displayed high level of understanding, during the period of getting the research work done.

The list will be incomplete if I fail to acknowledge the unrelenting support of Mr Emmanuel E. Igonor, Mr Wale Aromolaran, Adekola Taiwo and Adewale Sadiq, Olisa Olusegun; members of staff of the Oyo State Mineral Development Agency; Dr Alessandra Costanzo and Prof. Martin Feely of the National University of Ireland, Galway, and the members of staff of Wagner Petrographic, Utah, United State of America.

I also seize this opportunity to appreciate the support and encouragement of my boss and mentor, the Executive Governor of Oyo State, His Excellency, Sen. Abiola Ajimobi in the course of this research work. I also thank the members of the Executive Council of Oyo State, especially the Deputy Governor, Otunba Moses Alake Adeyemo, the Secretary to the State Government, Alh. Ishmael Olalekan Alli, the Chief of Staff to the Governor, Dr Gbade Ojo, the Commissioner for Environment and Water resources, Chief Isaac Ishola and others.

Also, I thank my big brother, Engr. Rauf Olaniyan for his support towards the achievement of this goal. I thank you all, may the Almighty increase all that you do.

Finally, I will like to appreciate Prof. S.O. Olobaniyi of the department of Geology, University of Lagos and Dr. Olutoyin Fashae of the department of Geography, University of Ibadan.

CERTIFICATION

I certify that this research work was carried out by **Oyedokun, Matthew Oyedele,** in the Department of Geology, University of Ibadan, Ibadan, Nigeria under my supervision.

…… …….

Date **Prof. O.A. Okunlola**

BSc (Ilorin), MSc (Zaria), PhD (Ibadan)

TABLE OF CONTENTS

Title	PAGE
Abstract	ii-iii
Dedication	iv
Acknowledgement	v
Certification	vii
Table of contents	viii
List of figures	xi-xvii
List of tables	xix-xx

CHAPTER ONE: Introduction

1.1: General Introduction	1
1.2: Formation and classification of pegmatite	8
1.3: Pegmatites of Nigeria	10
1.4: Fluid inclusion studies	19
1.4.1: Background	19
1.4.2: Classification of fluid inclusions	20
1.4.3: Methods of study of fluid inclusions	24
1.5: Justification	24
1.6: Aim and Objectives of the Study	24
1.6.1: Aim	24
1.6.2: Objectives	25
1.7: Scope	25
1.8: Location and accessibility	25
1.9: Climate, topography, relief and drainage	25

CHAPTER TWO: Geology of southwestern Nigeria and review of related previous works

2.1: Review of the Geology of Nigeria	29
2.1.1: The Migmatite-Gneiss Complex	32
2.1.2: The Schist Belt (Metasedimentary and Metavolcanic Rocks)	32
2.1.3: The Older Granites (Pan African Granitoids)	33
2.1.4 Undeformed Acid and Basic Dykes	36

2.2 Review of related previous works 37

CHAPTER THREE: Methodology
3.1: Field methods, mapping and sampling 42
3.2: Sample preparation 42
3.3: Geochemical analysis 42
3.4: Fluid inclusion study 43
3.4.1: sample preparation and instrumentation 43
3.4.2: Fluid inclusion petrography and microthermometry 47
3.4.3 Fluid Inclusion Microthermometry 47

CHAPTER FOUR: Results and discussion
4.1: Geological setting of the study areas 49
4.1.1: Geology of Olode-Falansa-Coco area 49
4.1.2: Geology of Komu-Igbojaye-Godondoya area: 57
4.1.3: Geology of Idiyan area 69
4.2: Geochemistry and fluid inclusion study of pegmatites 76
4.2.1: Geochemistry of pegmatite 76
4.2.1.1: Major elemental concentration 76
4.2.1.2: Trace elemental concentration 93
4.2.1.3: Rare earth elemental concentration 106
4.2.1.4: Comparison of selected trace elemental concentrations in whole rock, feldspars, biotite and muscovite extracts 118
4.2.1.5: Discussion 127
4.3: Fluid inclusion studies 148
4.3.1: Description of Fluid Inclusion Types 148
4.3.2: Fluid Inclusion photomicrographs for each sample 152
4.3.3: Fluid Inclusion Microthermometry 173
4.3.3.1: Abuja Leather, Komu 173
4.3.3.2: Omoba in Okeho 173
4.3.3.3: Owode, Ibarapa 182
4.3.3.4: Gbayo, Olode 187
4.3.3.5: Coco, Olode 192
4.3.4: Discussion: Modelling Trapping Pressure and Temperature (P-T)

of Aqueous Fluids 199
4.3.4.1: Abuja Leather, Komu 199
4.3.4.2: Omoba, Okeho 199
4.3.4.3: Owode, Ibarapa 199
4.3.4.4: Gbayo, Olode 204
4.3.4.5: Coco, Olode 204

CHAPTER FIVE: Summary, conclusion and recommendation

5.1: Summary 209
5.2: Conclusion 210
5.3: Recommendation 210

REFERENCES 211

LIST OF FIGURES

PAGE

Figure 1.1: Interior to marginal LCT pegmatites (after Cerny, 1991b) **4**

Figure 1.2: Regional zoning of LCT pegmatites around a parental pluton (Cerny 1991b) **5**

Figure 1.3: Schematic vertical section through a zoned fertile granite-pegmatite. 1: fertile granites with leucocratic and pegmatitic cupolas, 2: barren to beryl-baring pegmatites, 3: beryl type, columbite to phosphate-bearing pegmatites; 4: complex spodumene (or petalite) bearing pegmatites (with Sn, Ta and Cs mineralisation), 5: faults, Letters A through D, progressively deeper levels of erosion showing the types of pegmatites exposed (from Cerny, 1986) **6**

Figure 1.4: Relationship between parent granite plutons and surrounding pegmatites showing A) Exterior pegmatites which occurs in a pegmatite aureole surrounds a granitic pluton; B) Marginal pegmatites; C) Interior pegmatites (adapted from Ashworth, 2013) **7**

Figure 1.5: General geology of Nigeria showing the preconceived pegmatite zone (adapted from Akintola et al., 2012) **16**

Figure 1.6: Geological map of the Nigeria, showing locations of rare-metal and barren pegmatite (Garba, 2003) **17**

Figure 1.7: General geology of Nigeria showing pegmatite zones (Okunlola, 2005) **18**

Figure 1.8: Sketch of fluid inclusion classification (Goldstein and Reynolds, 1994) **22**

Figure 1.9: Topographical map of Ikomu area **26**

Figure 1.10: Topographical map of Olode area. **27**

Figure 1.11: Topographical map of Igangan area. **28**

Figure 2.1: Generalised geological map of Nigeria within the framework of the Geology of West Africa (Adapted from Wright, 1985) **31**

Figure 2.2: Geological Map of Nigeria (NGSA, 2004) **34**

Figure 2.3: Geological map of Nigeria showing the Schist belt (After Woakes et al., 1987) **35**

Figure 3.1: Pictures of the doubly polished wafers of pegmatite samples **44**

Figure 3.2: Transmitted Plane Polarised Light Microscope fitted with an incident UV light attachment used for microthermometric analysis of fluid inclusions at Geofluids Research Laboratory, National University of Ireland, Galway **45**

Figure 3.3: Transmitted Plane Polarised Light Microscope fitted with a stage mounted Linkam heating and cooling stage used for microthermometric analysis of fluid inclusions at Geofluids Research Laboratory, National University of Ireland, Galway **46**

Figure 4.1: Field picture showing pegmatite in Olode area **50**

Figure 4.2: Field picture showing granite in Olode area **51**

Figure 4.3: Field picture showing pegmatite in Olode area **52**

Figure 4.4: Photomicrograph of section of pegmatite from Falansa showing presence of Microcline (Mc) in abundance and Muscovite (Ms). **53**

Figure 4.5: Photomicrograph section of pegmatite from Falansa showing presence of Microcline (Mc) and Quartz (Qz). **54**

Figure 4.6: Photomicrograph of a section of pegmatite from Coco showing presence of Microcline (Mc), Muscovite (Ms) in abundance and Quartz (Qz) **55**

Figure 4.7: Geological map of Olode-Coco-Falansa area **56**

Figure 4.8: Field picture showing porphyritic granite in Komu area **58**

Figure 4.9: Field picture showing pegmatite in Komu area **59**

Figure 4.10: Field picture showing pegmatite in Komu area **60**

Figure 4.11: Field picture showing pegmatite in Igbojaye area **61**

Figure 4.12: Field picture showing pegmatite in Igbojaye area **62**

Figure 4.13: Field picture showing pegmatite intruding metasedimentary rocks in Igbojaye area **63**

Figure 4.14: Field picture showing pegmatite in Godondoya area **64**

Figure 4.15: Photomicrograph of a section of pegmatite from Abuja Leather **65**

Figure 4.16: Photomicrograph of a section of pegmatite from Balogun Ojo **66**

Figure 4.17: Photomicrograph of section of pegmatite from Doya showing presence of Microcline (Mc), Albite (Ab) and Quartz (Qz) **67**

Figure: 4.18: Geological map of Komu area **68**

Figure 4.19: Field photograph showing biotite granite around Idiyan area **70**

Figure 4.20: Field photograph showing quartz vein in granite gneiss in the Idiyan area **71**

Figure 4.21: Field pictures showing folded alternating layers of felsic and

mafic bands in migmatised gneiss in the Idiyan area **72**

Figure 4.22: Field pictures showing pegmatite mining pit in the Idiyan area **73**

Figure 4.23: Photomicrograph of section of pegmatite from Idiyan showing presence of Microcline (Mc) in abundance and Quartz (Qz). **74**

Figure 4.24: Geological map of Idiyan area **75**

Figure 4.25: Be concentration in whole rock pegmatites from the different locations **95**

Figure 4.26: Nb concentration in whole rock pegmatites from the different locations **96**

Figure 4.27: Sn concentration in whole rock pegmatites from the different locations **97**

Figure 4.28: Cs concentration in whole rock pegmatites from the different locations **98**

Figure 4.29: Ta concentration in whole rock pegmatites from the different locations **99**

Figure 4.30: W concentration in whole rock pegmatites from the different locations **100**

Figure 4.31: Be concentration in feldspars from the different locations **101**

Figure 4.32: Nb concentration in feldspars from the different locations **102**

Figure 4.33: Cs concentration in feldspars from the different locations **103**

Figure 4.34: Ta concentration in feldspars from the different locations **104**

Figure 4.35: W concentration in feldspars from the different locations **105**

Figure 4.36: Be concentration in muscovites from the different locations **107**

Figure 4.37: Be concentration in muscovites from the different locations **108**

Figure 4.38: Sn concentration in muscovites in the different locations **109**

Figure 4.39: Cs concentration in muscovites in the different locations **110**

Figure 4.40: Ta concentration in muscovites in the different locations **111**

Figure 4.41: W concentration in muscovites in the different locations **112**

Figure 4.42: Nb concentration in biotite extracts in the different locations **113**

Figure 4.43: Sn concentration in biotite extracts in the different locations **114**

Figure 4.44: Cs concentration in biotite extracts in the different locations **115**

Figure 4.45: Ta concentration in biotite extracts in the different locations **116**

Figure 4.46: W concentration in biotite extracts in the different locations **117**

Figure 4.47: comparative plot of Sn, Zn and W for whole rock and mineral extracts in Balogun-Ojo sample **119**

Figure 4.48: comparative plot of Cs,Ta and Nb for whole rock and mineral extracts in Balogun-Ojo sample **120**

Figure 4.49: comparative plot of Sn, Zn and W for whole rock and mineral extracts in Abuja leather sample **121**

Figure 4.50: comparative plot of Cs, Ta and Nb for whole rock and mineral extracts in Abuja leather sample **122**

Figure 4.51: comparative plot of Sn, Zn and W for whole rock and mineral extracts in Idiyan sample **123**

Figure 4.52: comparative plot of Cs, Ta and Nb for whole rock and mineral extracts in Idiyan sample **124**

Figure 4.53: comparative plot of Sn, Zn and W for whole rock and mineral extracts in Omo-Oba sample **125**

Figure 4.54: comparative plot of Cs, Ta and Nb for whole rock and minerals extracts in Omo-Oba sample **126**

Figure 4.55: Ternary plot of Na_2O-Al_2O_3-K_2O **128**

Figure 4.56: Plot of A/NK against A/CNK (after Shand 1943) **129**

Figure 4.57: K/Rb vs Rb plot for pegmatite and extracts (modified after Staurov et al., 1966). Blue represents whole rock samples, red represents feldspar extracts, brown muscovite extracts and green biotite extracts **130**

Figure 4.58: mineralisation potential and characterisation of the pegmatite (modified after Maniar and Piccoli, 1989) **131**

Figure 4.59: K/Rb vs Cs plot for pegmatites and extracts in the studied Localities. Blue represents whole rock samples, red represents feldspar extracts, brown muscovite extracts and green biotite extracts **132**

Figure 4.60: Relative degree of fractionation of pegmatites (after Larsen, 2002) **137**

Figure 4.61: Relative degree of fractionation of pegmatites **138**

Figure 4.62: Plot of Ta vs K/Cs for pegmatite and extracts (modified after Beus, 1966 and Gordiyenko, 1977). Blue represents whole rock samples, red represents feldspar extracts, brown muscovite extracts and green biotite extracts **139**

Figure 4.63: Plot Ta vs Rb for pegmatite and extracts modified after (modified after Beus, 1966 and Gordiyenko, 1977; a: Ta prospective; b: Ta mineralised), Blue represents whole rock samples, red represents

feldspar extracts, brown muscovite extracts and green biotite extracts **140**

Figure 4.64: Plot of Ta (ppm) against Cs + Rb (ppm) for mineral extracts from the study areas (after Gaupp et al., 1984). Blue represents whole rock samples, red represents feldspar extracts, brown muscovite extracts and green biotite extracts **141**

Figure 4.65: Ta vs Ga plot for pegmatites and extracts from the study area. Blue represents whole rock samples, red represents feldspar extracts, brown muscovite extracts and green biotite extracts **142**

Figure 4.66: Plot of Ta (ppm) against Cs (ppm) for mineral extracts from the study areas (after Moller and Morteani, 1987). Blue represents whole rock samples, red represents feldspar extracts, brown muscovite extracts and green biotite extracts **143**

Figure 4.67: condrite normalisation plot for group 1 pegmatite (values after Sun and McDonough, 1989). **144**

Figure 4.68: Chondrite-normalised plot of incompatible trace elements for group 2 pegmatites [normalisation values after Taylor and McLennan (1985)**145**

Figure 4.69: condrite normalisation plot for group 2 pegmatite (values after Sun and McDonough, 1989) **146**

Figure 4.70: Chondrite-normalised plot of incompatible trace elements for group 2 pegmatites [normalisation values after Taylor and McLennan (1985)] **147**

Figure 4.71: Schematic representation of the occurrence of quartz-hosted FIs in all samples. **149**

Figure 4.72: Photomicrographs of sample AB 006 (Abuja Leather). (a) General view of typical quartz and feldspar grains under low magnification. (b) Trail containing Type 3 that terminates at quartz grain boundary.**153**

Figure 4.73: Photomicrographs of sample AB 006 (Abuja Leather) (c) Trail containing Type 1 along annealed fracture in quartz. (d) Type 1 and 3 forming cluster of individual FIs in quartz grain. **154**

Figure 4.74: Photomicrographs of sample AB 007 (Abuja Leather). (a) General view of typical quartz and feldspar grains under low magnification. (b) Trail containing Type 1 and 3 and terminating at quartz grain boundary **155**

Figure 4.75: Photomicrographs of sample AB 007 (Abuja Leather). (c) Type 1 forming a cluster hosted in quartz grain. (d) Trail containing Type 1 in quartz grain. **156**

Figure 4.76: Photomicrographs of sample OM 009 (Omoba). (a) General view of typical FI-rich quartz grain under low magnification. (b) Type 1 and Type 3 forming a trail along an annealed fracture. **157**

Figure 4.77: Photomicrographs of sample OM 009 (Omoba). (c) Isolated individuals of Type 1. (d) Isolated Type 2 (L=Liquid, V=Vapour, S=Solid) inclusions. **158**

Figure 4.78: Photomicrographs of sample OM 010 (Omoba). (a) General view of typical quartz grain under low magnification. (b) Multiple crosscutting trails of Type 1 along annealed fractures in quartz. **159**

Figure 4.79: Photomicrographs of sample OM 010 (Omoba). (c) Trail of Type 1 along an annealed fracture in quartz. (d) Isolated Type 1 inclusions in quartz. **160**

Figure 4.80: Photomicrographs of sample OW 003 (Owode). (a) General view of typical quartz grain under low magnification. (b) Type 1 and Type 3 forming trail along annealed fracture. **161**

Figure 4.81: Photomicrographs of sample OW 003 (Owode) (c) Cluster containing Type 1 FI. (d) Isolated Type 2 (L=Liquid, V=Vapour, S=Solid) inclusions. **162**

Figure 4.82: Photomicrographs of sample OW 005 (Owode). (a) General view of typical quartz grain under low magnification. (b) Type 1 and Type 3 forming trail along annealed fracture **163**

Figure 4.83: Photomicrographs of sample OW 005 (Owode) (c) Trail containing Type 1 along annealed fracture. (d) Trail containing Type 2 (L=Liquid, V=Vapour, S=Solid) inclusions. **164**

Figure 4.84: Photomicrographs of sample GB 001 (Gbayo). (a) General view of typical quartz grain under low magnification. (b) Type 1 and Type 3 forming trails along annealed fracture. **165**

Figure 4.85: Photomicrographs of sample GB 001 (Gbayo) (c) Type 1 showing irregular shape due to stretching. (d) Multiple Type 1 inclusions displaying a variety of morphologies. **166**

Figure 4.86: Photomicrographs of sample GB 002 (Gbayo). (a) General view of typical quartz grain under low magnification. (b) Type 1 and Type 3 forming trails along annealed fractures **167**

Figure 4.87: Photomicrographs of sample GB 002 (Gbayo) (c) Multiple Type 1 forming trail along annealed fracture. (d) Higher magnification view of inset from (c) showing irregular shapes of FI and varying vapour bubble volumes. **168**

Figure 4.88: Photomicrographs of sample CO 003 (Coco). (a) General view

of typical quartz grain under low magnification. (b) Type 3 forming a trail along an annealed fracture. **169**

Figure 4.89: Photomicrographs of sample CO 003 (Coco) (c) Isolated Type 1. (d) Multiple Type 1 individuals forming cluster. **170**

Figure 4.90: Photomicrographs of sample CO 005 (Coco). (a) General view of typical quartz grain under low magnification. (b) Multiple crosscutting trails containing Type 1and Type 3 FI **171**

Figure 4.91: Photomicrographs of sample CO 005 (Coco) (c) Trail containing Type 1. (d) Isolated Type 2 (L=Liquid, V=Vapour, S=Solid). **172**

Figure 4.92: T_H frequency distribution histogram for Type 1 (n=28) FIs in Abuja leather Samples **176**

Figure 4.93: T_H versus salinity plot for Abuja leather samples. **177**

Figure 4.94: T_H frequency distribution histogram for Type 1 (n=18) and Type 2 (n=6) FIs in Omoba samples. **180**

Figure 4.95: T_H versus salinity plot for Omoba samples. **181**

Figure 4.96: T_H frequency distribution histogram for Type 1 (n=22) and Type 2 (n=3) FIs in Owode, Ibarapa samples. **184**

Figure 4.97: T_H versus salinity plot for Owode, Ibarapa samples. **186**

Figure 4.98: T_H frequency distribution histogram for Type 1 (n=33) and Type 2 (n=4) FIs in Gbayo, Olode samples. **190**

Figure 4.99: T_H versus salinity plot for samples Gbayo, Olode samples.

191

Figure 4.100: T_H frequency distribution histogram for Type 1 (n=24) and Type 2 (n=4) FIs in Coco samples. **195**

Figure 4.101: T_H versus salinity plot for Coco samples. **196**

Figure 4.102: Isochores calculated for Type 1 aqueous FIs in Abuja leather sample. Arrow indicates possible dilution trend. **201**

Figure 4.103: Isochore calculated for Type 1 aqueous FIs in samples from Omoba area **202**

Figure 4.104: Isochore calculated for Type 1 aqueous FIs in Owode samples **203**

Figure 4.105: Isochores calculated for Type 1 aqueous FIs in samples from Gbayo.

Arrow indicates possible dilution trend. **205**

Figure 4.106: Isochores calculated for Type 1 aqueous FIs in Coco samples. Arrow indicates possible dilution trend. **206**

Figure 4.107: A qualitative pressure-temperature-time (PTt) model for fluid trapping. **208**

LIST OF TABLES

Table 1.1: Pegmatite classification table: Modified from Cerny et al., (2012). **12**

Table 1.2: **Petrogenetic component of pegmatitie classification:** Modified from Cerny et at. (2012), rare elements; MI, miarolitic; *peraluminous, A/CNK>1: subaluminous, A/CNK-1: metaluminous, A/CNK<1 at A/NK>1; subalkaline, A/NK-1; peralkaline, A/NK<1, where A =$A1_20_3$, CNK = C_a0+Na_20 + K_20, and NK = Na_20+K_20 (all in molecular values; Cerny 1991a). **13**

Table 1.3: Classification of granitic pegmatites

15

Table 1.4: Fluid inclusion classification scheme based upon phases observed at room temperature **23**

Table 4.1: Major elements analytical results for whole rock pegmatites **77**

Table 4.2: Major elements analytical results for feldspars extracts **78**

Table 4.3: Major elements analytical results for biotite extracts **79**

Table 4.4: Major elements analytical results for muscovite extracts **80**

Table 4.5: Trace elemental analytical results for whole rock pegmatites **81**

Table 4.6: Trace elemental analytical results for feldspar extracts **82**

Table 4.7: Trace elemental analytical results for biotite extracts **83**

Table 4.8: Trace elemental analytical results for muscovite extracts **84**

Table 4.9: Rare earth elemental concentration for whole rock pegmatites **85**

Table 4.10: Rare earth elemental concentration for feldspar extracts **86**

Table 4.11: Rare earth elemental concentration for biotite extracts **87**

Table 4.12: Rare earth elemental concentration for muscovite extracts **88**

Table 4.13: Range of major elements composition in the analysed samples **89**

Table 4.14: Range of trace elements composition in the analysed samples **90**

Table 4.15: Rare earth elemental composition in the analysed samples (in ppm)

91

Table 4.16: Elemental ratios of whole rock pegmatites and mineral extracts **133**

Table 4.17: Classification of fluid inclusions observed in the study **150**

Table 4.18: Sample number and fluid inclusion type present in the pegmatite samples. **151**

Table 4.19: Microthermometric result of Abuja Leather samples **174**

Table 4.20: Microthermometric result of Abuja Leather samples **175**

Table 4.21: Microthermometric result of Omoba samples **178**

Table 4.22: Microthermometric result of Omoba samples **179**
Table 4.23: Microthermometric results of Owode Ibarapa samples **183**
Table 4.24: Microthermometric results of Owode Ibarapa samples **184**
Table 4.25: Microthermometric results of Gbayo samples **188**
Table 4.26: Microthermometric results of Gbayo samples **189**
Table 4.27: Microthermometric results of Coco samples. **193**
Table 4.28: Microthermometric results of Coco samples. **194**
Table 4.29: Salinity and homogenisation measurements of inclusion wafers **197**
Table 4.30: Range and average of homogenisation temperature per location **198**

CHAPTER ONE

INTRODUCTION

1.1 General Introduction

With the increase in technological advancement, and the search for new rare metal deposits all over the world, it becomes justified that a thorough study be carried out on the pegmatites of southwestern Nigeria with the intent of unravelling their origin, composition and their economic potential. This will add to the knowledge of the inventory of rare metal mineralisation in Nigeria for economic development.

Pegmatites are coarse grained igneous rocks mostly of granitic origin, composed essentially of quartz, feldspar, mica, which is similar to typical granite. However, they could also be mineralised with garnet, tantalite, niobite, columbite, tourmaline, lepidolite, and other economically viable minerals. For these minerals which pegmatites host, they have become a well sought after and much more explored rock type. These exploration activities have been further boosted by the current drive towards technological advancement and exploration of specialty metals such as tantalite, columbite, tin and a host of other rare metals. Gem mineralisation such as aquamarine, emerald, rubellite, topaz and other valued gemstones are known to be associated with pegmatites.

Pegmatites are generally crystalline, most times intrusive igneous rocks which are composed of interlocking crystals with the crystal size one of the most striking features observable in a hand specimen of a pegmatite which can sometimes grow beyond 5 cm in size.

Pegmatites size varies from veinlets of few centimetres to massive intrusive bodies which could extend for several kilometres. Nature of pegmatite bodies also varies; some occur as dike-like tubular intrusions while some occur as oval, lenticular or pipe-like bodies, lenses, veins, and dikes which are either simple or complex.

Pegmatites are known to serve as hosts to a wide range of economic deposits, such as gemstones, metallic and non-metallic (industrial) minerals. Gemstones;

precious and semi-precious stones such as ruby, opal, emerald, aquamarine, etc., which are used for their aesthetic values in jewellery, ornamental stones, etc. Tantalum (Ta) and Columbium/Niobium (Nb): these are rare metals that invariably occur together. They are used in vacuum tube synthetic rubber, dental and surgical instruments, abrasive, computer and electronics. Lithium (Li) is the lightest of all metals and does occur as native in nature. It is used as alloy of aluminium, magnesium and zinc for light aeroplane metals, ceramic and glass industries etc., while feldspar are used in ceramics industries, and also in the production of fillers in paints, as well as insulating materials in the electrical industry.

Pegmatites, depending on composition, texture and mineralogy, may be simple or complex (zoned). Generally, in unzoned/simple pegmatites which are the most common pegmatite type, mineralogical composition and texture are uniform within the pegmatite with no major variation along the strike. Simple pegmatite show uniformity in grain size from wall with no segregation of minerals; they also possess simple mineralogy of quartz, feldspars and mica; they may contain schorl, garnet as accessory minerals and they are common in metamorphic terranes.

Zoned pegmatites are pegmatites with noticeable textural, mineralogical or compositional dis-uniformity, though zones may not be well developed in certain areas. In zoned pegmatites, different zones which are mappable, non-uniform and differ in texture, grain size and mineralogical composition can be identified; and they are characterised by a core which is surrounded by other outer zones. In zoned pegmatite, grain size increases inwards towards the core of the pegmatite from the outer zones, indicating progressive grain size increase during progressive fractionation of the pegmatite. Furthermore, in zoned pegmatites, from the outer zones through intermediate zones to the pegmatite core, zones may change from an aplitic/granitic texture through graphic/heterogeneous texture in the intermediate zones to large sized coarse grains in the pegmatite core.

Also, in zoned pegmatites, mineralogical variations change from wall to core with the wall having a more complex mineralogy which becomes simpler towards the core, and silica content in the different mineralogical zones increasing towards the zones. In rare metal/rare element enriched pegmatites, different mineralogical zones may contain different elemental concentration of rare metals and rare elements (Okunlola and Ocan, 2009).

Pegmatites commonly occur in groups/swarms, which usually appear to be related to co-genetic large plutons of granitic rock in the area. Based on their distribution with respect to a related pluton, three pegmatite groups: interior, marginal and exterior have been recognised (figures 1.1-1.3) with the least fractionated end of the pluton which has the least complex structural and mineralogical characteristics located within the pluton (interior pegmatites); an intermediate section which lies at the pluton margin (marginal pegmatites), while the third group (exterior pegmatites) lies outside the granitic pluton in the metamorphic country rocks (Černý *et al*., 1981; Černý, 1991b).

Exterior pegmatites which are complex structurally, texturally and mineralogically, tend to be more common in LCT intrusive—pegmatite system while in NYF pegmatites, interior pegmatites are more common (figure 1.4, Simmons *et al*., 1987, 1999a, Cerny 1991b).

Regional zoning is believed to develop due to the ability of fluid rich in volatiles to travel great distances at lower temperatures and therefore greater distances from the source pluton due to the greater amount of volatiles they contain and their lower viscosity (Černý, 1991a and b). Regional zoning is common in LCT pegmatites and it is influenced by the nature, structure of the host rock, and the vertical level of exposure of the pegmatite. From the related granitic pluton, the mineralogical complexity increases outwards, the degree of fractionation increases while there is a decrease in the number of related associated exterior pegmatites. The sequence is:

- barren to Be-rich
- Be-Nb rich
- Li-Cs-Ta-Sn-rich

With an increase in complexity and degree of evolution of the pegmatite, there is a decrease in the number of pegmatite with one of lepidolite, albite-spodumene or albite, usually present in the most fractionated regional zones (figure 1.2, Cerny, 1986). The proposed explanation for this type of zoning is that the more fractionated melts are richer in volatiles. They are therefore less viscous and the volatile-rich fluids remain fluid to lower temperatures and can therefore travel greater distances from the source pluton.

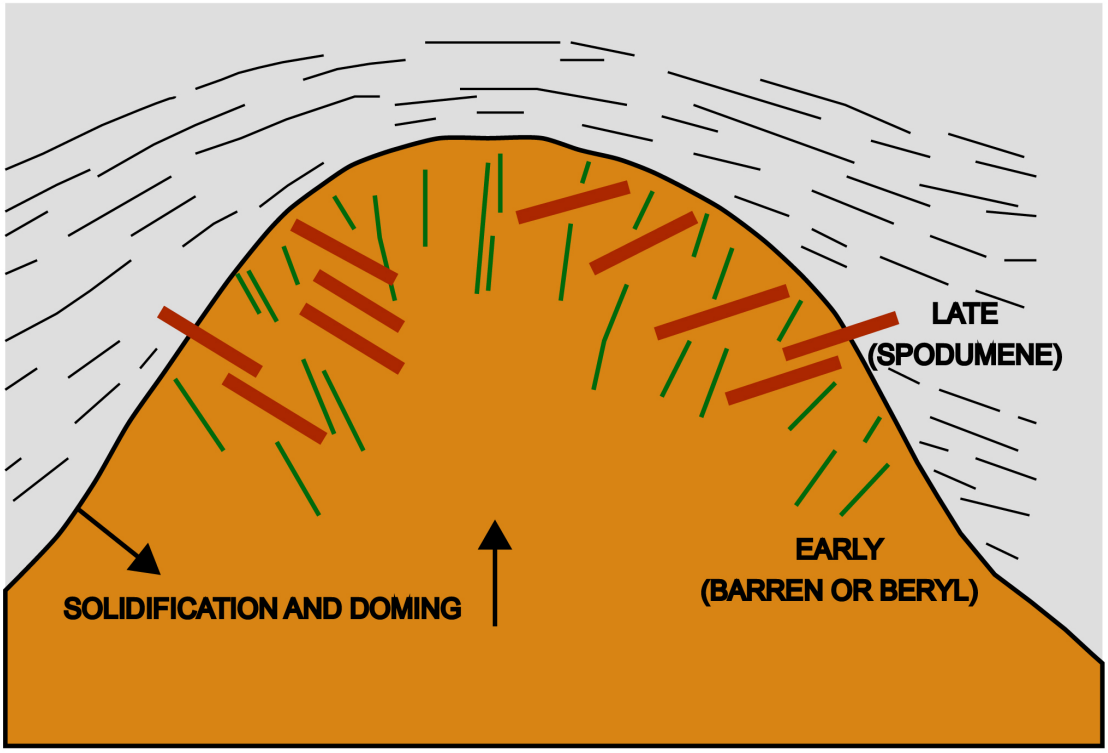

Figure 1.1: Interior to marginal LCT pegmatites (after Cerny 1991b)

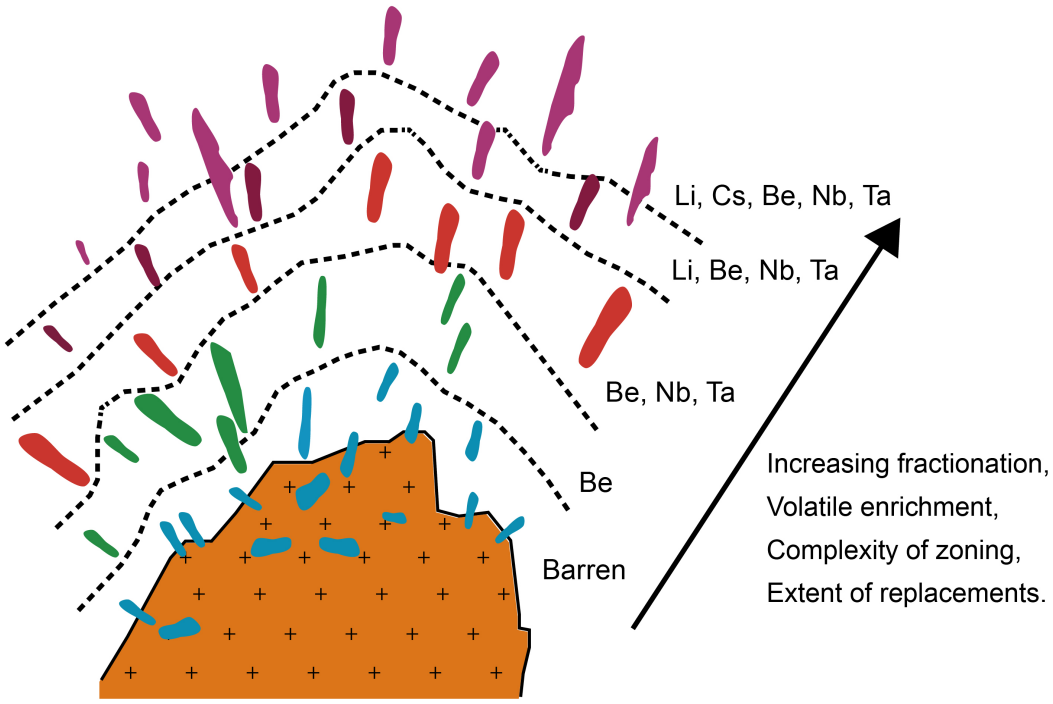

Figure 1.2: Regional zoning of LCT pegmatites around a parental pluton (Cerny 1991b)

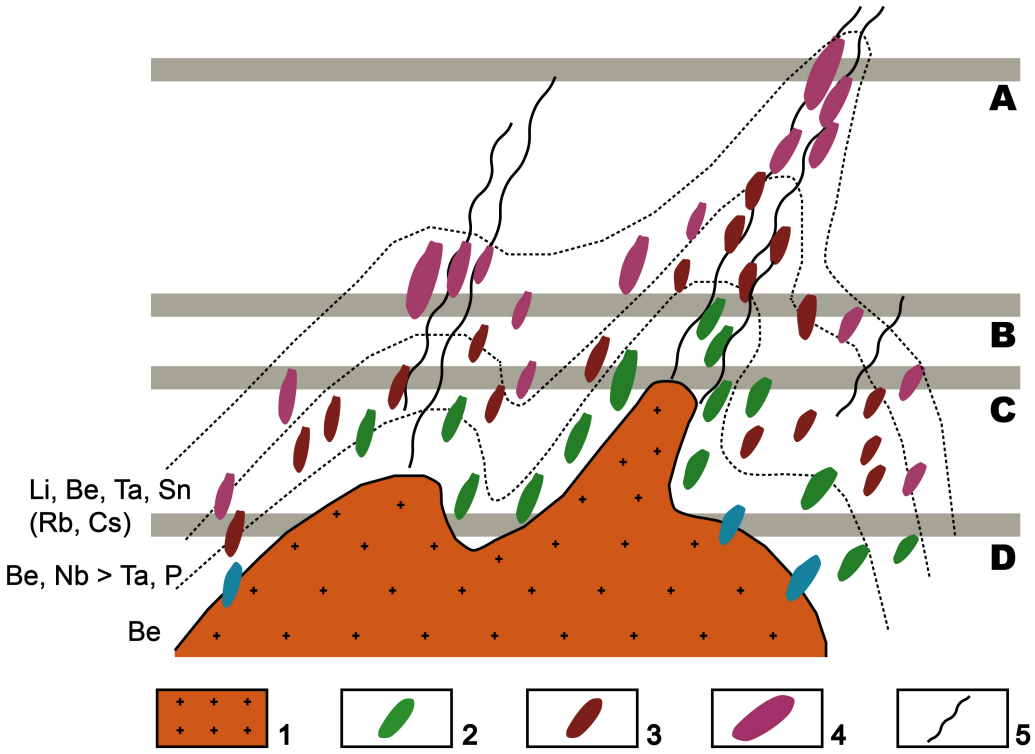

Figure 1.3: Schematic vertical section through a zoned fertile granite-pegmatite.1: fertile granites with leucocratic and pegmatitic cupolas, 2: barren to beryl-baring pegmatites, 3: beryl type, columbite to phosphate-bearing pegmatites; 4: complex spodumene (or petalite) bearing pegmatites (with Sn, Ta and Cs mineralisation), 5: faults, Letters A through D, progressively deeper levels of erosion showing the types of pegmatites exposed (from Cerny, 1986)

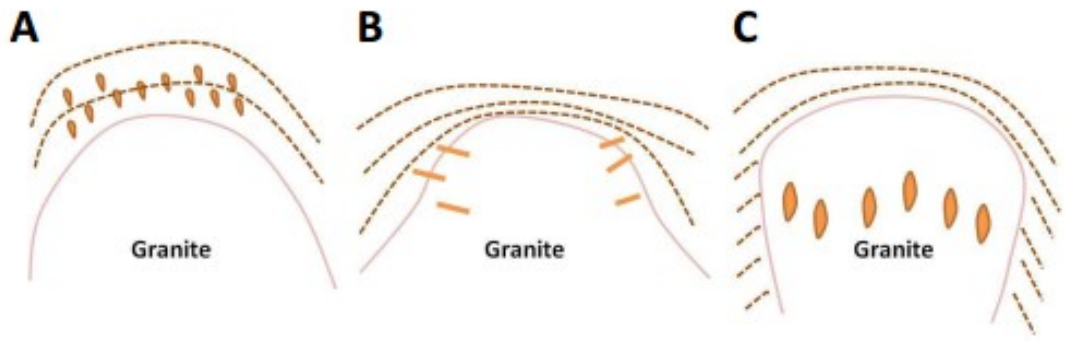

Figure 1.4: Relationship between parent granite plutons and surrounding pegmatites showing A) Exterior pegmatites which occurs in a pegmatite aureole surrounds a granitic pluton; B) Marginal pegmatites; C) Interior pegmatites (adapted from Ashworth, 2014)

1.2: Formation and classification of pegmatite

There are two different proposed models of pegmatite genesis, fractional crystallisation and anatexis, but fractional crystallisation of a granitic pluton to form pegmatitic melts is the most widely accepted model of pegmatite formation (Cameron et al., 1949; Jahns, 1953; Jahns and Burnharn, 1969; Cerny, 1991b). Based on this model, as the granite crystallizes, the earlier formed minerals are alkali feldspar, sodic plagioclase, quartz and minor muscovite, or biotite and the silicate minerals incorporate Si, Al, K, Na, and minor amounts of Fe and H_20 from the melt thereby depleting the melt in these constituents and enriching the residual melt in incompatible elements, volatiles and fluxes such as H_2O, B, F, CO_2, Li and P. The residual melt therefore has lower viscosity and crystallisation temperature compared to the parent granitic magma, and the melt becomes enriched in rare elements such as Ta, Nb, Cs, Zr, U REE and Sn (Cameron et al., 1949; Simmons, 2007; London, 2008; London and Morgan, 2012).

Two main models exist for crystallisation of pegmatites: fractional crystallisation (Cameron *et al*., 1949; Jahns, 1953; Jahns and Burnharn, 1969; Cerny 1991b) and constitutional zone refining (Morgan and London 1999). The Jahns, (1953) and Jahns and Burnham's 1969 theory which explained that aqueous fluid interacting with silicate melt is a necessary condition for formation of pegmatite was until recently the most widely accepted theory. However, this has been challenged by experiments of London *et al*., (1989) who cited a lack of supporting evidence, in particular the low solubility of Al in aqueous fluids. In addition, London, (2008) and London and Morgan, (2012) also cited experimental evidence showing that rapid crystallisation of undercooled melt results in the formation of a boundary layer highly enriched in volatile components.

Fractional crystallisation, however, produces the same effect by the exclusion of incompatible elements as the pegmatite solidifies. The concentration increase is more gradual in fractional crystallisation, but the concentrations of incompatible elements increase exponentially near the final stage of crystallisation (figure 1.2).

London proposed that this process is the mechanism for concentrating fluxes and other incompatible elements into the final products of crystallisation and he refers to this process as constitutional zone refining (CZR). This process allows for the concentration of incompatible elements into the boundary layer without having an initially aqueous vapor-saturated melt. One of the notable differences in the two models is that the Jahns and Burnham model requires aqueous vapor saturation and the London model does not.

The second proposed model for pegmatite genesis is anatexis with the abyssal and muscovite classes of pegmatites proposed to have been formed by anatexis (Cerny and Ercit 2005, Cempirek and Novak, 2006; Grew, 2002), while the rare element class pegmatitic melts are possibly formed by anatexis of rocks with an appropriate composition.

It was also proposed by Simmons *et al.* (1995, 1996) that in an orogenic environment, partial melting of migmatites around plutons could produce melts of similar composition as late-stage melts which are products of fractional crystallisation, thereby implying that pegmatitic melts could be directly produced from low-degree partial melts.

Classification of pegmatite

Different pegmatite classification schemes have been employed over time such as the pegmatite classification studies by Fersman, (1924) and Landes, (1933). But presently, the widely accepted classification scheme is that of Cerny, (1991a) which has been modified over the years to produce other classification other schemes by Cerny and Ercit, (2005) and Cerny *et al*., (2012).

Cerny's classification scheme of 1991 was based on several factors which includes emplacement depth of the pegmatite, minor elemental composition as well as metamorphic grade and he classified pegmatites into 5 major classes which are:

1. Abyssal (high metamorphic grade, high to low pressure),
2. Muscovite (high pressure, intermediate temperature),
3. Muscovite-Rare Element (high pressure, lower temperature),
4. Rare-Element (low temperature and pressure), and
5. Miarolitic (shallow level).

The pegmatite classes were further subdivided with the exception of the muscovite class into LCT and NYF families based on Li, Cs, Ta, Nb, Y and F elemental concentration while the Rare-Element pegmatite class was subdivided based on mineralogical or geochemical characteristics into different types and subtypes.

Cerny and Ercit, (2005) revised the classification scheme of Cerny, (1991a), they proposed changes on NYF pegmatite classification and produced a petrogenetic classification of pegmatites (table 1.1-1.2).

Martin and De Vito, (2005) also addressed the relationship of pegmatites to tectonic regime. They explained that the LCT and NYF classes cannot be based on

depth-zone classification and they concluded that pegmatites are of two main types, those of anatectic origin and those formed by fractional crystallisation of more primitive felsic plutons. They suggested that the nature/type of parent magma as well as derivatives of rare element enriched magmas are determined by the tectonic setting and they proposed that orogenic suites (compressional tectonic settings) produce LCT pegmatites while extensional tectonic settings (anorogenic suites) produces NYF pegmatites. In addition, they discussed pegmatites with 'mixed' LCT and NYF signatures and 'hybrid' pegmatites which are overprinted by fluids from the wall rocks.

1.3: Pegmatites of Nigeria

Several studies have been carried out on pegmatites in different areas of Nigeria. Raeburn (1927), who was one of the earliest workers of the Precambrian pegmatite of Nigeria, observed that the pegmatites of Calabar were characterised by the presence of tinstone and tourmaline. Jacobson and Webb (1946) in their study of pegmatite in the Central part of Nigeria, concluded that they are of the complex category and that the rare-metals bearing pegmatite of Nigeria are confined to a 400 km long NNE – SSW trending belt stretching from Ago-Iwoye in Southwestern Nigeria to Wamba area in Central Nigeria (figure 1.5-1.7).

Earlier workers such as Jacobson and Webb, (1946) concentrated their work on the geology of pegmatites around plateau tin fields which shows petrographic similarities in the leucogranites of Central and Southwest Nigeria around Wamba and Odoshin near Egbe. They suggested that the formation of the Southwest Nigeria pegmatite is analogous to the pegmatites of Central Nigeria around Wamba. Wright (1970) postulated that widespread pegmatite and aplite development marked the closing stages of the older granite emplacement and further adduced that mineralisation was due to Na rich hydrothermal solutions emanating from the mantle.

Matheis and Caen Vachette (1983); and Matheis (1987) dated the Egbe granites to be 100 Ma older than the 350 Ma recorded for the mineralised pegmatites of the area and postulated that the initial Sr ratios values obtained does not support cogenetic origin for the granites and the pegmatites, and the rare metal rich pegmatites of Southwest Nigeria are products of partial melting of rocks and leaching of the basement units with external fluid supply than truly a pegmatitic phase of proximal older granite.

Kuster, (1990) opined that the evolution of rare metal pegmatites of central Nigeria is related to the late tectonic granite magmatism which is characterised by multiphase intrusion and structurally controlled emplacement. Ekwueme and Matheis, (1995) suggested that the pegmatites appears to have been emplaced along major fault lineaments with albitisation and attendant rare metal mineralisation which may have been due to late stage fluids available at the close of Pan African Orogeny.

Table 1.1: Pegmatite classification table: Modified from Cerny et al., (2012).

Class	Subclass	Type	Subtype	Family
Abyssal	HREE LREE U			NYF
	B Be			LCT
Muscovite				
Muscovite-Rare Element	REE			LCT
	Li			
Rare Element	REE	allanite-monazite euxenite gadolinite		NYF
	Li	beryl complex	beryl-columbite beryl-columbite-phosphate spodumene petalite lepidolite elbaite amblygonite	LCT
Miarolite	REE	topaz-beryl gadolinite-fergusonite		NYF
	Li	beryl-topaz spodumene petalite lepidolite		LCT

TABLE 1.2: Petrogenetic component of pegmatitie classification: Modified from Cerny et at. (2012), rare elements; MI, miarolitic; *peraluminous, A/CNK>1: subaluminous, A/CNK-1: metaluminous, A/CNK<1 at A/NK>1; subalkaline, A/NK-1; peralkaline, A/NK<1, where A =$A1_20_3$, CNK = C_a0+Na_20 + K_20, and NK = Na_20+K_20 (all in molecular values; Cerny 1991a).

Family	Pegmatite subclass	Geochemical signature	Pegmatite bulk composition	Associated granite	Granite bulk composition*	Source lithologies
LCT	REL-Li mL-Li	Li, Rb, Cs, Bc, Sn,Ga, Ta>Nb, (B, P, F)	Peraluminous To subaluminous	Synoroganic to late- orogenic (toanorogenic); largely heterogeneous	Peraluminous S, 1 or mixed S+1 types	Undepleted upper to middle-crust supracrustal rocks and basement gneiss
NYF	REL- REE MI- REE	Nb>Ta, Ti Y, Sc, REE, Zr, Y, Th F	Subaluminous to metaluminous (to subalkaline)	Syn-, late, post-to mainly anorogenic; quasi-homogeneous	Peraluminous to subaluminous and metaluminous A and 1 types	Depleted middle to lower crustal granulite, or juvenile granitoid rocks
Mixed	Cross-bred: LCT an NYF	Mixed	Metaluminous to moderately peraluminous	Post orogenic to anorogenic heterogeneous	Subaluminous to slightly peraluminous	Mixed protoliths or assimilation of supracrustal rocks by NYF granite

However, studies by Ekwueme and Schlag, (1989); Ekwueme and Matheis, (1995) and Garba, (2002), show that pegmatites in Nigeria are not restricted to the "Tin Province" or "Pegmatite belt of Nigeria", but also occur in the southeastern part of Nigeria. These pegmatites are also to extend into northeastern Brazil (Garba, 2002; Ekwueme and Matheis, 1995).

Furthermore, Garba, (2003) delineated some newly discovered rare element pegmatites in Nigeria while Okunlola, (2005) defined 7 broad fields of the Precambrian rare-metals pegmatites of Nigeria namely: Anka-Birnin Gwari, Nasarawa-Keffi, Ijero-Aramoko, Ibadan-Oshogbo, Oke Ogun, Lema-Share and Kabba-Isanlu (figure 1.6-1.7) with rare metal enrichment increasing northwards, from the Ibadan-Oshogbo fields to the most enriched Lema-Ndeji field (Okunlola, 2017).

Okunlola, (2005) in his studies of metallogeny of Nb – Ta mineralisation in Precambrian basement pegmatites of Nigeria noted that rare metal pegmatites are not confined to an older tin belt only. He also noted that low to moderate degree of Na-metasomatism (albitisation) control rare metal mineralisation in some Nigerian pegmatites, this shows lower degree of evolution and thus in effect means lower mineralisation compared to other highly mineralised pegmatites in other parts of the world.

Nigerian pegmatites have also been associated with gemstone mineralisation with over ten varieties of gemstones documented mainly around the Ibadan-Osogbo and Oke-Ogun pegmatite fields (Okunlola and Ogedengbe, 2003; Okunlola and Omitogun, 2014) as well as some of the pegmatite fields in the northern central part of the country (Okunlola and Ocan 2009).

Okunlola, (2017) also explained that using geochemical signatures, structural characteristics and petrographic variations, Nigerian pegmatites can be classified into 3 main sub types—Beryl type, Albite type and complex (table 1.3 and 1.4) and some of the pegmatites variably comparable to that of Tanco (Canada), Homestead and Wodgna (Australia) pegmatites, while some overlap with the Buck Noumas rare pegmatite fields of South Africa.

Furthermore, Okunlola, (2017) explained that in some areas, mineralogical zonation are present, though they are complex; they are can be defined and in some pegmatites (for example, Keffi area; Okunlola and Ocan, 2009); they control mineralisation.

Table 1.3: Classification of granitic pegmatites

Class	Family	Typical minor element	Metamorphic environment	Relation to granite
Abyssal	-	U, Th, Zr, Nb, Ti, Y, REE, Mo. Poor to moderate mineralisation.	(Upper amphibolite) Low-to-high P granulite facies 4-9kb, 700-800^{o}C	None. Segregations of anatectic melt.
Muscovite	**-**	**Li, Be, Y, REE, Ti, U, Th, Nb>Ta.** **Poor to moderate mineralisation.**	**High-P, Barrovian amphibolite facies. Kyanite-sillimanite.** **5-8kb, 650-580^{o}C**	**None (anatectic bodies) to marginal and exterior.**
Rare element	**LCT**	**Li, Rb, Cs, Be, Ga, Sn, Hf, Nb><Ta, B, P, F.** **Poor to abundant mineralisation.**	**Low-P, Abukuma amphibolite to upper greenschist facies.** **(andalusite-sillimanite), 2-4kb, 650-500^{o}C**	**Interior to marginal exterior**
	NYF	Y, REE, Ti, U, Th, Zr, Nb>Ta,F. Poor to abundant mineralisation	Variable	Interior to marginal
Miarolitic	NYF	Be, Y, REE, Ti, U, Th, Zr, Nb>Ta, F, Poor Mineralisation.	Shallow to subvolcanic. 1-2kb.	Interior to marginal

Major pegmatite class for southwest Nigeria in red colour

LCT: Lithium caesium tantalum, NYF: niobium yttrium fluorine. Original Source: Cerny (1991 a)

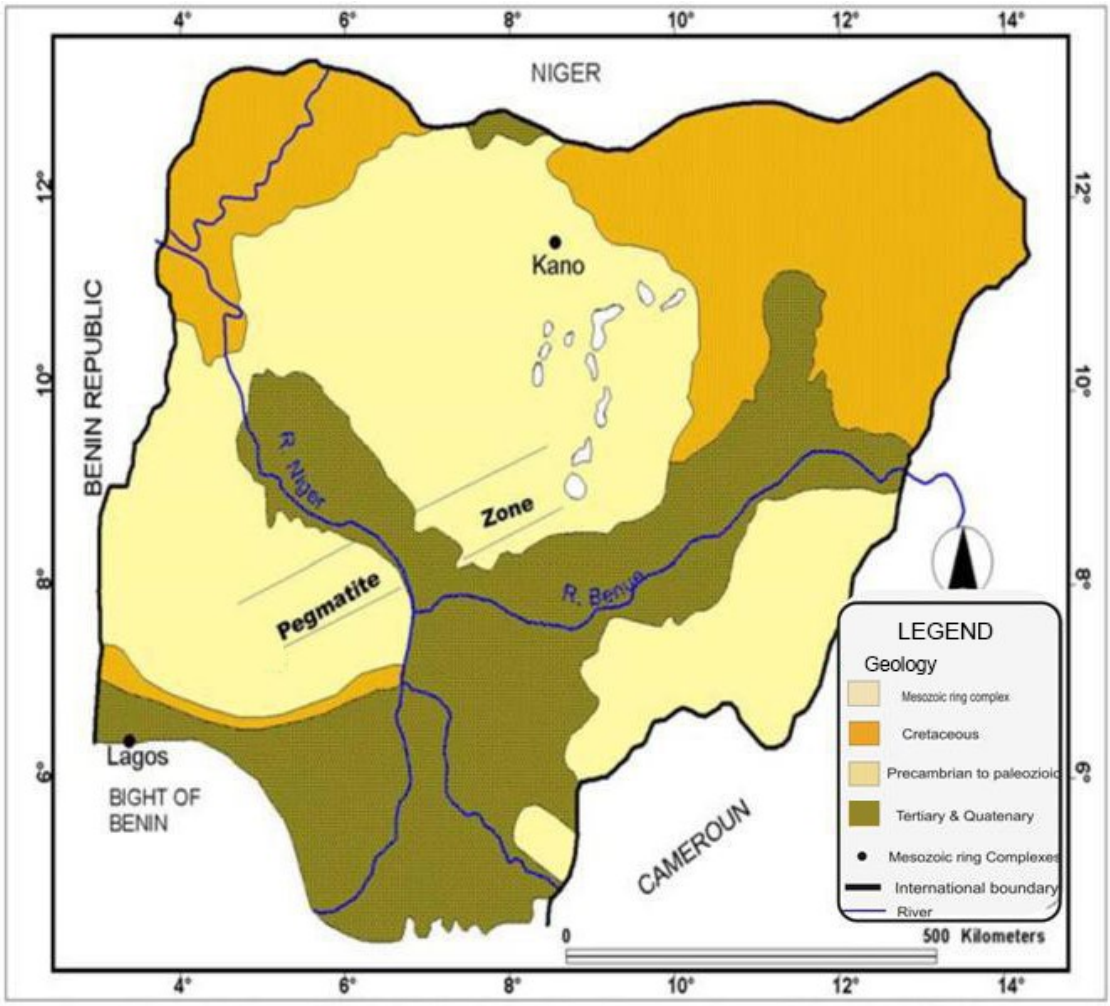

Figure 1.5: General geology of Nigeria showing the preconceived pegmatite zone (adapted from Akintola et al., 2012).

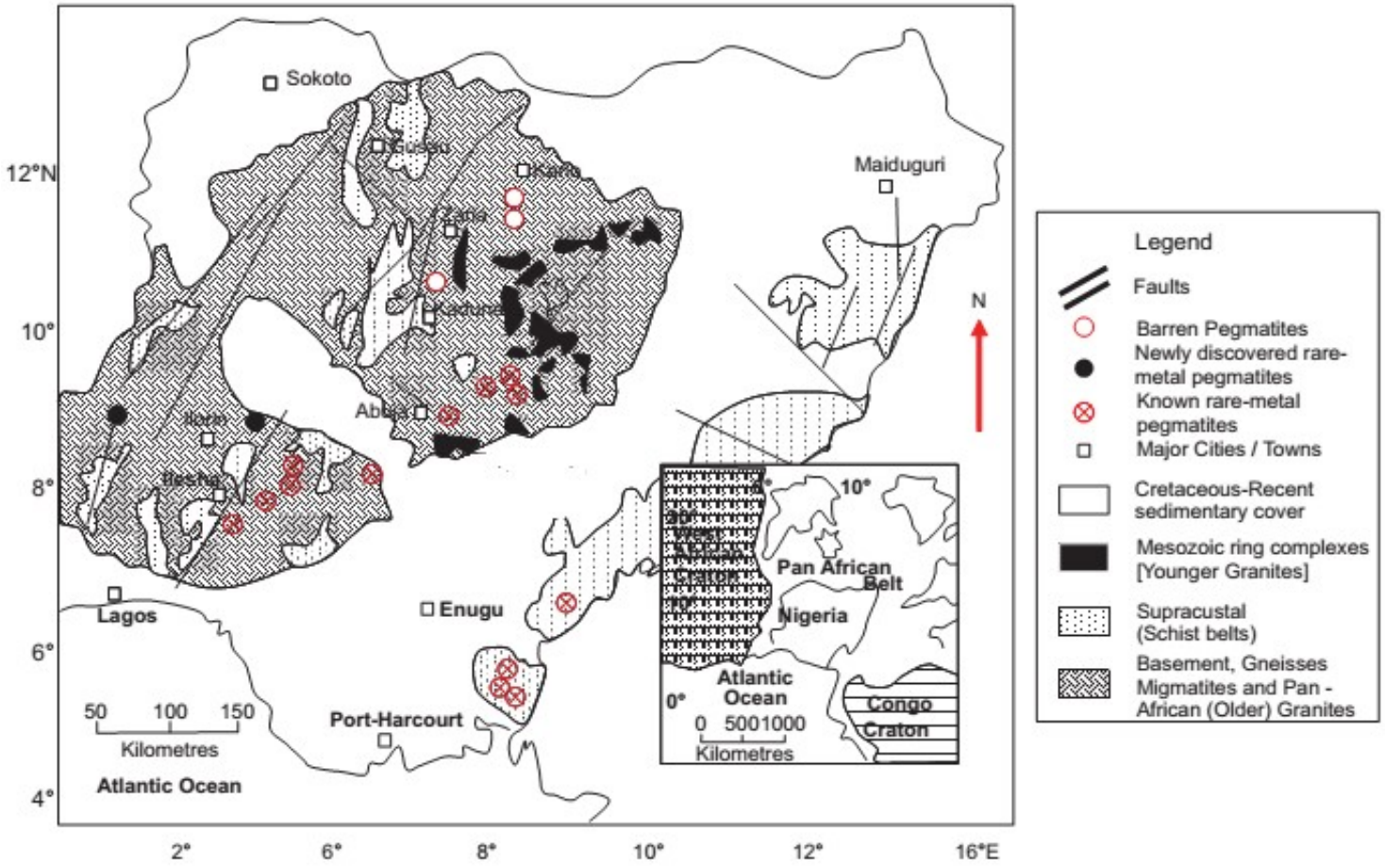

Figure 1.6 Geological map of the Nigeria, showing locations of rare-metal and barren pegmatite (Garba, 2003)

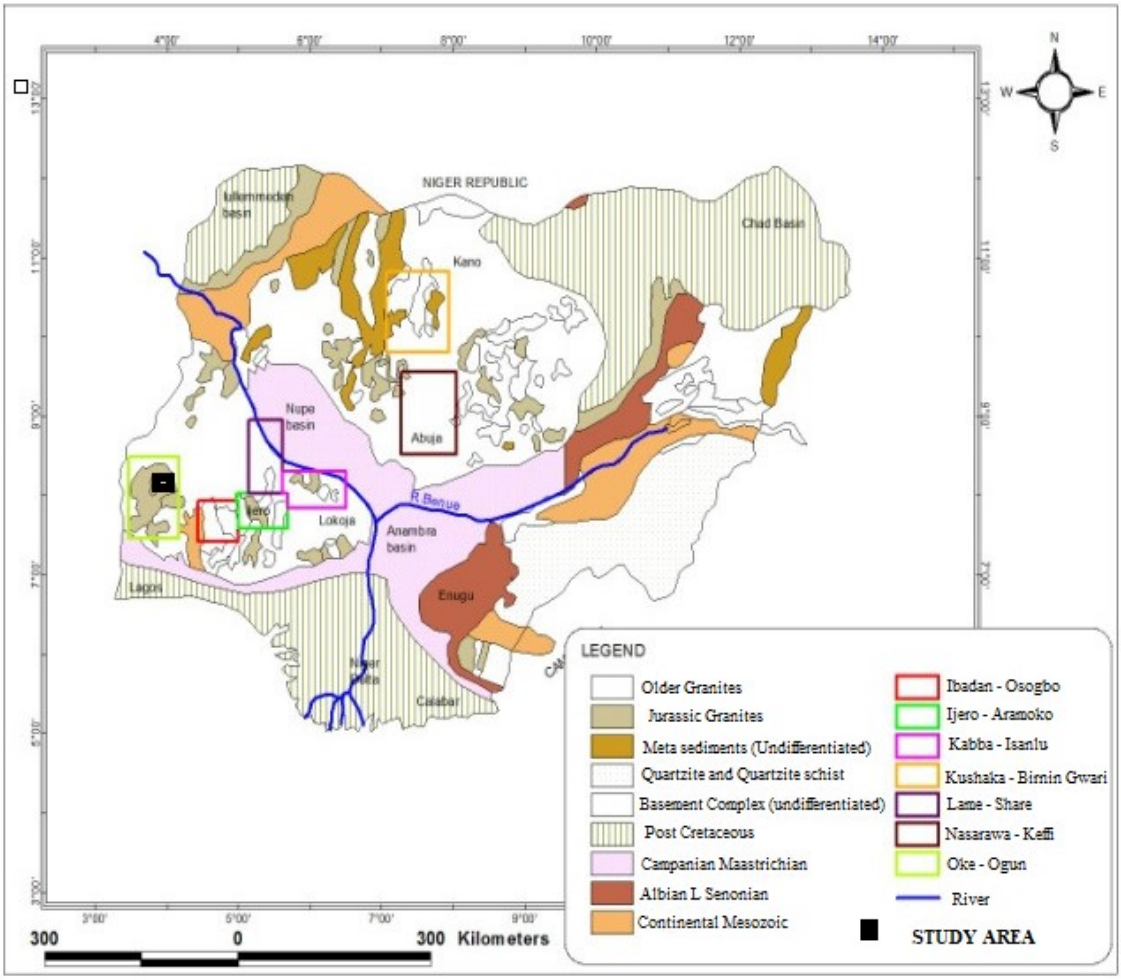

Figure 1.7: General geology of Nigeria showing pegmatite zones (Okunlola, 2005).

1.4: Fluid inclusion studies

1.4.1: Background

Fluid inclusions are minute quantities of fluid with size which are usually 5 – 30 μm, trapped in cavities within minerals (Van der Kerkhof and Hein., 2001). They are vacuoles within minerals which are fluid filled. Fluid inclusion studies in rocks and minerals were developed about 1000 years ago and they were first described in the 11th century though they were observed much earlier by ancient Greek and Roman scientists (Roedder, 1984; Leeder et al., 1987).

However, the use of fluid inclusions in the study of geological systems was pioneered by Henry Sorby in the 1800s. Sorby, (1858) reasoned that 'bubbles' within fluid inclusions in minerals are a result of differential thermal heating. He explained that systematic increment of the temperature of the inclusions will lead to the disappearance of the bubbles and temperatures at which the bubbles disappear may be used to estimate temperature at which the mineral was formed.

Today, various types of fluid inclusions in minerals have become an invaluable tool in the study of metamorphic and igneous petrology, ore deposits as well as in petroleum geology and if adequately studied, it can provide adequate information on the composition, temperature, pressure and density of ore forming fluid in geological systems:

1. Temperature of mineral crystallisation: fluid inclusions are useful in determination of the trapping temperature of inclusions at different levels of certainty depending on the study method employed and the type of fluid inclusion assemblage (FIA) present. Minimum temperature of trapping of inclusions can be obtained with the temperature of total homogenisation and sometimes, true temperature of trapping of the inclusions may be obtained.

2. Pressure of mineral crystallisation: pressure conditions during mineral crystallisation can also be obtained from fluid inclusion studies. Inclusions can also be useful in determination of true pressure of entrapment in certain cases while in some circumstances, pressure corrections are applied to derive true pressure at the time of crystallisation.

3. Fluid composition: composition of fluids (aqueous or carbonic) can be determined from fluid inclusion studies. Salinity of inclusions can be determined as well as the presence of organics. Other measurements that can be obtained include concentration of organics; identity and concentration of major and minor ion ratios, identity and concentration of dissolved components and gases, identity and composition of available solids as well as isotopic composition of fluids.

4. True temperature and pressure at the time of precipitation can also be obtained from fluid inclusion studies through the use of independent geothermometers such as stable isotope method.

Fluid inclusions occur in all geological environments in different rock forming minerals, but they are best studied using quartz, fluorite, halite, calcite, apatite, dolomite, sphalerite, barite, topaz and cassiterite. In ore deposit studies (porphyry deposits, skarn and hydrothermal deposits), fluid inclusions are best studied in large euhedral crystals in vugs, alterations and veins; in igneous rocks, apatite is used in carbonitite, phenocrysts of volcanic rocks can be studied while quartz is also used.

In pegmatites, minerals which can be used for fluid inclusion studies are quartz, beryl and tourmaline; quartz is from veins and pods can also be used for study in metamorphic rocks, while in sedimentary rocks; diagenetic fluids which are well preserved in pods, vugs, veins and diagenetic cement can be used for fluid inclusion studies.

1.4.2: Classification of fluid inclusions

Classification of fluid inclusion may be based on the timing of entrapment of the inclusions and also by the type and number of phases present in the inclusion at room temperature. Based on petrographic criteria (timing of entrapment in relation to mineral paragenesis), fluid inclusions can be classified into primary, secondary and pseudo-secondary inclusions. Primary inclusions are inclusions which were formed during mineral growth within the growth zone and they can be identified by their relationship to the growth zones in minerals. They commonly occur along grain boundaries or parallel to growth zonation they range in size and can be of different

shapes (figure 1.8); hence, primary inclusions are good indicators of the conditions of crystallisation of their host minerals.

Secondary inclusions are inclusions which are developed after crystal growth. After crystallisation of a mineral, minute cracks or deformational planes may form in the crystal trapping fluids present during the healing, thereby providing a record of fluids which are present after crystal growth. Sometimes, inclusions are trapped before crystal growth is completed and these inclusions bear all characteristics of secondary inclusions and are termed pseudosecondary inclusions but they terminate at a growth zone boundary while secondary inclusions may appear to cut across different growth zones of a crystal (figure 1.8).

The second classification scheme is based on the type and number of phases (solid, liquid and vapor) which are observed at room temperature in the inclusion (table 1.4). Inclusions are classified into:

1. Monophase liquid (L) inclusions: these are inclusions with 100% liquid content
2. Liquid-rich, two phase (L+V) inclusions: these are inclusions which contain a liquid phase and a vapor phase with a liquid phase occupying a larger percentage (>50%) while the present but smaller vapour phase occupies <50% of the total inclusion volume.
3. Vapor rich, two phase (V+L) inclusions: these are inclusions in which the vapor phase dominates and occupies between 50-80% of the volume of the inclusion with the liquid phase occupying less than 50% of the inclusion volume.
4. Monophase vapor (V) inclusions: these are inclusions which are entirely filled with vapor phase without a visible liquid phase.
5. Multiphase solid (S+L$\pm$V) and multi-solid (S+L$\pm$V) inclusions: these inclusions essentially contain at least one solid crystalline phase/daughter minerals which is usually less than 50% of the inclusion volume and in, liquid and vapour phases.
6. Immiscible liquid (L1+L2$\pm$V) inclusions: these inclusions contain two immiscible liquids; an aqueous phase and a CO_2 rich phase in addition to a vapour phase.
7. Glass inclusions: these are inclusions which contain over 50% of glass.

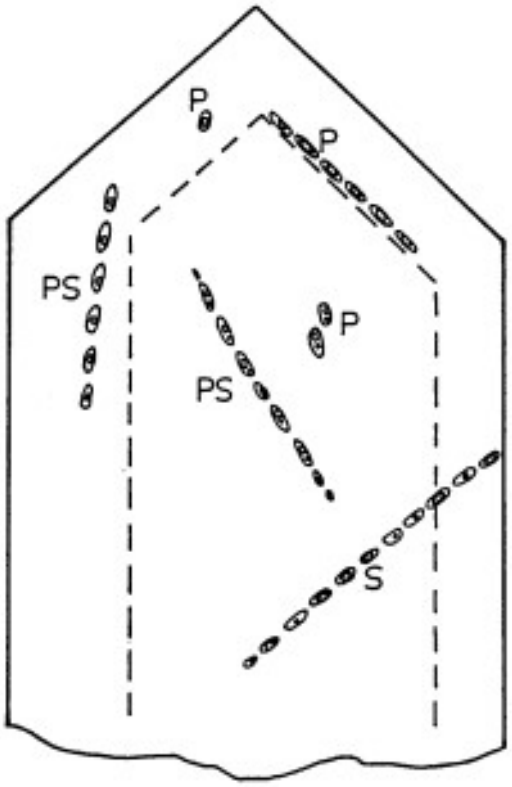

Figure 1.8: Sketch of fluid inclusion classification (Goldstein and Reynolds, 1994)

Table 1.4: Fluid inclusion classification scheme based upon phases observed at room temperature L=liquid, V= vapour, S=solid, GL=glass (adopted from: Shepherd et al., 1985)

INCLUSION TYPE	ESSENTIAL PHASES	TYPICAL EXAMPLES	ABBREVIATION
Monophase liquid	L = 100%		L
Liquid-rich, two-phase	L > 50%		L+V
Vapour-rich, two-phase	V = 50 to 80%		V+L
Monophase vapour	V ≙ 100%		V
Multiphase solid	L = variable S < 50%		S+L±V
Multisolid	S > 50% L, V variable		S+L±V
Immiscible liquid	L_1, L_2		$L_1+L_2±V$
Glass	GL > 50%	not shown	GL±V±S

1.4.3: Methods of study of fluid inclusions

Fluid inclusion studies begin with samples selection for production of doubly polished wafers of between 90 and120µm. Fluid inclusion petrography involves the determination of the textural relationship of fluid inclusions and the host rock/mineral. It involves observation of different types, generations and populations of inclusions to ensure that fluid inclusions which will be analysed will be representative of the processes which were prevalent during fluid genesis. Different fluid generations can be present in a mineral to be studied due to interaction of minerals with different fluids throughout its geological history. Petrography is therefore used to differentiate between these different set of fluid types and generations; and it provides adequate information on types of fluids present in minerals, the type of fluid inclusion assemblages (FIA) present, abundance of each inclusion type and their relationship/chronology. Fluid inclusion petrography is therefore a very important aspect of fluid inclusion study as it is the key which determines if and how the study should be carried out (Roedder, 1981; 1984; Touret, 2001).

There are various methods involved in the study of fluid inclusions. Fluid inclusion analysis involves destructive and non-destructive methods. Destructive methods of analysis includes mechanical crushing, decrepitometry, gas and mass spectrometry, crush and leach analysis for bulk analysis; and EPMA/SIMS and LA-ICPMS for single inclusions. Non-destructive analysis methodology includes optical microscopy, microthermometry, Raman spectrometry, laser induced breakdown spectrometry, Fourier Transform Infra-Red etc.

1.5: Justification

Over the years, different researches have been carried out on pegmatites of Nigeria. These studies have been focused on appraisal of the pegmatites for their economic potential and suitability of their constituents for industrial applications with little or no focus on pegmatite genesis. Hence, the study is aimed at determining the fluid characteristics of pegmatites in selected areas of southwestern Nigeria.

1.6: Aim and Objectives of the Study

1.6.1: Aim

The study is aimed at unravelling the origin and economic mineralisation potential of pegmatites from selected parts of southwestern Nigeria.

1.6.2: Objectives

i. Determination of the mineralisation potential of the pegmatites.
ii. Determination of the fluid characteristics of the pegmatite.
iii. Determination of the origin of pegmatites in the study area

1.7 Scope

To achieve the objectives of the study, the following scope were covered;

i. systematic geologic mapping of the study areas, with detailed study of field relationship and lithological associations between the pegmatites and host rocks.
ii. petrographic studies and geochemical analyses of pegmatites and mineral extracts.
iii. fluid inclusion study using pegmatitic quartz
iv. determination of the genesis of the pegmatites

1.8: Location and accessibility

The study areas are assessible from different areas. Gonandoya, Abuja Leather, Owode, Idiyan, Omoba, and Balogun-Ojo within the Oke-Ogun pegmatite field while Gbayo, Coco and Falansa are located with the Ibadan-Oshogbo pegmatite field.

Komu, Okeho and Igbojaye can be accessed through the Ibadan-Iseyin road network. Owode and Idiyan can be accessed through the Eleyele – Eruwa road network from Ibadan. Gbayo, Coco and Falansa are easily accessible through the road network in the ancient city of Ibadan through Olomi - Olode road (figure 1.9 – 1.11).

1.9: Climate, topography, relief and drainage

Climate in the study areas is of the typical tropical climate with high temperatures, high humidity with rains from March to October and with temperatures at the peak towards the end of the harmattan period which runs from January to March. (Online Nigeria, 2003).

Average temperatures range 24°C to 25°C during the rainy season with 800-1500mm of rain in different areas. The study areas are mostly drained by rivers with dendritic drainage pattern and vegetation in the study area is characterised by rain forest.

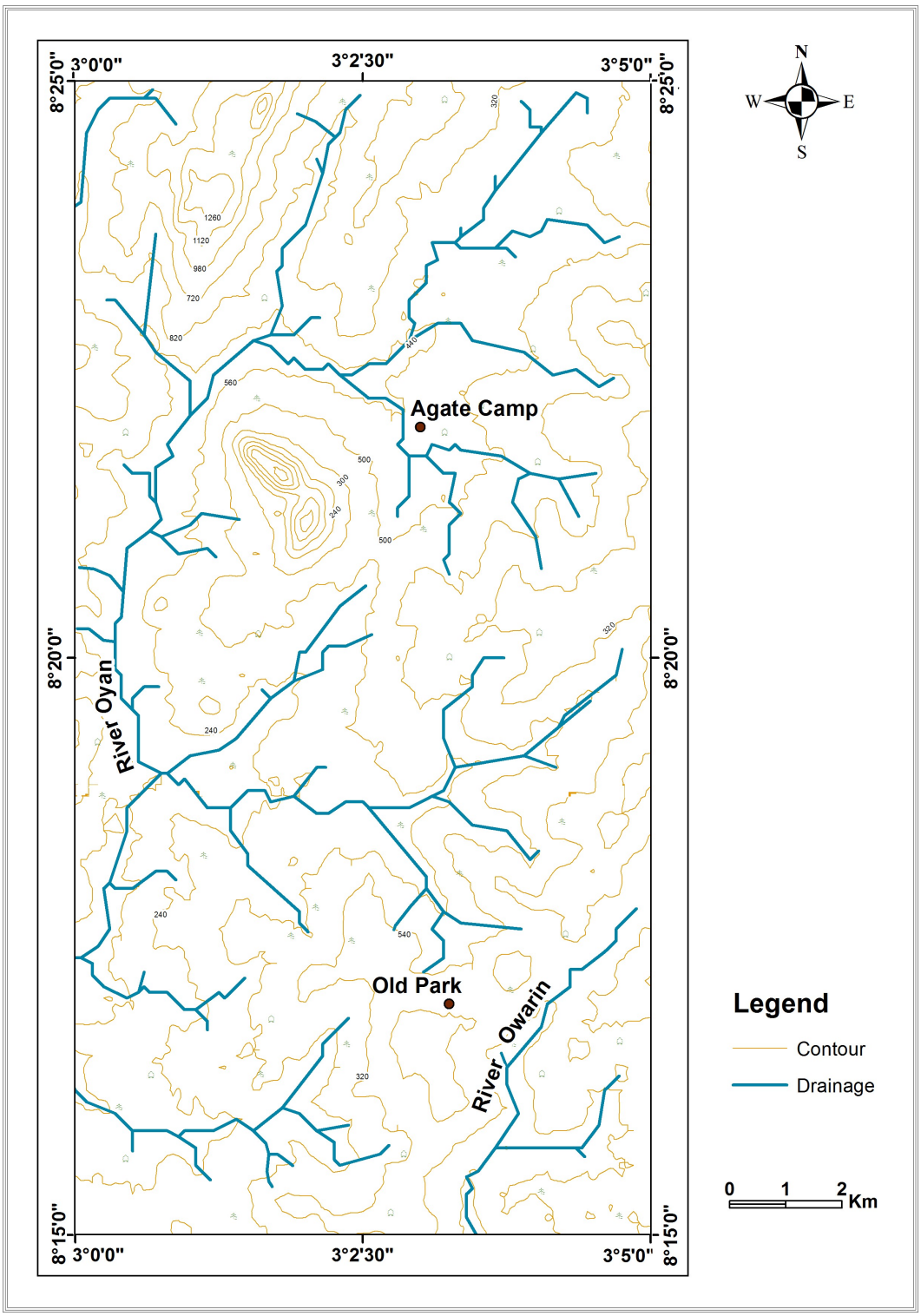

Figure 1.9: Topographical map of Ikomu area.

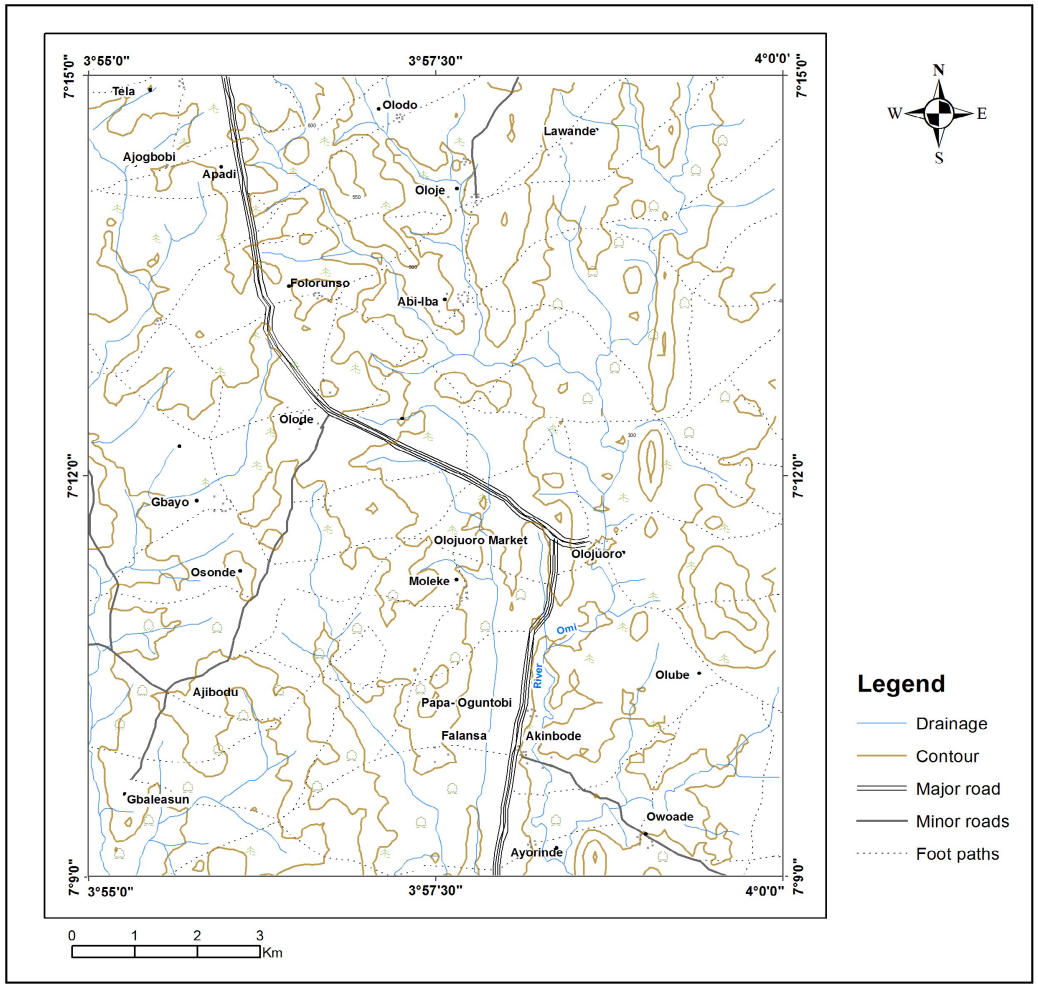

Figure 1.10: Topographical map of Olode area.

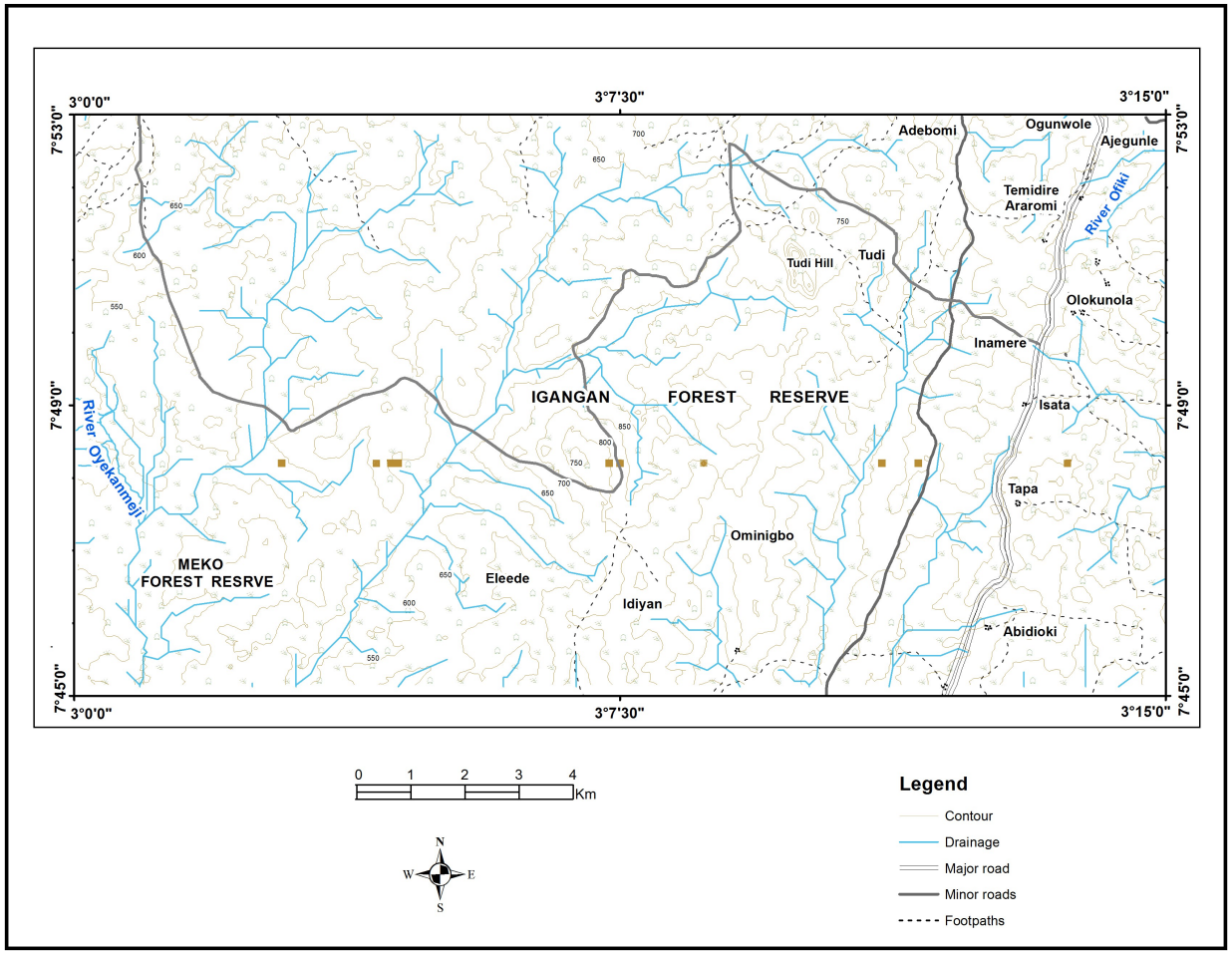

Figure 1.11: Topographical map of Igangan area.

CHAPTER TWO

GEOLOGY OF NIGERIA AND REVIEW OF RELATED PREVIOUS WORKS

2.1: Regional Geology of Nigeria

Nigeria lies within the boundaries of Latitudes 4^{o}N and 15^{o}N and Longitudes 3^{o}E and 14^{o}E.it is located within the Pan African mobile belt, which is between the West African and Congo Cratons (figure 2.1). Geologically, Nigeria is made up:

i. The Basement Complex,
ii. Younger Granites, and
iii. Sedimentary Basins. (Obaje, 2009).

The basement complex bears imprints of the 600 Ma Pan-African orogeny (figure 2.2). It lies within the reactivated region which was produced by the collision or active Pharusian continental margin and the passive continental margin of the West African craton (Burke and Dewey, 1972; Dada, 2006). These rocks are believed to be results of over four major orogenic cycles (Liberian, eburnean, Kibaran and Pan-African orogeny) between 2700-600 Ma which produced tectonic activities such as metamorphism, deformation and fluid remobilisation.

The Liberian, Eburnean and Kibaran orogenic cycles were characterised by deformation, structural events (isoclinal folding) alongside large-scale regional metamorphism, after which large scale migmatisation occurred. The fourth orogeny involved regional metamorp0hism, migmatisation, granitisation and gneissification which lead to the evolution of syntectonic granites and homogeneous gneisses (Abaa, 1983). The late stage of the Pan-African Orogeny was typified by the emplacement of different suites of granitic rocks and granodiorites as well as contact metamorphism while fracturing and faulting marked the end of the orogenic episode (Gandu et al., 1986; Olayinka, 1992).

Within the basement complex of Nigeria, there are four distinguishable major petro-lithological units (Figure 8) namely:

1. The Migmatite–Gneiss Complex (MGC),

2. The Schist Belt (Metasedimentary and Metavolcanic rocks),
3. The Older Granites (Pan African granitoids),
4. Undeformed Acid and Basic Dykes.

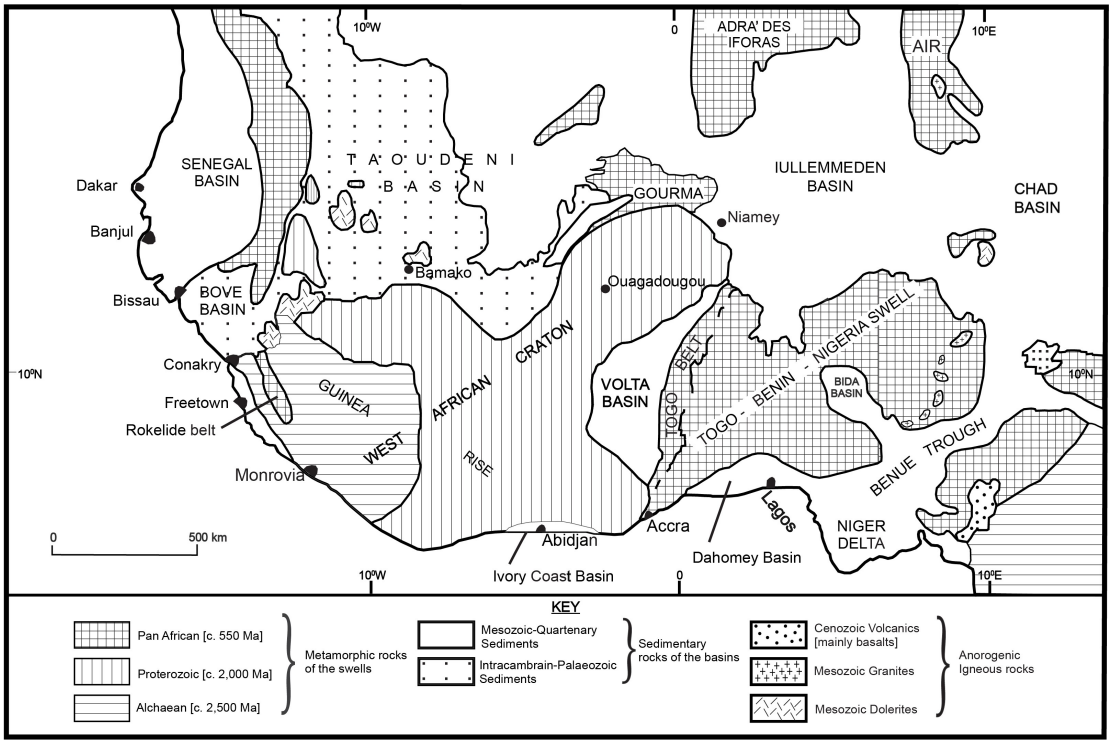

Figure 2.1: Generalised geological map of Nigeria within the framework of the Geology of West Africa (Adapted from Wright, 1985).

2.1.1 The Migmatite-Gneiss Complex

This is the most widespread of the units in the Nigerian basement. The migmatite- gneiss complexes comprised of an heterogeneous assemblage of rocks which include migmatites, ortho-gneisses, para-gneisses, as well as metamorphosed basic and ultrabasic rocks. The mineralogy of these rock units have been reworked by geological processes which are associated with the Pan-African which led to the recrystallisation of a large percentage of the constituent minerals by partial melting. Age of the migmatite gneiss complex ranges from Pan-African to Eburnean with the rocks displaying metamorphic assemblage which ranges from medium to upper amphibolite facies.

This unit makes up a large area of the Nigerian basement (Rahaman and Ocan, 1978) and they record three major geological events (Rahaman and Lancelot, 1984);

i. the earliest, at 2,500 Ma, which involved crust forming processes and crustal growth by sedimentation and orogeny;
ii. this was followed by the Eburnean, 2,000 ± 200 Ma, marked by the Ibadan type granite gneisses
iii. Pan-African event of 900 to 450 which led to structural overprinting of the older rocks and resetting of geochronological clocks in the older basement rocks and also giving rise to granite gneisses, migmatites and other similar lithological units.

2.1.2 The Schist Belt (Metasedimentary and Metavolcanic Rocks)

The Schist Belts comprises of low grade, metasedimentary rocks which are more prominent in the western side of Nigeria (figure 2.2 - 2.3). These N–S trending rocks are as wide as 300km and they have been infolded into the migmatite gneiss rocks complex. Lithologically, the schist belt of Nigeria contains different lithologies which vary from fine to coarse grained clastics, phyllites, pelitic schists, carbonate rocks, banded iron formation and metavolcanics rocks of mafic composition (amphibolite).

Different workers over the years have suggested different origins for the schists belts of Nigeria. Rahaman (1976) and Grant (1978) suggested several depositional basins were involved in the evolution while Oyawoye (1972) and McCurry (1976) suggested they are relicts of a single supracrustal cover. Furthermore, Olade and Elueze (1979) also considered the schist belts to be fault-controlled rift-like structures

while Grant (1978), Holt (1982) and Turner (1983) suggested different ages for the sediments based lithological on structural information while Ajibade et al., (1979) proposed that the schist belt contains series of rocks which have similar deformation history.

Detailed absolute age determination of the schist belts of Nigeria has remained indefinite though the relative ages of the intrusive older granites cross-cuts the schistose rocks and provided a lower age limit of 750 Ma. Rb/Sr dating also provided an age of 1,040 ± 25 Ma as obtained by Ogezi, (1977) and this was accepted as metamorphic age for the Maru Belt phyllites. Finally, the metasedimentary rocks are considered Upper Proterozoic in age.

The schist belts have been mapped and studied over the decades in detail in the following localities: Maru, Anka, Zuru, Kazaure, Kusheriki, Zungeru, Kushaka, Iseyin Oyan, Iwo, and Ilesha where they are known to be generally associated with gold mineralisation.

2.1.3 The Older Granites (Pan African Granitoids)

Falconer, (1911) introduced the term "Older Granite" as a means of distinguishing between the deep-seated granites which are commonly concordant or semi discordant with the Basement Complex and the tin bearing Mesozoic younger granites of North Central Nigeria which occurs as highly discordant granites. It is believed that they are 450-750Ma in age and comprises of believed are pre tectonic, syn-tectonic and post tectonic rocks which cross-cut the older lithologies.

They are representative of a varied and extensive magmatic cycle which is associated with the Pan-African orogeny with varying composition such as tonalities, granodiorites, diorites, syenites and true granites. Rahaman, (1981) noted that they are high level intrusions with anatexis playing an integral role in their evolution. Generally, they generally lack any form of associated mineralisation which might be due to the role thermal effects may have played in remobilisation of mineralizing fluids (Obaje, 2009).

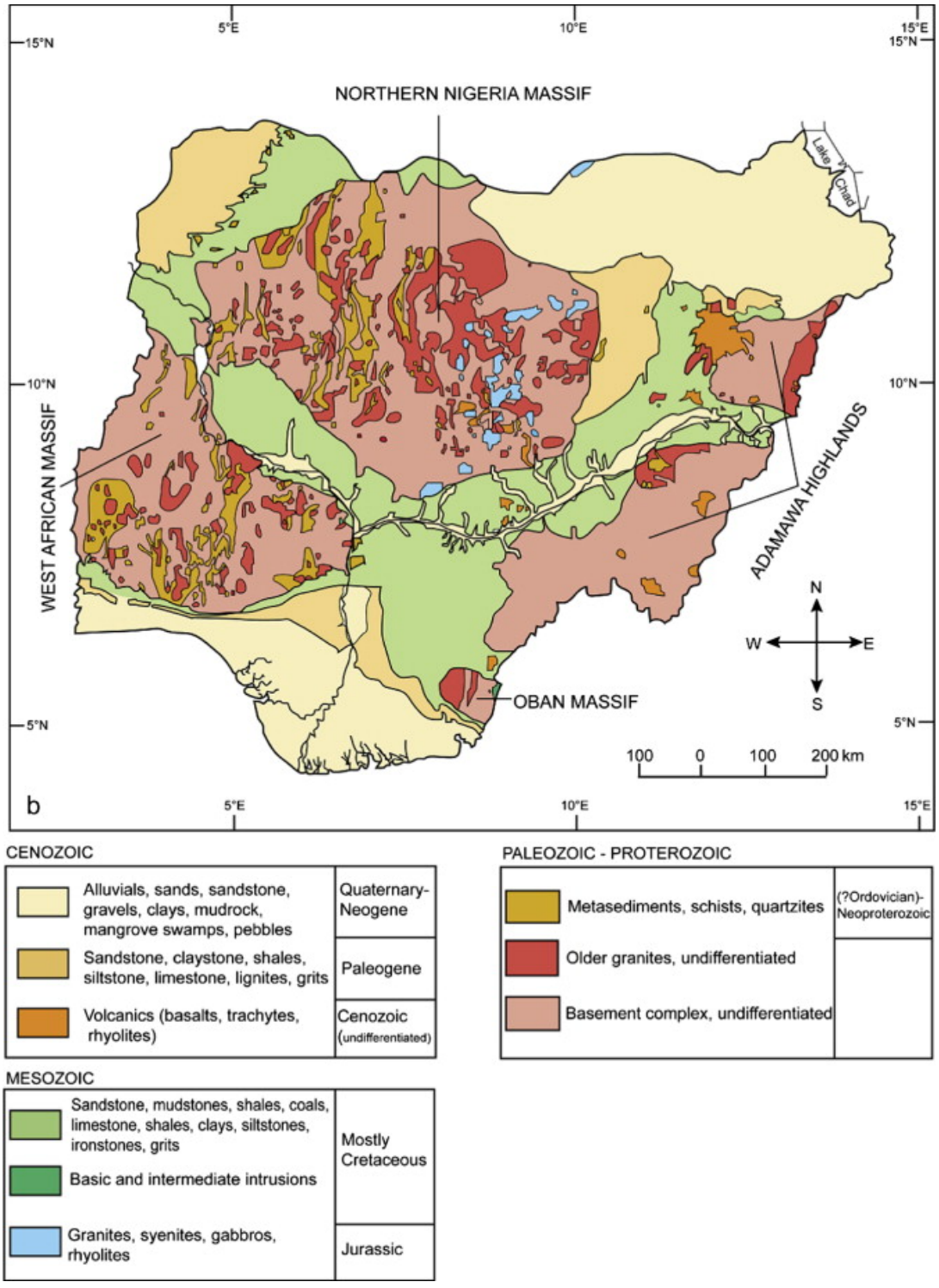

Figure 2.2: Geological Map of Nigeria (NGSA, 2004).

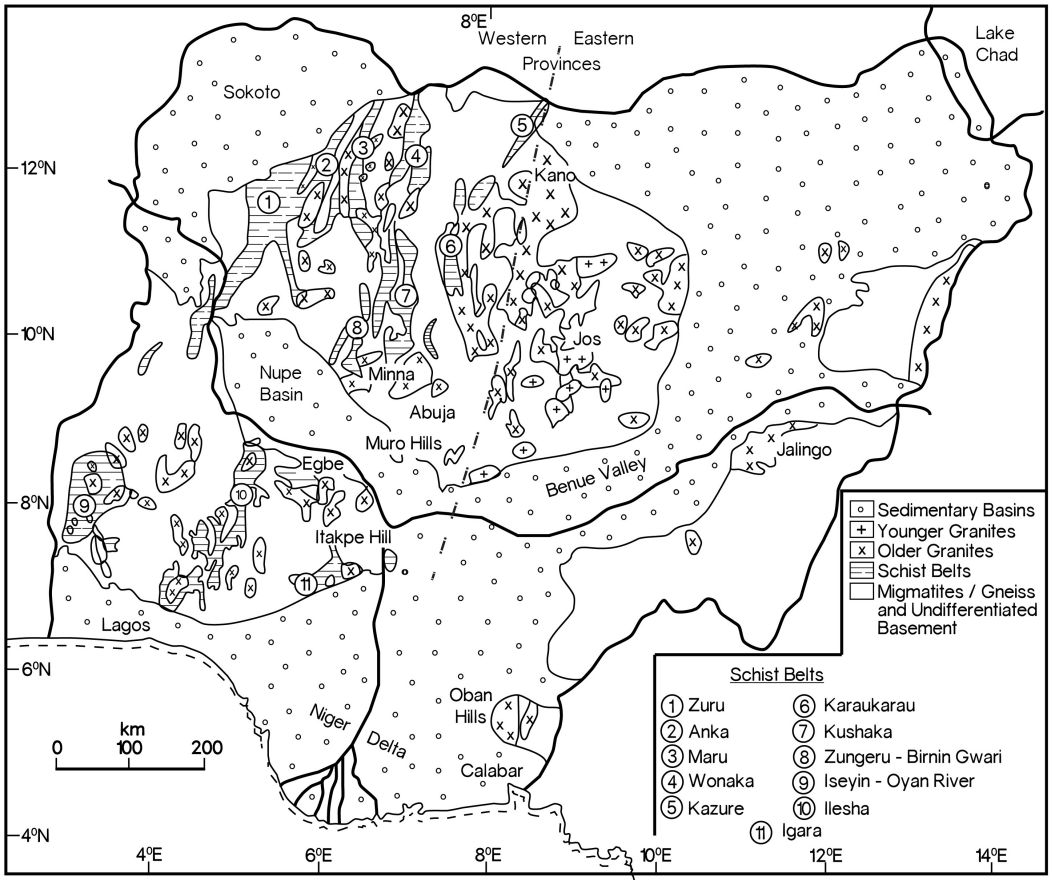

Figure 2.3: Geological map of Nigeria showing the Schist belt (After Woakes et al., 1987).

The older granites also encompass various petrologicaly important groups which were formed at the same time (Dada, 2006); they occur within the basement complex as the most visible product of the Pan-African orogeny with different levels of addition of materials which may be as high as 70% in some places (Rahaman, 1988). Within the schist belts, various types of granitoids such as biotite granites, charnokites, anorthoites and serpentinites outcrop.

Rahaman, (1988) on the basis of texture, emplacement period and mineralogical variations discarded the earlier classification of members of the Older Granites suite. In its place, based on textural characteristics, he proposed six members of the Older Granite suite as follows:

1. Migmatitic granite;
2. Granite gneiss;
3. Early pegmatites and fine-grained granite;
4. Homogeneous to coarse porphyritic granite;
5. Slightly deformed pegmatite aplites and vein quarz; and
6. Undeformed pegmatites, two-mica granites and vein quartz.

The older granites occur majorly as intrusives associated with the schist belt; and the migmatite gneiss complex rocks. They outcrop at Akwanga, Bauchi, Abuja, Ado-Ekiti, Zaria and Obudu areas.

2.1.4 Undeformed Acid and Basic Dykes

These are late to post-tectonic rocks which are of Pan African rocks age and cross-cut the Migmatite-Gneiss Complex rocks, the Schistose rocks and the Older Granites. They occur as two groups of intrusive rocks which are:

a. Felsic dykes associated with granitoids of Pan African age on the terrain such as the tourmaline, muscovite and beryl bearing pegmatites, microgranites, aplites and syenite dykes (Dada, 2006),

b. Basic dykes such as dolerites as well as the less common felsite, basaltic and lamprophyric dykes which are regarded as the youngest units in the Nigerian basement.

Geochronological studies have revealed ages of 535-580Ma from Rb-Sr isotopic studies on whole rocks for the felsic dykes (Matheis and Caen-Vachette, 1983; Dada, 2006); an age of 500Ma has been suggested for the basic dykes (Grant, 1970).

2.2 Review of related previous works

All over the world, pegmatites have received tremendous attention, which is mostly due to the gemstones, industrial minerals and rare-earth elements they host which play significant roles in technological and economic advancement. However, most of the studies carried out have been focused towards the rare metal and rare earth economic mineralisation potential of pegmatites, with less research on delineating pegmatite genesis using fluid inclusion approach.

Globally, authors who used results from the analyses of mineral extracts to investigate pegmatites. Jiang, (1998) similarly carried out radiogenic isotope studies of tourmaline and opined that stable and radiogenic isotopic studies of tourmaline is a powerful tools for tracing the origin of hydrothermal fluids and for determination of the period of tourmalinisation and associated other hydrothermal alteration, mineralisation or metamorphism.

Quemeneur and Lagache, (1999), did a comparative study of two pegmatite fields in Brazil using results data from the chemical analyses of micas and feldspars. Results indicated that crystallisation mode of the pegmatite fields occurred in a homogenous melt. Scares et al., (2000) studied and tourmaline from pegmatite of Brazil using electron microprobe and Inductively Coupled Plasma Atomic Emission Spectroscopy (ICP-AES) analytical methods and concluded that there are indicative of crystal fractionation as the main magmatic differentiation process for the formation of these pegmatites.

Beurlen et al., (2008) using petrography, scanning electron microscopy-energy dispersive x-ray spectroscopy and U-Pb dating reported that the mineralised pegmatites of the BPP region could have been sourced from associated pegmatitic granite.

Raslan and Ali, (2011) opined that the main mineralizing event in the rare metal pegmatite of Egypt was magmatic with later hydrothermal alteration coupled with local remobilisation of high-field-strength elements. This inference was drawn from the data obtained from heavy mineral analysis, field emission scanning, and X-ray micro analyses of the whole rock pegmatite.

Fredriksson, (2017) studied the rare-element pegmatite bodies of Altim and Tamanduá; in North-eastern Brazil. The two pegmatite bodies were found to have clearly different elemental compositions with high Zn concentration observed in the Altim pegmatite which clearly denotes the two pegmatites as two different formations.

Fluid inclusion study revealed the two pegmatites have different fluid characteristics with low–moderate salinity aqueous-carbonic fluid inclusion in the Tamanduá and moderate–high salinities in the Altim pegmatite. Laser ablation on fluid inclusions revealed Nb and Ta concentrations of 0.1 – 3.2 ppm.

Swanson and Veal, (2010) studied the pegmatites of Spruce Pine District, USA to delineate the mineralogy and petrogenesis. They reported that pegmatites are associated with granodiorites they have similar mineralogy to the granodiorite. The pegmatites varied from zoned to unzoned pegmatite and that the pegmatites crystalized at 20-30km based on feldspar thermobarometry and experimental petrology.

Beurlen et al., (2014) studied the petrogenesis and mineralisation style in the Borborema Pegmatite Province, Brazil. They reported liquidos temperature of 580°C and solidus temperature of 400°C with pressure of 3.8kbar as crystallisation conditions. They surmised that the pegmatite crystallised from a peraluminous melt which was saturated in an aqueous-carbonic fluid of low to medium salinity, peralkaline flux enriched fluid fraction. Based on mineral chemistry studies, the pegmatites are classified as complex-spodumene of lepidolite subtype pegmatite.

Ollila, (1987) also studied the pegmatites of Damaran Orogeny in Namibia. He reported that with respect to Nb, Li, Ta, Be and Sn; the pegmatites are mineralized. Fluid inclusion results from the study revealed that fluid pressure at crystallisation did not exceed 2kb. He surmised that pegmatites crystallised from residual fraction of volatile rich granitic melts during the waning stages of the orogeny.

Deveau et al., (2015) conducted a study on the genesis of LCT pegmatites of French Massif Central using Li isotopes in the mica extracts. They reported $^{\delta}7$Li values, of -3.6 to +3.4‰ with Li concentration increasing with increasing degree of magmatic evolution of the pegmatite, hence they surmised that partial melting of rare element bearing protoliths is responsible for the isotopic fractionation rather than fractionation crystallisation.

Vapnik and Moroz, (2000) studied the fluid characteristics of inclusions in emerald from Jos, North Central Nigeria using microthermometry and Raman Spectrometry. They reported the occurrence of primary and pseudosecondary inclusions of two types, an highly saline type I inclusion with up to 45% NaCl wt% eq. which contained a low density volatile phase as well as daughter minerals and type II

inclusions which are volatile free and occur with water bearing CO_2 inclusions. They concluded that emerald mineralisation occurred at 400-450°C and 0.2-0.3kbar.

Levasseur, (1997) in his fluid inclusion study of the rare element pegmatite south platte district, Colorado reported concentric zoning with fluorite, Y, Nb and REE enrichment in the pegmatites relative to the associated granite. He reported the presence of four different fluid types in the pegmatites; three sets of aqueous inclusions with salinity of 0-12, 18-24 and 26-30 wt.% eq. and also, a low salinity, CO_2 bearing fluid. He concluded that low salinity fluids were responsible for rare element mineralisation at temperatures of 349-500C, while the other fluid types postdate the mineralisation.

Furthermore, Gagnon *et al*., (2004) also carried out a study to delineate the origin of hydrothermal fluids in the same NYF pegmatite studied by Levasseur, (1997) with microthermometry and laser ablation ICP-MS. They also reported the presence of four different fluid types in the pegmatites and homogenisation temperatures of 93-149°C. Though the properties of these inclusions could not be detected by microthermometry, LA-ICPMS however revealed detectable differenced in Ca concentration in some inclusions while the lower salinity inclusions are characterized by a Na + K+ Sr + Ba solution.

Esmail and Moharem, (2009) carried out a study of fluid characteristics of radioactive mineralized pegmatites in Egypt using microthermometry on pegmatitic quartz and fluorite. They reported that at least two stages of late magmatic hydrothermal alteration was involved; the first stage involved high temperature, low saline fluids while the second stage involved low temperature, highly saline fluids. They surmised that fluid mixing lead to a pH change which remobilised the metals and lead to precipitation of REEs and radioactive minerals.

Whitworth and Rankin, (1989) studied the spodumene bearing pegmatites of southeast Ireland with the aim of evaluating the evolution of the pegmatites from inclusions trapped in quartz. Petrography and microthermometry revealed two different fluid types. Type I inclusions with low to moderate salinities which homogenized at 400°C and type II inclusions which were more saline and homogenized at temperatures below 250°C. Based on pressure temperature modelling, they concluded that type I fluids are associated with magmatic/hydrothermal fluids from the associated granite.

Ackerman et al., (2007) also carried out a thermobarometric and fluid evaluation of pegmatites from the Bohemian Massif, Czech Republic using fluid inclusions on quartz, fluorite, titanite and apatite. Two fluid types were identified; an early aqueous-carbonic fluid and a late aqueous fluid; the barren pegmatites are associated withH_2O-CO_2 low salinity fluids of 2-6 wt % eq while fluids associated with Li mineralized pegmatites are more saline and contain H_2O–CO_2/N_2–H_3BO_3–NaCl. They reported P-T conditions of 600-640 °C and 420-580Mpa for barren pegmatites and 500-570 C and 310-430MPa for Li mineralized pegmatite.

Zarasvandi et al., (2014) also carried out a fluid investigation of the Farsesh barite deposit, Iran using microthermometry. They identified two types of primary/pseudo-primary inclusions with low salinity values of 4.2-20 eq wt% NaCl which homogenized into the liquid phase at low homogenisation temperature of 125-200°C and they concluded that the barite deposited precipitated from hydrothermal basinal fluids of low to medium salinity.

Shafaroudi and Karimpour, (2015) examined the evolution of the Sechangi lead-zinc deposit of Eastern Iran using mineralogical, fluid and sulfur isotopic characteristics. Microthermometry results revealed homogenisation temperatures of 151-352°C with salinity of 0.2-16.5 wt. %NaCl eq. They surmised that ore forming fluids are low-medium temperature and low-medium salinity with fluid mixing playing an important role in mineralisation.

Sasmaz and Yavuz, (2007) also carried out a study to investigate the genesis and physiochemical conditions of fluorite mineralisation in syenites of Yildizeli-Sivas, Turkey using geochemical method and microthermometry. They reported that fluorites in the study area have characteristics which are typical of primary crystallisation and remobilization based on REE geochemistry and they were formed from fluids at temperatures of 161-243°C.

Oyebamiji, (2013) studied the compositional characteristics of pegmatite bodies in Oro, southwestern Nigeria with a view to elucidating the rare metal mineralisation characteristics. He surmised that the pegmatites in the areas are mineralized.

Taylor and Friedrichsen, (1983) studied the stable isotopic characteristics of the Landsverk pegmatite, Norway. They reported light ^{18}O values which are characteristic

of meteoric-hydrothermally altered rocks and δD values in one fluid inclusion which supports evidence of the presence meteoric water in the area.

Garba and Akande, (1992) studied the origin and significance of the carbonic inclusion associated with gold mineralisation in Bin Yauri, northwestern Nigeria. They reported that fluid immiscibility of low salinity CO_2 rich hydrothermal fluids lead to selective entrapment and loss of H_2O phase during gold mineralisation which lead to increased oxidation effects. The fluids are believed to have originated from dewatering of subducted metasedimentary rocks along the Anka fault system.

Sirbescu and Nabalek, (2003) examined the petrogenesis of the Tin Mountain pegmatite in South Dakota, USA. They reported the presence of Dawsonite in primary inclusions within pegmatitic quartz and this confirmed using SEM-EDS and Raman spectroscopy. They explained that the presence of the mineral is evidence of carbonate ions in pegmatite evolution and carbonates, as well borate minerals play important roles in pegmatite formation.

Arribas *et al.,* (1995) studied the gold alunite deposits of Spain using a combined approach of geology, geochronology, fluid and isotopic characteristics. Based on results from fluid and isotopic studies, an hydrothermal system characterized by an early acidic wall rock alteration and late gold mineralisation was inferred. They also reported that the presence of a significant magmatic fluid and salinity values in inclusions which are higher than 40% wt. eq. NaCl.

Akcay *et al.,* (1995) in their study of the fluid characteristics and chemistry of tourmalines from the Sb-Hg+ W deposit of Niode massif, Turkey reported that tourmalinasation is a common feature of associated granitic rocks. Fluid characterization of the tourmaline revealed salinity measurements of 5.5-10.5 wt. % eq. NaCl which may be indicative of a magmatic origin for the tourmaline.

CHAPTER THREE

METHODOLOGY

3.1 Field methods, mapping and sampling

The study involved systematic geological mapping of selected areas within the Ibadan-Oshogbo and Oke-Ogun pegmatite field to delineate the geology and obtain representative samples of pegmatites. Geological mapping involved observation of the pegmatites and the associated lithologies as well as basic pegmatite mineralogy.

3.2 Sample preparation

From the systematic mapping exercise, 58 samples of pegmatites were collected; samples with very low degree of alteration were selected for thin section and geochemical analysis. Thin sections were prepared at the Department of Geology, University of Ibadan while doubly polished wafer were prepared at Wagner Petrographic, Utah, United States of America.

3.3: Geochemical analysis

Pegmatite samples from five areas (Komu Olode gbayo Idiyan and Owode) in the Oke-Ogun and Ibadan-Oshogbo pegmatite fields were collected. Unaltered samples of pegmatites were selected and 48 samples comprising of 16 whole rock samples, 11 feldspars extracts, 13 muscovite extracts and 8 biotite extracts were pulverised at the petrological laboratory of the Department of Geology, University of Ibadan and thereafter analysed at Activation Laboratories, Ontario, Canada for major, trace and rare-earth elemental concentrations using Inductively Coupled Plasma Optical Emission Spectrometry (ICP-OES) and Inductively Coupled Plasma Mass Spectrometry (ICP-MS) techniques.

3.4: Fluid inclusion study

3.4.1: Sample preparation and instrumentation

The doubly polished wafers were studied at the Geofluids Research Laboratory (figure 3.1); National University of Ireland, Galway to develop a fluid inclusion paragenetic classification using transmitted light microscopy with a Nikon Eclipse E200 polarising microscope. Microthermometric analyses were carried out using a Linkam THMGS 600 heating-freezing stage, mounted on an Olympus transmitted plane polarised light microscope (figure 3.2 - 3.3) equipped with a long working distance objective lenses with up to 100x magnification.

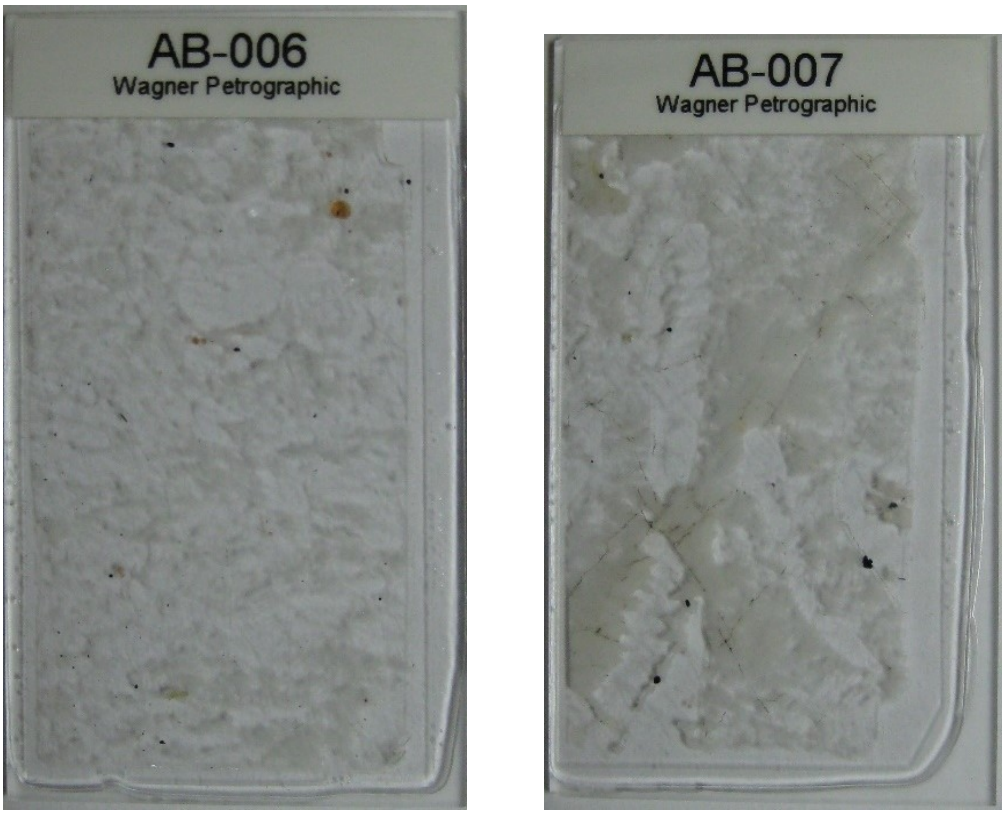

Figure 3.1: Pictures of the doubly polished wafers of pegmatite samples

Figure 3.2: Transmitted Plane Polarised Light Microscope fitted with an incident UV light attachment used for microthermometric analysis of fluid inclusions at Geofluids Research Laboratory, National University of Ireland, Galway

Figure 3.3: Transmitted Plane Polarised Light Microscope fitted with a stage mounted Linkam heating and cooling stage used for microthermometric analysis of fluid inclusions at Geofluids Research Laboratory, National University of Ireland, Galway

3.4.2: Fluid inclusion petrography and microthermometry

Fluid inclusion petrography involves the determination of the types and generation of fluid inclusion in the doubly polished wafers as well as their properties. Microthermometry is a non-destructive fluid inclusion study analytical method. It is the most common method and it is used in the determination of physical and compositional properties of the inclusions. It involves cooling and heating of the inclusions in other to determine fluid composition, salinity and density through the observation of subtle phase changes. Inclusions were subjected to cooling up to -100°C and phase changes were measured during progressive heating. After all low temperature measurements were obtained, heating was carried out up to temperatures of 450°C to determine the homogenisation temperature. Measurements obtained during microthermometry for the study are the temperature of last melting (TLM) and the temperature of homogenisation (Th).

3.4.3 Fluid Inclusion Microthermometry

Aqueous fluid inclusions were subjected to cooling/freezing and heating to observe and record the temperature at which phase changes occur. Temperature of first ice melting (TFM) and temperature of last ice melting (TLM) were recorded by cooling the inclusions to temperatures in excess of -110°C and the heating..

- The TFM is equivalent to the eutectic melting point of an aqueous saline solution. TFM values below -20.8ºC are indicative of other salt components in the solution (e.g. Ca or Mg).
- TLM values are used to estimate the salinity of the fluid. The TLM values are indicative of the type of salts available in the aqueous solution and TLM is reported as equivalent weight % of NaCl.

Subsequent heating of the two-phase (liquid + vapour) aqueous fluid inclusion, allows for measurement of the temperature of homogenisation (T_H). This is the temperature at which liquid and vapour phases homogenise to the single phase and yields a minimum fluid trapping temperature for an aqueous fluid inclusion. Isochores were thereafter constructed using the program FLUIDS of Bakker, (2003).

Two samples were collected from the same pegmatite (i.e. two samples from each of five pegmatites), therefore the microthermometric data is presented as a series of paired samples to reflect this. T_H and salinity data for each sample pair is presented

as frequency distribution histogram (frequency versus T_H) and bivariate plots (T_H versus salinity).

The microthermometric data includes temperature of last ice melting (T_{LM}), temperature of total homogenisation (T_H) and salinity (equivalent weight % NaCl).

CHAPTER FOUR
RESULTS AND DISCUSSION

RESULTS

4.1 Geological setting of the study areas

Pegmatite samples from different areas were used for the study. The geological settings of the areas are described below:

4.1.1: Geology of Olode-Falansa-Coco area

The geology of the study area comprises the geology of Ibadan, Oke-Ogun and Ibarapa zones. The geology of Olode-Falansa area comprises of rock types; granite gneiss, sillimanite quartzite, medium grained granite and pegmatite. The granite gneiss was observed to occupy the eastern half of the area. Granite gneiss in the Olode area are characterised by alternating bands of felsic and mafic minerals, they are medium to coarse grained and are closely associated with pegmatites in the area (figure 4.1-4.3).

N-S trending sillimanite quartzites also outcrop in the area with gradational contact with the granite gneisses and granites. The granites in the Olode area are low lying in some areas and are massive outcrops in other areas, they are medium grained.

In the Olode area, pegmatites occur as NE-SW trending outcrops of various shapes, sizes and length. They are composed of quartz, plagioclase, orthoclase and muscovites, while tourmaline, beryl, garnets are associated accessory minerals (figure 4.4- 4.6).

Figure 4.1: Field picture showing pegmatite in Olode area

Figure 4.2: Field picture showing granite in Olode area

Figure 4.3: Field picture showing pegmatite in Olode area

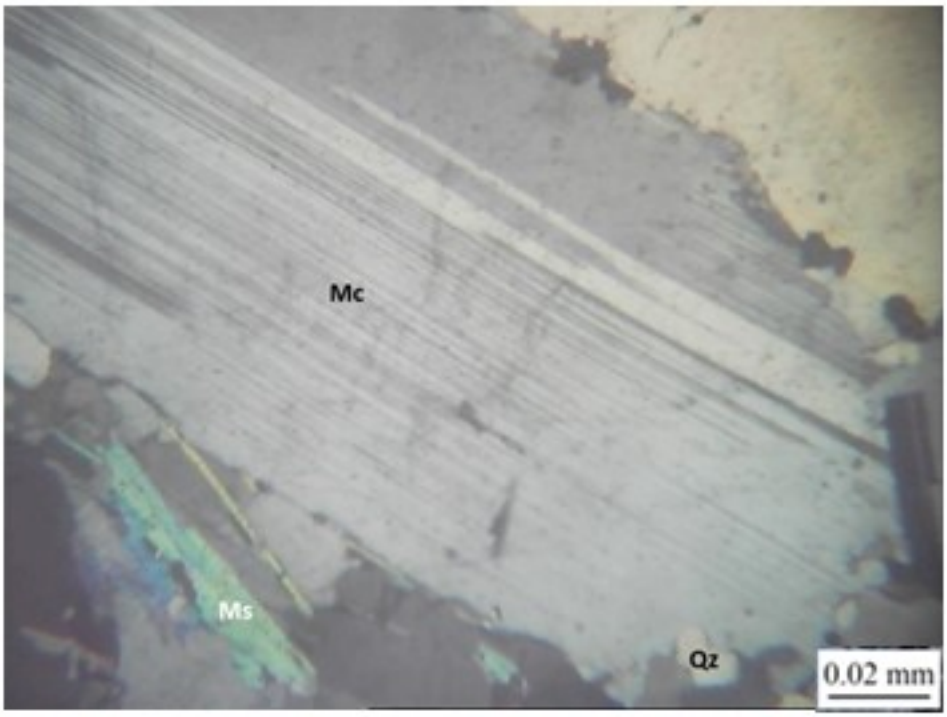

Figure 4.4: Photomicrograph of section of pegmatite from Falansa in transmitted light showing presence of Microcline (Mc) in abundance and Muscovite (Ms).

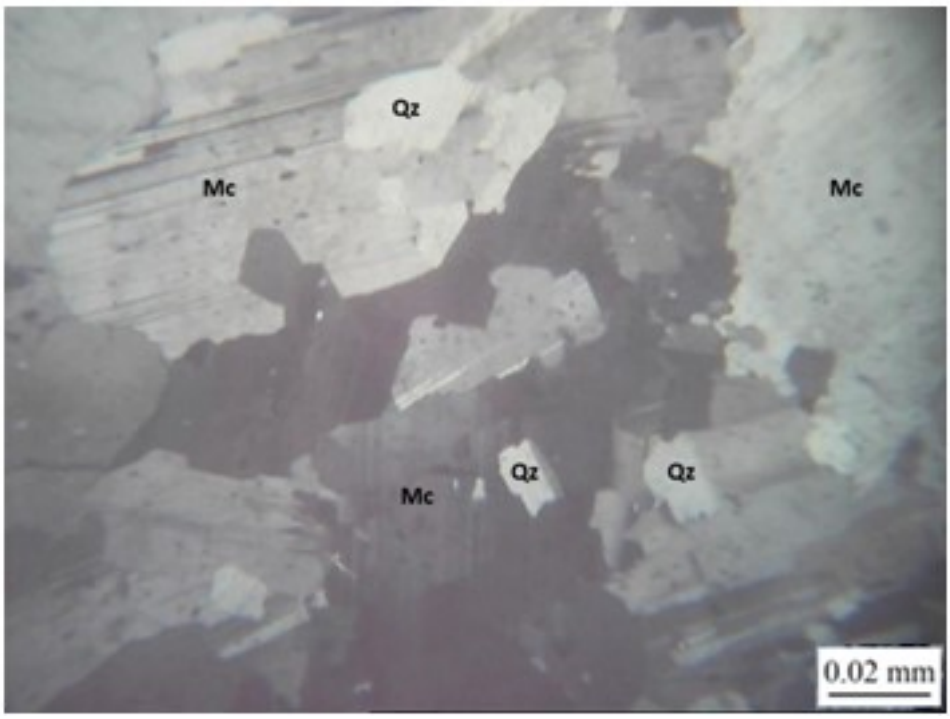

Figure 4.5: Photomicrograph section of pegmatite from Falansa in transmitted light showing presence of Microcline (Mc) and Quartz (Qz).

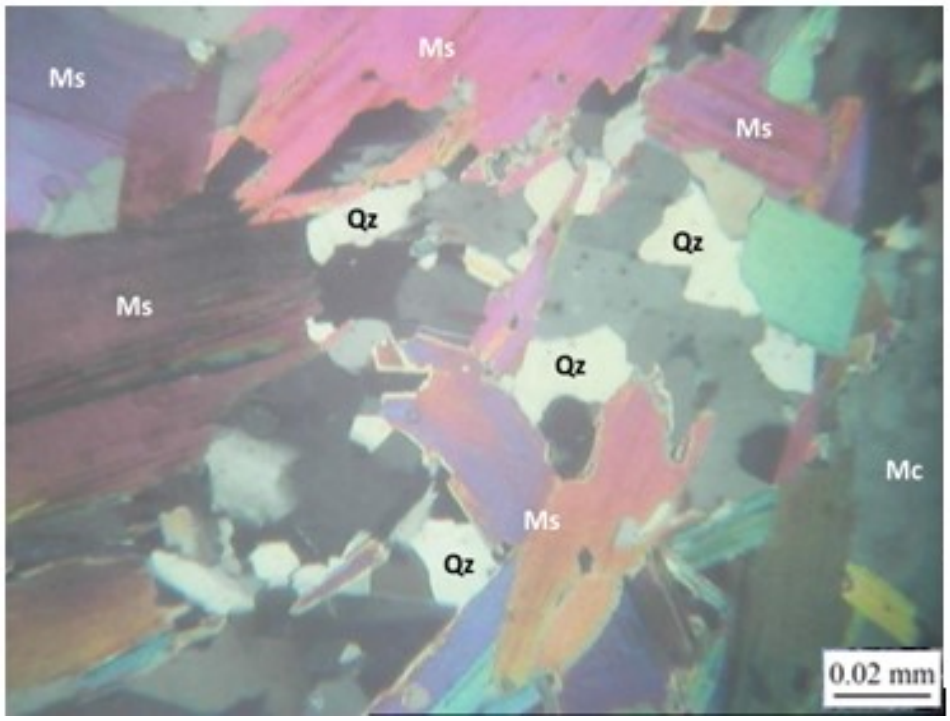

Figure 4.6: Photomicrograph of a section of pegmatite from Coco in transmitted light showing presence of Microcline (Mc), Muscovite (Ms) in abundance and Quartz (Qz).

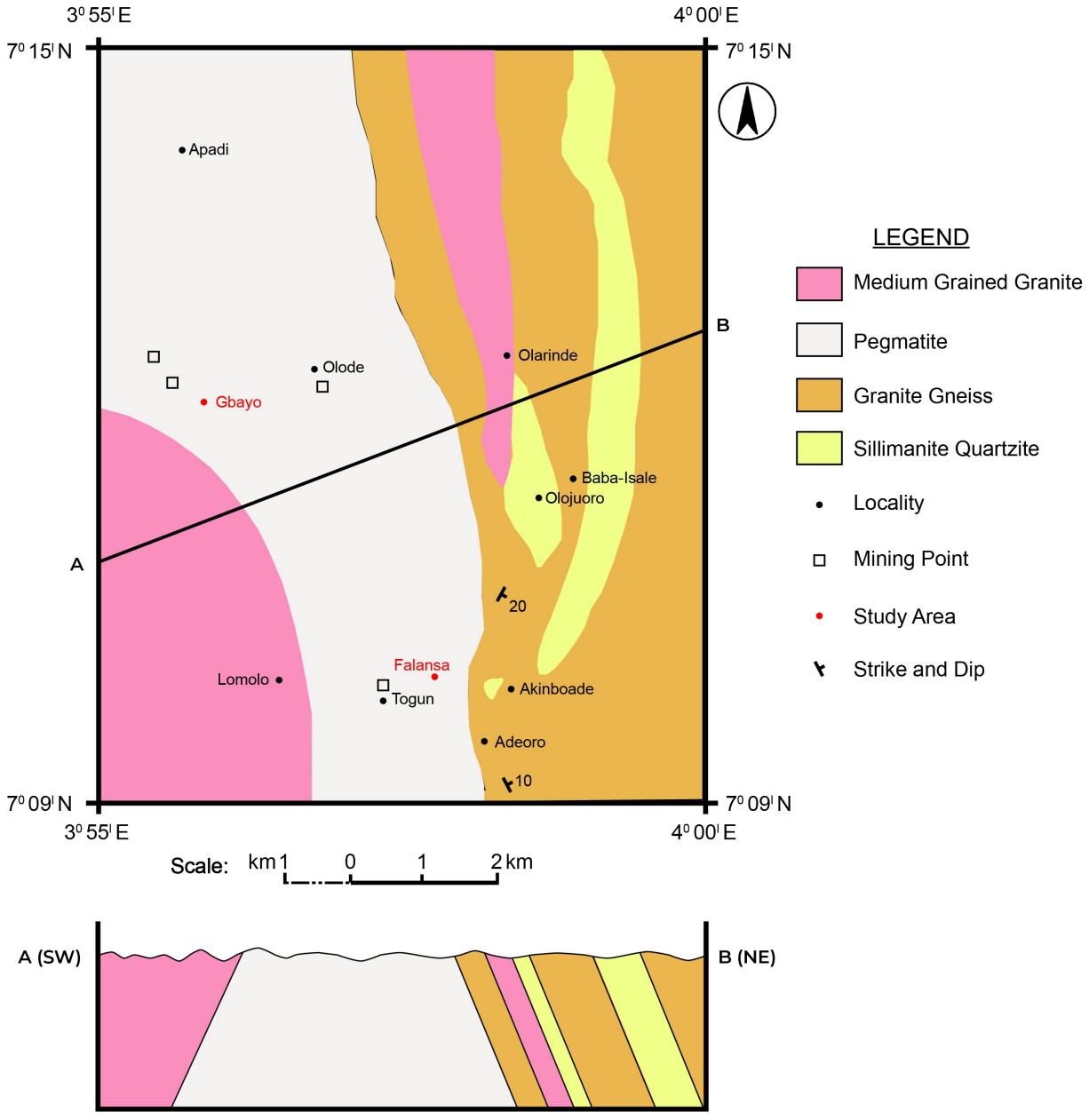

Figure 4.7: Geological map of Olode-Coco-Falansa area

4.1.2: Geology of Komu-Igbojaye-Godondoya area:

The komu area is underlain by granite gneiss, amphibolite, mica schist and pegmatite with quartz veins associated with the larger rock bodies (figure 4.8- 4.14).

Granite Gneiss

Granite gneisses are the predominant rock type in the Komu area. Mineralogically, they contain biotite, quartz and ferromagnesian minerals with prominent mafic and felsic bands. The less prominent mafic bands are dominantly composed of biotite while the dominant felsic bands are composed mainly of feldspars. Petrographic studies revealed an assemblage of quartz, biotite, microcline and plagioclase. Petrographically, biotite was observed as elongated brown crystals and distinct cleavage; alkali feldspar shows low birefigerence with low relief while microcline shows crosshatching while quartz is subhedral, clear and elongate with no preferred orientation.

Amphibolites

Amphibolites occur and are widely distributed in the Komu area. They commonly occur as dark greenish lensoid bodies which are composed of amphiboles, plagioclase and minor quantities of quartz. Petrographic studies revealed the amphiboles are mainly hornblende.

Pegmatites

In the Komu area, pegmatites occur as intrusives in the gneisses and amphibolites. Pegmatites occur as coarse grained rocks composed of quartz, feldspars and tourmaline of varying length which intrude amphibolites and gneisses with a NNW-SSE trend and gradational contact obvious between pegmatites and host lithologies. As regards gemstone mineralisation, it was observed that large crystals of quartz, k-feldspar and micas occur closer to areas with gemstone mineralisation.

Petrographically, plagioclase, quartz, microcline, biotite, tourmaline and muscovite were observed. Quartz is characterised by low relief, and occurs as an interwoven intergrowth with feldspars which vary from plagioclase to microcline while perthite was observed in some sections (figure 4.15-4.17).

Figure 4.8: Field picture showing porphyritic granite in Komu area

Figure 4.9: Field picture showing pegmatite in Komu area

Figure 4.10: Field picture showing pegmatite in Komu area

Figure 4.11: Field picture showing pegmatite in Igbojaye area

Figure 4.12: Field picture showing pegmatite in Igbojaye area

Figure 4.13: Field picture showing pegmatite intruding metasedimentary rocks in Igbojaye area

Figure 4.14: Field picture showing pegmatite in Godondoya area

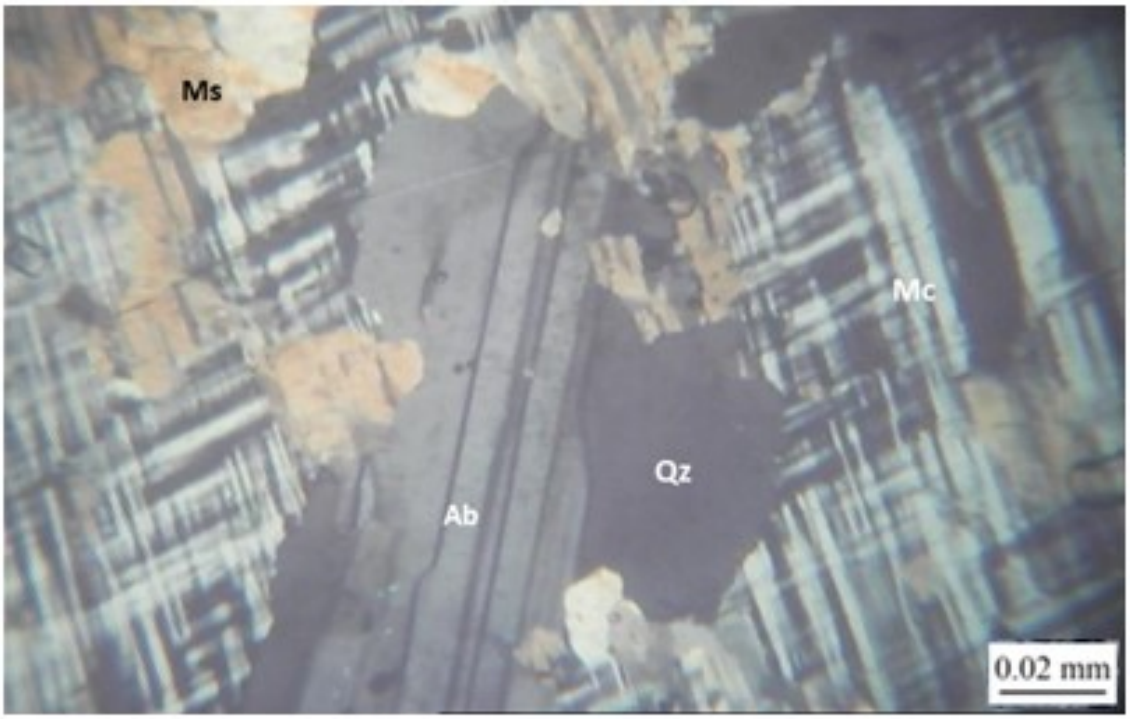

Figure 4.15: Photomicrograph of a section of pegmatite from Abuja Leather in transmitted light showing presence of Quartz (Qz), Muscovite (Ms) and Microcline (Mc).

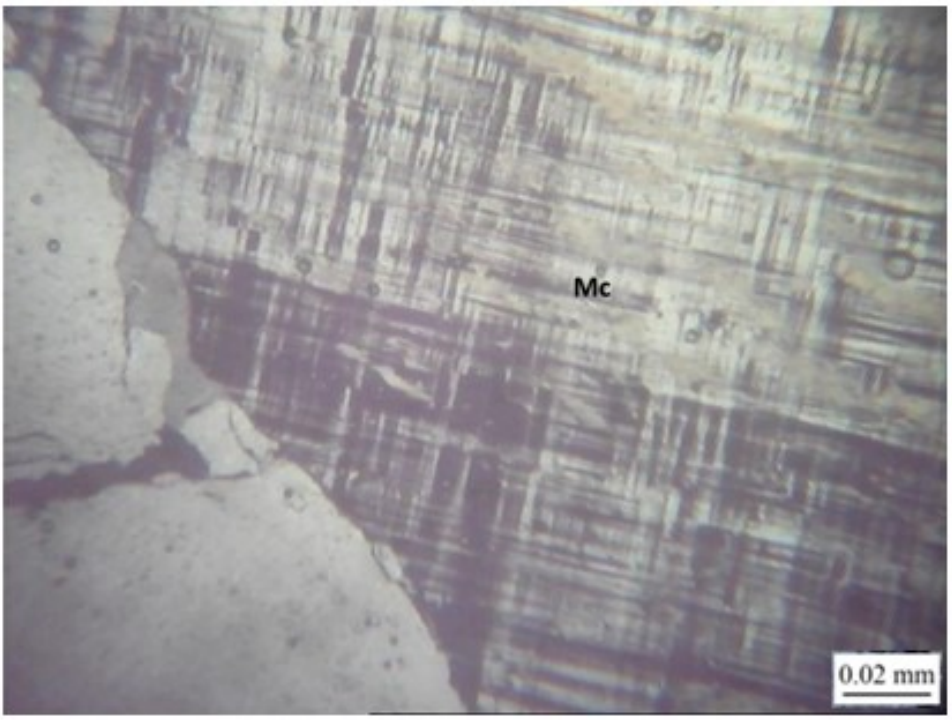

Figure 4.16: Photomicrograph of a section of pegmatite from Balogun Ojo in transmitted light showing abundance of Microcline (Mc).

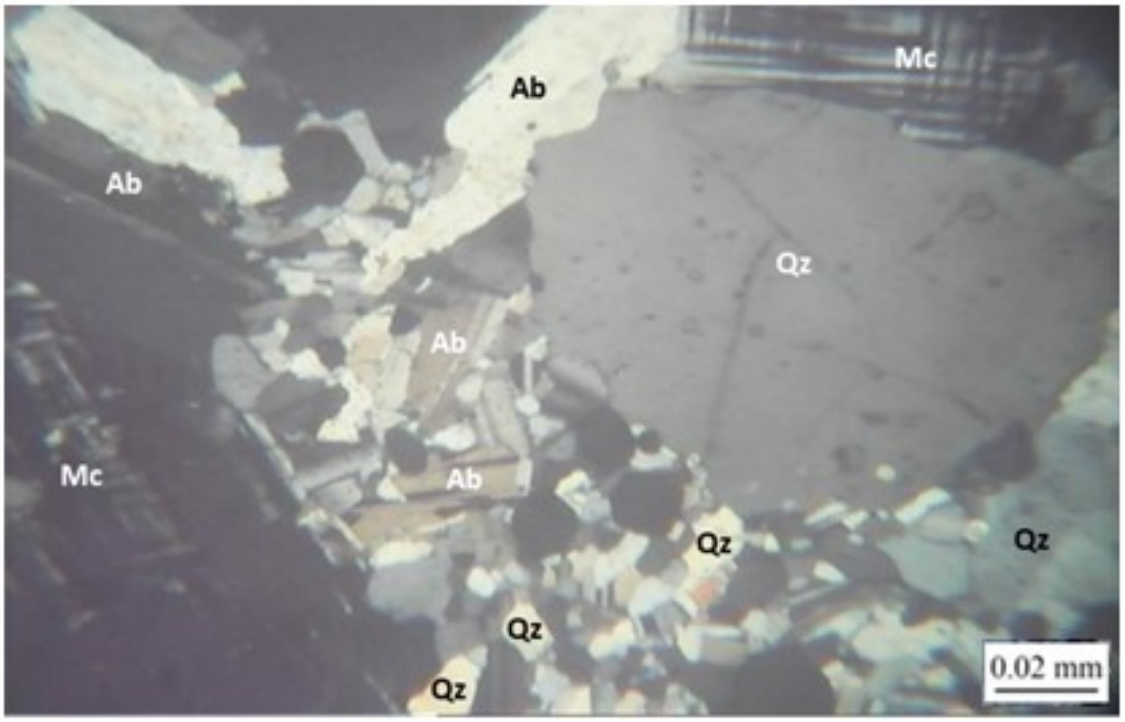

Figure 4.17: Photomicrograph of section of pegmatite from Doya in transmitted light showing presence of Microcline (Mc), Albite (Ab) and Quartz (Qz).

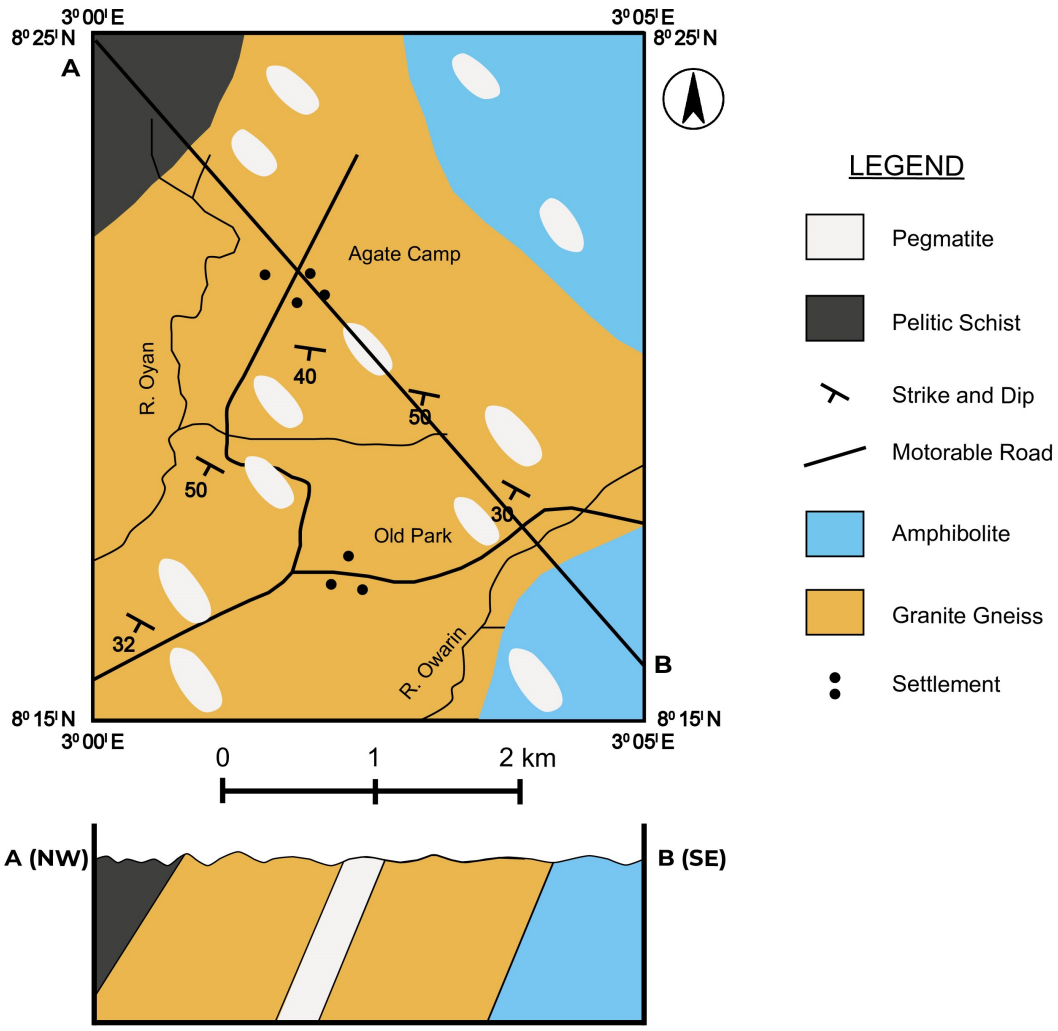

Figure: 4.18: Geological map of Komu area.

4.1.3: Geology of Idiyan area

The Idiyan area is dominated by mica schist, granite gneisses, and migmatites with NW-SE trending pegmatites intruding the quartz mica schists. Granite gneisses around the Idiyan area have a NNE-SSW trend, they are medium grained, grey, and slightly foliated; biotite, quartz and feldspars observed on hand specimen. Mica schist in the Idiyan area occurs as low lying disjointed, highly weathered outcrops with an N-S strike and they dip westernly (figure 4.19-4.22).

The migmatite gneiss is a mixture of different rock types which include granite gneiss intruded by quartz, pegmatitic and granitic intrusions of various sizes dimensions around Ominigbo and Abidioki. They are characterised by faults, folds and foliation with alternating dark and light layers (figure 4.21). Felsic material occurs as cross cutting veins of coarser granitic material and pegmatite. They are fine to medium grained and color is based on mineral assemblage with pitch and swell structures present in few areas.

In thin section, brown biotite crystals are present with muscovite, quartz and albite. No mymerkitic texture was observed but in some areas on the section, microcline encloses some quartz grains and all minerals display subhedral shape. It is composed of plagioclase, biotite, quartz, and microcline with hornblende occurring with other opaques as accessory minerals. Quartz is abundant and it occurs as subhedral crystals which are medium to fine grained. Alkaline feldspar is mostly microcline and shows typical cross hatch twinning.

The western flank of the study area is overlain by biotite granites which are mafic in color, with greater than 65% mafic minerals and low percentage of felsic minerals. Pegmatites are worked in this area for this feldspar content and gemstone prospects (figure 4.22). Petrographically, composed of quartz and orthoclase with subordinate mica; petrographic analysis revealed a preponderance of microcline (figure 4.23).

Geological maps of the study locations are shown in figures 4.7, 4.18 and 4.24.

Figure 4.19: Field photograph showing biotite granite around Idiyan area

Figure 4.20: Field photograph showing quartz vein in granite gneiss in the Idiyan area.

Figure 4.21: Field pictures showing folded alternating layers of felsic and mafic bands in migmatised gneiss in the Idiyan area

Figure 4.22: Field pictures showing pegmatite mining pit in the Idiyan area.

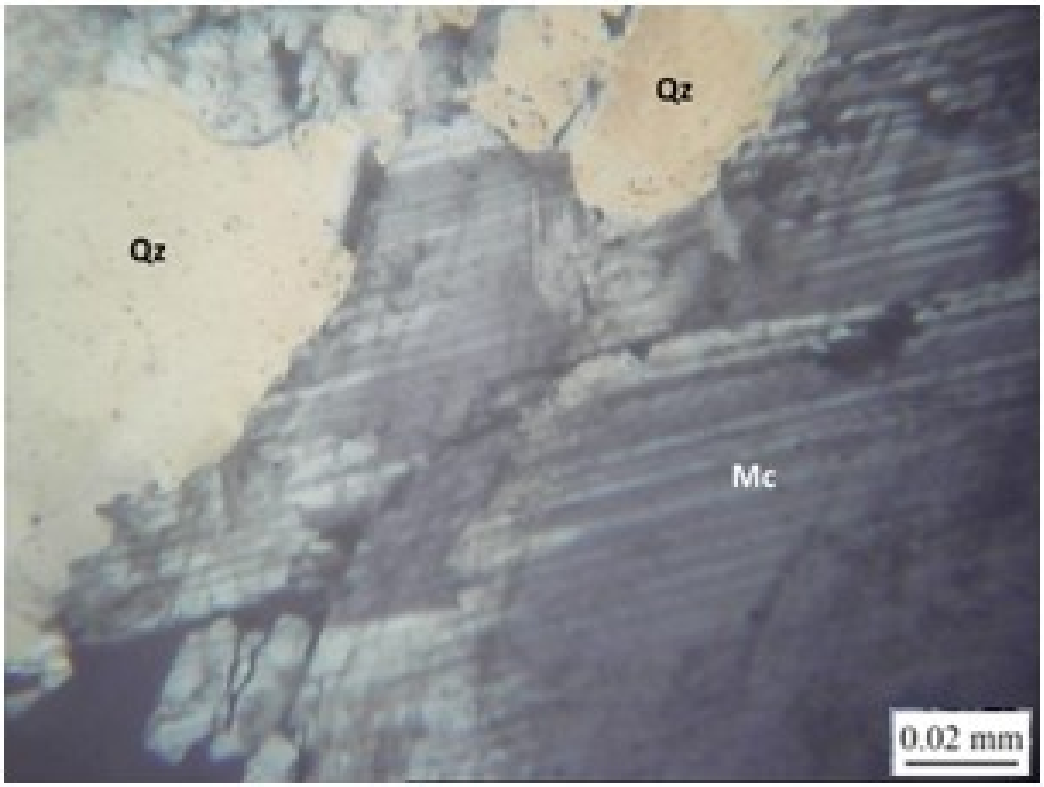

Figure 4.23: Photomicrograph of section of pegmatite from Idiyan in transmitted light showing presence of Microcline (Mc) in abundance and Quartz (Qz).

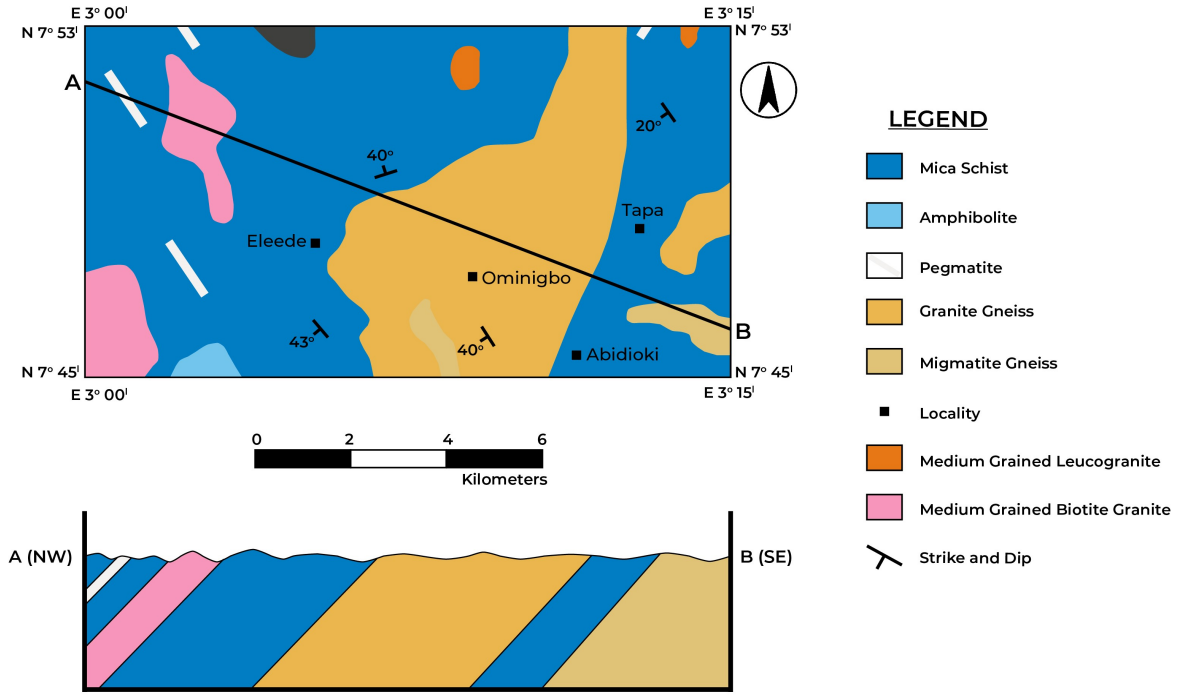

Figure 4.24: Geological map of Idiyan area

4.2: Geochemistry and fluid inclusion study of pegmatites

Major, trace and rare elemental concentration of whole rock pegmatites and extracts are presented in tables 4.1-4.15 while results of fluid inclusion analysis is presented in tables 4.17- 4.30.

4.2.1: Geochemistry of pegmatite

4.2.1.1: Major elemental concentration

Whole rock pegmatite and feldspar extracts

Geochemical analytical results (table 4.1- 4.3; tables 4.4 -4.15)**,** revealed pegmatites in the locations have SiO_2 ranging from 47.76% to 82.17%. Samples from Omo-Oba had the lowest SiO_2 concentration while pegmatites from Idiyan had the highest SiO_2 concentration. TiO_2 ranges from 0.01 to 0.34%, samples from Owode had the lowest TiO_2 concentration while pegmatites from Idiyan had the highest TiO_2 concentration; Al_2O_3 ranges from 9.84% to 18.92% with samples from Idiyan having the lowest Al_2O_3 concentration while pegmatites from Omo-Oba had the highest Al_2O_3 concentration. Fe_2O_3 ranges from 0.20% to 4.25% with samples from Falansa having the lowest Fe_2O_3 concentration while pegmatites from Omo-Oba had the highest Fe_2O_3 concentration.

For whole rock pegmatites, other oxides ranged: MnO (0.01% to 1.21%), MgO (0.02% to 1.21%), CaO (0.11% to 2.24%), Na_2O (0.09% to 10.16%), K_2O (0.08% to 11.36%) and P_2O_5 (0.01% to 0.23%). Highest concentrations of MnO, MgO, CaO, Na_2O, K_2O and P_2O_5 in whole rock pegmatites were observed at Doya, Omo-oba, Omo-oba, Balogun-Ojo and Owode respectively while lowest concentration of MnO, MgO, CaO, Na_2O, K_2O and P_2O_5 were observed at Falansa, Doya, Falansa, Omo-Oba and Balogun-Ojo respectively.

For feldspar extracts, SiO_2 ranges from 43.09% to 73.70%. Feldspar extracts from Omo-Oba had the lowest SiO_2 concentration while feldspar extracts from Doya had the highest SiO_2 concentration. TiO_2 ranges from 0.002 to 0.02%, feldspar extracts from Falansa had the lowest TiO_2 concentration while feldspars extracts from Omo-Oba had the highest TiO_2concentration; Al_2O_3 ranges from 16.38% to 21.13% with feldspar extracts from Doya having the lowest Al_2O_3 concentration while feldspar extracts from Balogun-Ojo had the highest Al_2O_3 concentration. Fe_2O_3 ranges from 0.10% to 0.61%, feldspar extracts from Gbayo had the lowest Fe_2O_3 concentration while feldspars extracts from Doya had the highest Fe_2O_3 concentration.

Table 4.1: Major elements analytical results for whole rock pegmatites

	AB-001	AB-002	BAO-001	BAO-008	CO-001	CO-002	DO-001	DO-003	FA-003	FA-004	ID-004	ID-005	OM-004	OM-008	OW-004	OW-005
SiO_2	71.81	76.44	67.75	76.55	77.08	75.24	73.84	72.45	74.61	71.69	82.17	74.81	98.01	47.76	69.68	71.61
Al_2O_3	16.76	14.55	17.72	13.56	13.7	15.14	15.56	16.4	14.86	15.04	9.84	14.36	0.73	38.85	18.92	16.33
$Fe_2O_3(T)$	2.32	0.51	0.28	0.53	0.38	1.08	0.94	0.87	0.52	0.2	0.53	1.09	0.39	4.25	0.33	0.33
MnO	0.048	0.016	0.008	0.034	0.067	0.196	0.649	1.206	0.077	0.008	0.058	0.061	0.008	0.053	0.269	0.331
MgO	0.33	0.04	0.09	0.11	0.03	0.09	0.03	0.02	0.07	0.02	0.12	0.3	0.08	1.21	0.04	0.04
CaO	0.49	0.45	0.18	1.92	0.41	0.17	0.16	0.27	0.39	0.11	0.73	0.47	0.32	2.24	0.12	0.33
Na_2O	6.31	5.88	2.31	5.05	6.19	2.65	4.67	8.6	7.05	2.8	5.43	4.44	0.09	2.39	10.16	8.85
K_2O	0.44	0.85	11.36	1.17	0.62	2.74	3.16	0.32	0.81	8.43	0.35	4.27	0.08	1.98	0.4	0.34
TiO_2	0.044	0.02	0.013	0.026	0.008	0.034	0.013	0.004	0.014	0.003	0.033	0.061	0.008	0.339	0.003	0.003
P_2O_5	0.03	0.04	0.01	0.01	0.11	0.03	0.04	0.06	0.17	0.12	0.04	0.03	0.06	0.01	0.06	0.23
LOI	0.52	0.44	0.29	0.23	0.45	1.57	0.62	0.1	0.42	0.19	0.18	0.3	0.23	1.34	0.32	0.37
Total	99.1	99.23	100	99.2	99.03	98.95	99.69	100.3	98.99	98.6	99.48	100.2	100	100.4	100.3	98.77

Table 4.2: Major elements analytical results for feldspars extracts

	DO/F	FA/F	BAO/F6	ID/F2	ID/F	BAO/F	OM/F	OM/F2	CO/F	GB/F	AB/F
SiO_2	73.7	66.31	66.52	66.72	66.43	66.38	65.47	43.09	70.62	66.09	65.77
Al_2O_3	16.38	18.88	21.13	17.94	19.48	18.27	19.11	55.56	19	18.78	17.95
Fe_2O_3(T)	0.61	0.12	0.22	0.2	0.12	0.14	0.15	0.48	0.32	0.1	0.11
MnO	0.949	0.006	0.008	0.008	0.004	0.004	0.006	0.006	0.096	0.004	0.01
MgO	0.01	< 0.01	0.03	0.03	0.01	0.02	0.03	0.09	0.03	< 0.01	< 0.01
CaO	0.26	0.04	2.61	0.16	0.25	0.08	0.09	0.07	0.46	0.16	0.05
Na_2O	8.12	2.6	8.81	2.94	3.52	2.22	2.56	0.23	8.53	2.91	2.33
K_2O	0.39	12.31	0.77	11.5	10.54	12.66	12.6	0.22	0.75	11.74	12.54
TiO_2	0.003	0.002	0.007	0.005	0.003	0.004	0.007	0.022	0.007	0.003	0.002
P_2O_5	0.07	0.18	0.03	< 0.01	< 0.01	0.01	0.22	< 0.01	0.07	0.02	0.15
LOI	0.12	0.2	0.32	0.25	0.24	0.23	0.15	0.66	0.62	0.2	0.17
Total	100.6	100.6	100.5	99.77	100.6	100	100.4	100.4	100.5	100	99.09

Table 4.3: Major elements analytical results for biotite extracts

	ID/B1	ID/B2	OM/B2	AB/B	AB/B2	OM/B	BAO/Bw	BAO/B
SiO_2	35.22	42.51	37.86	35.85	36.43	39.68	43.35	45.21
Al_2O_3	27.79	18.22	23.88	32.61	32.78	27.69	17.8	24.6
Fe_2O_3(T)	19.79	15.82	18.36	15.9	15.84	15.5	18.96	11.83
MnO	0.73	1.693	0.121	0.291	0.299	0.082	0.619	0.374
MgO	1.93	8.55	5.69	1.6	1.57	4.75	4.92	4.64
CaO	0.38	0.16	0.46	0.1	0.09	0.86	0.32	0.48
Na_2O	2.4	0.83	0.74	1.86	1.85	1.06	0.68	2.12
K_2O	0.12	7.11	7.24	0.21	0.2	5.91	7.37	0.09
TiO_2	0.752	2.067	2.105	0.238	0.246	1.799	2.155	0.625
P_2O_5	0.01	0.01	0.03	< 0.01	< 0.01	0.05	0.03	< 0.01
LOI	1.79	1.73	2.37	1.95	1.92	1.78	3.31	2.16
Total	90.91	98.71	98.85	90.59	91.23	99.16	99.52	92.13

Table 4.4: Major elements analytical results for muscovite extracts

	CO/M	DO/M2	DO/M	FA/M2	GB/M	GB/M2	ID/M3	AB/M	BAO/M	AB/M2	ID/M	ID/M2	OW/M
SiO_2	52.2	48.23	47.55	45.9	48.28	49.26	49.67	46.64	46.81	45.51	48.09	48.82	46.19
Al_2O_3	31.18	32.65	33.04	34.81	34.2	31.67	32.44	33.3	33.9	34.45	34.6	33.49	34.22
Fe_2O_3(T)	2.12	2.99	2.96	3.24	2.69	2.78	2.6	3.3	1.92	3.32	2.67	2.61	2.17
MnO	0.048	0.128	0.12	0.097	0.07	0.069	0.123	0.091	0.156	0.098	0.104	0.119	0.165
MgO	0.23	0.11	0.11	0.14	0.25	0.25	0.06	0.13	0.38	0.14	0.05	0.05	0.31
CaO	0.03	0.03	0.03	0.01	< 0.01	0.01	0.02	0.02	0.04	0.02	0.02	0.03	0.03
Na_2O	1.31	0.95	0.84	0.66	0.66	0.65	0.92	0.75	0.9	0.67	0.93	0.92	0.72
K_2O	8.01	9.01	9.37	9.72	9.44	9.54	8.95	9.54	9.68	9.67	9.23	9.21	10.09
TiO_2	0.098	0.101	0.088	0.112	0.044	0.047	0.078	0.132	0.1	0.117	0.077	0.076	0.098
P_2O_5	0.01	0.02	0.02	0.03	< 0.01	0.02	< 0.01	0.02	0.04	< 0.01	< 0.01	< 0.01	0.03
LOI	4.16	4.39	4.67	5.14	4.56	4.52	4.26	4.57	4.78	5.11	4.42	4.45	4.83
Total	99.39	98.61	98.79	99.87	100.2	98.82	99.12	98.5	98.71	99.1	100.2	99.78	98.85

Table 4.5: Trace elemental analytical results for whole rock pegmatites

	AB-001	AB-002	BAO-001	BAO-008	CO-001	CO-002	DO-001	DO-003	FA-003	FA-004	ID-004	ID-005	OM-004	OM-008	OW-004	OW-005
Be	6	6	2	5	23	7	384	243	215	4	5	4	< 1	4	49	13
Zn	210	< 30	< 30	< 30	< 30	< 30	210	< 30	< 30	< 30	30	80	< 30	< 30	570	< 30
Ga	40	33	14	15	17	32	48	41	22	12	21	33	1	35	33	28
Rb	45	139	267	30	64	348	> 1000	21	88	668	23	337	6	86	53	37
Sr	6	7	73	134	20	9	3	< 2	28	85	22	28	3	124	4	5
Nb	30.4	35.6	0.8	1.7	8.5	20.4	66.9	60.1	18.2	1.2	11.8	32.2	0.6	7.2	72.9	5.4
Sn	8	15	< 1	< 1	3	17	23	4	4	< 1	1	2	< 1	2	< 1	< 1
Cs	2.8	4	13.3	3.6	4.8	11	29.2	4	9.9	26.7	10.6	49.6	0.7	3.9	29.8	21.6
Ba	5	6	630	139	8	12	5	4	11	182	9	48	13	523	29	7
Hf	< 0.1	0.4	0.2	0.1	0.4	0.9	3.3	5.4	0.6	< 0.1	1.3	1.2	< 0.1	4.2	7.1	0.9
Ta	5.07	7.06	0.54	0.87	9.86	33.5	34.9	76.1	17.6	0.96	3.25	14.8	1.45	0.93	64.1	8.86
W	251	255	217	274	352	428	177	97.4	215	191	217	230	933	141	112	172
Th	0.2	9.76	0.81	10.9	0.83	6.8	7.92	11	0.69	0.11	6.28	13.2	< 0.05	10.2	1.35	0.95
U	0.45	4.8	0.83	1.2	0.92	2.86	8.72	10.1	1.62	0.29	6.96	13.1	0.04	1.67	3.37	1.93

Table 4.6: Trace elemental analytical results for feldspar extracts

	AB/F	OM/F	OM/F2	BAO/F6	BAO/F	CO/F	DO/F	FA/F	GB/F	ID/F	ID/F2
Be	4	4	< 1	9	< 1	8	171	5	< 1	3	3
Zn	< 30	< 30	< 30	< 30	< 30	30	< 30	< 30	< 30	< 30	< 30
Ga	14	14	46	22	13	30	41	14	14	39	37
Rb	> 1000	954	9	14	273	379	36	976	247	> 1000	> 1000
Sr	97	74	8	130	115	17	< 2	70	131	42	36
Nb	2.3	1	0.8	1.8	0.6	18	61.4	1.7	1.7	8	7.2
Sn	< 1	< 1	< 1	< 1	< 1	15	4	< 1	< 1	1	< 1
Cs	30.7	37.8	0.9	1.4	11.4	11.8	3.5	30.3	6.5	351	285
Ba	179	163	17	67	1912	8	4	162	2260	138	96
Hf	< 0.1	0.1	< 0.1	0.1	< 0.1	0.4	5.2	< 0.1	< 0.1	< 0.1	0.1
Ta	1.28	0.58	0.94	0.55	0.32	7.67	69.1	0.76	0.49	1.33	1.62
W	151	118	600	123	153	592	281	166	199	204	159
Th	< 0.05	0.11	0.96	0.24	0.17	0.79	2.78	< 0.05	0.08	0.21	0.32
U	0.3	0.27	0.11	0.34	0.19	0.55	5.08	0.44	0.18	0.93	1.25

Table 4.7: Trace elemental analytical results for biotite extracts

	BAO/Bw	BAO/B	AB/B	AB/B2	ID/B1	ID/B2	OM/B2	OM/B
Be	5	2	4	4	2	5	2	3
Zn	550	1340	1970	2000	3800	2220	110	120
Ga	71	126	144	145	178	102	37	35
Rb	> 1000	3	11	13	5	> 1000	373	310
Sr	17	18	< 2	< 2	12	11	36	49
Nb	267	312	16.7	4.8	5.4	248	36.8	31.5
Sn	41	26	25	25	19	70	6	4
Cs	195	2.1	0.7	0.7	1.5	475	16.2	15.2
Ba	242	16	22	12	< 2	52	1650	1185
Hf	0.6	1	0.4	0.5	0.1	1.3	15	13.5
Ta	56.1	68.7	2.97	1.35	1.16	26.5	2.89	2.54
W	61.3	699	327	361	444	333	28	52.5
Th	2.31	63.5	1.11	2.5	0.22	3.58	33.6	28.9
U	3.94	43	0.94	1.21	0.56	8.28	6.69	5.45

Table 4.8: Trace elemental analytical results for muscovite extracts

	AB/M	AB/M2	ID/M	ID/M2	ID/M3	BAO/M	GB/M	GB/M2	CO/M	DO/M2	FA/M2	DO/M	OW/M
Be	23	29	26	19	21	72	23	23	15	19	28	18	28
Zn	240	280	310	310	450	560	280	280	70	180	280	160	590
Ga	271	281	243	249	247	171	104	103	96	242	281	249	177
Rb	> 1000	> 1000	> 1000	> 1000	> 1000	> 1000	> 1000	> 1000	> 1000	> 1000	> 1000	> 1000	> 1000
Sr	7	8	14	14	14	5	6	5	6	15	8	17	5
Nb	330	302	253	265	252	266	238	239	244	265	297	263	237
Sn	319	263	222	233	218	2	46	46	75	194	260	178	8
Cs	194	248	183	172	173	126	44.8	40.2	53.2	216	246	252	127
Ba	5	4	28	32	34	11	59	54	16	82	5	80	10
Hf	1.4	0.7	0.7	0.7	0.6	0.7	0.1	0.1	0.3	0.9	0.7	0.5	0.3
Ta	87.7	107	63.8	82.4	75.4	58.7	34.8	32.8	55.4	96.5	103	74	58.3
W	89.5	21.6	108	114	58.4	17.2	70.7	107	127	69.5	25.9	214	20.6
Th	0.24	0.16	0.59	0.32	0.46	0.33	0.07	0.07	0.69	0.65	0.16	0.52	0.09
U	2.76	2.29	0.81	0.8	0.93	0.8	0.09	0.03	0.96	1.65	2.19	0.36	0.21

Table 4.9: Rare earth elemental concentration for whole rock pegmatites

	AB-001	AB-002	BAO-001	BAO-008	CO-001	CO-002	DO-001	DO-003	FA-003	FA-004	ID-004	ID-005	OM-004	OM-008	OW-004	OW-005
La	0.68	0.6	2.26	192	0.57	3.34	1.19	1.53	0.35	< 0.05	3.32	3.8	0.14	47.4	< 0.05	0.71
Ce	1.34	1.37	4.27	269	1.13	7.46	3.67	4.51	0.67	0.18	8.61	11	0.4	86.4	0.08	2.08
Pr	0.15	0.16	0.48	22.5	0.13	0.88	0.54	0.61	0.07	0.01	1.24	1.63	0.04	9	< 0.01	0.29
Nd	0.31	0.63	1.76	60	0.47	2.99	1.81	2.02	0.22	0.1	5.36	7.44	0.18	30.6	< 0.05	0.99
Sm	0.15	0.91	0.45	5.68	0.09	1.11	2.52	3.15	0.04	0.02	2.17	4.12	0.04	5.44	< 0.01	1.28
Eu	0.014	0.01	0.47	1.25	0.02	0.087	< 0.005	< 0.005	0.02	0.01	0.115	0.166	0.017	2.16	< 0.005	0.024
Gd	0.14	2.02	0.5	2.24	0.1	1.11	3.02	4.79	0.05	0.04	2.4	4.63	0.05	4.17	0.09	1.16
Tb	0.02	0.51	0.11	0.25	0.02	0.22	0.56	0.87	< 0.01	< 0.01	0.43	0.9	0.01	0.55	0.03	0.14
Dy	0.11	3.05	0.76	1.33	0.11	1.19	2.36	3.66	0.05	0.05	2.96	5.37	0.09	3.1	0.15	0.32
Ho	0.01	0.42	0.16	0.21	0.02	0.2	0.17	0.2	< 0.01	< 0.01	0.62	0.89	0.03	0.6	0.01	0.01
Er	0.03	1.11	0.41	0.56	0.04	0.6	0.23	0.23	0.02	0.02	1.99	2.67	0.14	1.77	0.02	0.02
Tm	< 0.005	0.192	0.06	0.088	< 0.005	0.099	0.024	0.021	< 0.005	< 0.005	0.416	0.504	0.027	0.27	< 0.005	< 0.005
Yb	0.04	1.7	0.48	0.56	0.05	0.83	0.14	0.11	0.03	0.05	3.47	4.32	0.3	2.17	0.01	0.02
Lu	0.007	0.265	0.081	0.105	0.006	0.135	0.019	0.015	0.006	0.006	0.649	0.654	0.067	0.356	< 0.002	0.005

Table 4.10: Rare earth elemental concentration for feldspar extracts

	OM/F	OM/F2	AB/F	BAO/F6	BAO/F	CO/F	DO/F	FA/F	GB/F	ID/F	ID/F2
La	0.3	20.4	< 0.05	2.57	1.27	1.08	0.25	< 0.05	0.71	1.56	1.18
Ce	0.6	28.2	0.12	4.37	2.05	1.76	1.06	0.12	0.86	1.14	1.09
Pr	0.07	2.39	< 0.01	0.46	0.23	0.23	0.15	0.01	0.09	0.25	0.21
Nd	0.28	6.32	< 0.05	1.6	0.8	0.77	0.5	< 0.05	0.3	0.78	0.72
Sm	0.04	0.52	< 0.01	0.43	0.25	0.25	1.06	< 0.01	0.1	0.22	0.25
Eu	0.03	0.137	0.014	0.599	0.747	0.041	< 0.005	0.006	0.683	0.074	0.066
Gd	0.04	0.15	0.02	0.52	0.42	0.22	1.93	0.02	0.16	0.22	0.28
Tb	< 0.01	0.02	< 0.01	0.11	0.07	0.04	0.31	< 0.01	0.03	0.04	0.05
Dy	0.02	0.11	0.03	0.73	0.42	0.3	1.46	< 0.01	0.17	0.22	0.29
Ho	< 0.01	0.02	< 0.01	0.13	0.06	0.06	0.07	< 0.01	0.03	0.04	0.06
Er	0.02	0.05	< 0.01	0.33	0.13	0.16	0.08	< 0.01	0.08	0.15	0.21
Tm	< 0.005	< 0.005	< 0.005	0.046	0.018	0.025	< 0.005	< 0.005	< 0.005	0.027	0.036
Yb	0.02	0.04	< 0.01	0.29	0.14	0.22	0.05	< 0.01	0.09	0.21	0.31
Lu	0.005	0.007	0.004	0.042	0.024	0.038	0.007	0.006	0.016	0.035	0.055

Table 4.11: Rare earth elemental concentration for biotite extracts

	ID/B1	BAO/Bw	BAO/B	AB/B	AB/B2	ID/B2	OM/B2	OM/B
La	2.57	6.31	12.6	3.33	2.83	3.08	105	93.7
Ce	7.15	12.4	32.3	6.94	6.54	9.05	215	187
Pr	0.61	1.47	5.67	0.78	0.76	1.26	24.1	21.1
Nd	1.71	5.13	24.9	2.62	2.7	5.41	86.2	75.4
Sm	0.31	1.3	15.3	0.6	1.01	2.43	16.2	14.5
Eu	0.042	0.179	0.481	0.049	0.022	0.088	2.43	2.34
Gd	0.16	1.21	15.2	0.47	0.56	2.85	13.1	11.4
Tb	0.02	0.19	3.12	0.07	0.07	0.55	1.87	1.5
Dy	0.09	1	17.7	0.38	0.28	3.48	10.1	8.06
Ho	0.02	0.17	2.69	0.06	0.03	0.69	1.81	1.35
Er	0.04	0.46	7.6	0.14	0.06	2.23	4.95	3.53
Tm	0.006	0.061	1.45	0.018	0.011	0.43	0.674	0.478
Yb	0.05	0.48	10.3	0.11	0.11	4.02	4.67	3.18
Lu	0.011	0.074	1.57	0.016	0.018	0.673	0.722	0.502

Table 4.12: Rare earth elemental concentration for muscovite extracts

	ID/M2	DO/M	BAO/M	CO/M	DO/M2	FA/M2	ID/M3	GB/M	GB/M2	AB/M	AB/M2	ID/M	OW/M
La	< 0.05	< 0.05	< 0.05	0.24	< 0.05	< 0.05	0.06	< 0.05	0.06	< 0.05	< 0.05	0.05	< 0.05
Ce	0.13	0.2	0.24	0.64	0.17	0.17	0.16	0.5	1.26	0.24	0.13	0.22	0.1
Pr	0.01	0.02	0.04	0.08	0.02	< 0.01	0.02	0.01	0.02	0.01	< 0.01	0.03	< 0.01
Nd	0.05	0.1	0.15	0.35	0.06	< 0.05	0.08	< 0.05	0.09	0.09	0.08	0.1	< 0.05
Sm	0.07	0.08	0.21	0.2	0.11	0.07	0.09	< 0.01	< 0.01	0.11	0.09	0.11	0.03
Eu	< 0.005	< 0.005	< 0.005	0.062	< 0.005	< 0.005	< 0.005	0.005	< 0.005	< 0.005	< 0.005	< 0.005	< 0.005
Gd	0.13	0.16	0.21	0.5	0.24	0.13	0.15	0.02	0.02	0.15	0.15	0.14	0.03
Tb	0.02	0.02	0.03	0.1	0.04	0.03	0.02	< 0.01	< 0.01	0.04	0.03	0.01	< 0.01
Dy	0.06	0.1	0.07	0.62	0.18	0.17	0.06	0.01	0.01	0.27	0.18	0.04	< 0.01
Ho	< 0.01	< 0.01	< 0.01	0.12	0.02	0.02	< 0.01	< 0.01	< 0.01	0.03	0.02	< 0.01	< 0.01
Er	< 0.01	0.02	< 0.01	0.3	0.03	0.05	< 0.01	< 0.01	< 0.01	0.08	0.06	< 0.01	< 0.01
Tm	< 0.005	< 0.005	< 0.005	0.037	< 0.005	< 0.005	< 0.005	< 0.005	< 0.005	0.013	< 0.005	< 0.005	< 0.005
Yb	< 0.01	0.04	< 0.01	0.25	0.04	0.13	< 0.01	< 0.01	< 0.01	0.13	0.09	< 0.01	< 0.01
Lu	0.002	0.007	0.003	0.045	0.009	0.023	< 0.002	< 0.002	0.003	0.031	0.016	< 0.002	0.003

Table 4.13: Range of major elements composition in the analysed samples

	Whole rock pegmatite (n=16)	Feldspar extracts (n=11)	Muscovite extracts (n=13)	Biotite extracts (n=8)
SiO_2	45.51-82.17	43.09-73.70	45.51-52.20	35.22-45.21
TiO_2	Bdl- 0.34	BDL-0.02	0.04-0.13	0.24-2.16
Al_2O_3	9.84-18.92	16.38-21.13	31.18-34.81	17.80-32.78
Fe_2O_3	0.20-4.25	0.10-0.61	1.92-3.32	11.83-19.79
MnO	0.01-1.21	BDL-0.95	0.05-0.17	0.08-1.69
MgO	0.02-1.21	0.01-0.09	0.05-0.38	1.57-8.55
CaO	0.11-2.24	0.04-2.61	0.01-0.04	0.09-0.86
Na_2O	0.09-10.16	0.23-8.81	0.65-1.31	0.68-2.40
K_2O	0.08-11.36	0.22-12.66	8.01-10.09	0.09-7.37
P_2O_5	0.01-0.23	0.01-0.22	0.01-0.04	0.01-0.05

Table 4.14: Range of trace elements composition in the analysed samples

	Whole rock pegmatite (n=16)	Feldspar extracts (n=11)	Muscovite extracts (n=13)	Biotite extracts (n=8)
Pb	8-61	7-86	5-13	13-51
Zn	Bdl-570	Bdl-30	Bdl-590	110-3800
Co	10-73	11-95	1-16	22-46
U	0.04-13.10	0.11-5.08	0.03-2.76	0.56-43.00
Th	0.11-13.20	0.08-2.78	0.07-0.69	0.22-63.5
Sr	3-134	8-131	5-17	11-49
Cd	-	-	-	-
Sb	-	-	-	-
Bi	0.2-1.5	0.2-2.6	0.2-2.8	0.1-50.6
Ba	4-630	4-2260	4-82	12-1650
W	97-933	118-600	17-214	28-699
Zr	2-166	1-30	3-10	2-621
Sn	1-23	1-15	2-319	4-70
Be	2-384	3-171	15-72	2-5
Sc	1-13	Bdl-1	1-40	29-389
Y	0.6-38.2	1.3-4.9	0.8-4.1	1.2-81.5
Hf	0.10-7.10	0.10-5.20	0.1-1.4	0.1-15.0
Rb	6-668	9-976	45->1000	3-373
Ta	0.54-76	0.32-69	33-107	1-69
Nb	0.60-73	0.6-61	237-330	4.8-312
Cs	0.70-50	0.90-351	40-252	0.7-475
Ga	1-48	13-46	96-281	35-178
Tl	0.21-4.91	0.7-7.51	5.61-26.4	2.23-9.39

Table 4.15: Rare earth elemental composition in the analysed samples (in ppm)

	Whole rock pegmatite (n=16)	Feldspar extracts (n=11)	Muscovite extracts (n=13)	Biotite extracts (n=8)
La	0.14-192	0.25-20.40	-	2.57-105
Ce	0.08-269	0.12-28.20	0.13-0.64	6.54-215
Pr	0.01-23	0.01-2.39	0.01-0.08	0.61-24.10
Nd	0.10-60	0.28-6.32	0.05-0.35	1.71-86.2
Sm	0.02-5.68	0.04-1.06	0.07-0.21	0.31-16.2
Eu	0.01-2.16	0.01-0.75	-	0.02-2.43
Gd	0.04-4.79	0.02-1.93	0.02-0.50	0.16-15.20
Tb	0.01-0.90	0.02-0.31	0.02-0.10	0.02-3.12
Dy	0.05-5.37	0.02-1.46	0.01-0.62	0.09-17.70
Ho	0.01-0.89	0.02-0.13	-	0.02-2.69
Er	0.02-2.67	0.02-0.33	0.02-0.30	0.04-7.60
Tm	0.02-0.50	0.02-0.05	-	0.01-1.45
Yb	0.01-4.32	0.02-0.31	0.04-0.25	0.05-10.30
Lu	0.01-0.65	0.01-0.06	0.01-0.05	0.01-1.57
∑REE	0.4-194.0	0.2-58.4	0.16-3.4	12.8-486.8

For feldspar extracts, other oxides range is as follows; MnO (0.01% to 0.95%), MgO (0.01% to 0.09%), CaO (0.04% to 2.61%), Na_2O (0.23% to 8.81%), K_2O (0.22% to 12.66%) and P_2O_5 (0.01% to 0.22%). Highest concentrations of MnO, MgO, CaO, Na_2O, K_2O and P_2O_5 in feldspar extracts were observed at Doya, Omo-Oba, Balogun-Ojo, and Omo-Oba respectively while lowest concentration of MnO, MgO, CaO, Na_2O, K_2O and P_2O_5 were observed at Idiyan,, Falansa Omo-Oba, Coco and Idiyan respectively.

Mica extracts

Muscovite extracts

For muscovite extracts, SiO_2 ranges from 45.51% to 52.20. Muscovite extracts from Abuja leather had the lowest SiO_2 concentration while muscovite extracts from Coco had the highest SiO_2 concentration. TiO_2 ranges from 0.04 to 0.13%, muscovite extracts from Gbayo had the lowest TiO_2 concentration while muscovites extracts from Abuja leather had the highest TiO_2 concentration; Al_2O_3 ranges from 31.18% to 34.81% with muscovite extracts from Coco having the lowest Al_2O_3 concentration while muscovite extracts from Falansa had the highest Al_2O_3 concentration. Fe_2O_3 ranges from 1.92% to 3.32%, muscovite extracts from Balogun-Ojo had the lowest Fe_2O_3 concentration while muscovites extracts from Abuja leather had the highest Fe_2O_3 concentration.

Other major oxides in the muscovite extracts are as follows; MnO (0.05% to 0.17%), MgO (0.05% to 0.38%), CaO (0.01% to 0.04%), Na_2O (0.65% to 1.31%, K_2O (8.01% to 10.09%) and P_2O_5 (0.01% to 0.04%). Highest concentrations of MnO, MgO, CaO, Na_2O, K_2O and P_2O_5 in muscovite extracts were observed at Owode, Coco, Balogun-ojo, Coco, Coco and Balogun-Ojo respectively while lowest concentration of MnO, MgO, CaO, Na_2O, K_2O and P_2O_5 were observed at Coco, Idiyan, Gbayo, Gbayo, Coco and Idiyan respectively.

Biotite extracts

For biotite extracts, SiO_2 ranges from 35.22% to 45.21%. Biotite extracts from Idiyan had the lowest SiO_2 concentration while biotite extracts from Balogun-Ojo had the highest SiO_2 concentration. TiO_2 ranges from 0.24 to 2.16%, biotite extracts from Abuja leather had the lowest TiO_2 concentration while biotites extracts from Balogun-Ojo had the highest TiO_2 concentration; Al_2O_3 ranges from 17.80% to 32.78% with

biotite extracts from Balogun-Ojo having the lowest Al_2O_3 concentration while biotite extracts from Abuja leather had the highest Al_2O_3 concentration. Fe_2O_3 ranges from 11.83% to 19.79%. Biotite extracts from Balogun-Ojo had the lowest Fe_2O_3 concentration while biotites extracts from Idiyan had the highest Fe_2O_3 concentration.

For biotite extracts, other oxides ranged; MnO (0.08% to 1.69%), MgO (1.57% to 8.55%), CaO (0.09% to 0.86%), Na_2O (0.68% to 2.40%), K_2O (0.09% to 7.37%) and P_2O_5 (0.01% to 0.52%). Highest concentrations of MnO, MgO, CaO, Na_2O, K_2O and P_2O_5 in biotite extracts were observed at Idiyan, Idiyan, Omo-oba, Abuja leather, Balogun-Ojo and Omo-Oba respectively while lowest concentration of MnO, MgO, CaO, Na_2O, K_2O and P_2O_5 were observed at Omo-oba, Abuja leather, Abuja leather, Balogun-Ojo, Idiyan an Omo-Oba respectively.

4.2.1.2: Trace elemental concentration

Range of selected trace elements (in ppm) in whole rock pegmatites are as follows (table 4.2): U (0.04-13) Th (0.1-13), W (97-933), Sn (1.0-23.0), Be (2-384), Rb (6.0-668.0), Ta (0.5-76.1), Nb (0.6-72.9), Sr (3.0-134.0), Ba (4.0-630.0) and Cs (0.7-49.6). Whole rock pegmatite samples from Doya has elevated concentration of Be relative to other pegmatites which had concentration less than 50ppm except one of the samples from Falansa which also revealed elevated concentration of Be. Samples from Doya also revealed highest concentration of Nb (67ppm) and Ta (76ppm). For W, all whole rock pegmatites have values in excess of 97ppm with one of the samples from Omo-Oba having the highest concentration (figure 4.25-4.30).

Range of selected trace elements (in ppm) in feldspar extracts are as follows: U (0.11-5.08) Th (0.1-2.8), W (118.0-600.0), Sn (1.0-15.0), Be (3-171), Rb (9.0-976.0), Ta (0.3-69.1), Nb (0.6-61.4), Sr (8.0-131.0), Ba (4.0-2260.0) and Cs (0.9-351.0). Be, Nb and Ta concentration is generally low in feldspars with concentration below 10ppm, 20ppm and 8ppm respectively in all samples except the feldspar extract sample from Doya with concentration of 171ppm, 61ppm and 69ppm for Be, Nb and Ta. Furthermore, W concentration varies in feldspar extracts with values above 118ppm in all extracts; with elevated concentrations in excess of 590ppm recorded in feldspar extracts from Omo-Oba and Coco (figure 4.31-4.35).

Range of selected trace elements (in ppm) in muscovite extracts are as follows: U (0.03-2.8) Th (0.1-0.7), W (17-214), Sn (2.0-319.0), Be (15-72), Rb (45->1000.0), Ta (32.8-107.0), Nb (237.0-330.0), Sr (5.0-17.0), Ba (4.0-82.0) and Cs (0.7-49.6).

Compared to other mineral extracts and whole rock pegmatites, muscovite extracts revealed the lowest concentration values of W and the highest concentration values of Sn, Nb and Ta. All muscovite extracts from the study have with the exception of Balogun-Ojo and Owode samples have Sn concentration above 45ppm, Nb values are above 237ppm in all muscovite extracts, values higher than Nb concentration in whole rock and feldspar extracts while 107ppm of Ta; the highest Ta value in pegmatites and extracts in this study was recorded in muscovite extracts from Abuja leather area. Highest concentrations of Nb and Sn were also recorded in samples from Abuja Leather (figure 4.36 - 4.41).

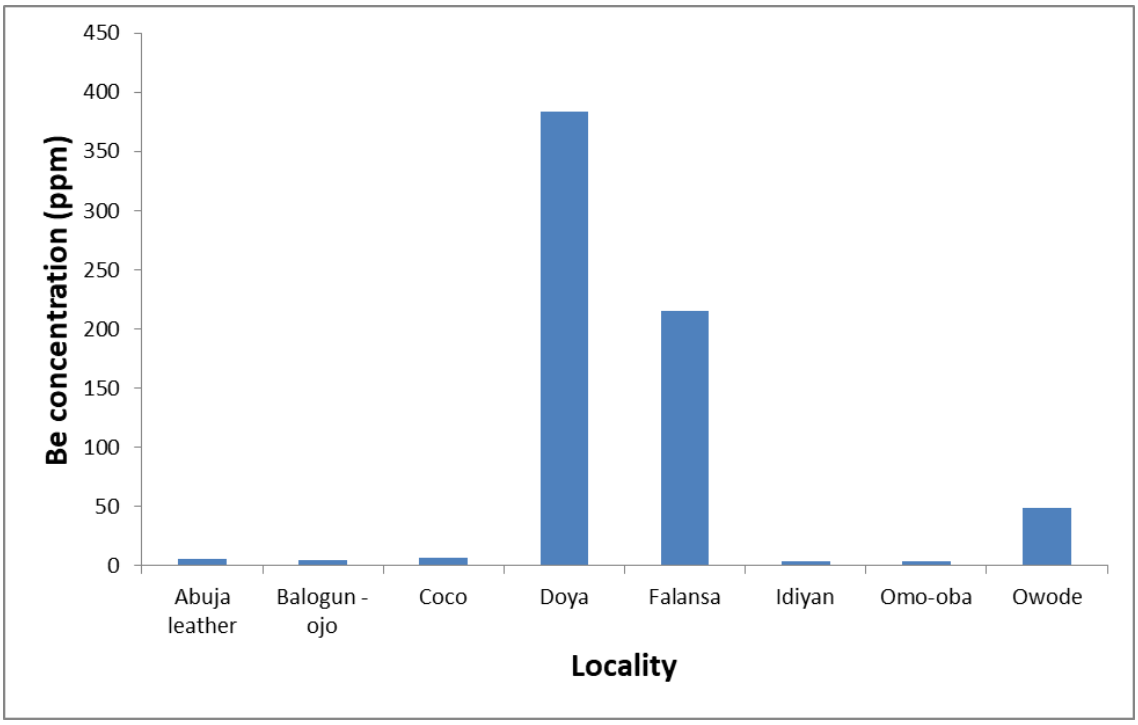

Figure 4.25: Be concentration in whole rock pegmatites from the different locations

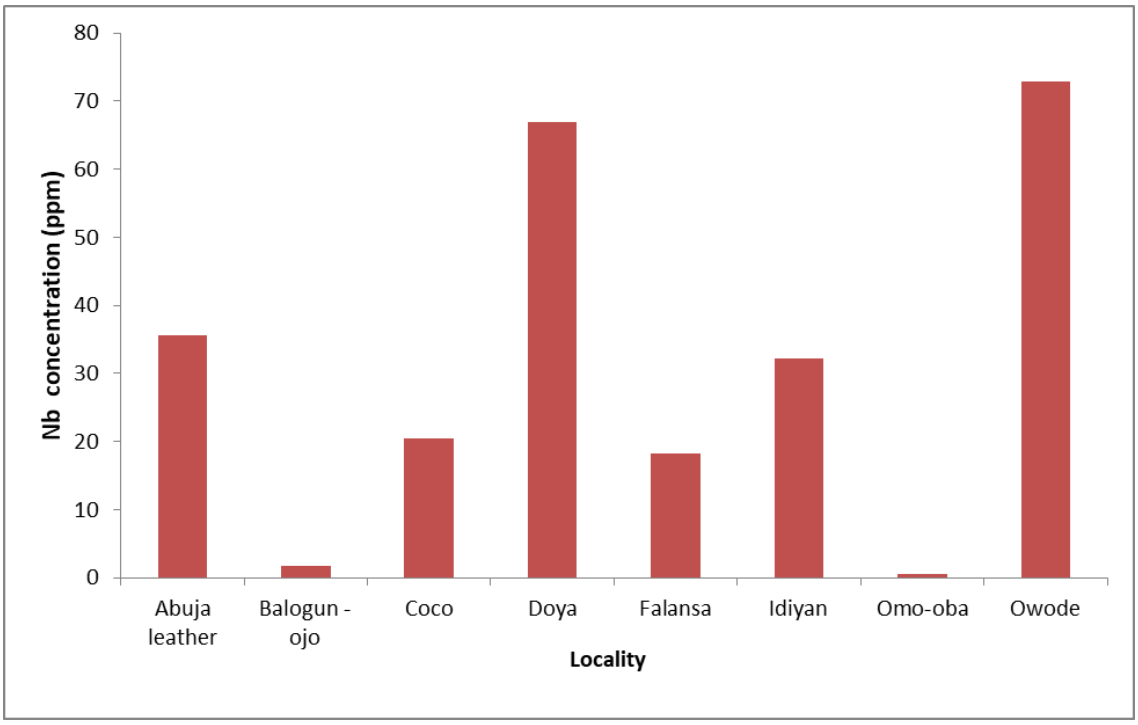

Figure 4.26: Nb concentration in whole rock pegmatites from the different locations

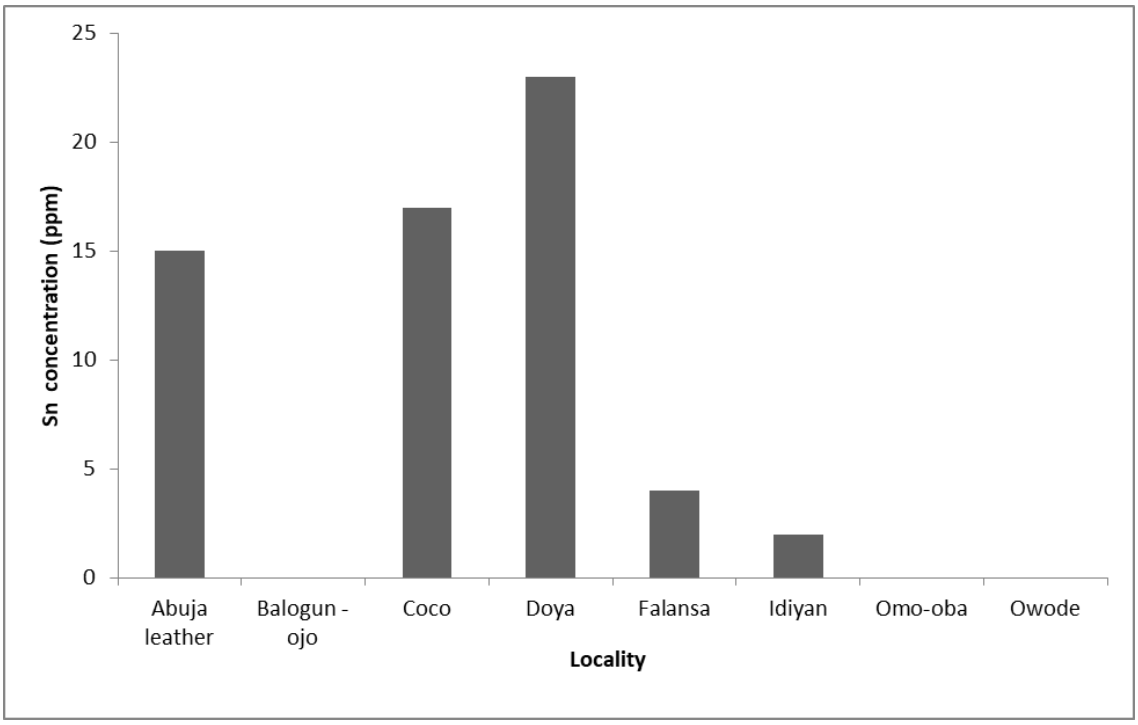

Figure 4.27: Sn concentration in whole rock pegmatites from the different locations

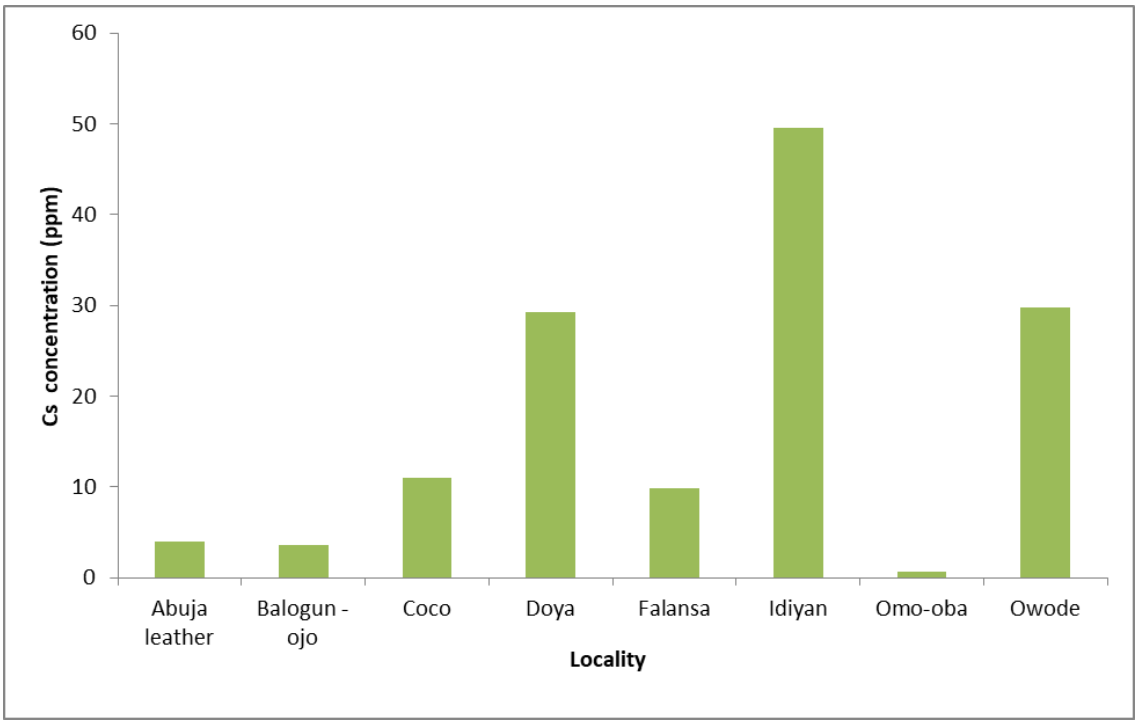

Figure 4.28: Cs concentration in whole rock pegmatites from the different locations

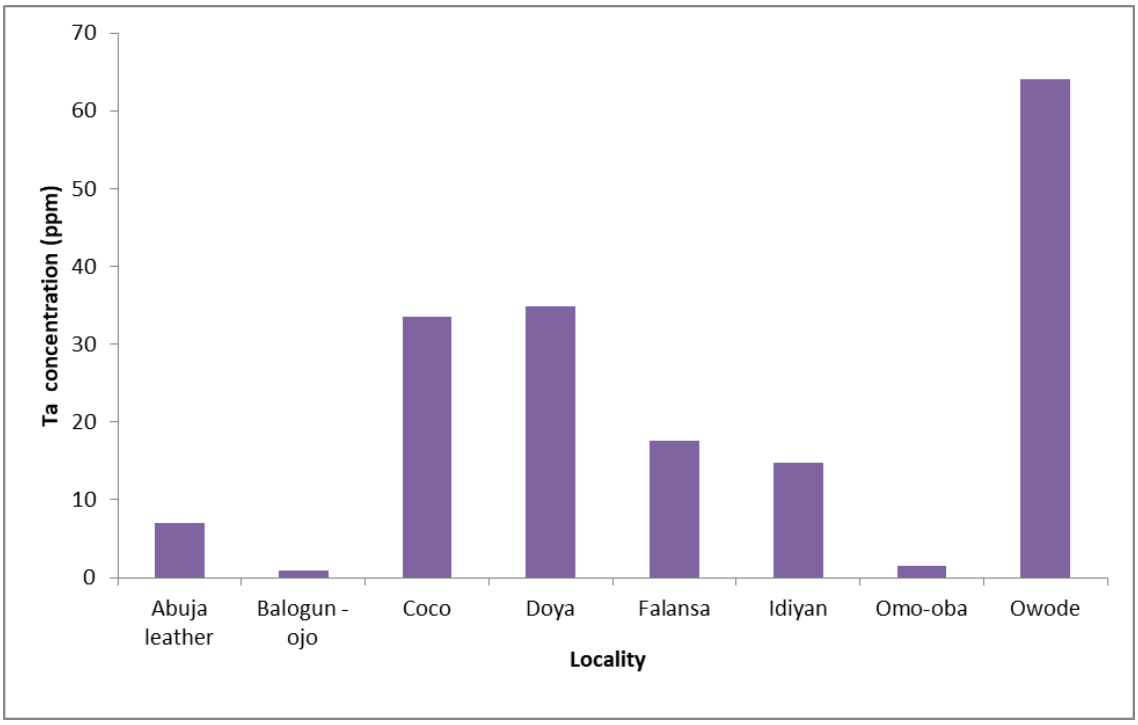

Figure 4.29: Ta concentration in whole rock pegmatites from the different locations

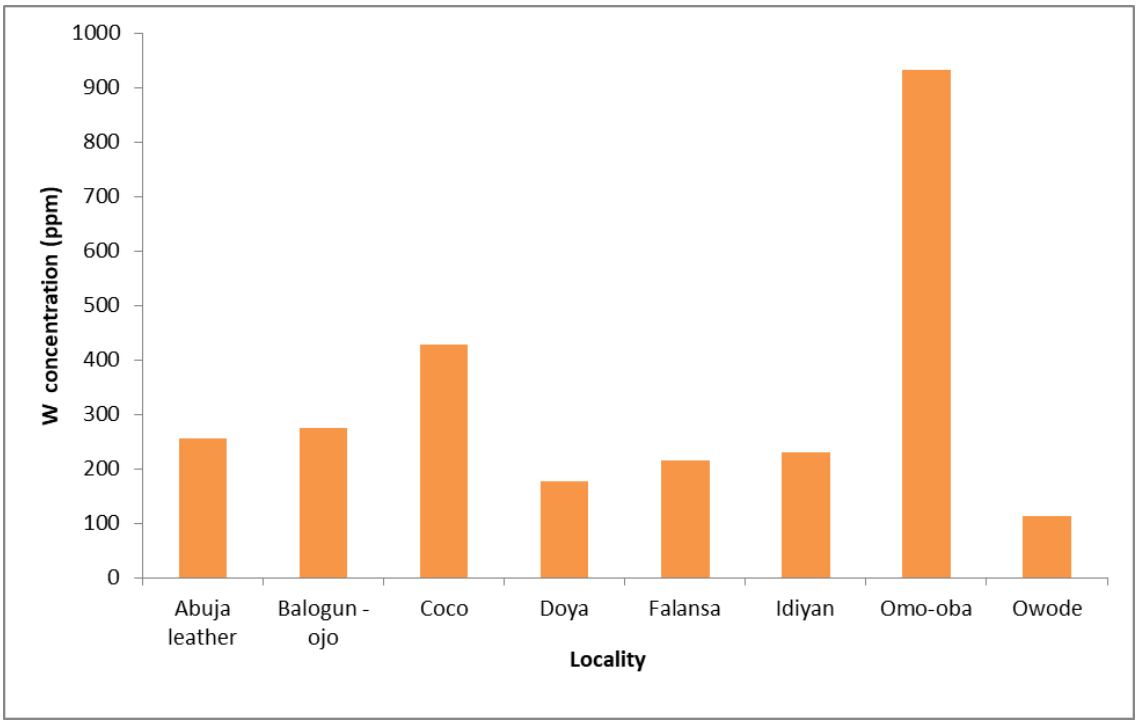

Figure 4.30: W concentration in whole rock pegmatites from the different locations

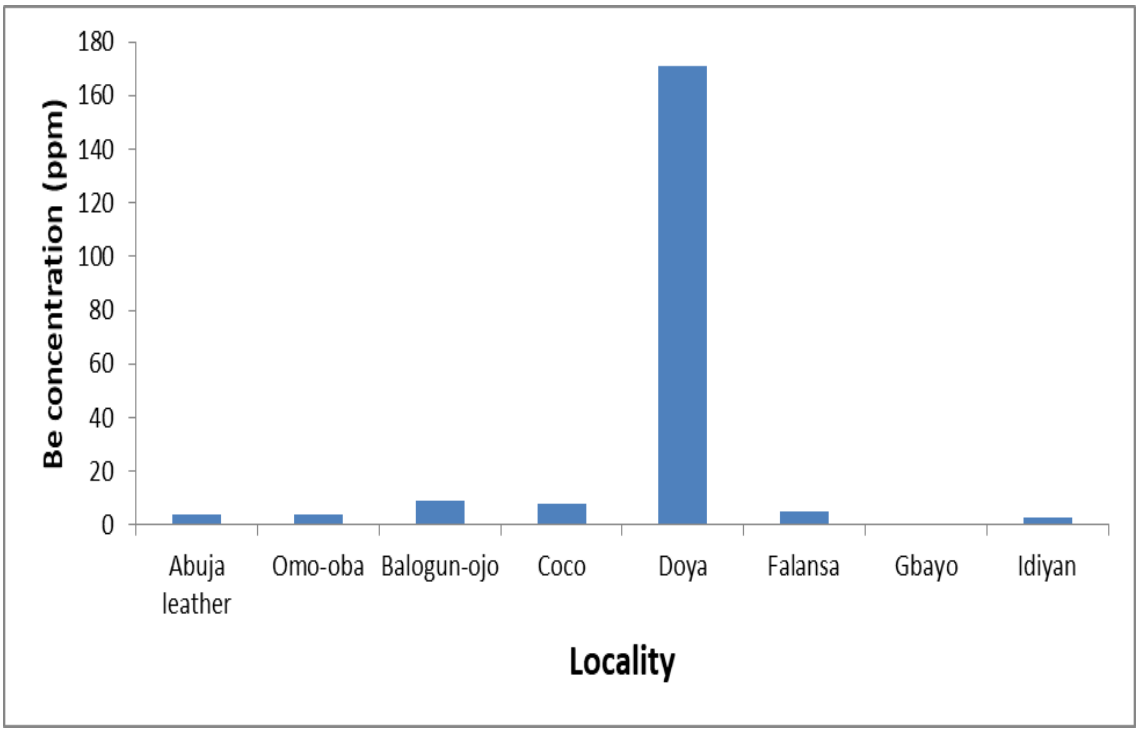

Figure 4.31: Be concentration in feldspars from the different locations

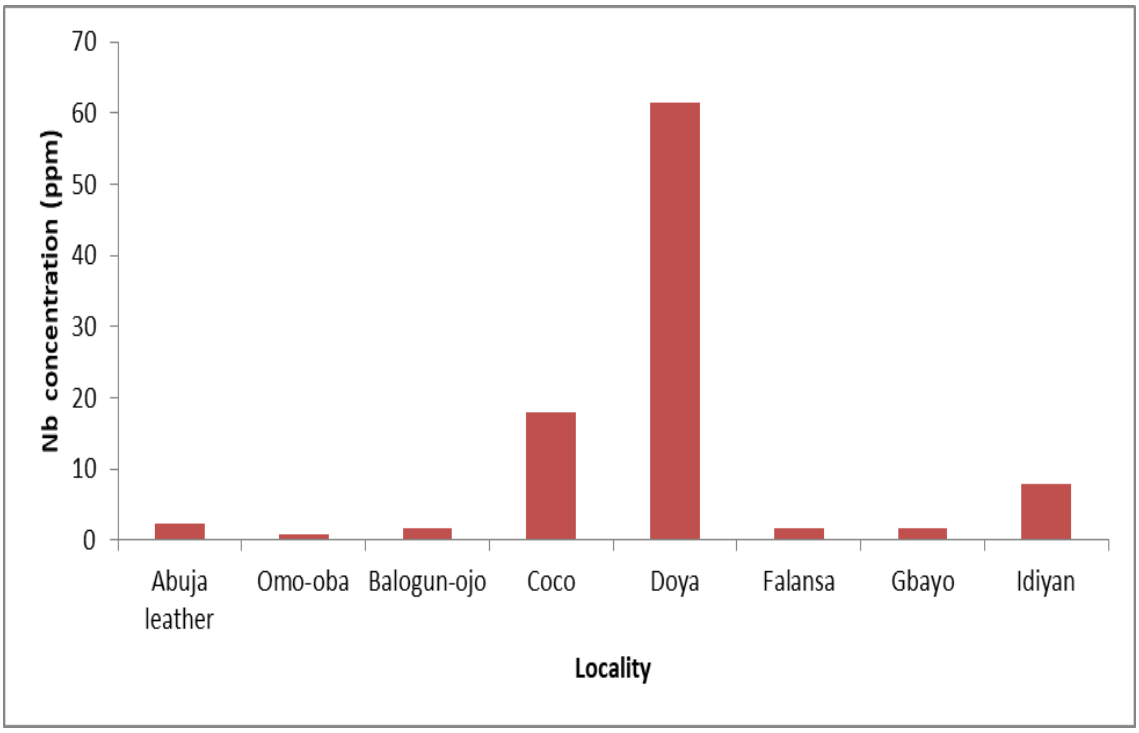

Figure 4.32: Nb concentration in feldspars from the different locations

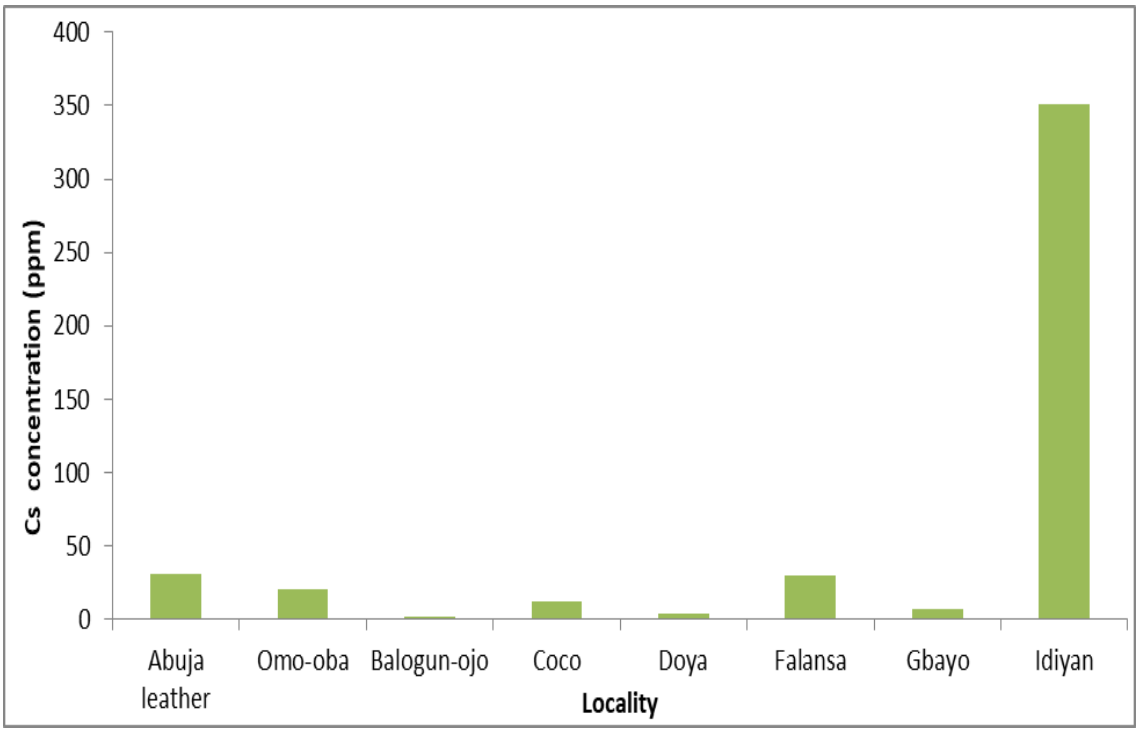

Figure 4.33: Cs concentration in feldspars from the different locations

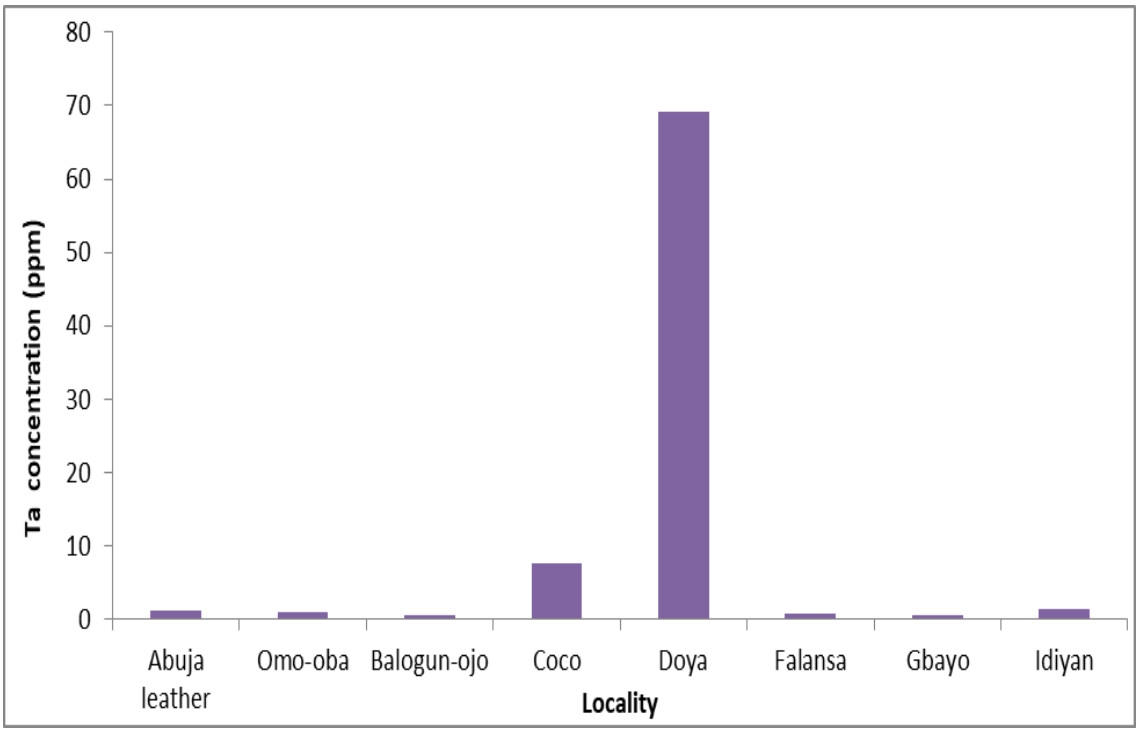

Figure 4.34: Ta concentration in feldspars from the different locations

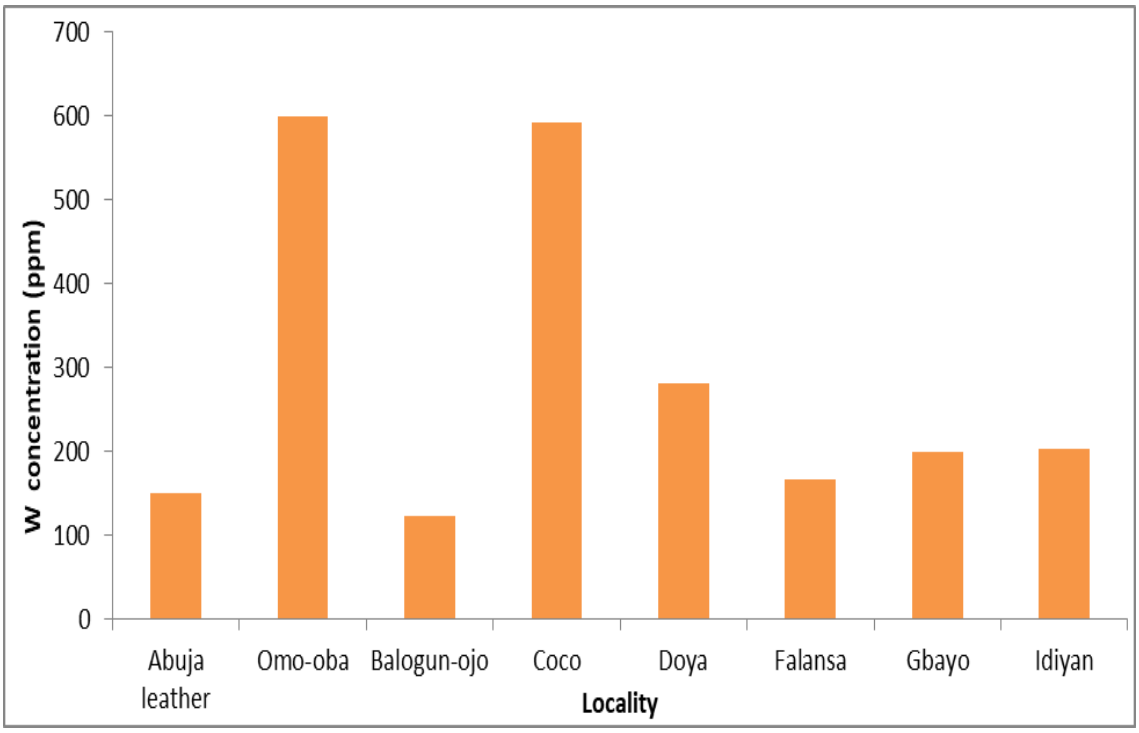

Figure 4.35: W concentration in feldspars from the different locations

Range of selected trace elements (in ppm) in biotite extracts are as follows: U (0.56-43.0) Th (0.2-64), W (28.0-699.0), Sn (4.0-70.0), Be (2-5), Rb (3.0-6373.0), Ta (1.2-68.7), Nb (04.8-312.0), Sr (11.0-49.0), Ba (12.0-1650.0) and Cs (0.7-475.0).compared to muscovite extracts, the biotite extracts have elevated concentration of W in excess of 326 in all locations except Omo-Oba but lower concentrations of Ta which is below 27ppm in all locations except Balogun-Ojo with Ta concentration of 69ppm (figure 4.42-4.46)

4.2.1.3: Rare Earth Elemental concentration

Pegmatite whole rock samples revealed low to moderate REE abundance; the value ranged 0.4-555.8ppm. Range of selected rare earth elements in whole rock pegmatites are as follows (table 4.3): La (0.14-192.0ppm), Nd (0.1-60.0ppm), Eu (0.1-2.16ppm), Sm (0.2-5.68ppm), Gd (0.04-4.8ppm), Ce (0.08-269.0ppm), Er (0.02-2.67ppm) and Yb (0.01-4.32ppm). REE abundance in feldspar extracts is low (0.2-58.4ppm). Selected rare earth elements in feldspar extracts ranged (table 4.15): La (0.25-20.40ppm), Nd (0.28-6.32ppm), Eu (0.1-0.75ppm), Sm (0.4-1.06ppm), Gd (0.2-1.93ppm), Ce (0.12-28.20ppm), Er (0.02-0.3 ppm) and Yb (0.02-0.31ppm).

REE abundance in muscovite extracts is low (0.2-3.5ppm). Selected rare earth elements in feldspar extracts ranged (table 18): Nd (0.05-0.35ppm), Sm (0.1-0.21ppm), Gd (0.02-0.5ppm), Ce (0.13-28.20.0ppm), Er (0.02-0.3 ppm) and Yb (0.02-0.31ppm). For biotite extracts, REE abundance is low (0.2-58.4ppm). Selected rare earth elements in biotite extracts ranged (table 18): La (0.25-20.40ppm), Nd (0.28-6.32ppm), Eu (0.1-0.75ppm), Sm (0.4-1.06ppm), Gd (0.2-1.93ppm), Ce (0.12-0.64ppm), Er (0.02-0.3 ppm), Yb (0.04-0.25ppm) and Yb (0.04-0.25ppm).

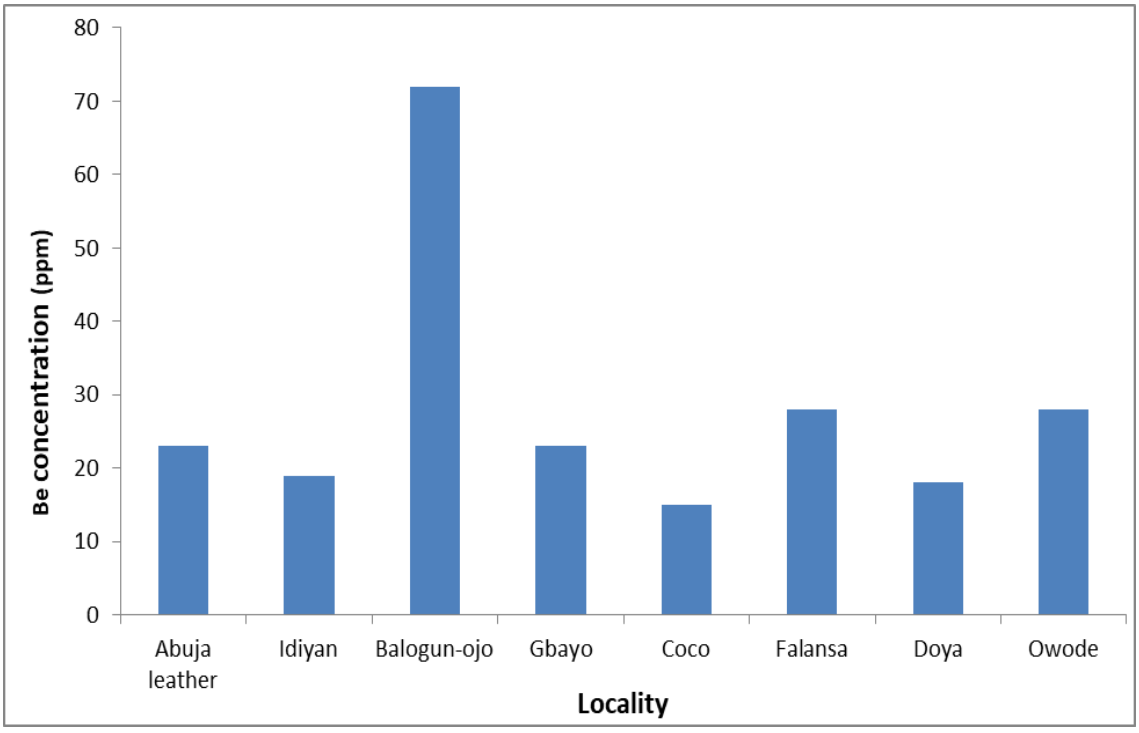

Figure 4.36: Be concentration in muscovites from the different locations

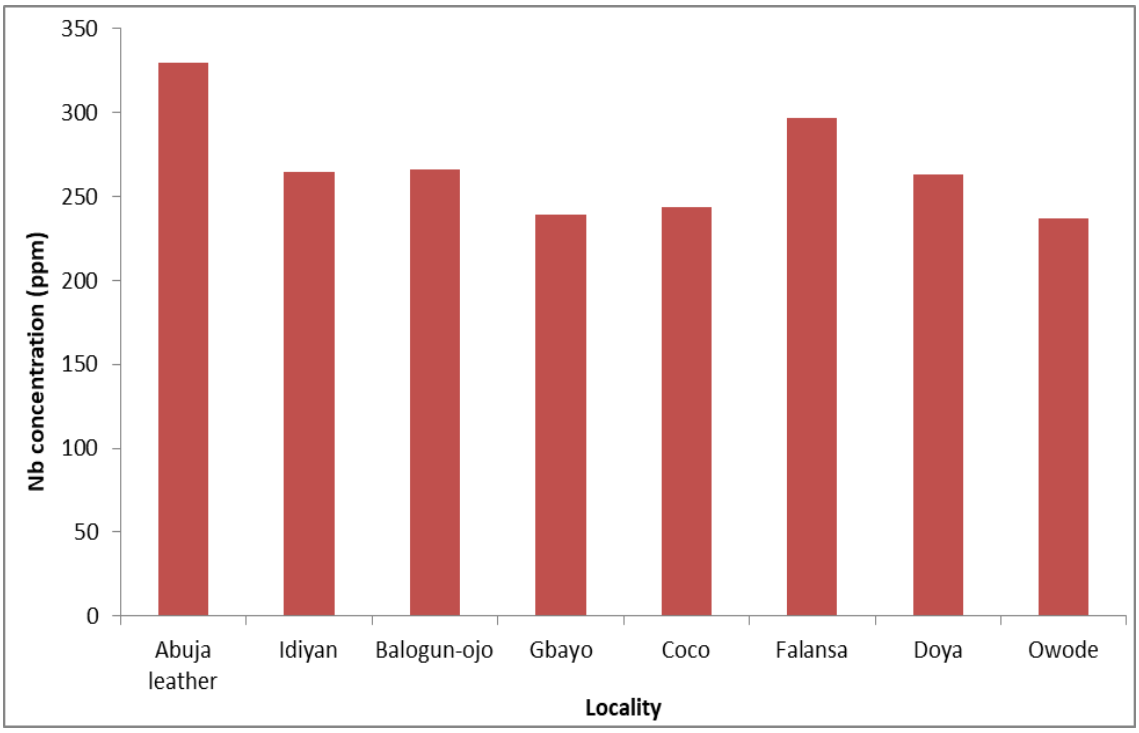

Figure 4.37: Nb concentration in muscovites from the different locations

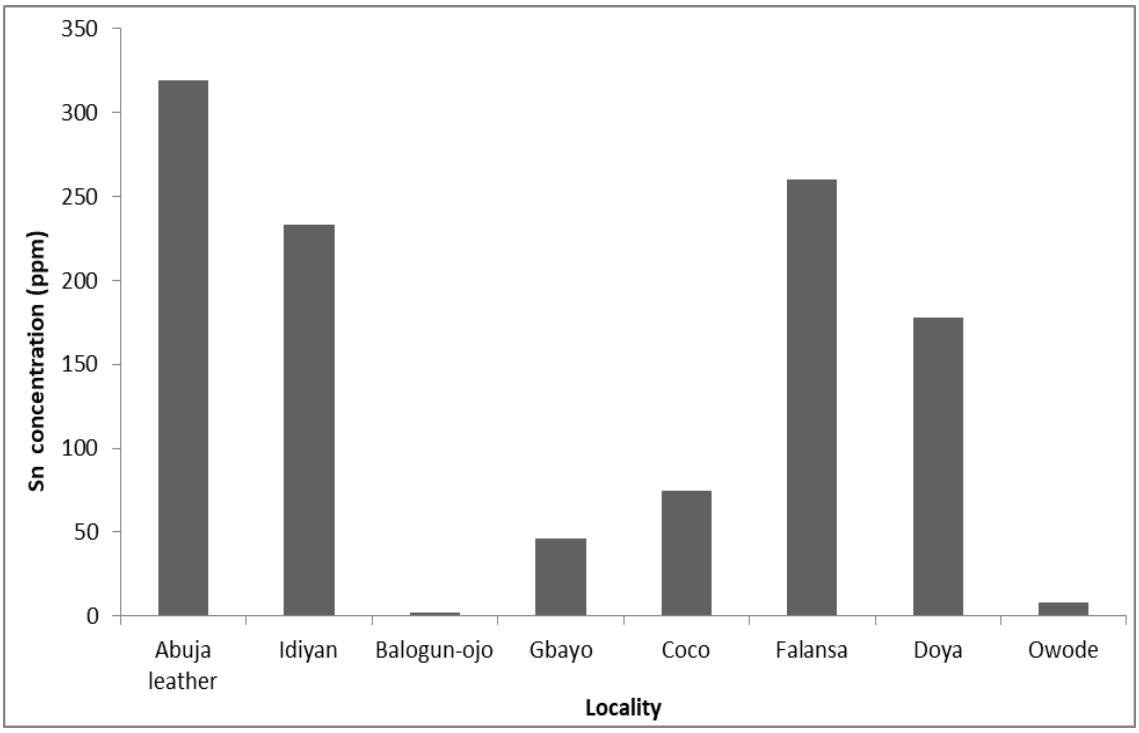

Figure 4.38: Sn concentration in muscovites in the different locations

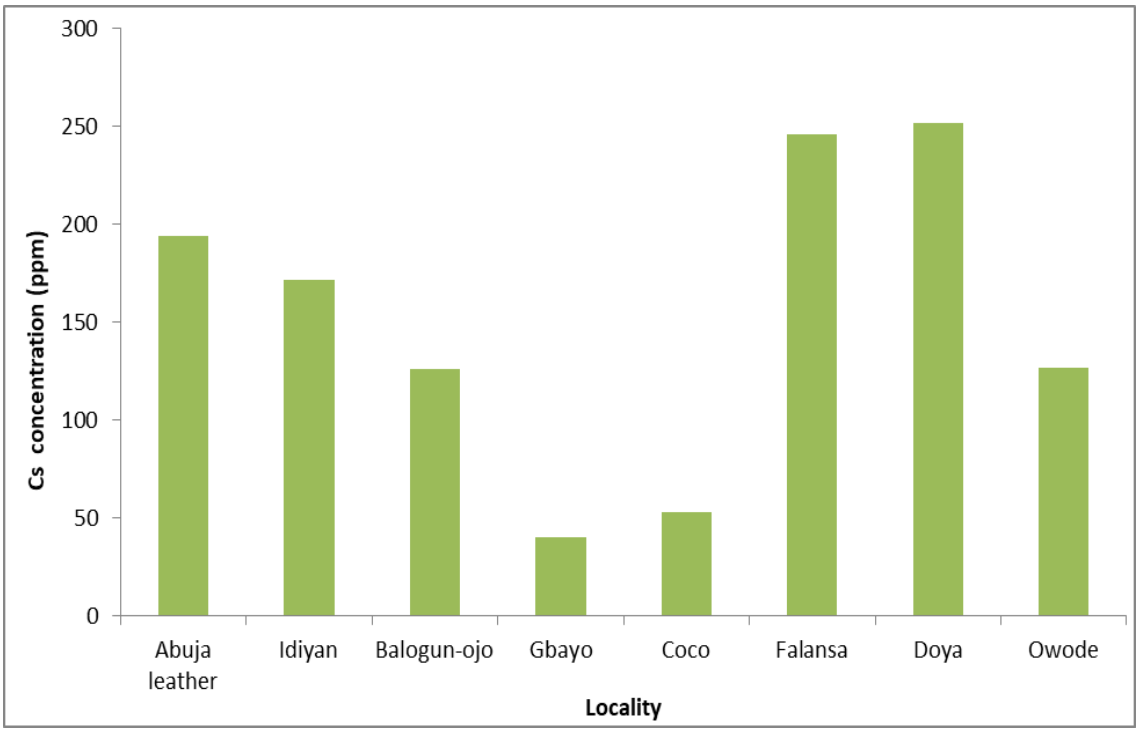

Figure 4.39: Cs concentration in muscovites in the different locations

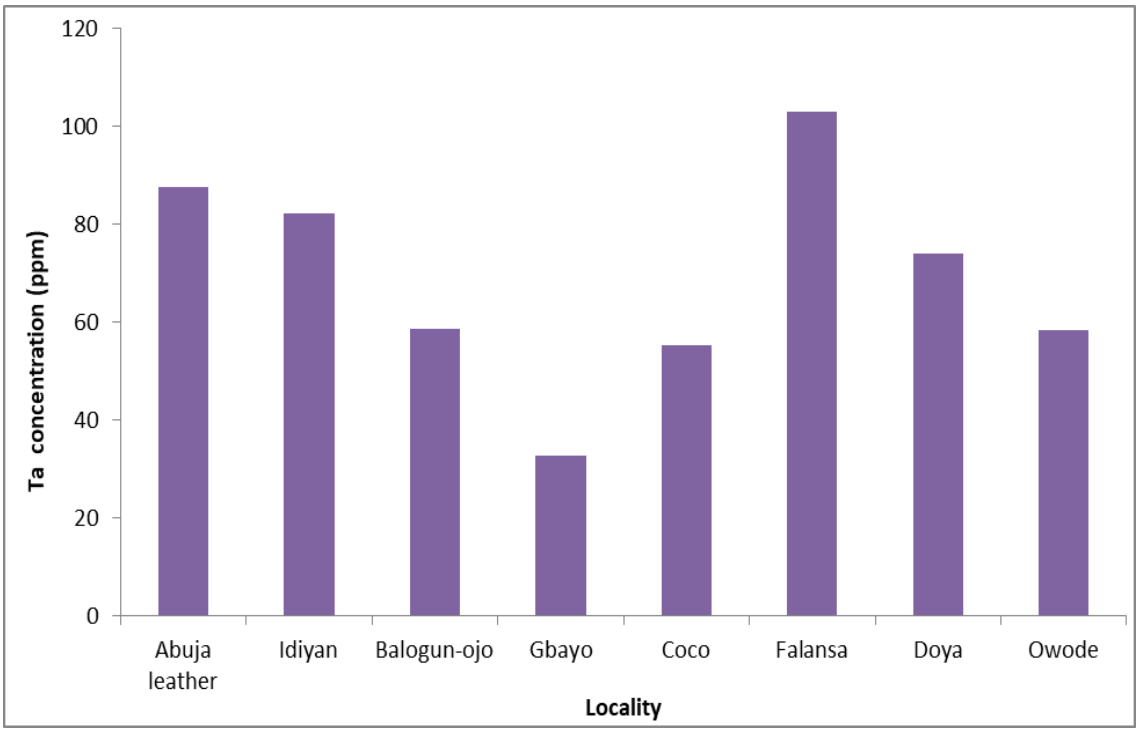

Figure 4.40: Ta concentration in muscovites in the different locations

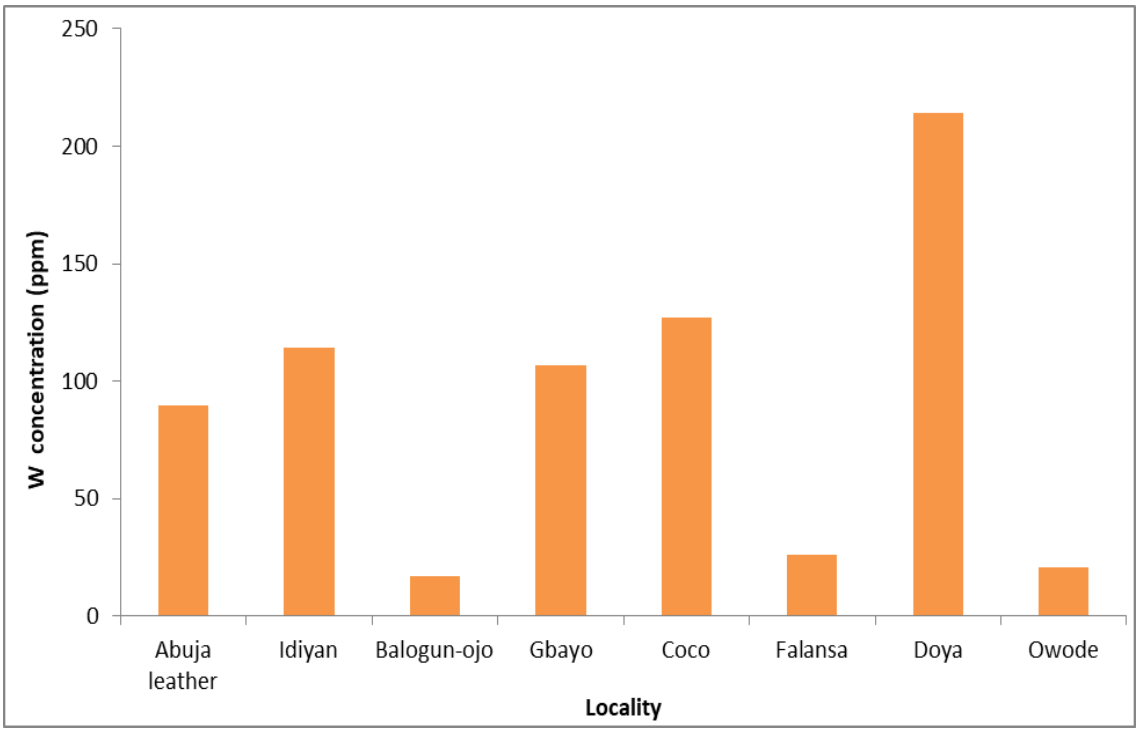

Figure 4.41 W concentration in muscovites in the different locations

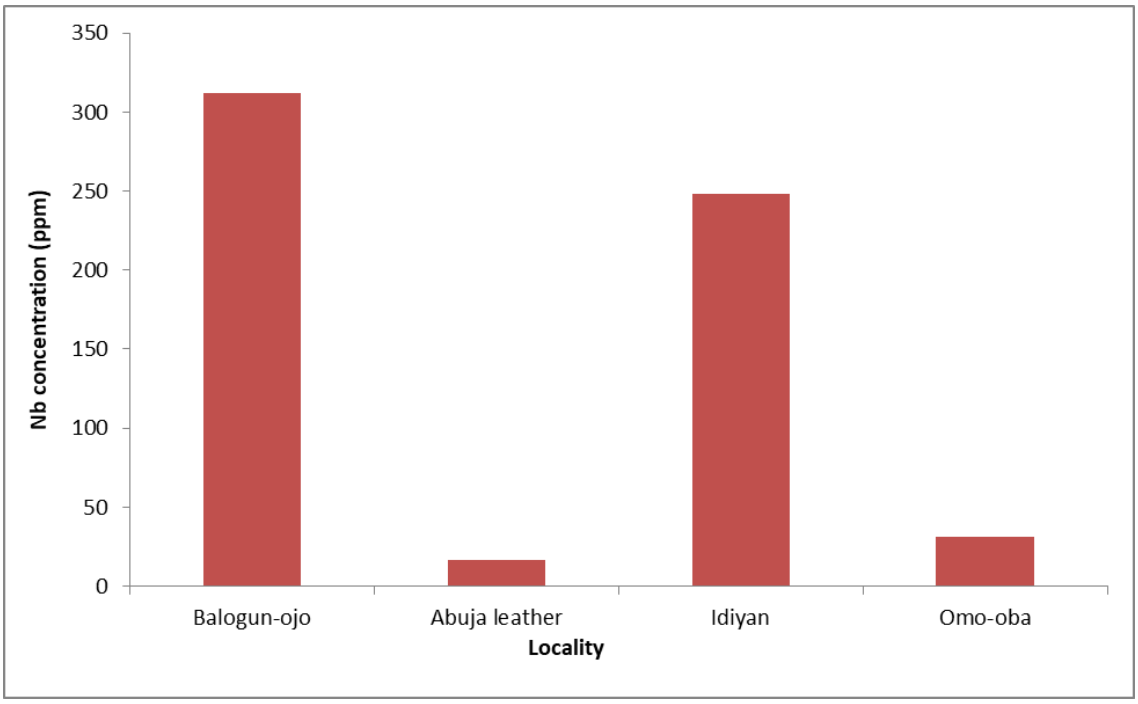

Figure 4.42: Nb concentration in biotite extracts in the different locations

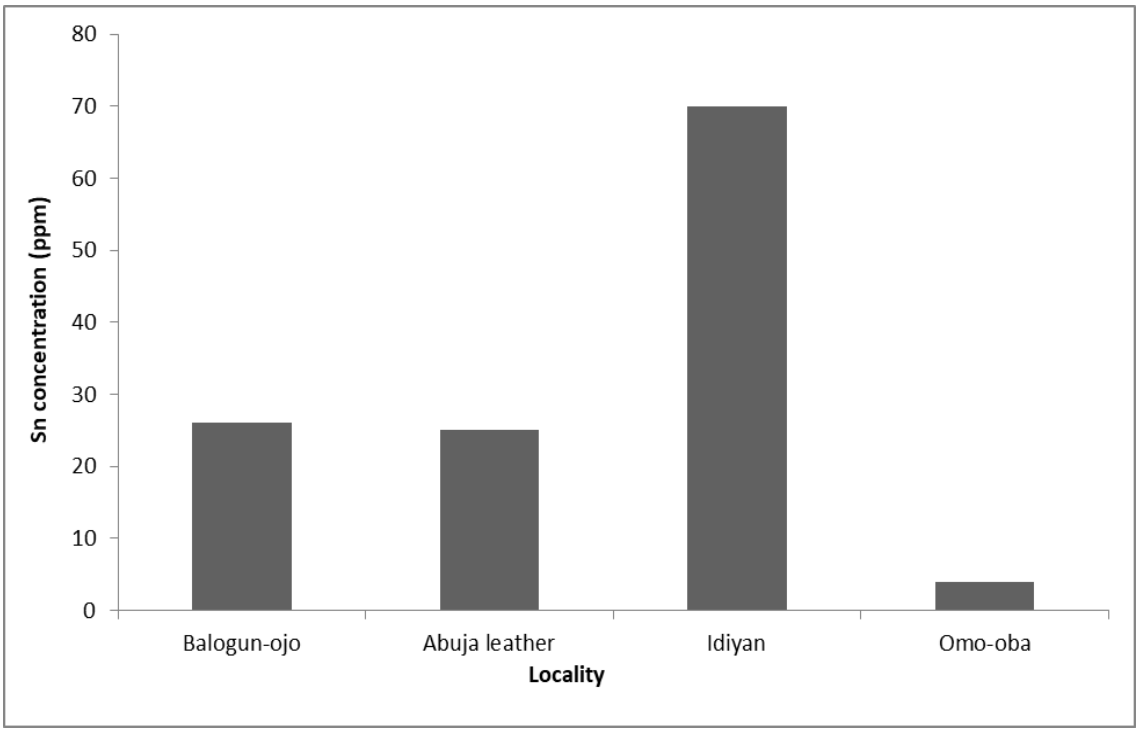

Figure 4.43: Sn concentration in biotite extracts in the different locations

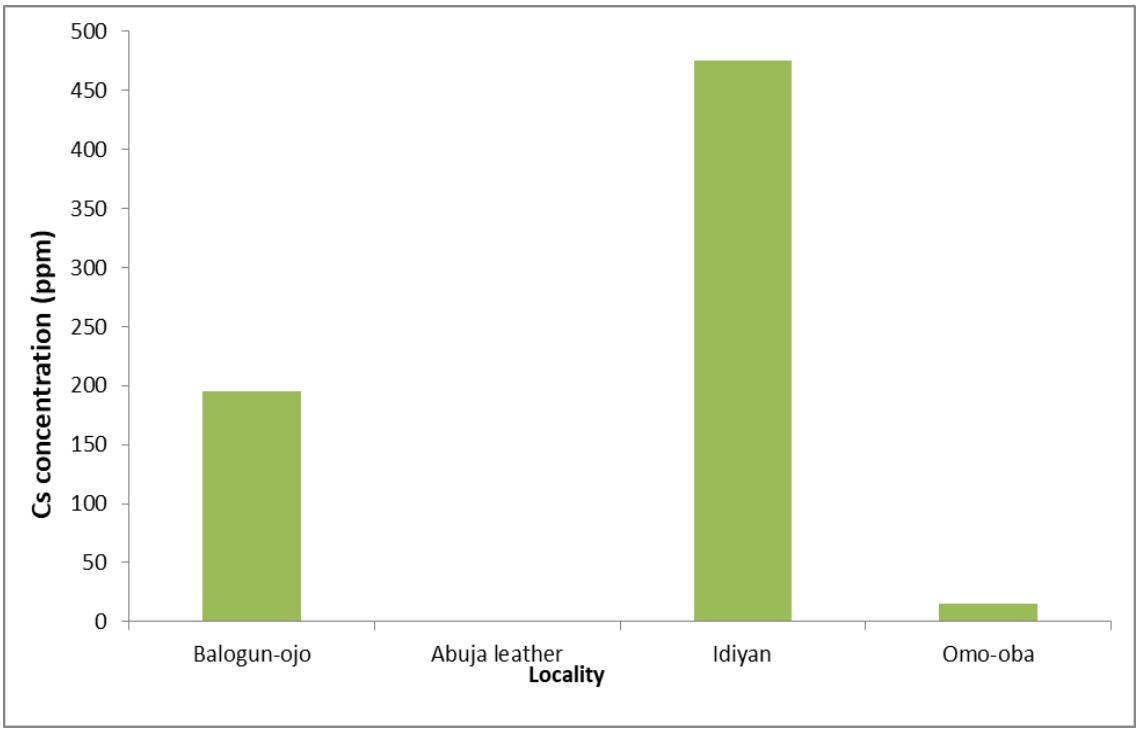

Figure 4.44: Cs concentration in biotite extracts in the different locations

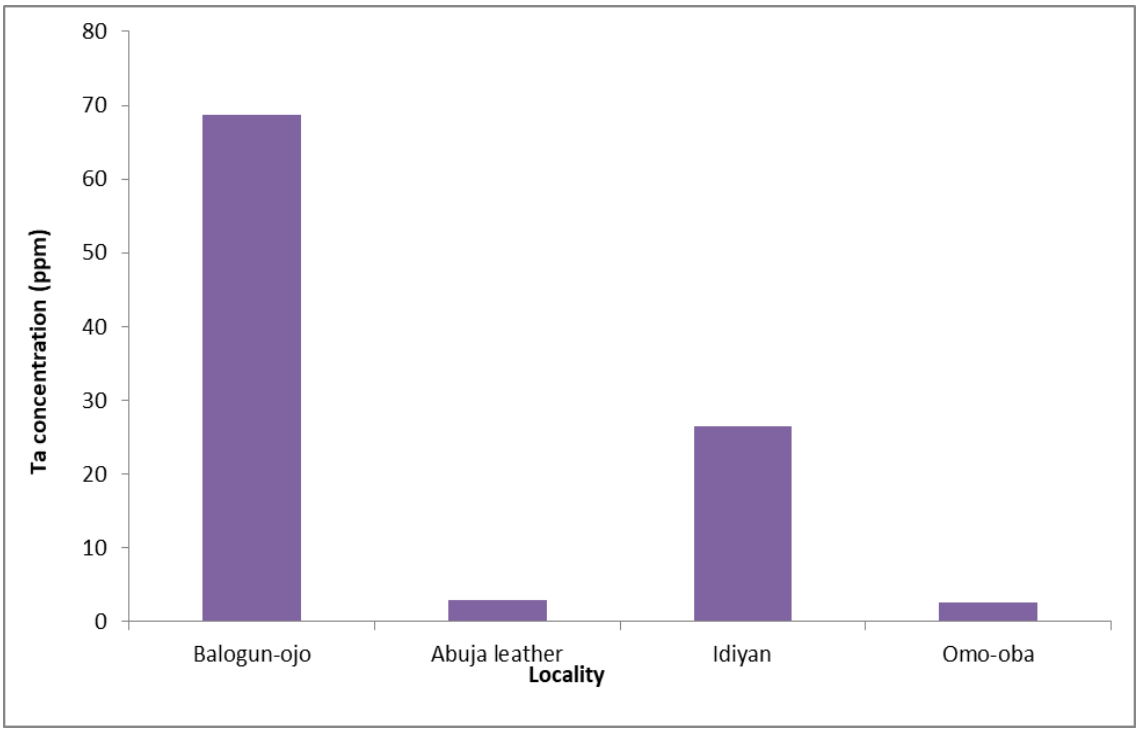

Figure 4.45: Ta concentration in biotite extracts in the different locations

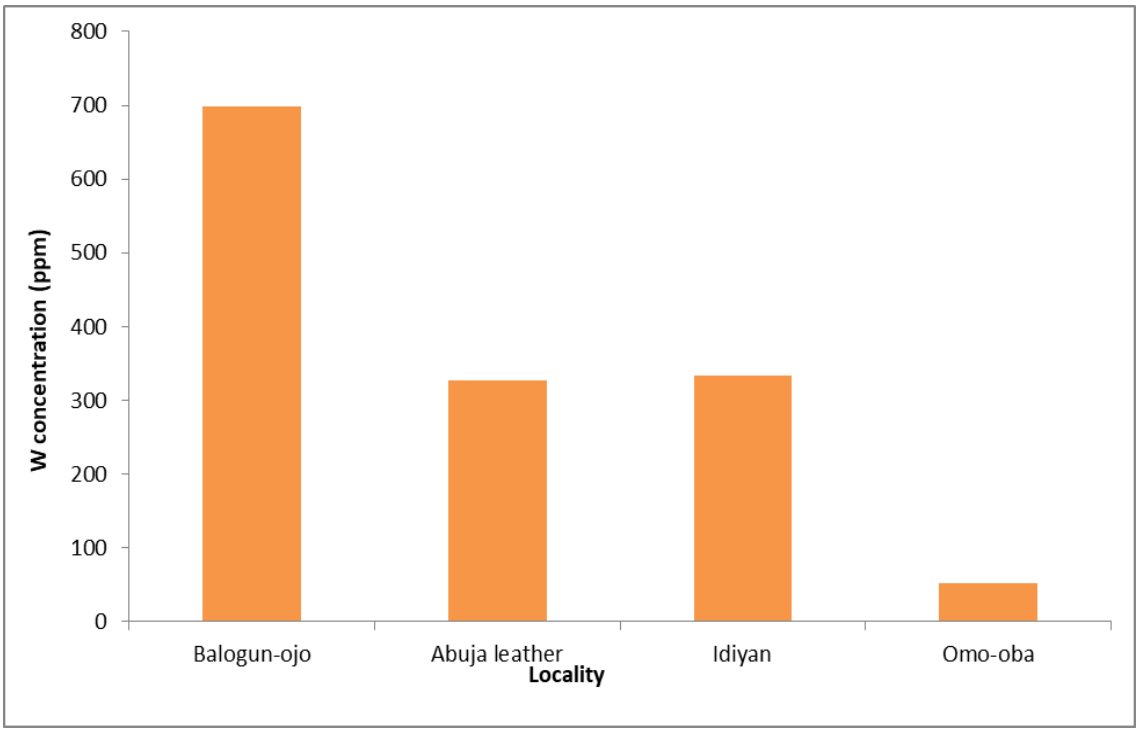

Figure 4.46: W concentration in biotite extracts in the different locations

4.2.1.4: Comparison of selected trace elemental concentrations in whole rock, feldspars, biotite and muscovite extracts

Comparison of trace elemental concentration of Sn, Zn, W, Ta, Nb and Cs was also carried out to assess the mineralisation pattern of these elements within the different sample types analysed. Trace elemental plots of samples from Balogun-Ojo (figures 4.47-4.48) revealed higher concentration of Cs, Ta and Nb in the biotite and muscovite extracts. Feldspars and whole rocks have lower concentration of Cs, Ta and Nb; W concentration showed no preference for any mineral phase while higher concentration of Zn was observed in biotite and muscovite extracts.

In Abuja-leather samples, elevated concentrations of Cs, Ta, Nb and Sn was observed in muscovite extracts compared to other extracts and whole rock samples, high concentration of Zn was observed in biotite extracts and W shows no preference for any mineral phase (figure 4.49-4.50).

Plots for whole rock pegmatites and extracts from Idiyan area revealed W has no preference for any mineral phase while Sn is elevated in the biotite and muscovite extracts. Elevated concentration of Zn was also observed in biotite extracts while elevated concentration of Cs and Nb was observed in biotites and muscovite extracts; feldspars extracts also revealed high Cs concentration (figure 4.51-4.52). In the Omo-Oba area, results also indicate elevated concentration of Nb, Cs and Zn in biotite extracts (figure 4.53-4.54).

Prefential enrichment of some elements observed in the biotite and muscovite extracts is possibly due to the ability of the micas to incorporate a wide range of rare elements by substitutions at various sites in its crystal structure (Belyankina and Petrov 1983; Bailey, 1984).

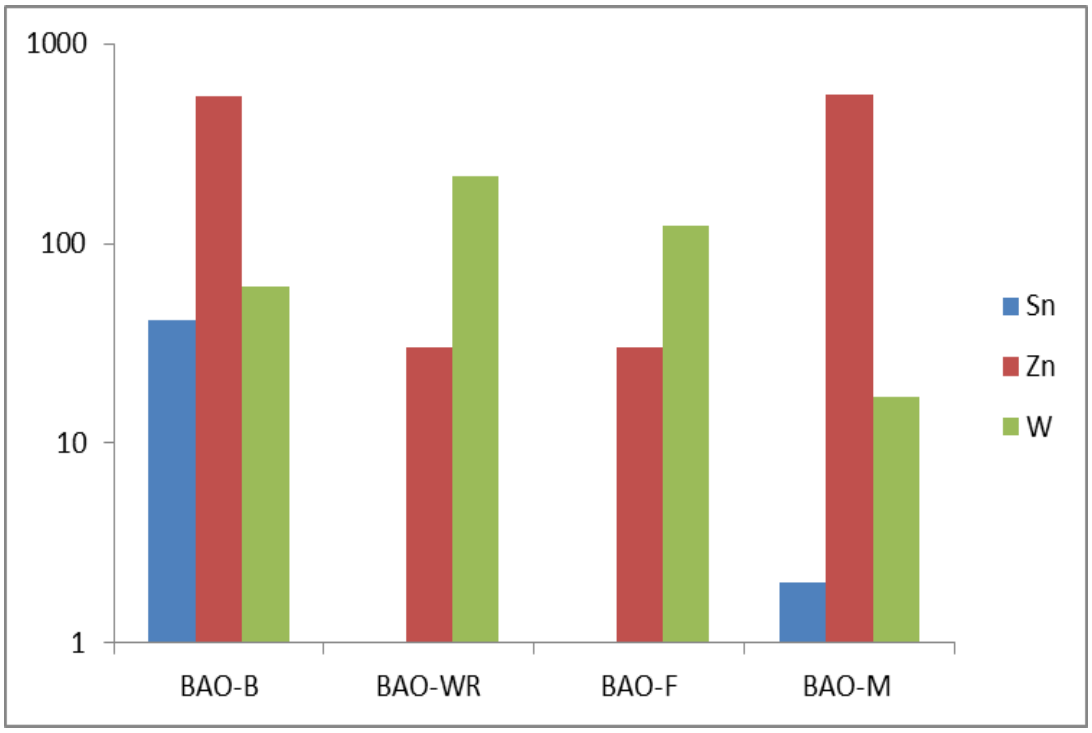

Figure 4.47: comparative plot of Sn, Zn and W for whole rock and mineral extracts in Balogun-Ojo sample

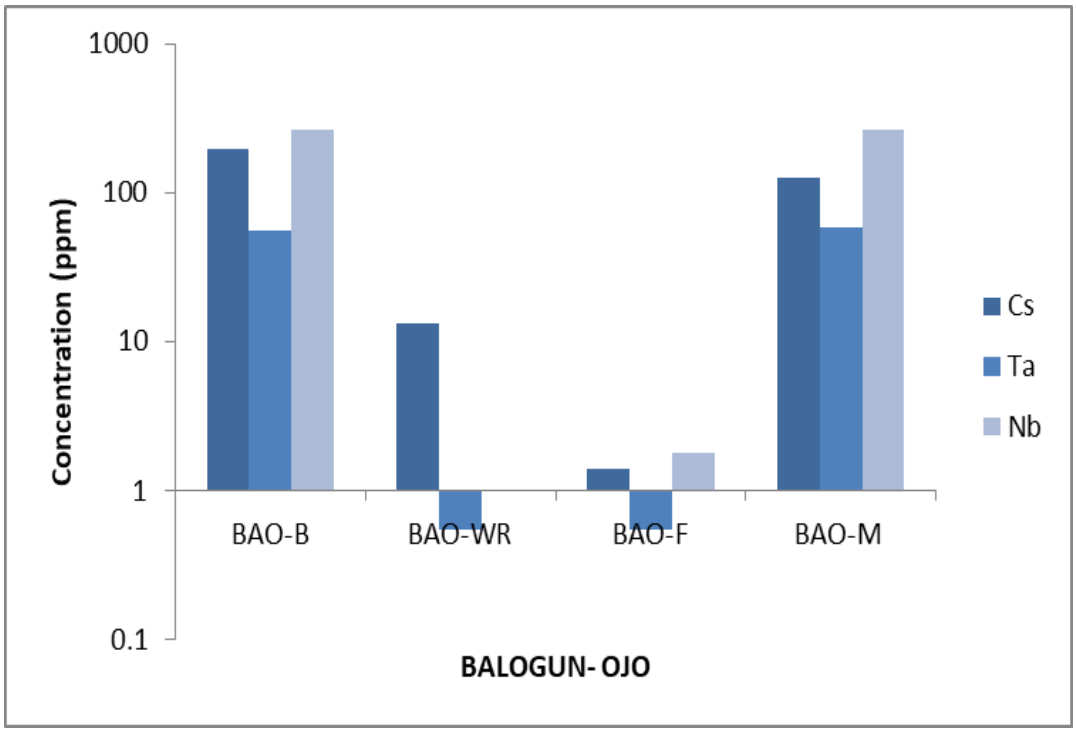

Figure 4.48: comparative plot of Cs,Ta and Nb for whole rock and mineral extracts in Balogun-Ojo sample

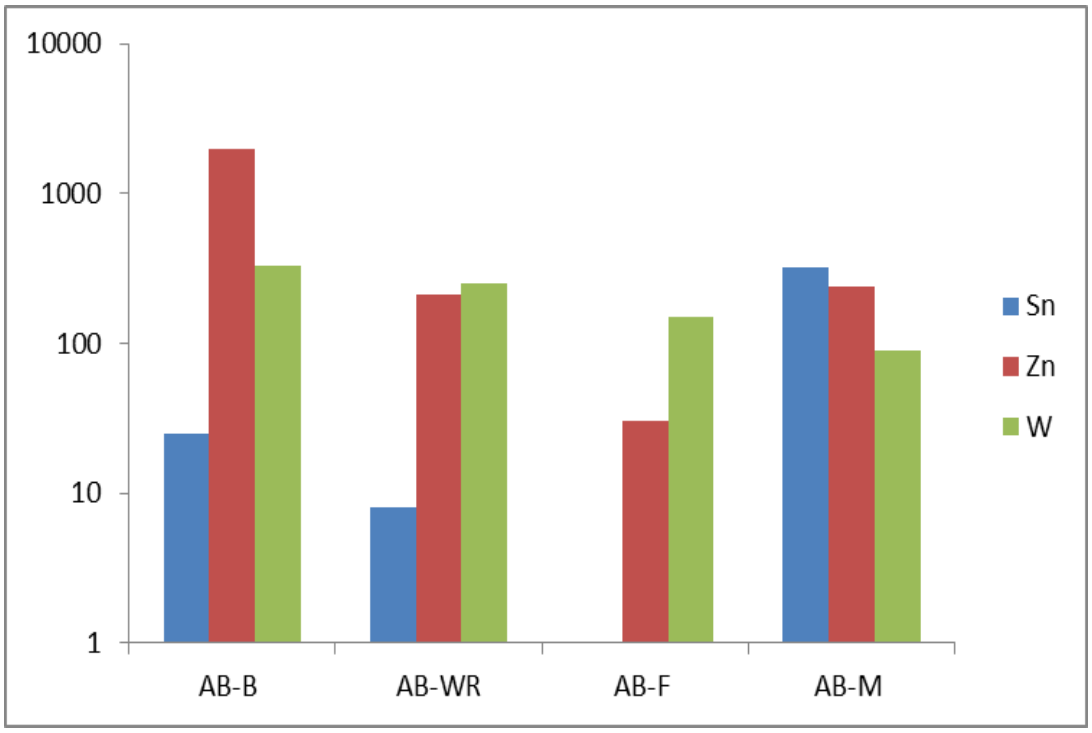

Figure 4.49: comparative plot of Sn, Zn and W for whole rock and mineral extracts in Abuja leather sample

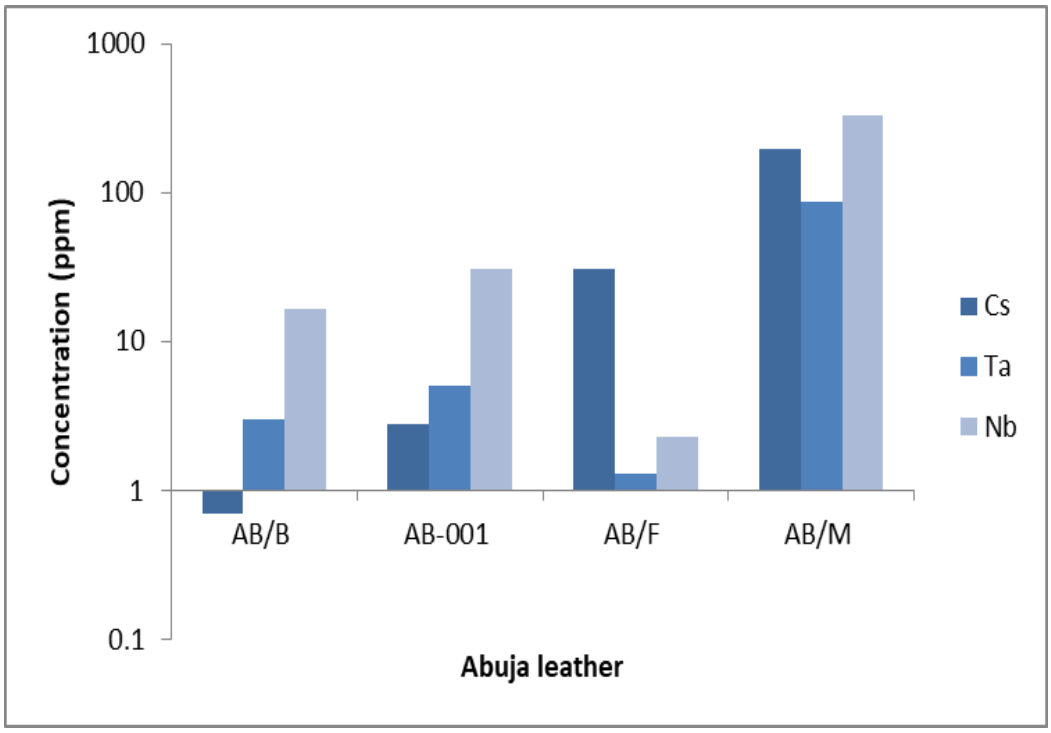

Figure 4.50: comparative plot of Cs, Ta and Nb for whole rock and mineral extracts in Abuja leather sample

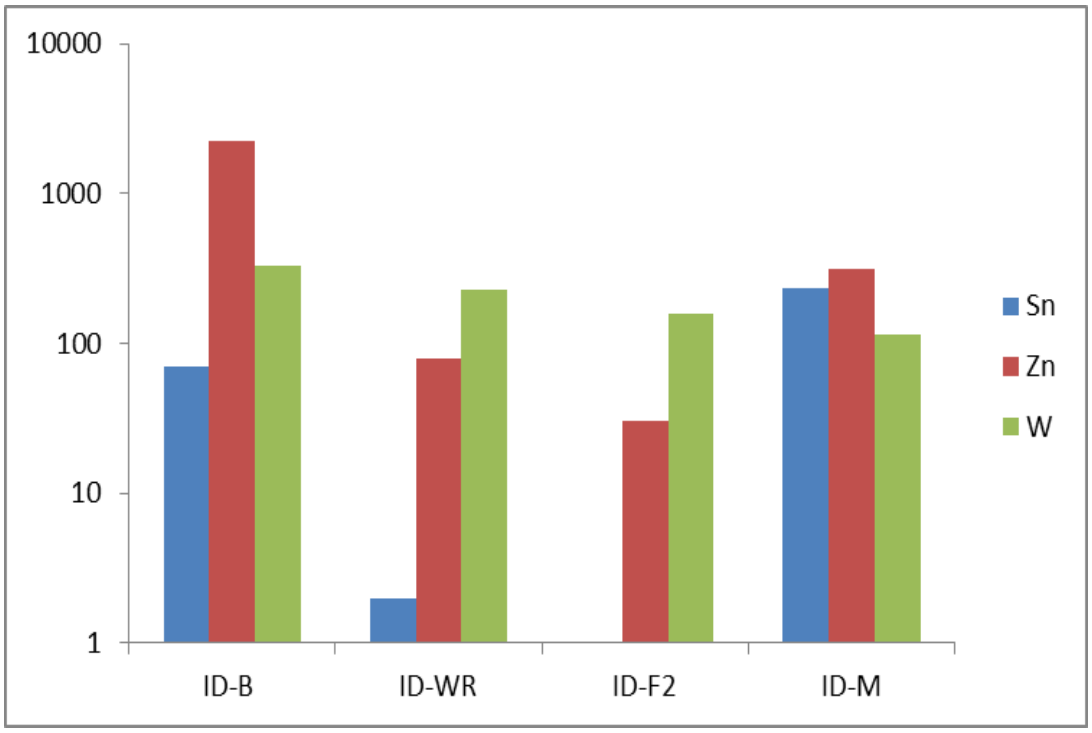

Figure 4.51: comparative plot of Sn, Zn and W for whole rock and mineral extracts in Idiyan sample

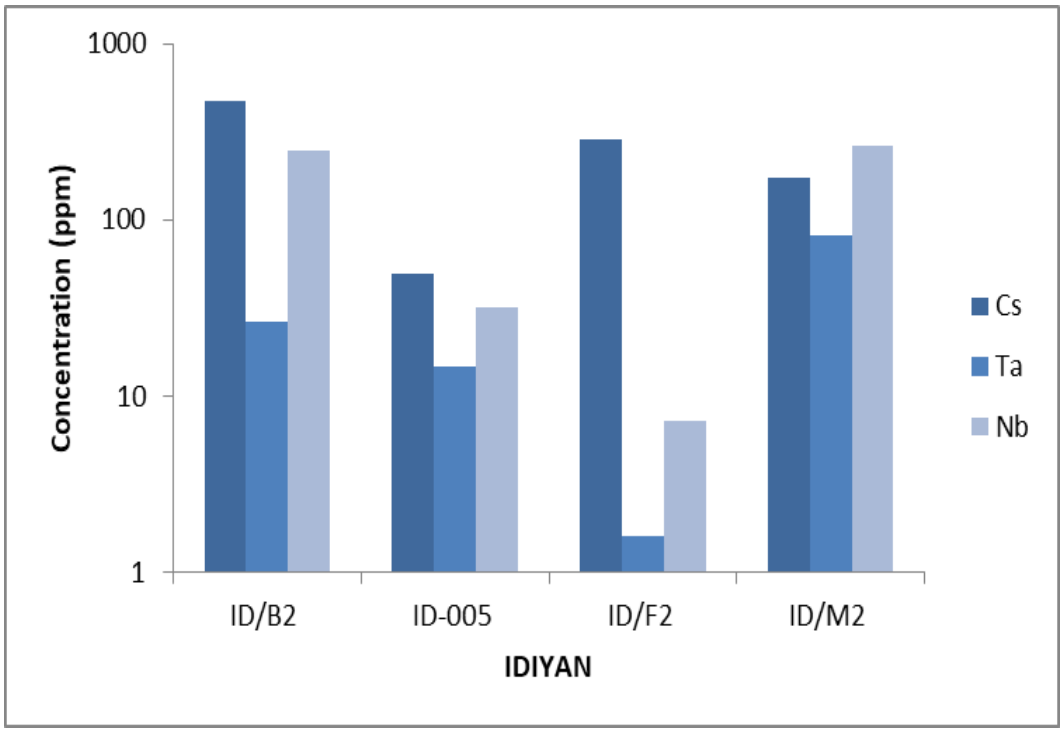

Figure 4.52: comparative plot of Cs, Ta and Nb for whole rock and mineral extracts in Idiyan sample

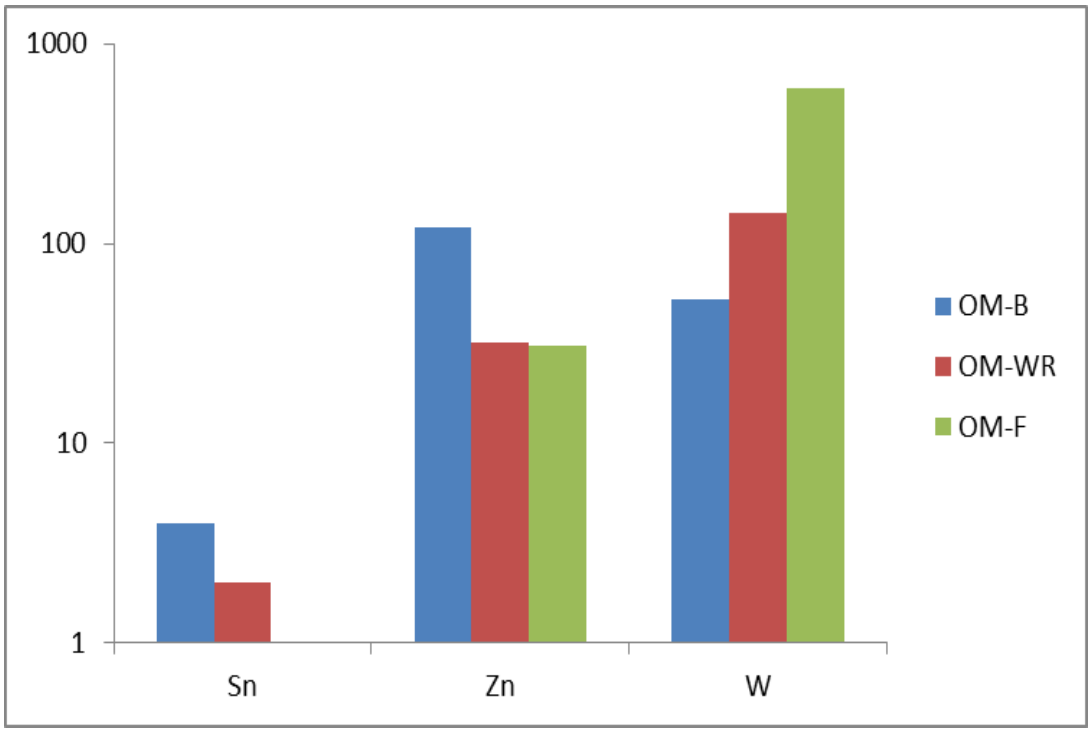

Figure 4.53: comparative plot of Sn, Zn and W for whole rock and mineral extracts in Om-Oba sample

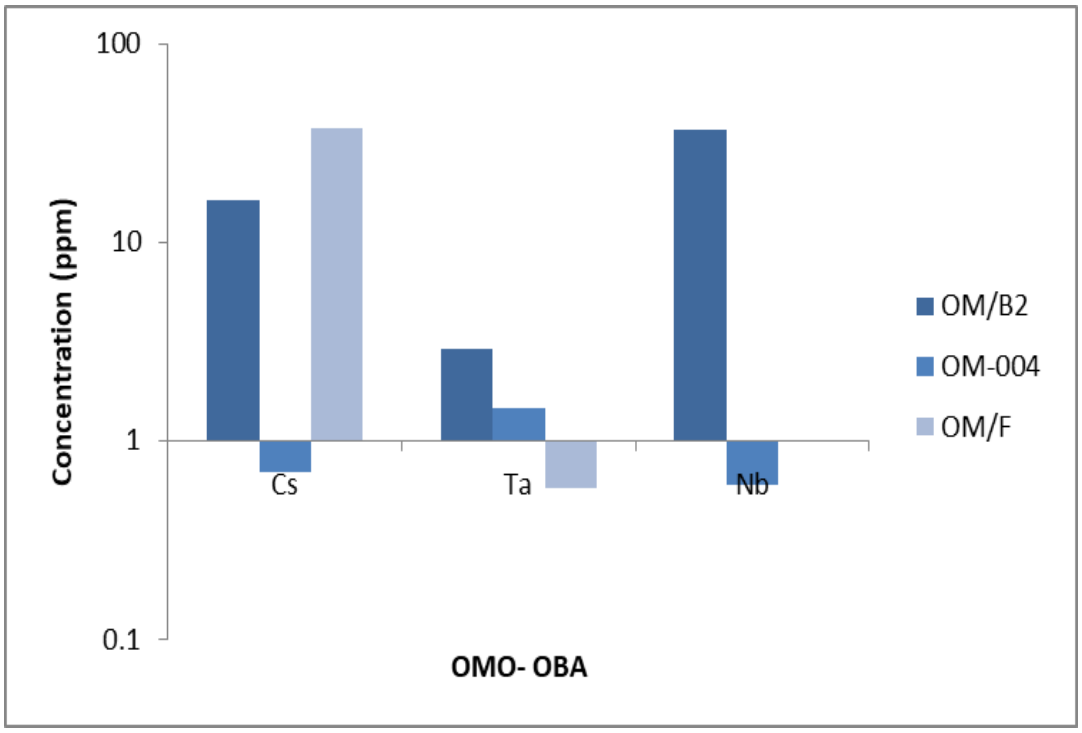

Figure 4.54: comparative plot of Cs, Ta and Nb for whole rock and minerals extracts in Omo-Oba sample

4.2.1.5: Discussion

Na_2O-Al_2O_3-K_2O ternary plot and the plot of A/NK against A/CNK revealed pegmatites are peraluminous with the aluminium saturation index (ASI) greater than 1.0 in all samples with the exception of the samples from Omoba and Idiyan which are metaluminous (figure 4.55-4.56).

High levels of fractionation of lithophilic elements (e.g. Rb, Cs) is believed to be a common characteristics of rare metal pegmatite (Garba, 2003) During late fractional crystallisation, there is a decrease in the K/Rb ratio hence the lower the K/Rb, the higher the degree of fractionation crystallisation and the more mineralised the pegmatites.

In this study, some pegmatites do not reveal chemical signatures associated with economically mineralised pegmatite which is delineated by K/Rb ratios, which is below 100 (Tischendorff, 1977). K/Rb ratios range from 26-353 in whole rock pegmatites with about eight of the samples studied having K/Rb ratios less than 100 and only one sample (Doya) revealing high fractionation with K/Rb values of 26 (table 4.16a-e). K/Rb vs Rb plots revealed pegmatites are un-mineralised pegmatites with the exception of the 'Doya" sample while the K/Rb vs Ba revealed that pegmatites mostly belong to the muscovite class. From the K/Rb vs Ba plot, pegmatites from Doya are rare element pegmatites while those of Idiyan, Balogun –Ojo, Falansa,Omo-Oba and Owode are muscovite class pegmatites.

The plot of Ta vs Ga shows that the pegmatites from the localities have low mineralisation potential with few of the pegmatite whole rock (Abuja leather, Coco, Doya and Falansa) and biotite samples (Abuja leather, Baba-ode and Doya) plotting above the Beus , (1966) mineralisation line; only one feldspar sample (Doya) reveals mineralisation potential while all muscovite mineral extracts plotted above the Ta-line of mineralisation of Beus, (1966) with some plotting above the Gordiyenko, (1971) mineralisation line. Preferential enrichment in muscovite and biotite extracts is believed to be due to the ability of the muscovite extracts to selectively accommodate certain elements in its crystal lattice during fractional crystallisation.

Similar observation was observed in the plot of Ta vs K/Cs and the Ta vs Cs + Rb plot; this further emphasises the low Ta-Nb mineralisation potential of the pegmatites studied (figure 4.57-4.59).

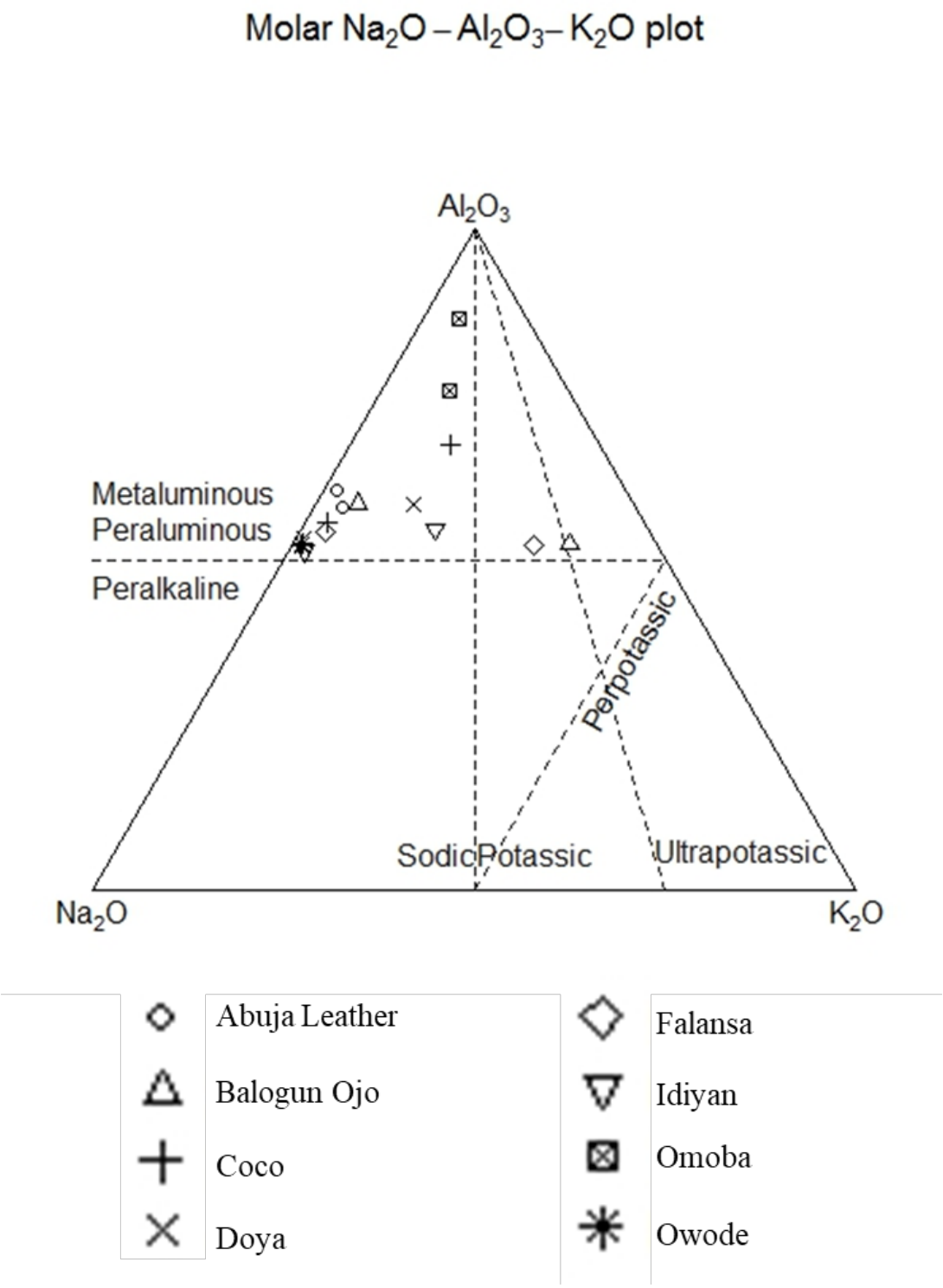

Figure 4.55: Ternary plot of Na_2O-Al_2O_3-K_2O.

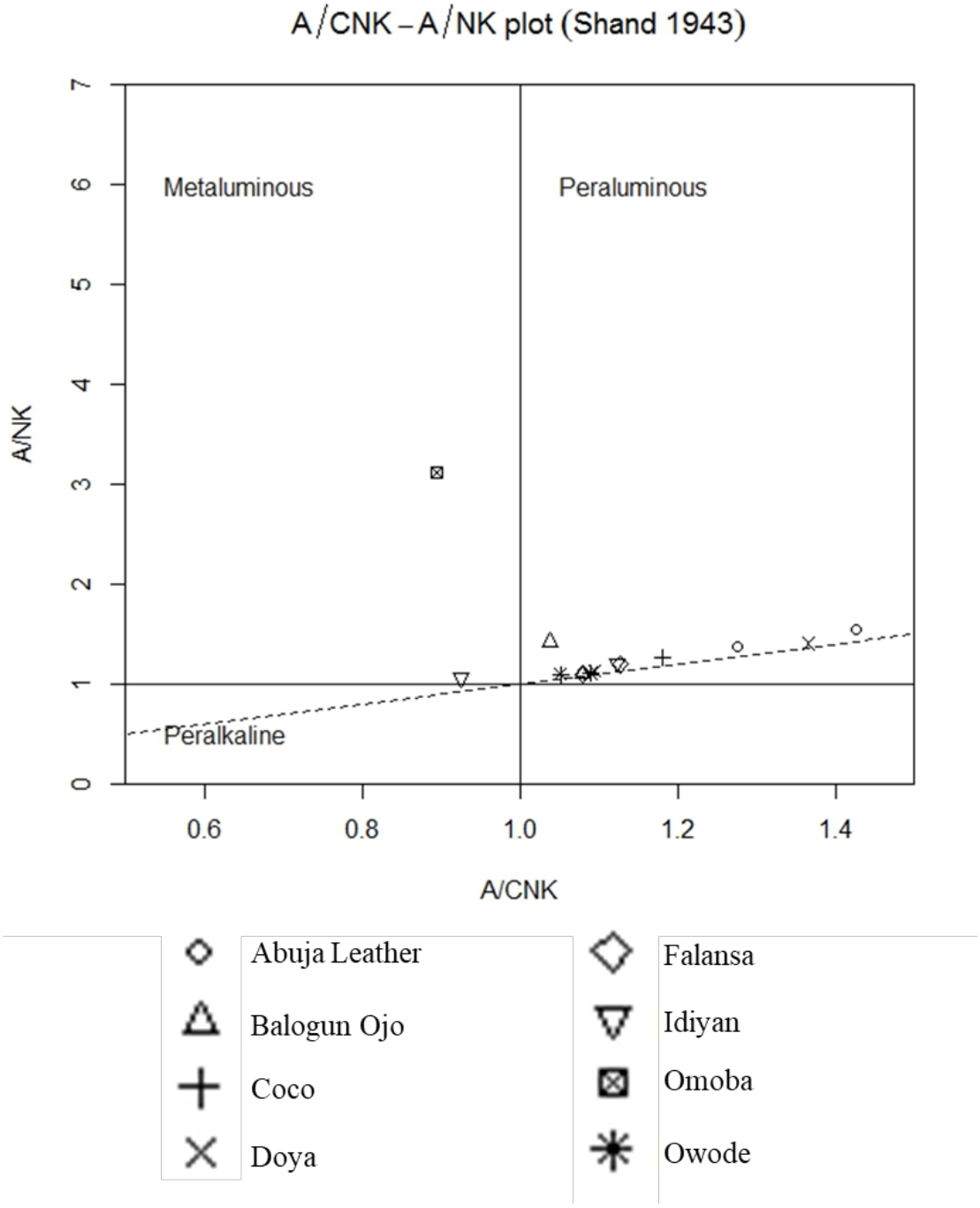

Figure 4.56: Plot of A/NK against A/CNK (after Shand 1943).

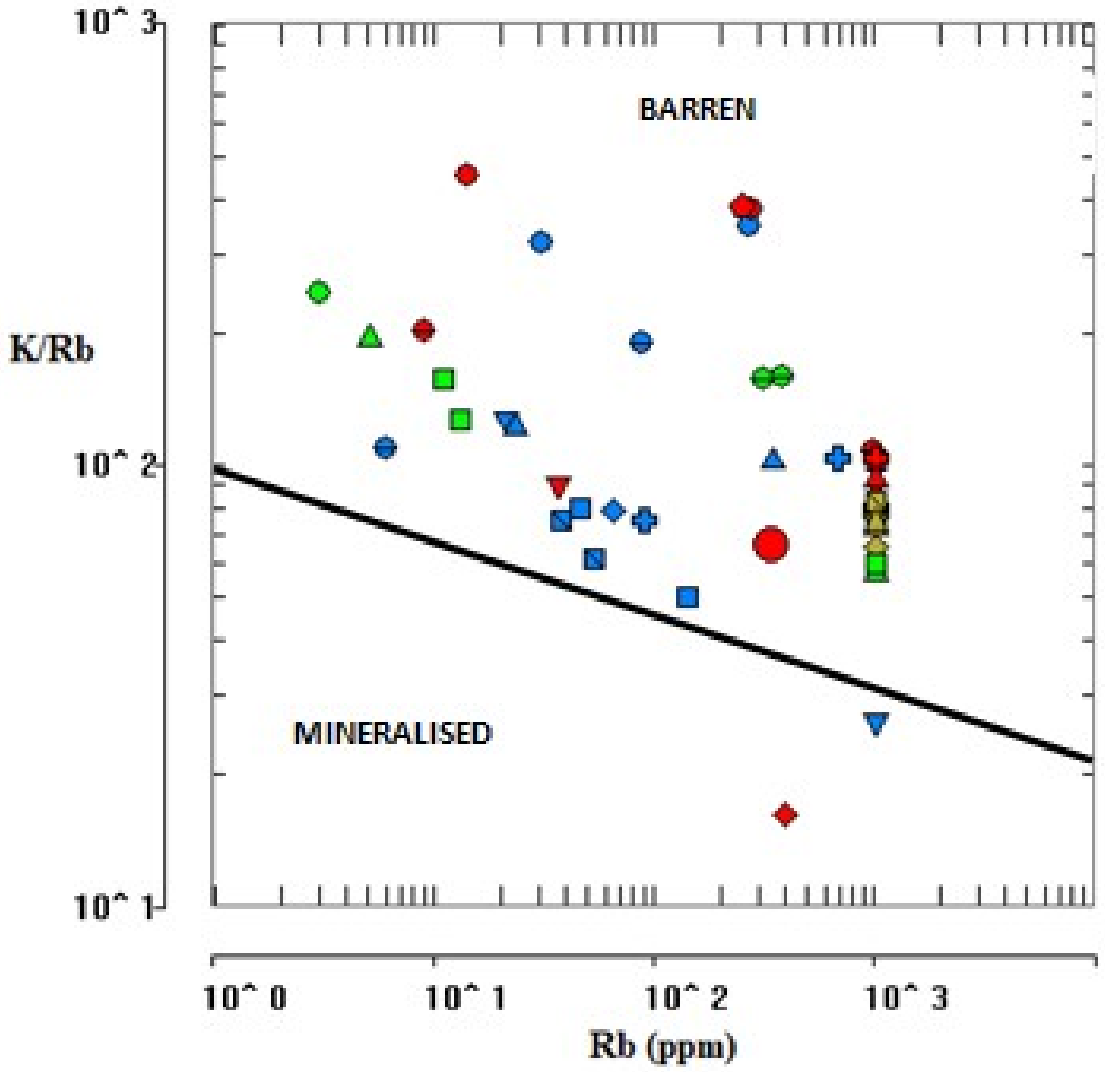

Figure 4.57: K/Rb vs Rb plot for pegmatite and extracts (modified after Staurov et al., 1966). Blue represents whole rock samples, red represents feldspar extracts, brown muscovite extracts and green biotite extracts

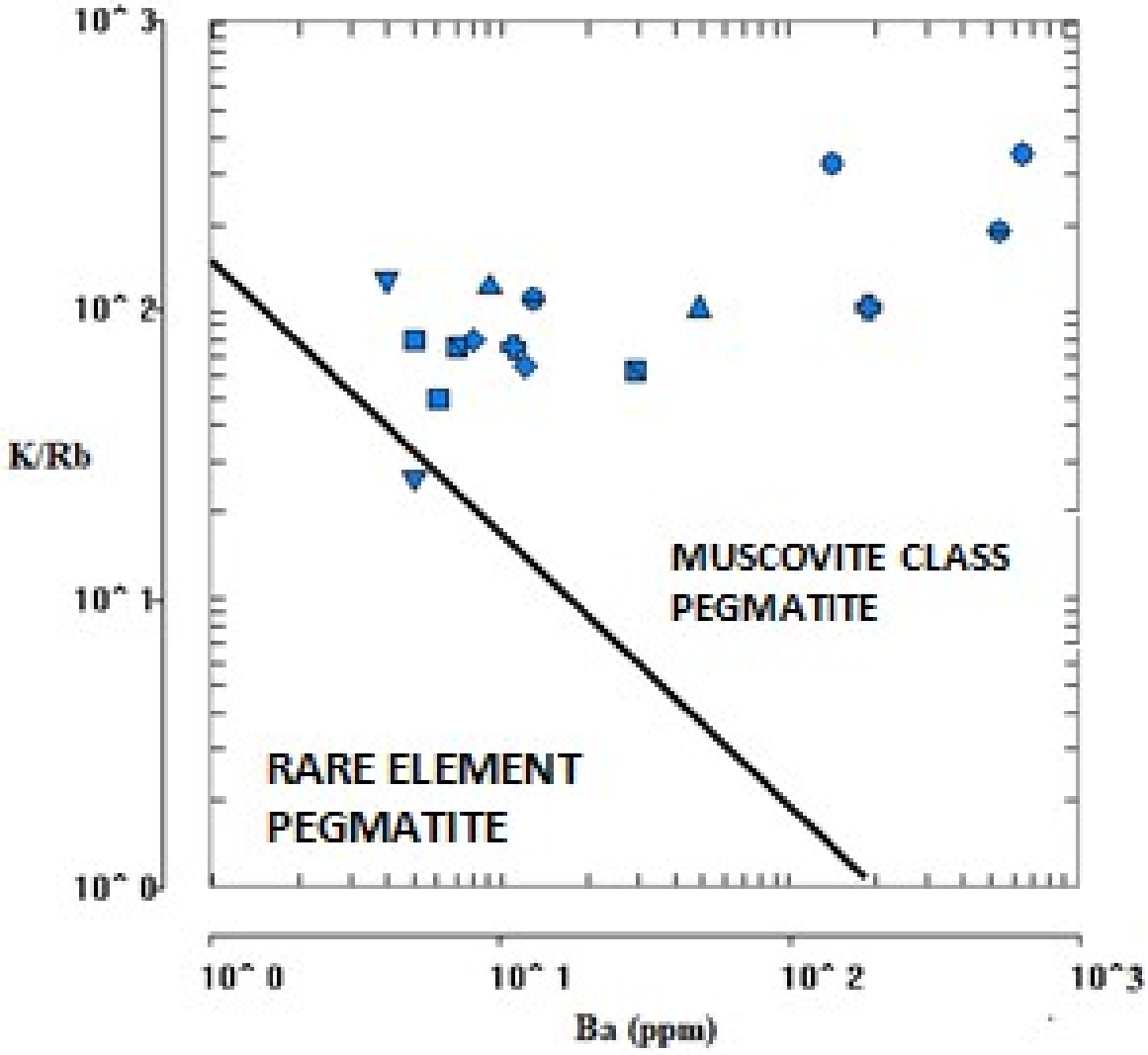

Figure 4.58: mineralisation potential and characterisation of the pegmatite (modified after Maniar and Piccoli, 1989)

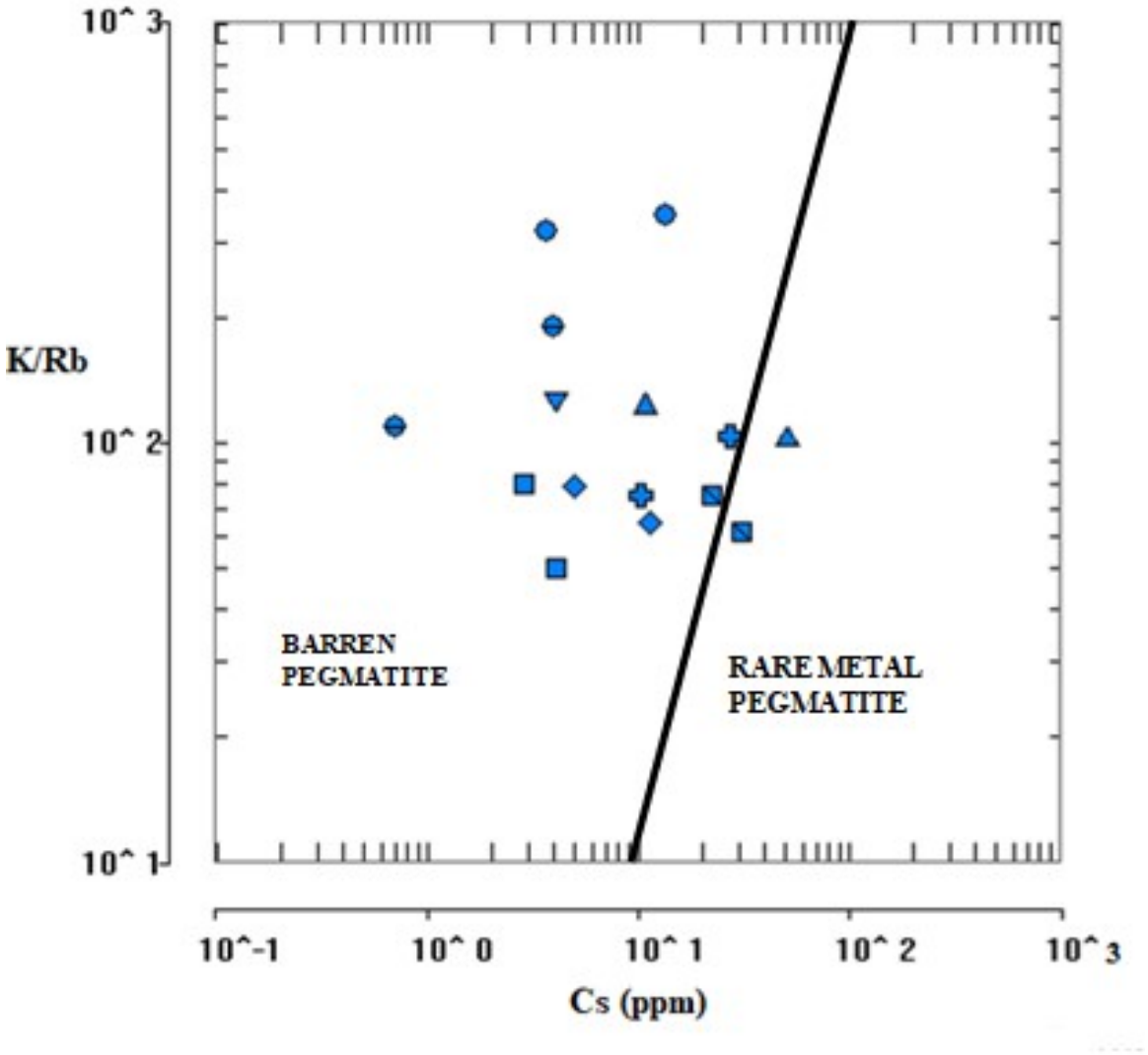

Figure 4.59: K/Rb vs Cs plot for pegmatites in the studied areas,

Table 4.16a: Elemental ratios of whole rock pegmatites and mineral extracts

Sample number	1	2	3	4	5	6	7	8	9	10
K/Rb	81	51	353	324	80	65	26	126	76	105
K/Ba	1.262	0.98	0.004	0.036	0.774	0.221	0.934	2.15	0.641	0.015
Ta/W	0.02	0.028	0.002	0.003	0.028	0.078	0.197	0.781	0.082	0.005
Zr/Hf	40	22.5	25	60	17.5	15.56	10	7.41	13.33	20
Ba/Rb	0.11	0.04	2.36	4.63	0.13	0.03	0.01	0.19	0.13	0.27
Rb/Sr	7.5	19.86	3.66	0.22	3.2	38.67	333.33	21	3.14	7.86
Rb/Cs	16.07	34.75	20.08	8.33	13.33	31.64	34.25	5.25	8.89	25.02
Nb/Ta	6	5.04	1.48	1.95	0.86	0.61	1.92	0.79	1.03	1.25
Th/U	0.08	3.9	0.43	6.41	0.21	1.79	1.55	1.47	0.14	0.03

Table 4.16b: Elemental ratios of whole rock pegmatites and mineral extracts

Sample number	11	12	13	14	15	16	17	18	19	20
K/Rb	126	105	111	191	63	76	110	203	104	456
K/Ba	0.603	0.093	0.007	0.005	0.35	1.264	0.016	0.014	0.013	0.131
Ta/W	0.015	0.064	0.002	0.007	0.572	0.052	0.005	0.002	0.008	0.004
Zr/Hf	11.54	10.83	20	39.52	9.15	10	40	20	30	60
Ba/Rb	0.39	0.14	2.17	6.08	0.55	0.19	0.17	1.89	0.18	4.79
Rb/Sr	1.05	12.04	2	0.69	13.25	7.4	12.89	1.13	10.31	0.11
Rb/Cs	2.17	6.79	8.57	22.05	1.78	1.71	25.24	10	32.57	10
Nb/Ta	3.63	2.18	0.41	7.74	1.14	0.61	1.72	0.85	1.8	3.27
Th/U	2.17	3.22	0.07	4.86	0.18	0.13	0.03	0.33	0.01	0.13

Table 4.16c: Elemental ratios of whole rock pegmatites and mineral extracts

Sample number	21	22	23	24	25	26	27	28	29	30
K/Rb	385	90	105	394	87	95	16	80	79	80
K/Ba	0.001	2.03	0.016	0.001	0.026	0.031	1.066	0.082	0.15	0.168
Ta/W	0.002	0.246	0.005	0.002	0.007	0.01	0.013	3.413	0.98	4.954
Zr/Hf	20	5.77	20	10	20	40	17.5	11.43	7.14	7.14
Ba/Rb	7	0.11	0.17	9.15	0.14	0.1	0.02	0.01	0.01	0
Rb/Sr	2.37	18	13.94	1.89	23.81	27.78	22.29	200	142.86	125
Rb/Cs	23.95	10.29	32.21	38	2.85	3.51	32.12	7.94	5.15	4.03
Nb/Ta	1.88	0.89	2.24	3.47	6.02	4.44	2.35	4.53	3.76	2.82
Th/U	0.09	0.34	0.01	0.05	0.04	0.06	0.23	0.06	0.05	0.03

Table 4.16d: Elemental ratios of whole rock pegmatites and mineral extracts

Sample number	31	32	33	34	35	36	37	38	39	40
K/Rb	76	66	75	78	79	81	74	78	84	77
K/Ba	0.029	0.082	0.012	0.011	0.012	0.132	0.027	0.011	0.072	0.033
Ta/W	0.723	0.436	1.388	0.492	0.307	3.977	1.291	0.346	2.83	0.591
Zr/Hf	7.14	13.33	6.67	30	30	7.14	6.67	10	13.33	5.71
Ba/Rb	0.03	0.02	0.08	0.06	0.05	0.01	0.03	0.08	0.01	0.03
Rb/Sr	71.43	166.67	66.67	166.67	200	125	71.43	58.82	200	71.43
Rb/Cs	5.81	18.8	4.63	22.32	24.88	4.07	5.78	3.97	7.87	5.46
Nb/Ta	3.22	4.4	2.75	6.84	7.29	2.88	3.34	3.55	4.07	3.97
Th/U	0.08	0.18	0.15	0.02	0.02	0.03	0.12	0.12	0.02	0.15

Table 4.16e: Elemental ratios of whole rock pegmatites and mineral extracts

Sample number	41	42	43	44	45	46	47	48
K/Rb	59	161	158	128	61	199	249	158
K/Ba	0.016	0	0.085	0.154	0.003	1.2	0.133	0.001
Ta/W	0.08	0.103	0.009	0.004	0.915	0.003	0.098	0.048
Zr/Hf	10	41.4	27.5	24	25	20	10	40.96
Ba/Rb	0.05	4.42	2	0.92	0.24	0.4	5.33	3.82
Rb/Sr	90.91	10.36	5.5	6.5	58.82	0.42	0.17	6.33
Rb/Cs	2.11	23.02	15.71	18.57	5.13	3.33	1.43	20.39
Nb/Ta	9.36	12.73	5.62	3.56	4.76	4.66	4.54	12.4
Th/U	0.48	17.68	0.43	0.96	0.62	0.05	17.16	14.45

Sample 1-16 are whole rock pegmatites. 17-27 are feldspar extracts, 28-40 are muscovite extracts and samples 41-48 are biotite extrcats

Fractionation degree of the pegmatites was also assessed using plots of Sr/Rb vs Rb/Ba and Rb/K vs. Sr/Rb (figure 4.60-4.61). The plots show the same trend for pegmatites in the locations with increasing fractionation. Furthermore, Nb/Ta ratio ranges from 0.41-7.74 in whole rock pegmatites, 0.85-6.02 in feldspar extracts, 2.35-7.29 in muscovite extracts and 3.54-12.73 in biotite extracts while Ta/W ranged 0.01-0.80 in whole rock pegmatites, 0.01-0.25 in feldspar extracts, 0.31-4.95 in muscovite extracts and 0.01-0.92 (table4.4) in biotite extracts which suggest the pegmatites whole rock and the extracts have higher concentration of Nb and W with respect to tantalum and could be more a Niobium and Tungsten prospect (figure 4.62-4.66).

Rare earth elemental normalisation pattern revealed two distribution patterns with no preferential enrichment of LREE or HREE.. Normalisation plots revealed no Ce anomalies but they revealed negative Europium anomaly is indicative of fractionation and late metasomatic effects (Taylor et al., 1986). Based on Eu/Eu* values and the presence/absence or Eu anomalies. Negative Eu anomalies was observed in all samples with K/Rb less than 100 and in just one sample with K/Rb value above 100. In this group of samples, Eu/EU* values ranged 0.04-0.65, with an average of 0.17 while in the samples with higher K/Rb values, Eu/Eu* values ranges from 0.90-3.03with an average of 1.48 which implies variable fractionation in the pegmatite studied.

In the other set of pegmatites with low K/Rb values, incompatible elemental plots revealed as expected, an enrichment in Cs, Rb, Ta, Nb relative to primordial mantle (values after Sun and McDonough, 1985) and a depletion in Ba, K and Sr. Enrichment in Rb, Cs, Ta and Nb with the depletion in K and Ba suggesting the pegmatites are formed as a result of progressive fractionation; and Rb enrichment coupled with Ba depletion is a due to late stage fractional crystallisation (figure 4.67-4.70).

In the other set of pegmatites, with high K/Rb values, negative Ce and negative Europium anomalies were not observed though some samples have a low positive Eu anomaly. It is inferred from the negative Eu and Ce anomalies that these pegmatites did not undergo considerable fractionation and they were not subjected to considerable metasomatism. For these samples, incompatible element plots revealed various patterns. It revealed a lower enrichment in Cs, Rb, Nb and in some cases Ta as well as lower depletions in Sr and Ba which suggests they were formed from a more unfractionated melt.

Furthermore, in pegmatites with low K/Rb ratios, (La/Yb)N ratios ranged 0.26-3.47 and they range 1.37-18.54 in pegmatites with higher K/Rb values which further indicates the difference in fractionation pattern between the two groups of pegmatites.

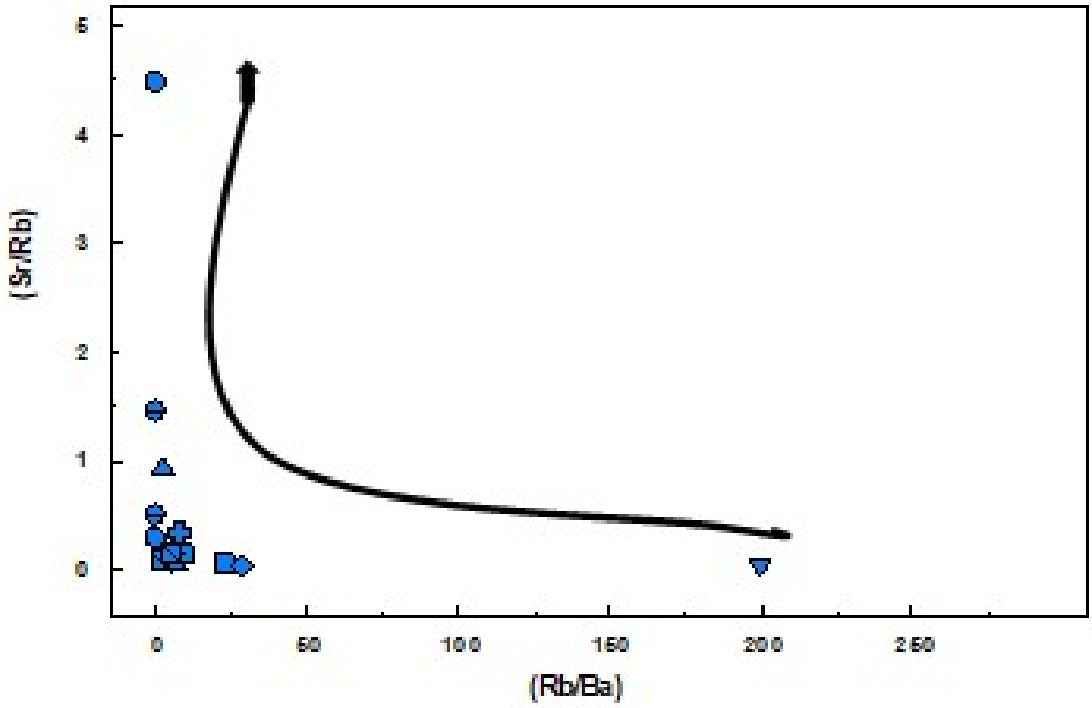

Figure 4.60: Relative degree of fractionation of pegmatites (after Larsen, 2002)

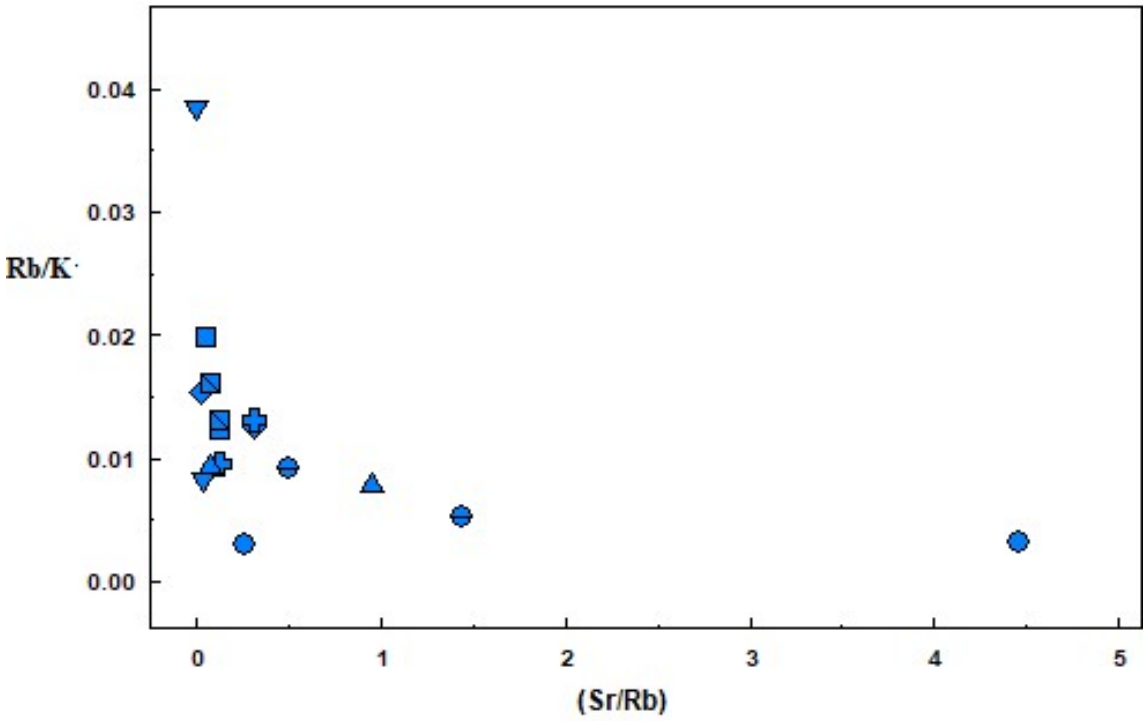

Figure 4.61: Relative degree of fractionation of pegmatites

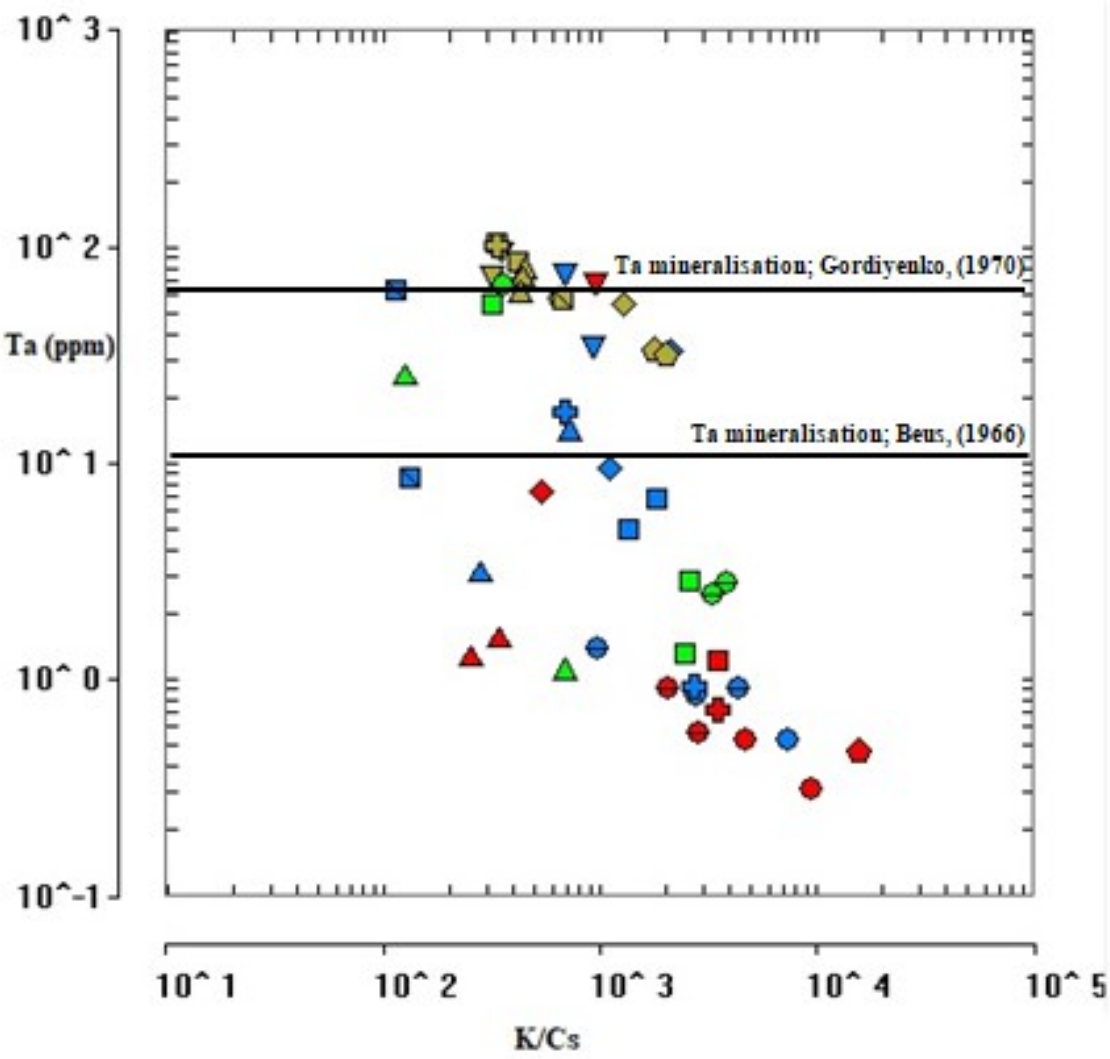

Figure 4.62: Plot of Ta vs K/Cs for pegmatite and extracts (modified after Beus, 1966 and Gordiyenko, 1977). Blue represents whole rock samples, red represents feldspar extracts, brown muscovite extracts and green biotite extracts

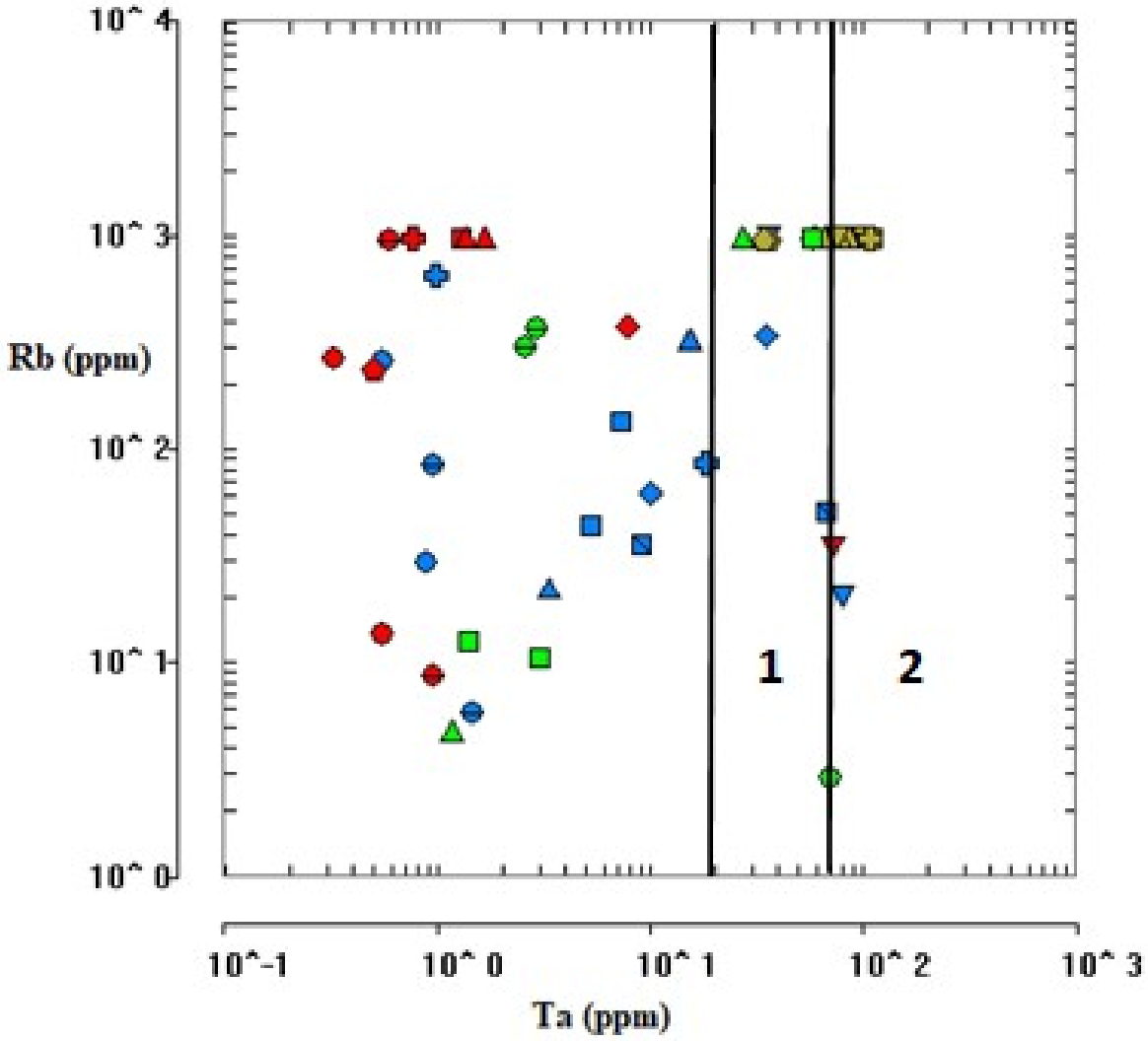

Figure 4.63: Plot Ta vs Rb for pegmatite and extracts modified after (modified after Beus, 1966 and Gordiyenko, 1977; a: Ta prospective; b: Ta mineralised) Blue represents whole rock samples, red represents feldspar extracts, brown muscovite extracts and green biotite extracts

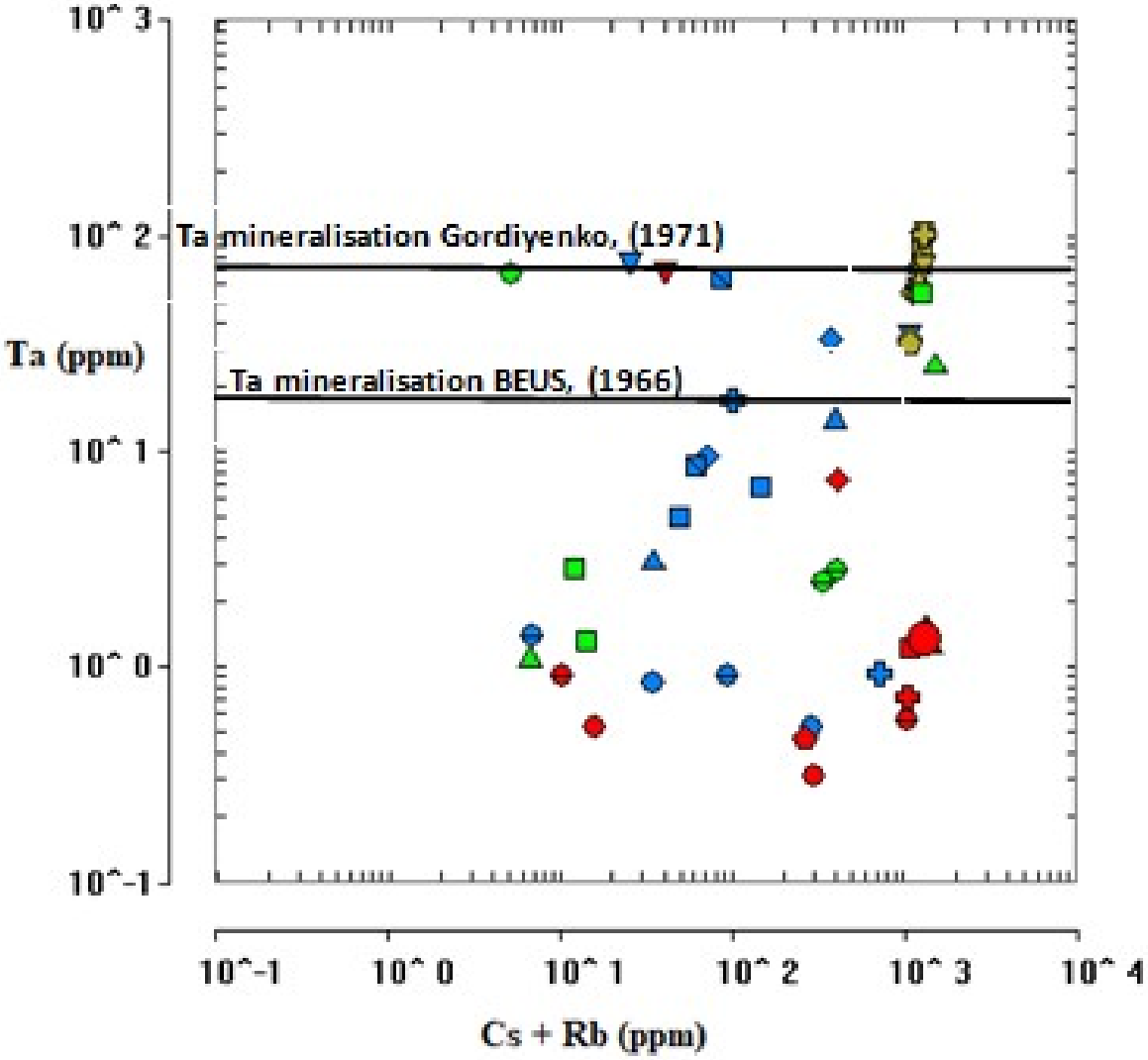

Figure 4.64: Plot of Ta (ppm) against Cs + Rb (ppm) for mineral extracts from the study areas (after Gaupp et al., 1984). Blue represents whole rock samples, red represents feldspar extracts, brown muscovite extracts and green biotite extracts

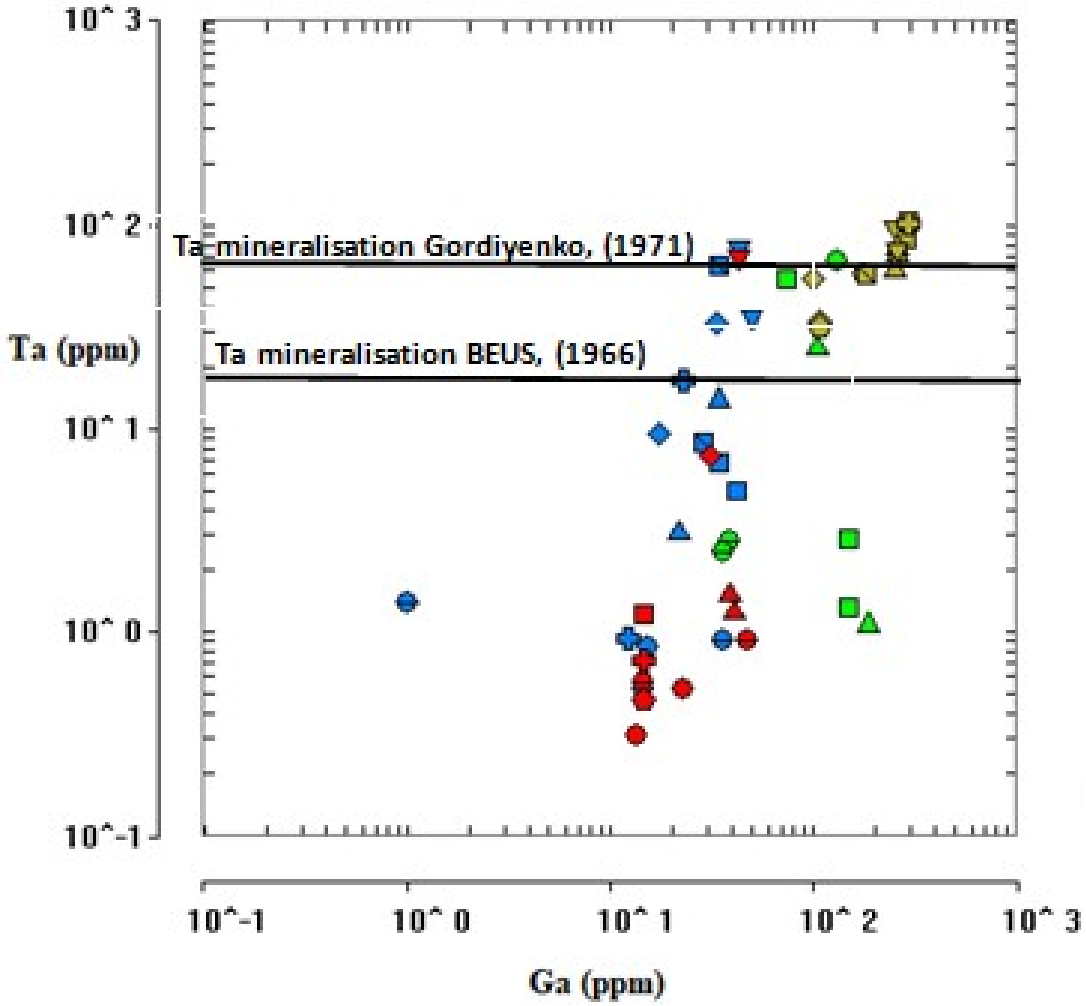

Figure 4.65: Ta vs Ga plot for pegmatites and extracts from the study area. Blue represents whole rock samples, red represents feldspar extracts, brown muscovite extracts and green biotite extracts

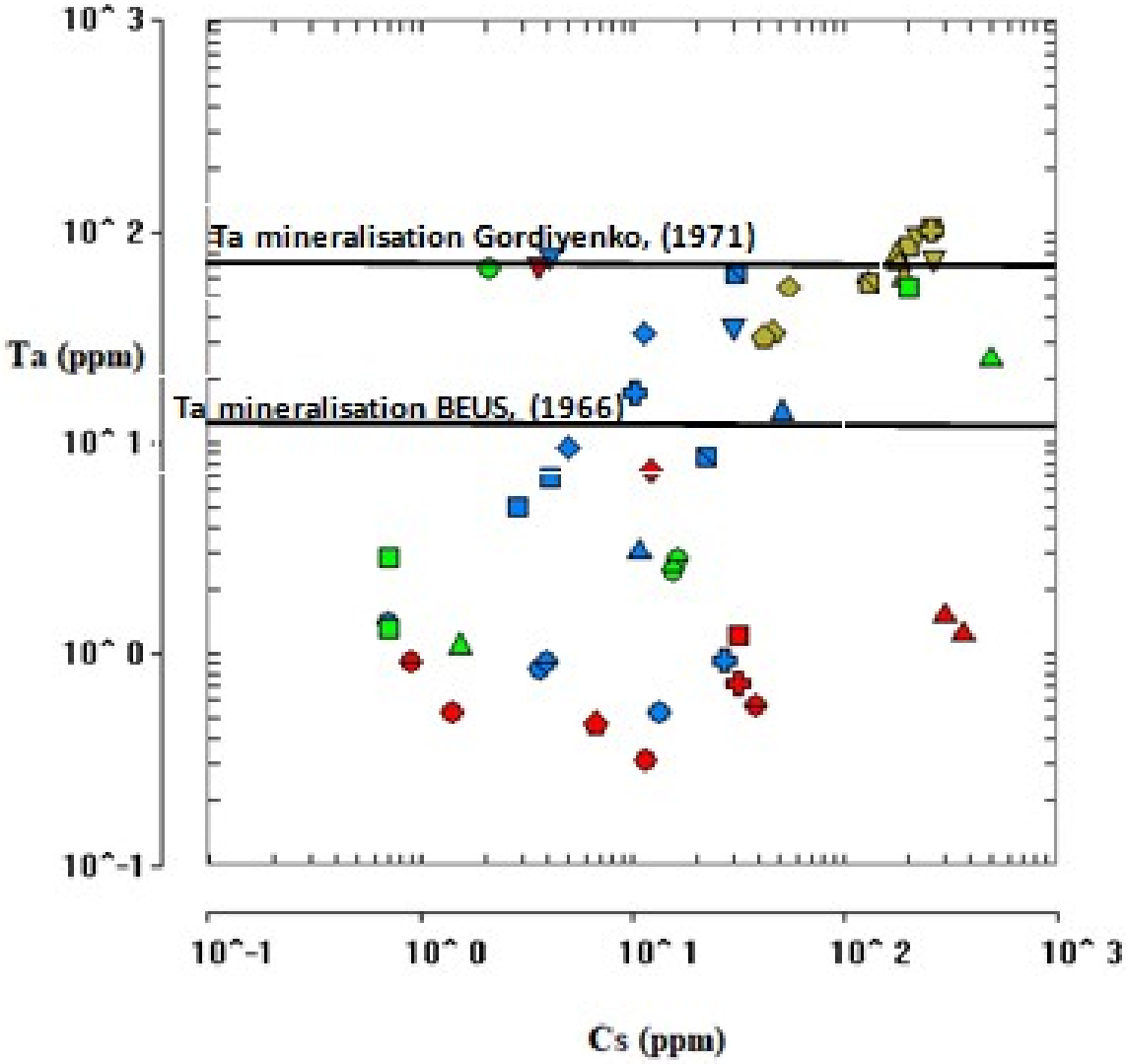

Figure 4.66: Plot of Ta (ppm) against Cs (ppm) for mineral extracts from the study areas (after Moller and Morteani, 1987). Blue represents whole rock samples, red represents feldspar extracts, brown muscovite extracts and green biotite extracts

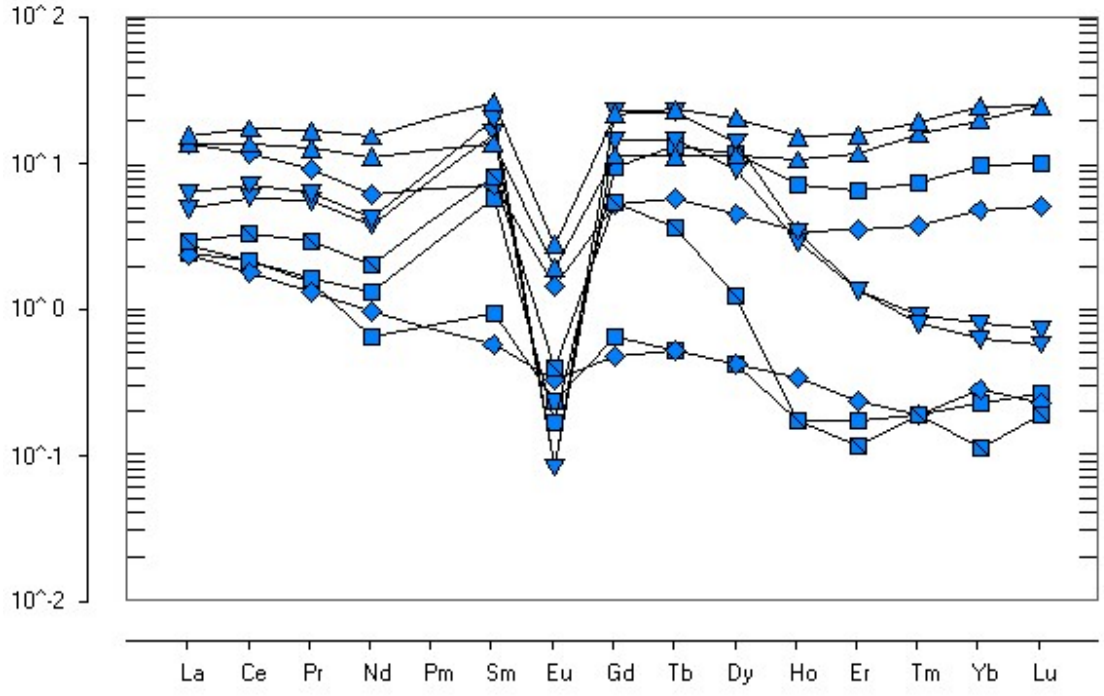

Figure 4.67: condrite normalisation plot for group 1 pegmatite (values after Sun and McDonough, 1989).

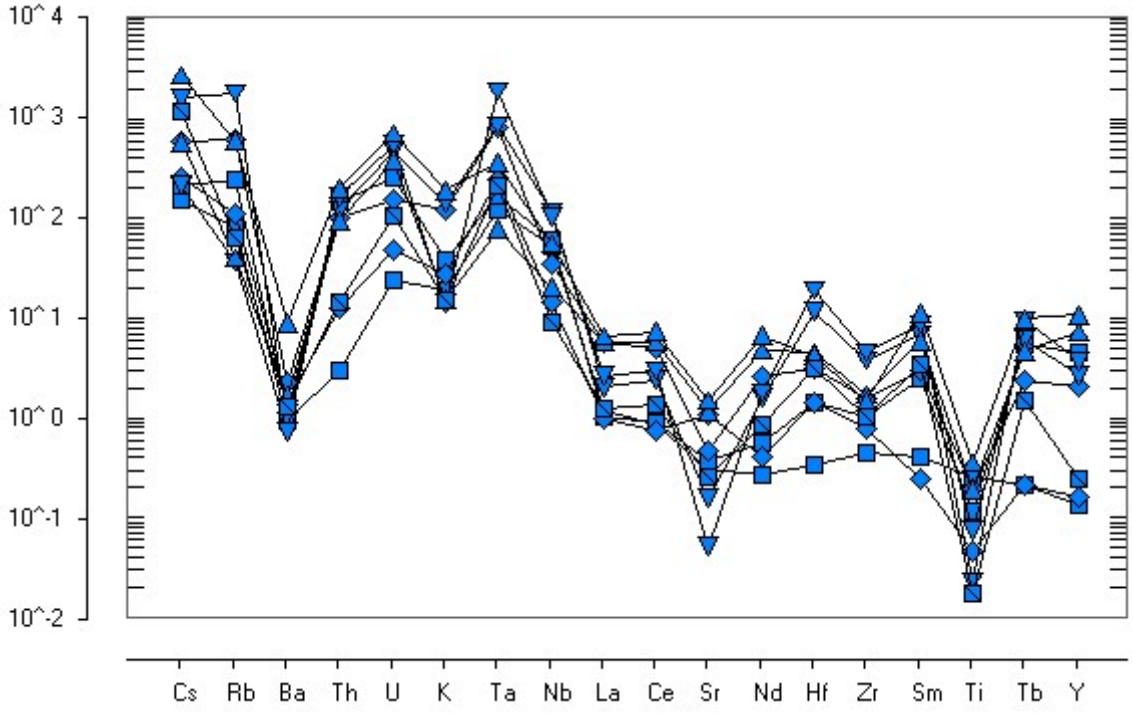

Figure 4.68: Chondrite-normalised plot of incompatible trace elements for group 2 pegmatites [normalisation values after Taylor and McLennan (1985)]

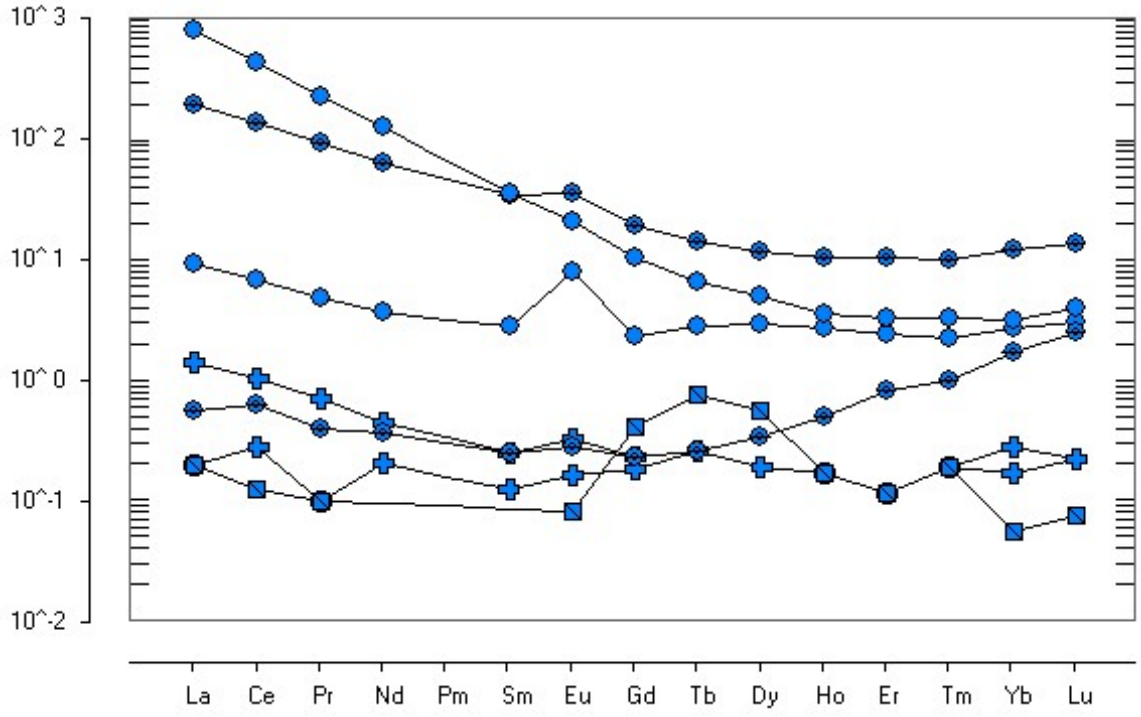

Figure 4.69: condrite normalisation plot for group 2 pegmatite (values after Sun and McDonough, 1989).

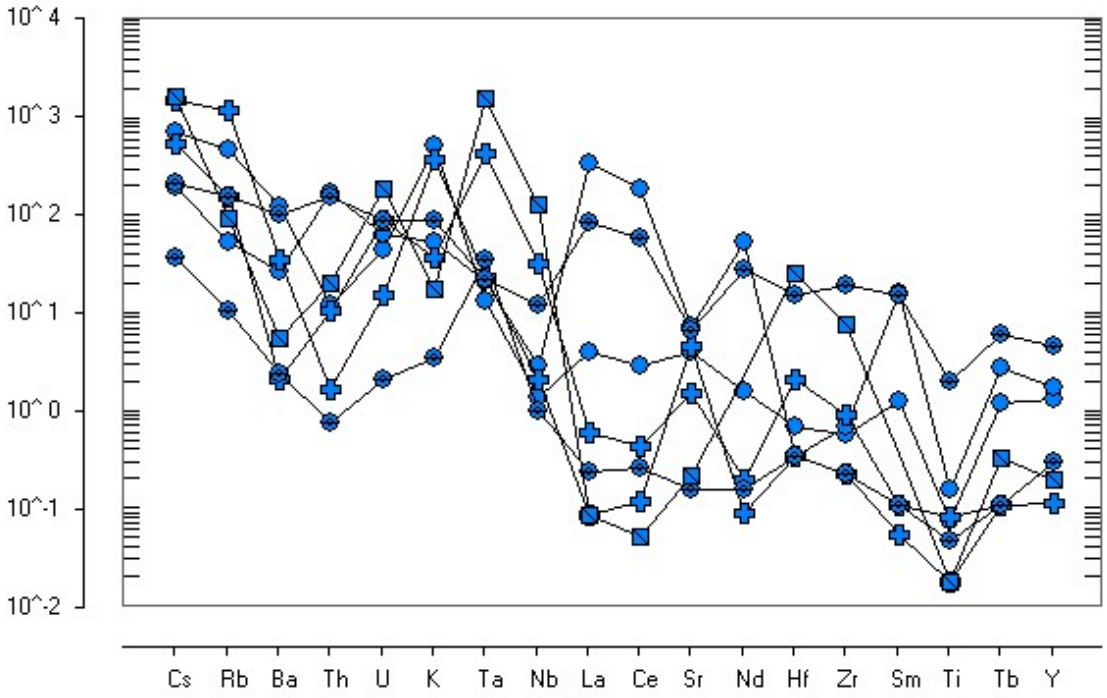

Figure 4.70: Chondrite-normalised plot of incompatible trace elements for group 2 pegmatites [normalisation values after Taylor and McLennan (1985)]

4.3 Fluid inclusion studies

4.3.1 Description of Fluid Inclusion Types

Availability, type and distribution of inclusions were determined by petrographic study on the doubly polished wafer. Inclusions observed were classified using the petrographic criteria of Shepherd et al., (1985) through a combination of distribution (e.g. isolated individuals or as trails along annealed fractures), phases present at room temperature and composition.

Using these criteria, the fluid inclusions present in a grain can were classified as primary (isolated individuals which are commonly aligned to crystal growth planes), secondary (fluid inclusion trails crosscut grains and are aligned with and contained within annealed fractures) and pseudosecondary (fluid inclusion trails begin and terminate abruptly within individual crystals). For this study, only primary and pseudosecondary inclusions were analysed as these fluid inclusions provide data on pressure, temperature and composition (PTX) properties of fluid trapped during quartz crystallisation and subsequent fluid migration events.

Inclusions occur as isolated individuals or in trails along annealed micro-fractures that cross-cut quartz grains in all samples. Fluid inclusion morphologies range from ellipsoidal to tabular to irregular and the sizes range from <2 μm to 100 μm (figure 4.71). Three types of aqueous inclusions (type 1, type 2 and type 3) were observed (table 4.17-4.18).

Type 1 inclusions are two-phase liquid + vapour (L+V; L>V) with high degree of fill (F) i.e. F~ 0.90 (**F= vol. of liquid/[vol. of liquid + vapour]**). They occur in all samples hosted in quartz grains as isolated individuals, in random groupings and as trails along post-crystallisation annealed fractures with size ranging from 2 μm to 100 μm. They display a range of shapes varying from tabular to ellipsoidal to irregular.

Type 2 are three phase (liquid + vapour + solid) inclusions with a high degree of fill i.e. F~0.85. They are ellipsoidal in shape with size of 2 μm to 15 μm. The trapped solid phases are generally < 3 μm in the longest dimension. They occur in trails or as isolated individuals within quartz grains. They are uncommon and only occur in five samples.

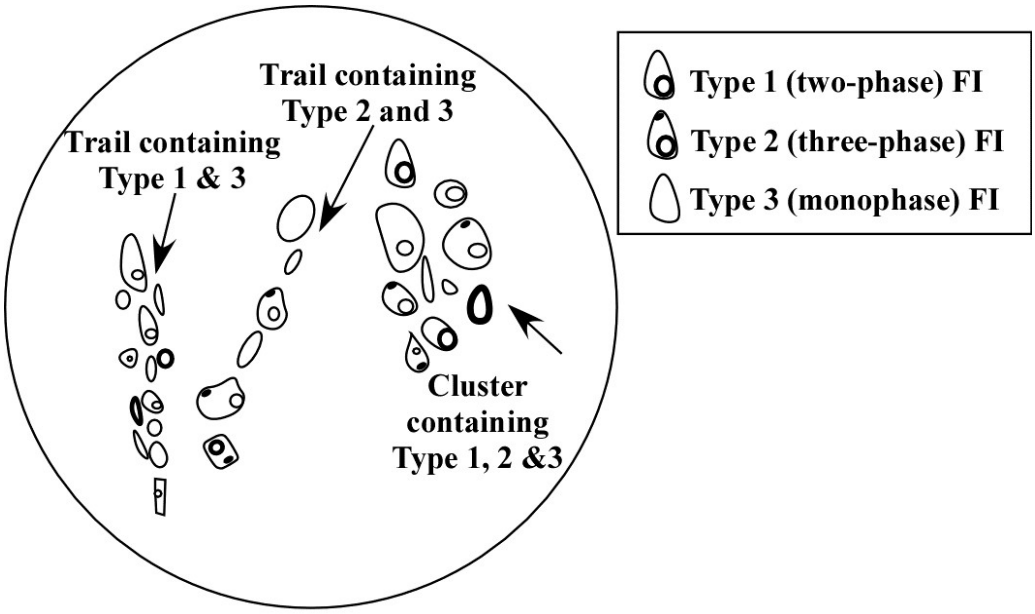

Figure 4.71: Schematic representation of the occurrence of quartz-hosted FIs in all samples.

Table 4.17: Classification of fluid inclusions observed in the study

TYPES	1	2	3
Phases Present	L + V	L + V + S	L
Composition	Aqueous	Aqueous	Aqueous
Size	2-100μm	2-15μm	<1-10μm
Occurrence	Quartz	Quartz	Quartz
Distribution	FI trails, clusters of individual FIs	FI trails, isolated individual FIs	FI trails, clusters of individual FIs

L=liquid, V=vapour, S=solid.

Table 4.18: Sample number and fluid inclusion type present in the pegmatite samples.

Sample number/FI type	1	2	3	4	5	6	7	8	9	10
1	XXX	XXX	XXX	XXX	XXX	XXX	XXX	XXX	XXX	XXX
2	-	-	X	-	X	X	-	X	-	X
3	XX	XX	XX	XX	XX	XX	XX	XX	XX	XX

X: present; XX: medium relative abundance; XXX: high relative abundance.

4.3.2 Fluid Inclusion photomicrographs for each sample

The following photomicrographs (figure 4.72-4.91) contain the range of fluid inclusion types recorded during this study. Each photomicrograph is annotated and annealed fractures hosting fluid inclusions are highlighted.

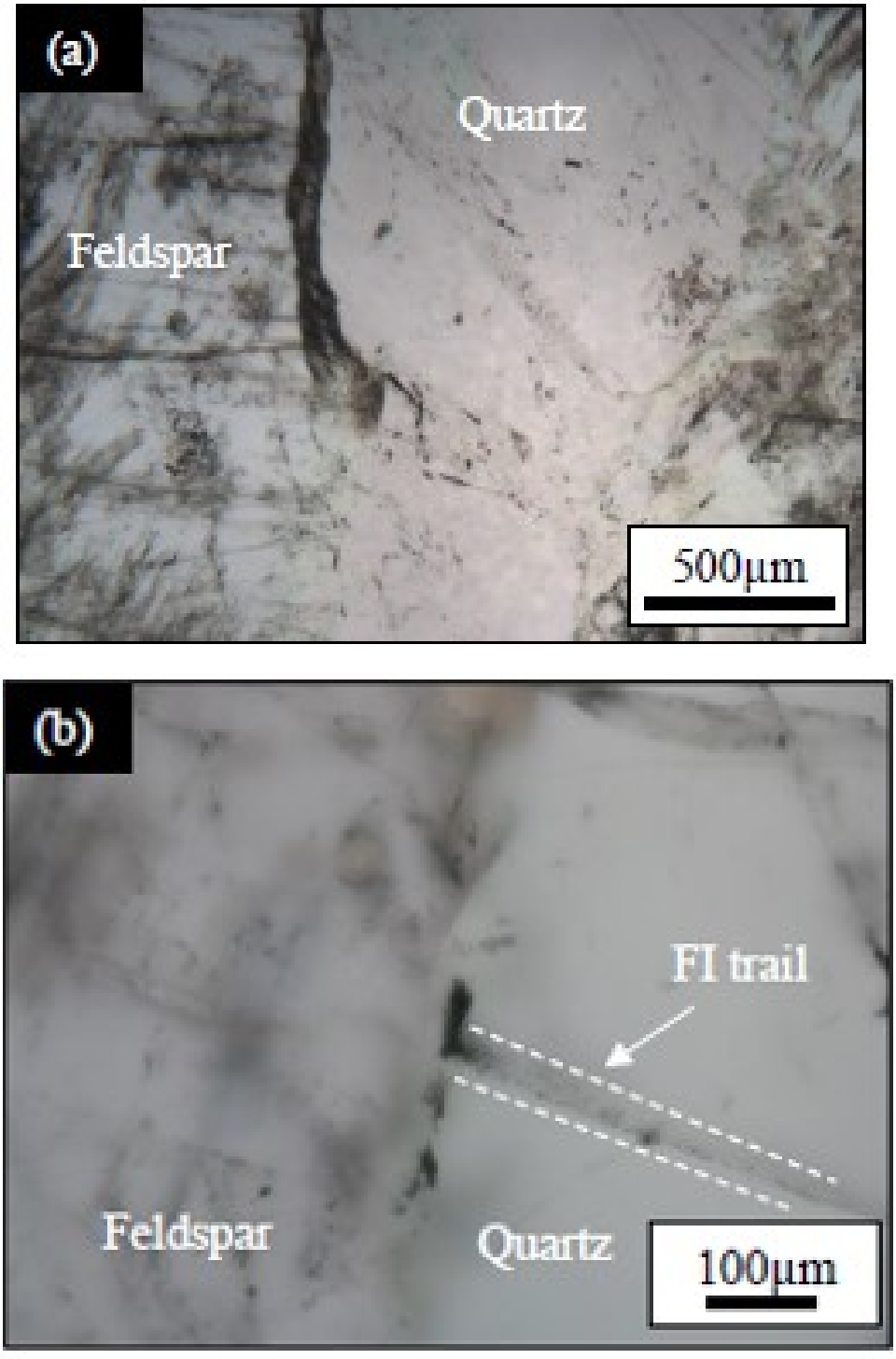

Figure 4.72: Photomicrographs of sample AB 006 (Abuja Leather). (a) General view of typical quartz and feldspar grains under low magnification. (b) Trail containing Type 3 that terminates at quartz grain boundary.

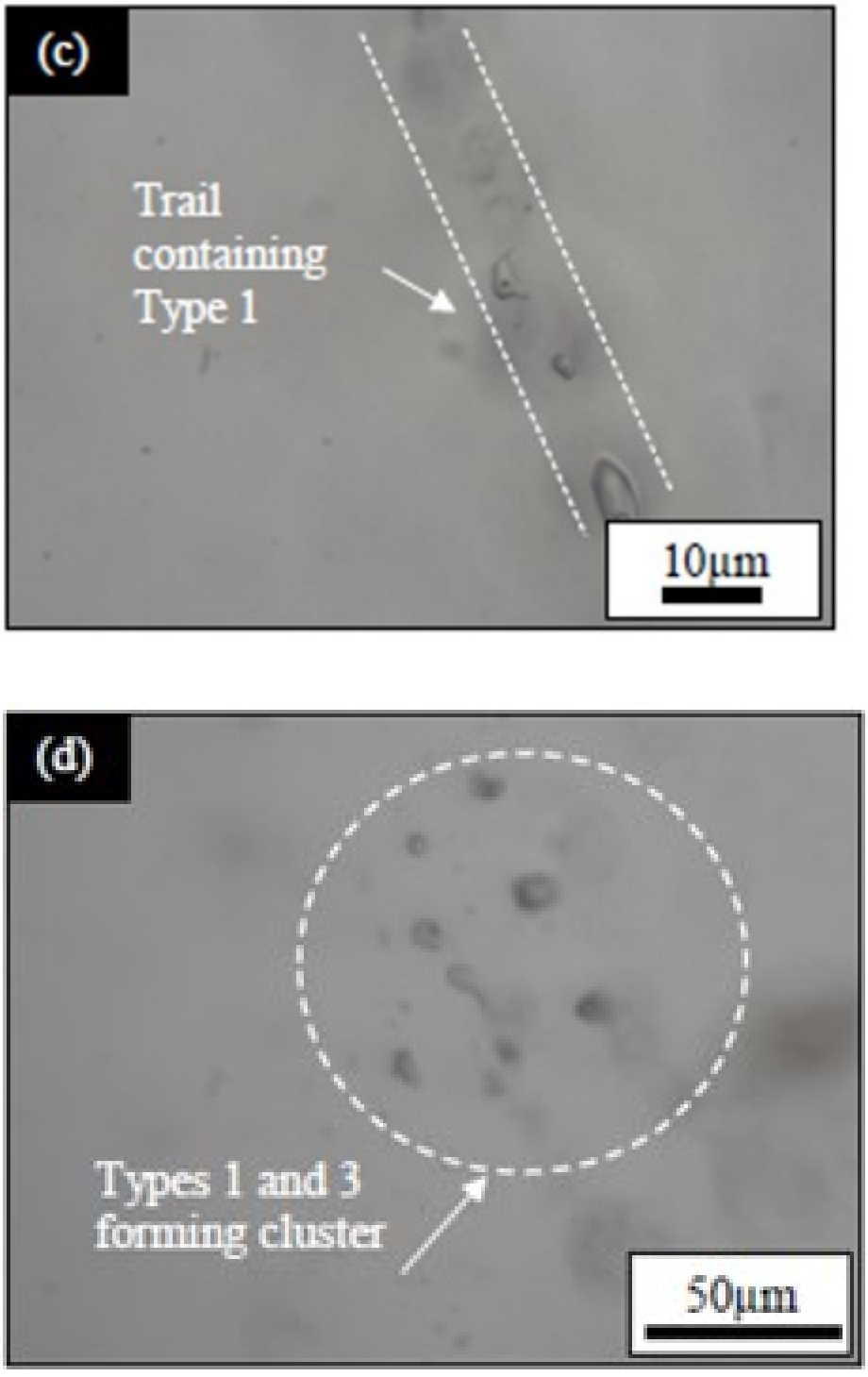

Figure 4.73: Photomicrographs of sample AB 006 (Abuja Leather) (c) Trail containing Type 1 along annealed fracture in quartz. (d) Type 1 and 3 forming cluster of individual FIs in quartz grain.

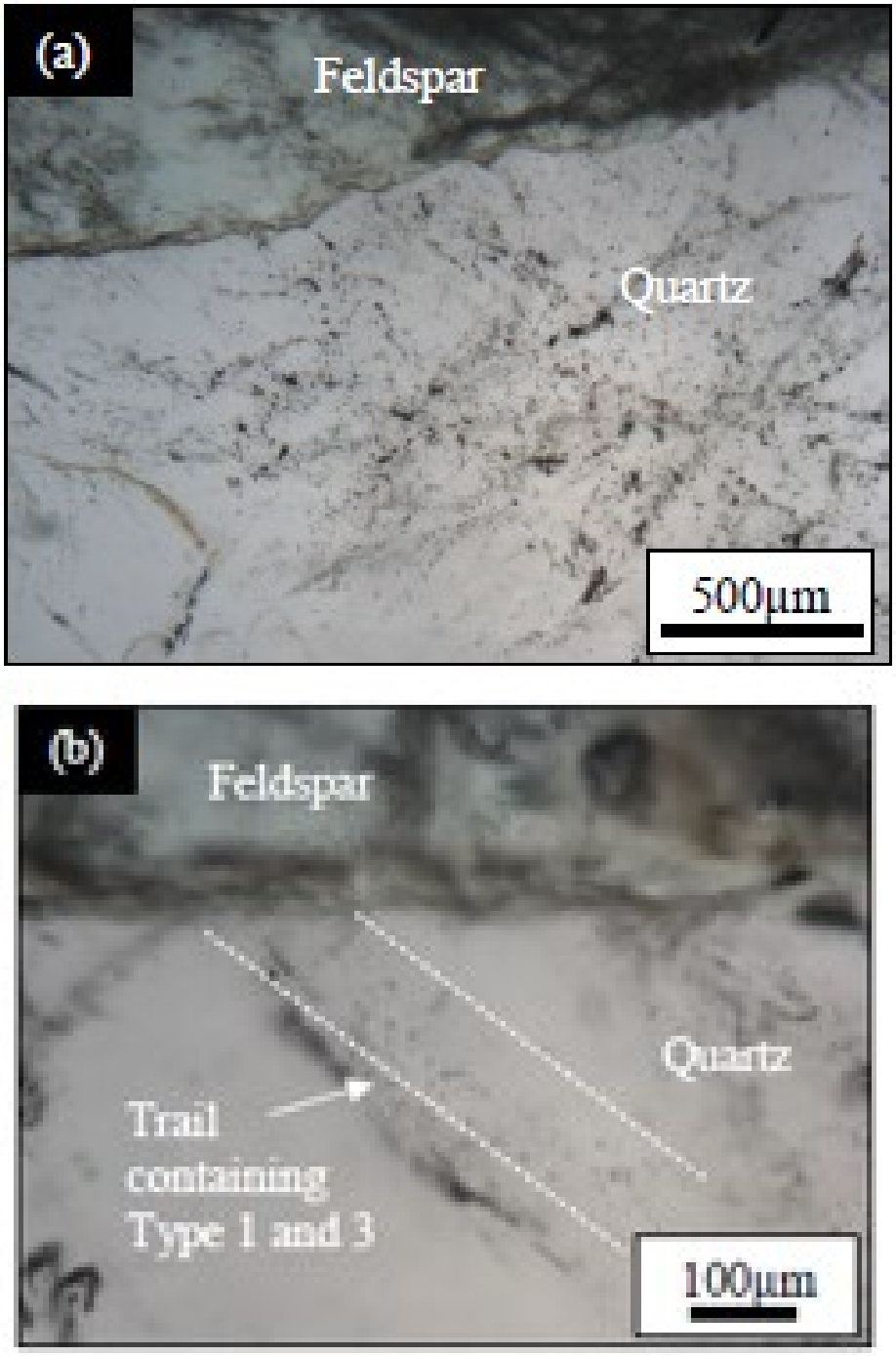

Figure 4.74: Photomicrographs of sample AB 007 (Abuja Leather). (a) General view of typical quartz and feldspar grains under low magnification. (b) Trail containing Type 1 and 3 and terminating at quartz grain boundary

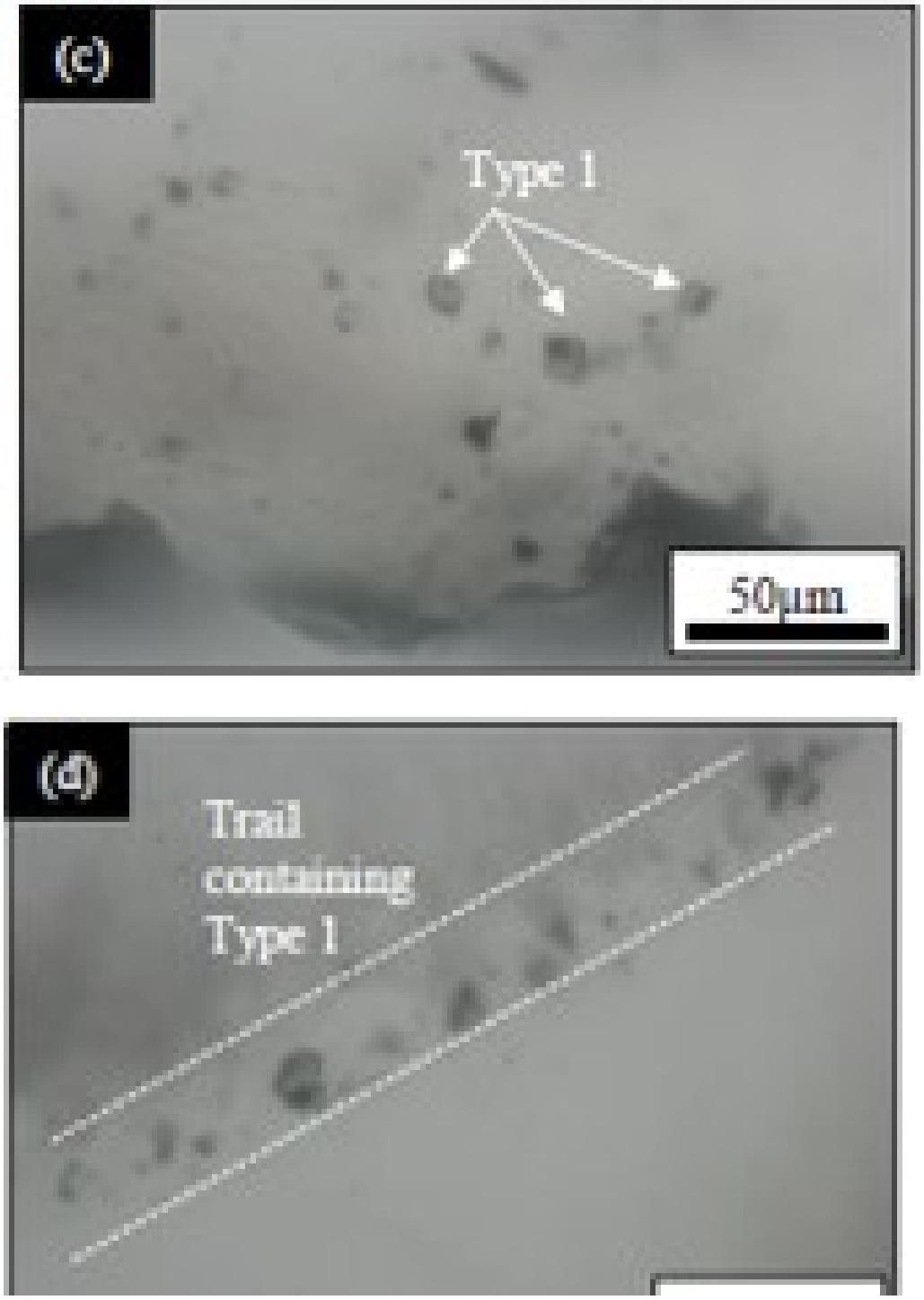

Figure 4.75: Photomicrographs of sample AB 007 (Abuja Leather). (c) Type 1 forming a cluster hosted in quartz grain. (d) Trail containing Type 1 in quartz grain.

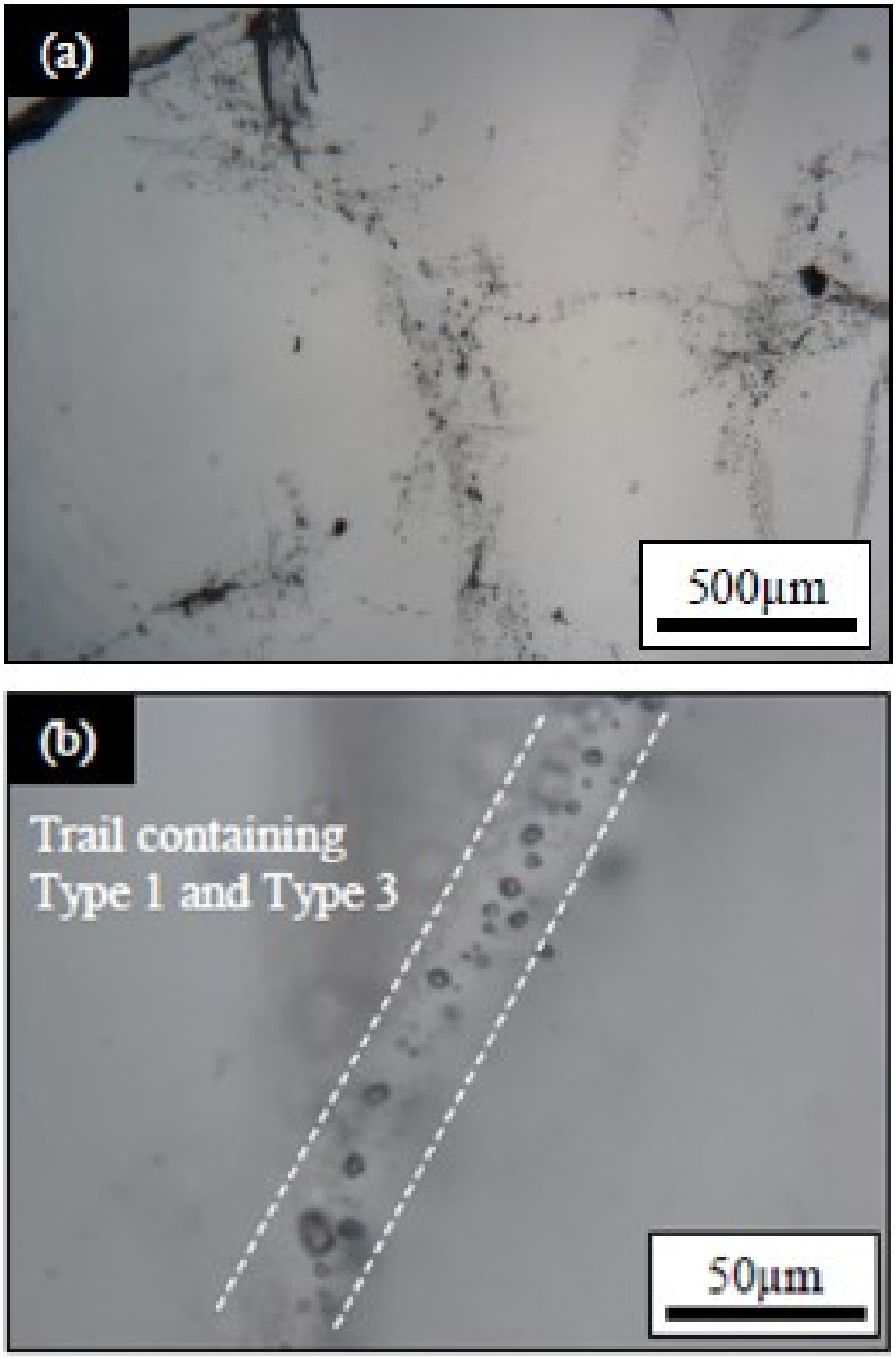

Figure 4.76: Photomicrographs of sample OM 009 (Omoba). (a) General view of typical FI-rich quartz grain under low magnification. (b) Type 1 and Type 3 forming a trail along an annealed fracture.

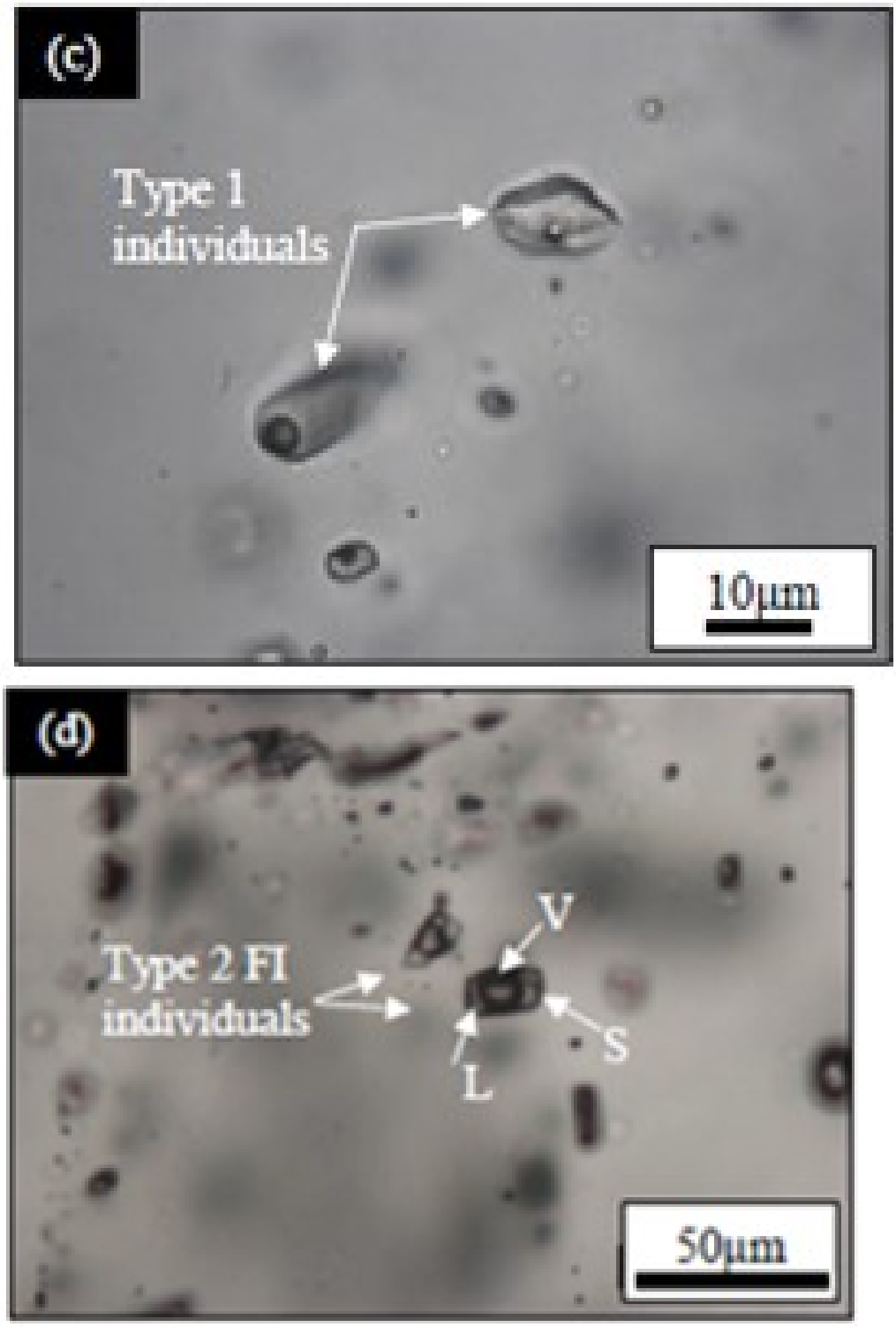

Figure 4.77: Photomicrographs of sample OM 009 (Omoba). (c) Isolated individuals of Type 1. (d) Isolated Type 2 (L=Liquid, V=Vapour, S=Solid) inclusions.

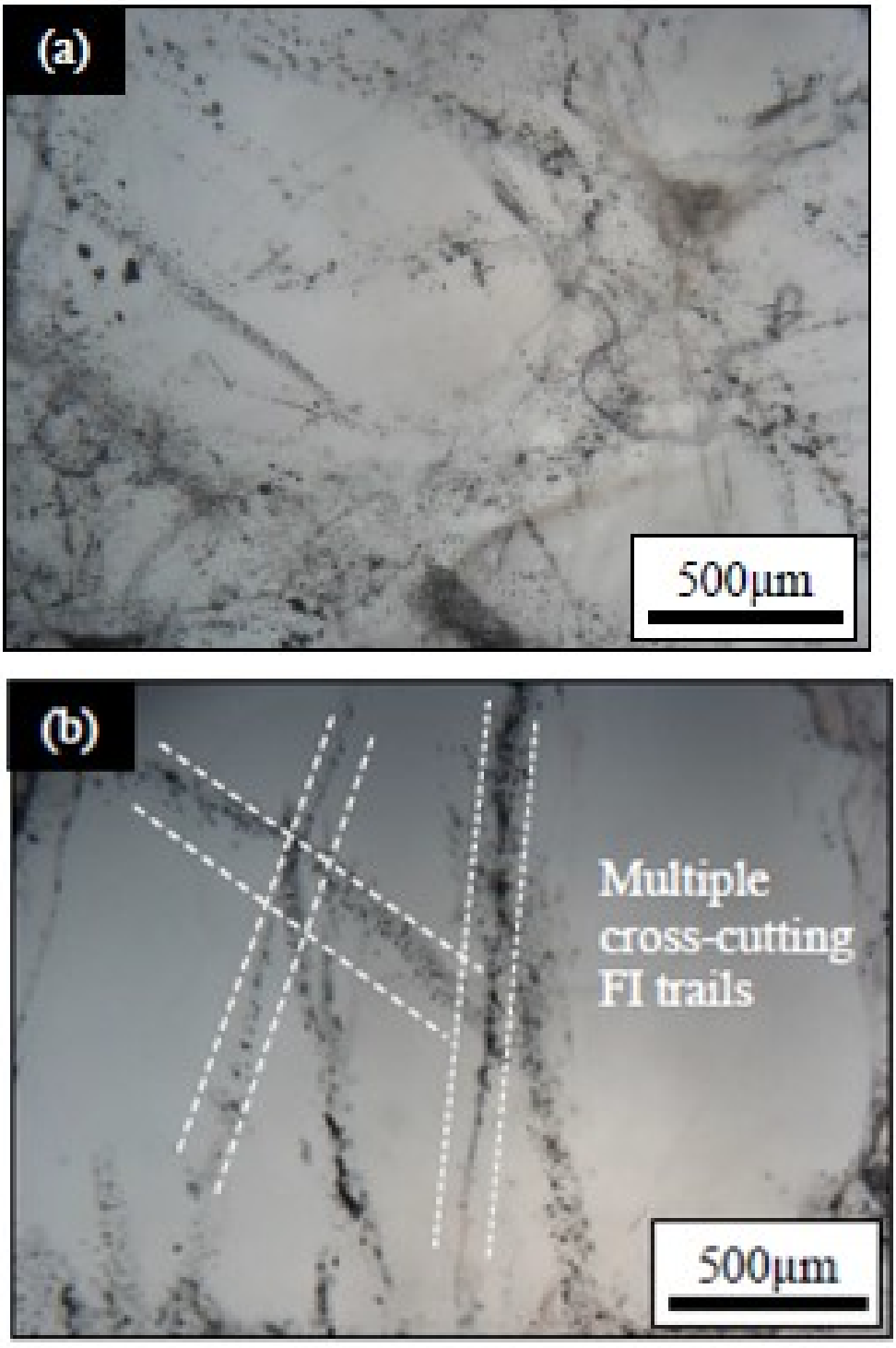

Figure 4.78: Photomicrographs of sample OM 010 (Omoba). (a) General view of typical quartz grain under low magnification. (b) Multiple crosscutting trails of Type 1 along annealed fractures in quartz.

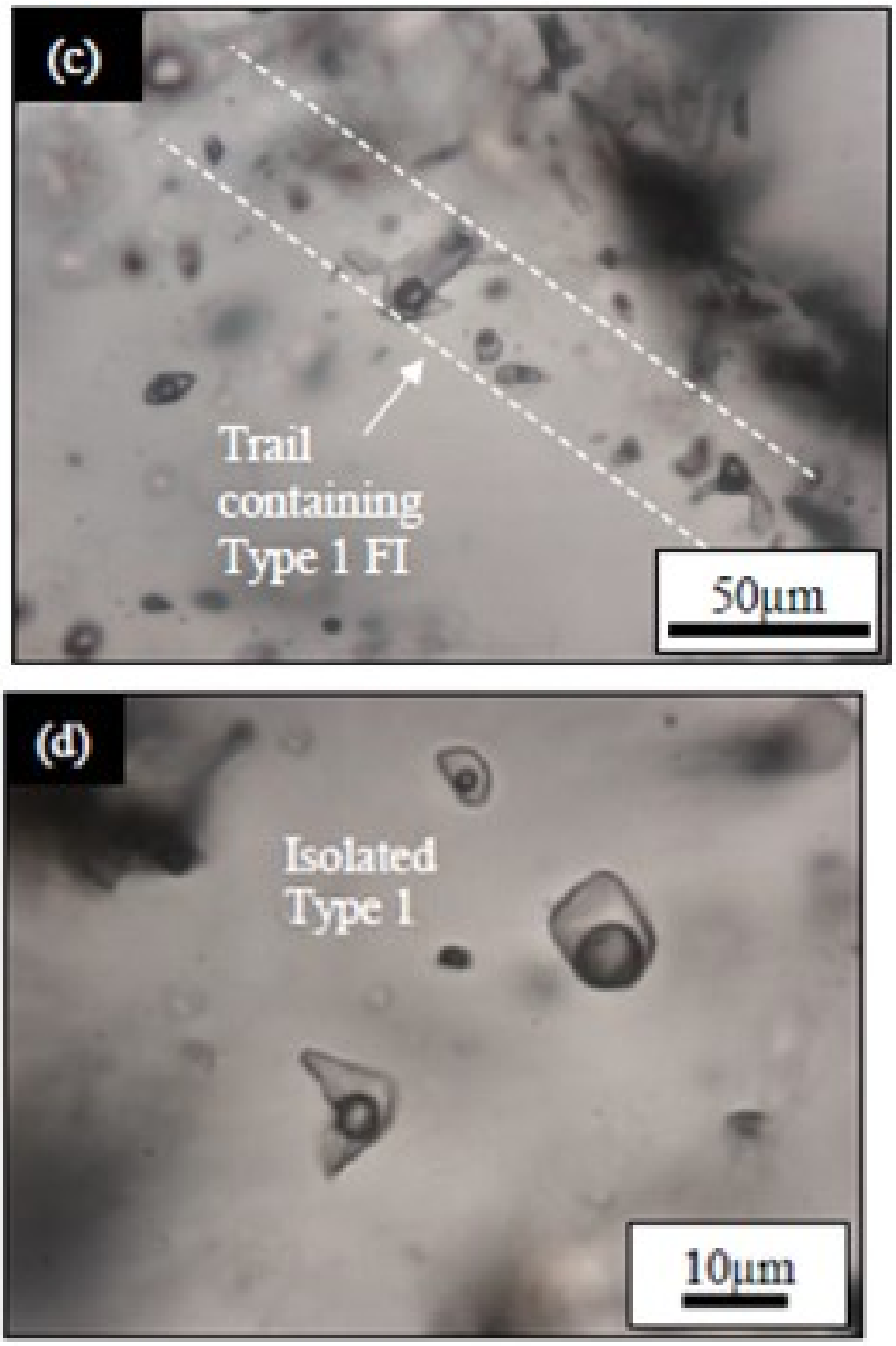

Figure 4.79: Photomicrographs of sample OM 010 (Omoba). (c) Trail of Type 1 along an annealed fracture in quartz. (d) Isolated Type 1 inclusions in quartz.

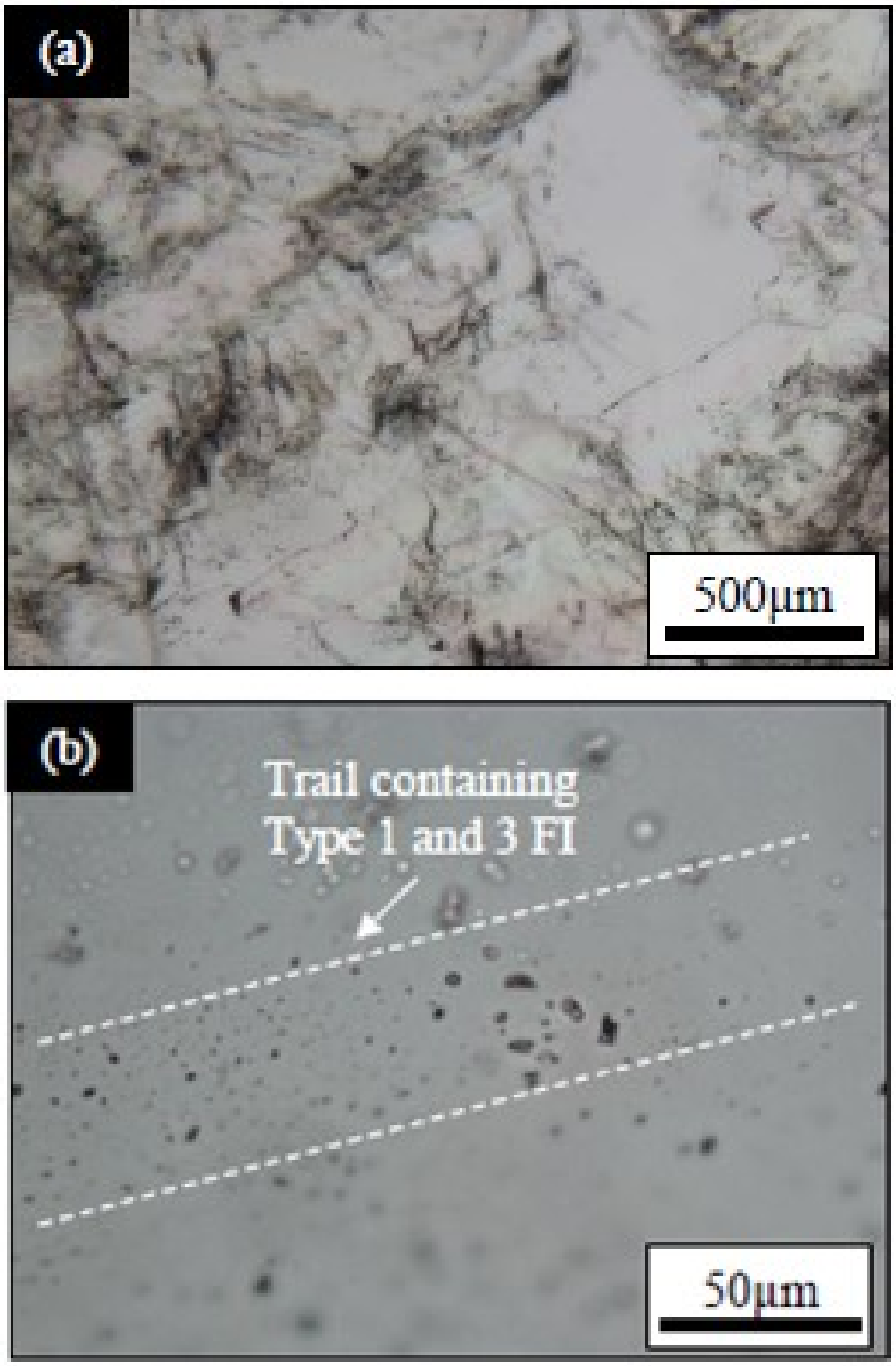

Figure 4.80: Photomicrographs of sample OW 003 (Owode). (a) General view of typical quartz grain under low magnification. (b) Type 1 and Type 3 forming trail along annealed fracture.

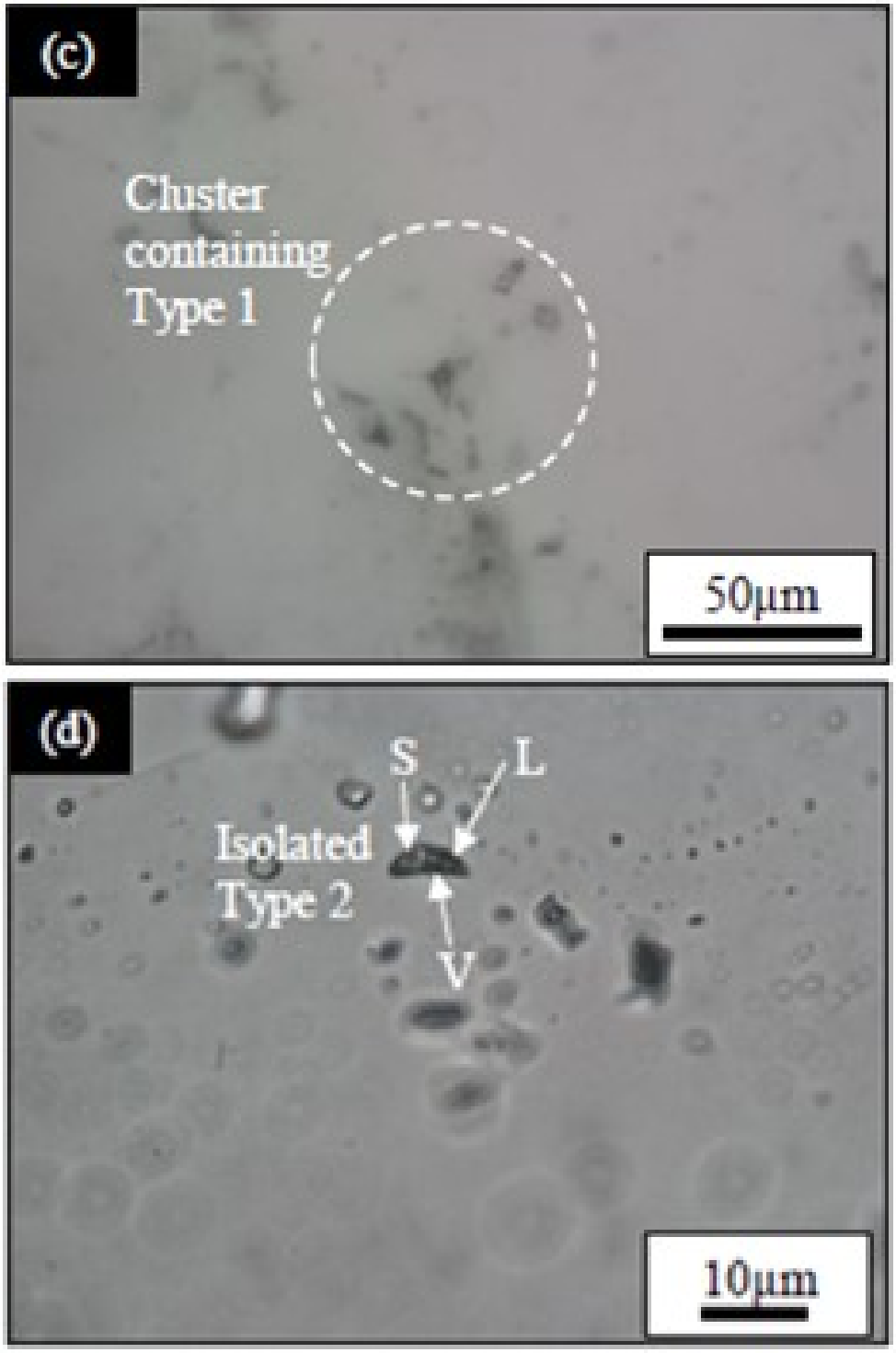

Figure 4.81: Photomicrographs of sample OW 003 (Owode) (c) Cluster containing Type 1 FI. (d) Isolated Type 2 (L=Liquid, V=Vapour, S=Solid) inclusions.

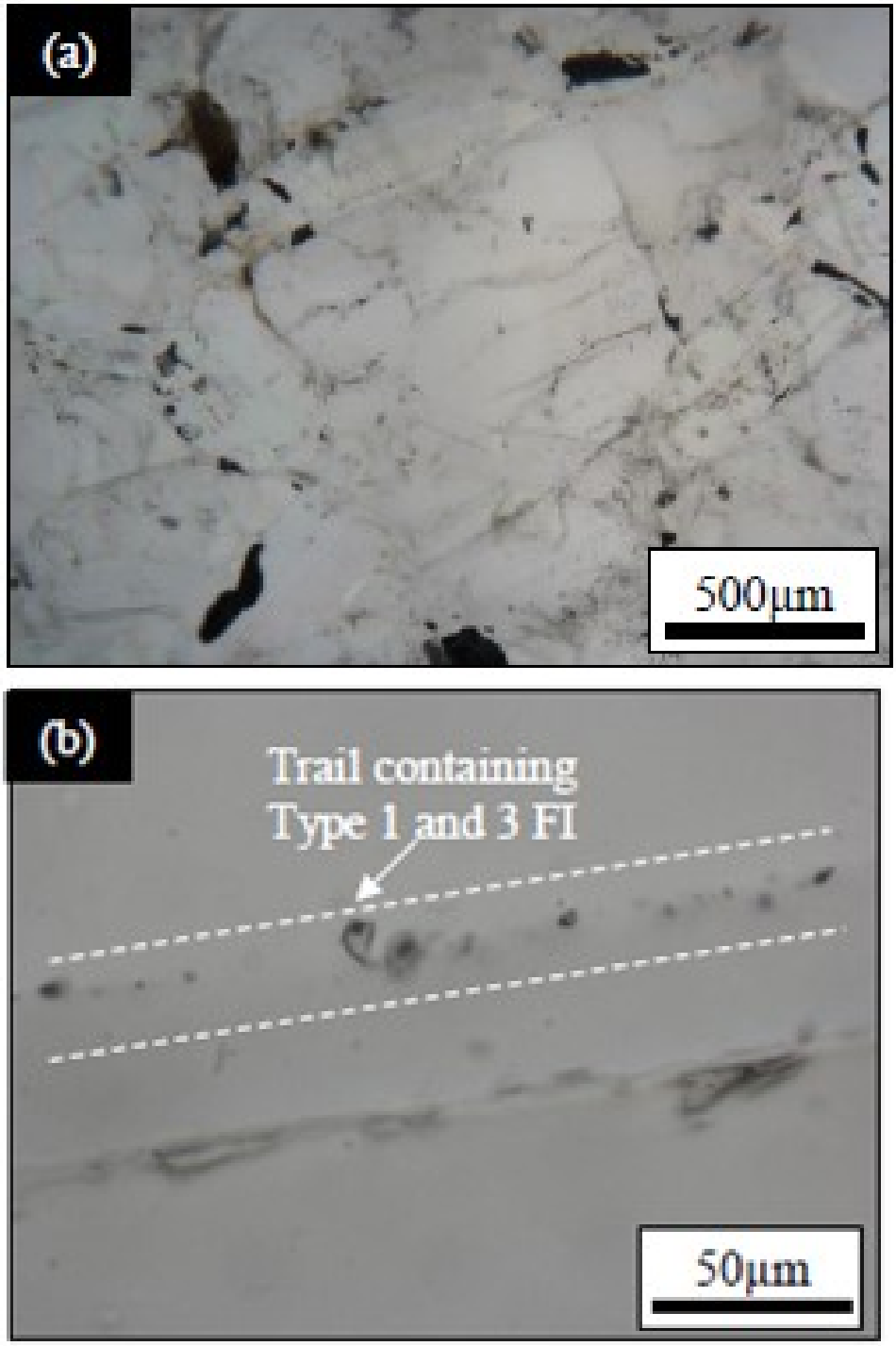

Figure 4.82: Photomicrographs of sample OW 005 (Owode). (a) General view of typical quartz grain under low magnification. (b) Type 1 and Type 3 forming trail along annealed fracture

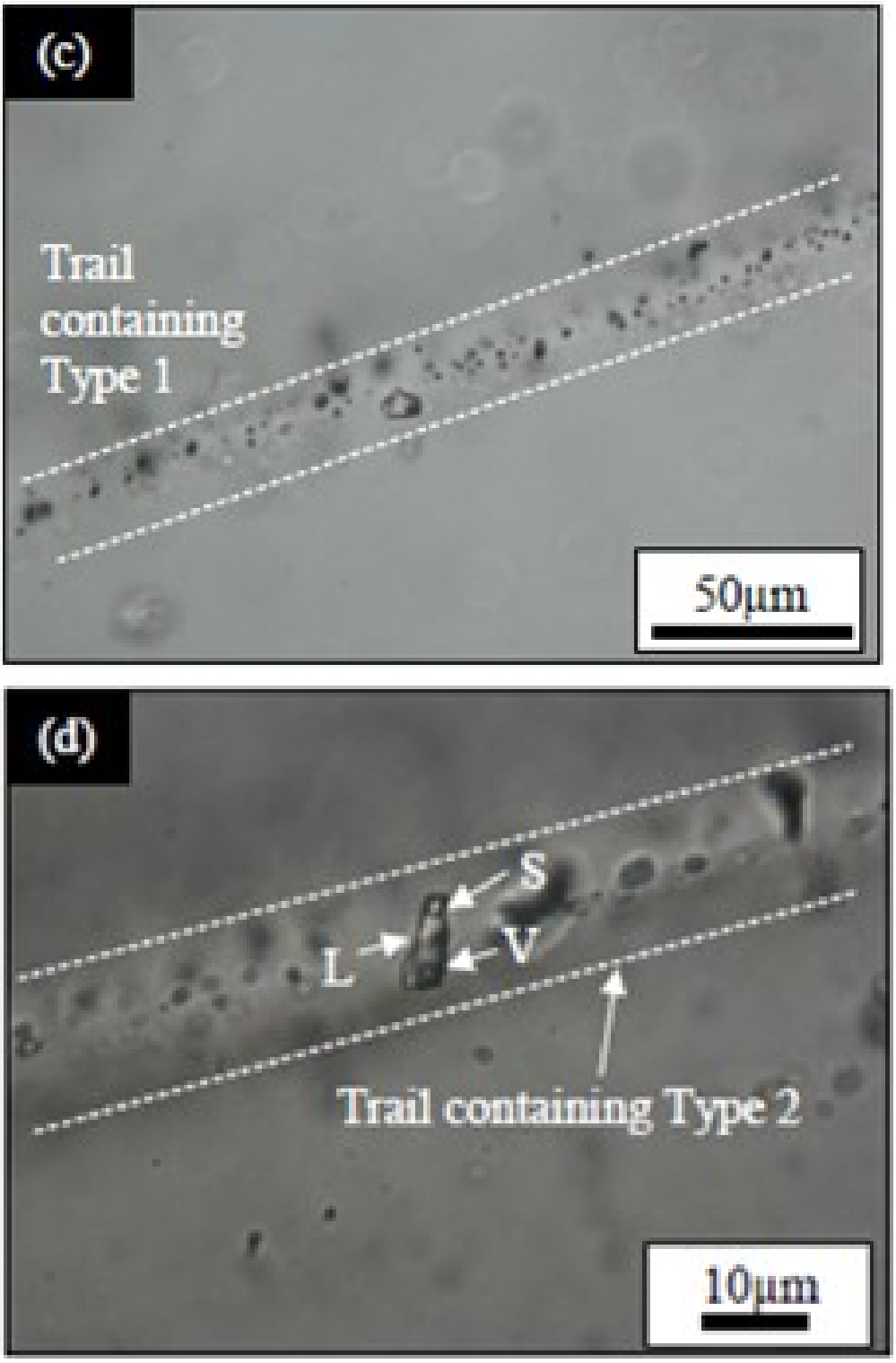

Figure 4.83: Photomicrographs of sample OW 005 (Owode) (c) Trail containing Type 1 along annealed fracture. (d) Trail containing Type 2 (L=Liquid, V=Vapour, S=Solid) inclusions.

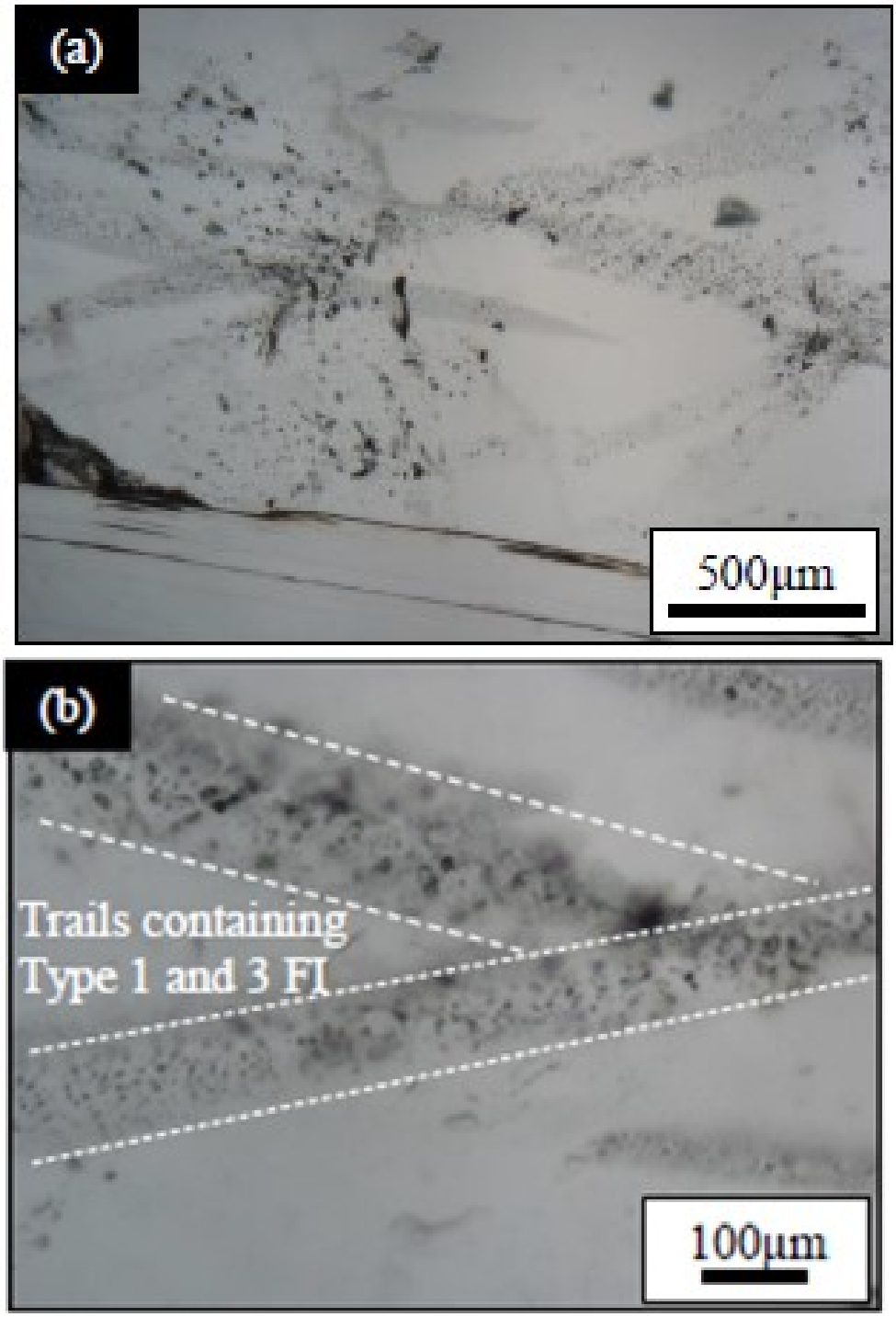

Figure 4.84: Photomicrographs of sample GB 001 (Gbayo). (a) General view of typical quartz grain under low magnification. (b) Type 1 and Type 3 forming trails along annealed fracture.

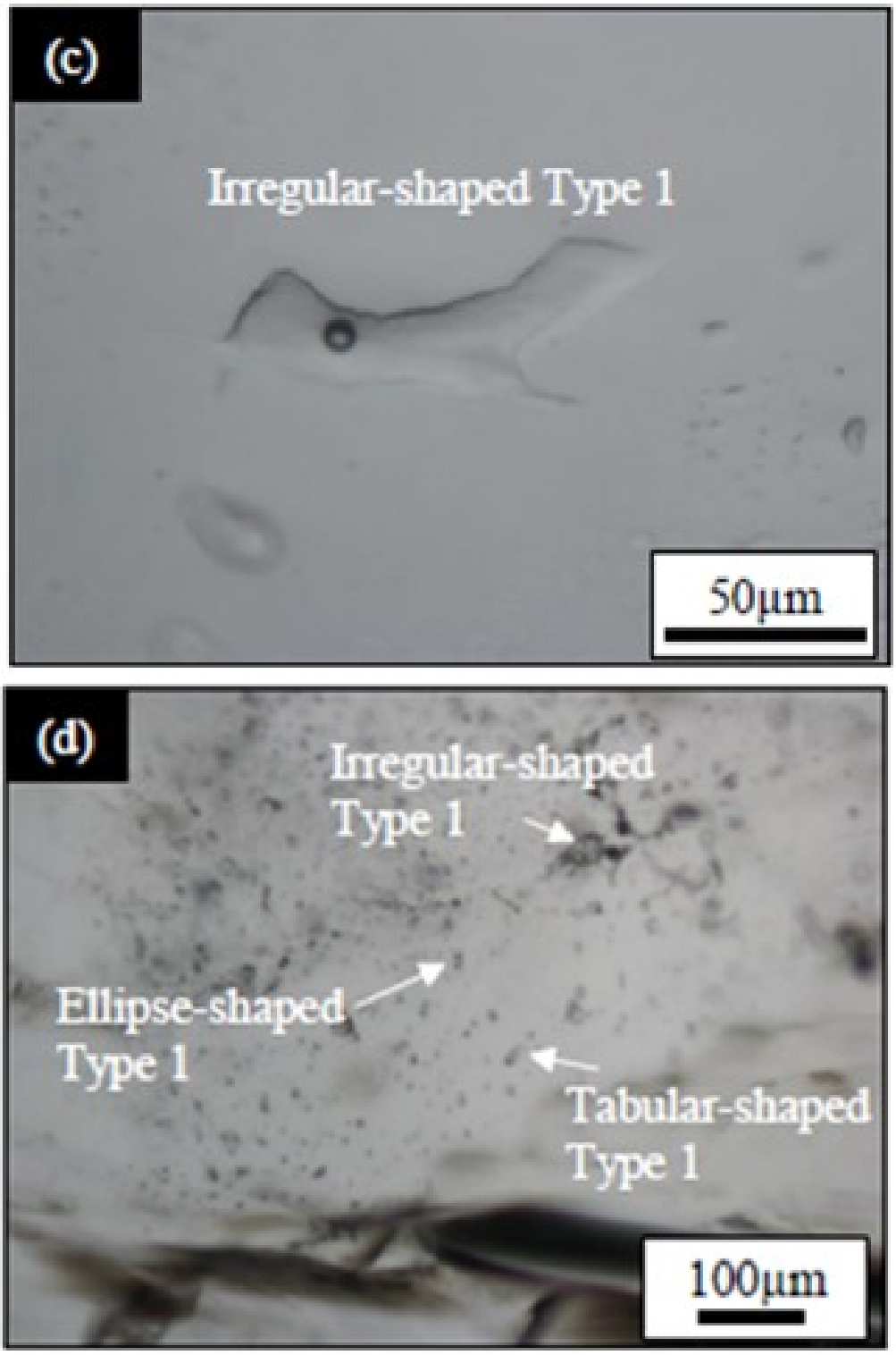

Figure 4.85: Photomicrographs of sample GB 001 (Gbayo) (c) Type 1 showing irregular shape due to stretching. (d) Multiple Type 1 inclusions displaying a variety of morphologies.

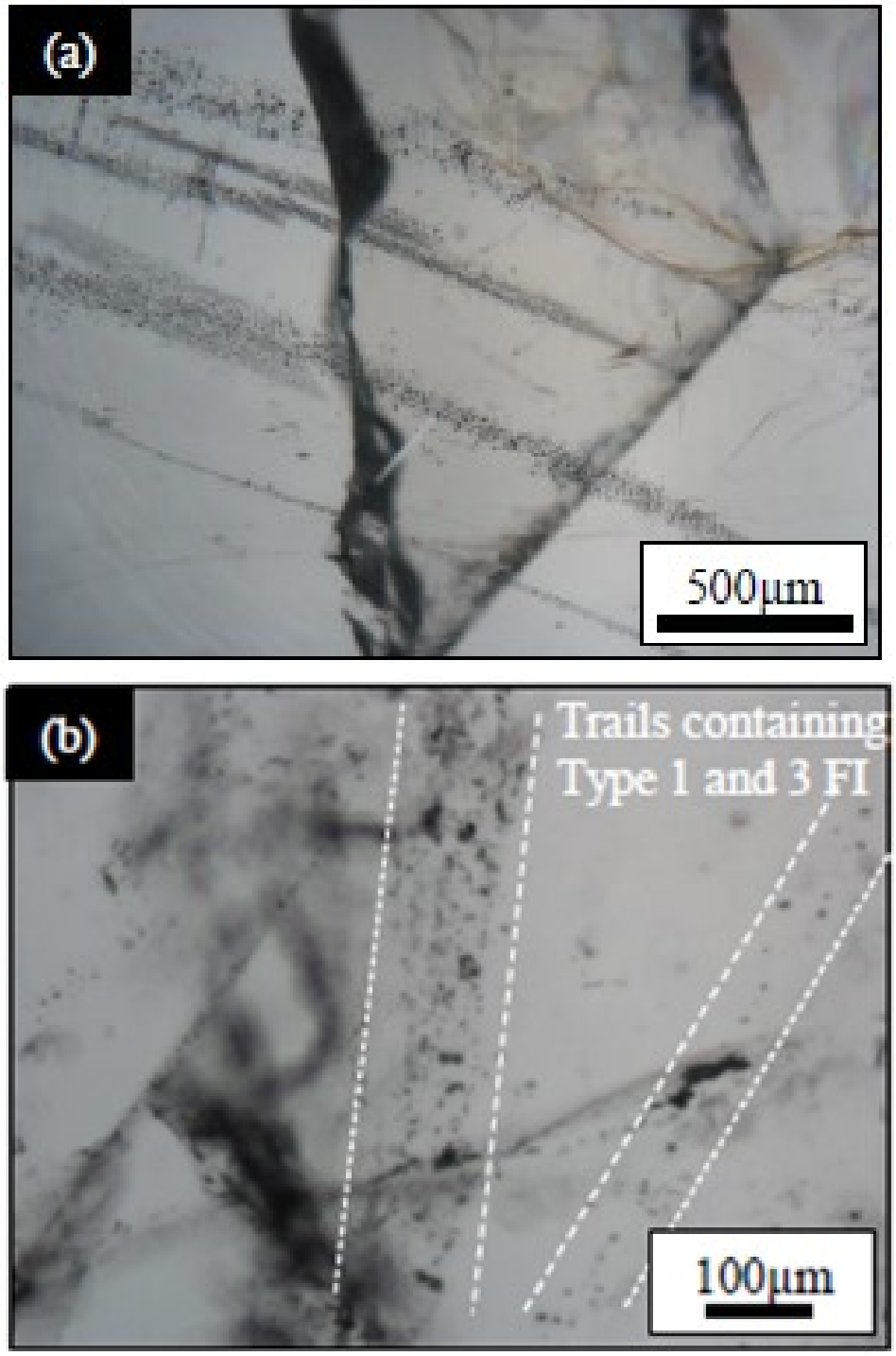

Figure 4.86: Photomicrographs of sample GB 002 (Gbayo). (a) General view of typical quartz grain under low magnification. (b) Type 1 and Type 3 forming trails along annealed fractures

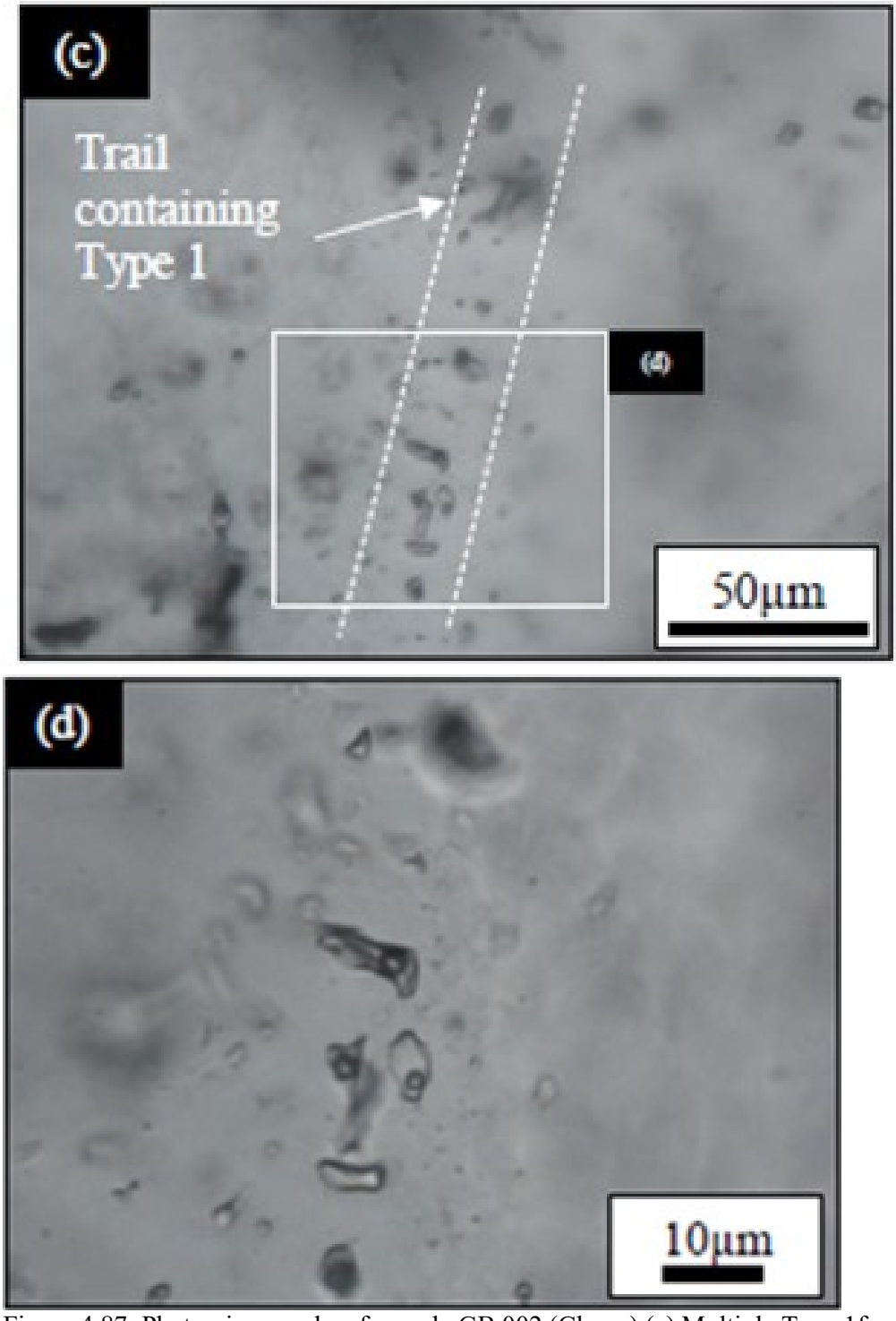

Figure 4.87: Photomicrographs of sample GB 002 (Gbayo) (c) Multiple Type 1forming trail along annealed fracture. (d) Higher magnification view of inset from (c) showing irregular shapes of FI and varying vapour bubble volumes.

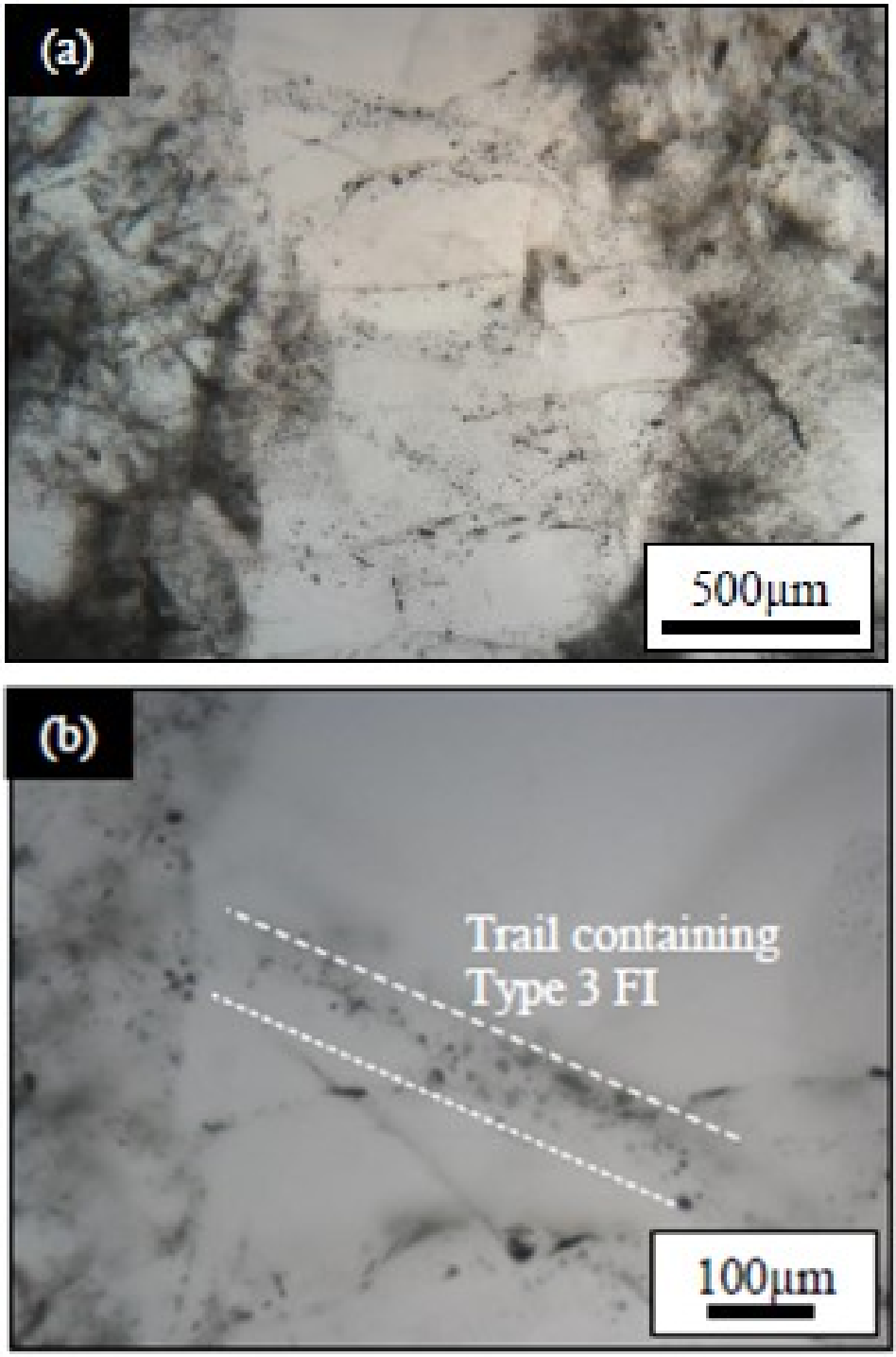

Figure 4.88: Photomicrographs of sample CO 003 (Coco). (a) General view of typical quartz grain under low magnification. (b) Type 3 forming a trail along an annealed fracture.

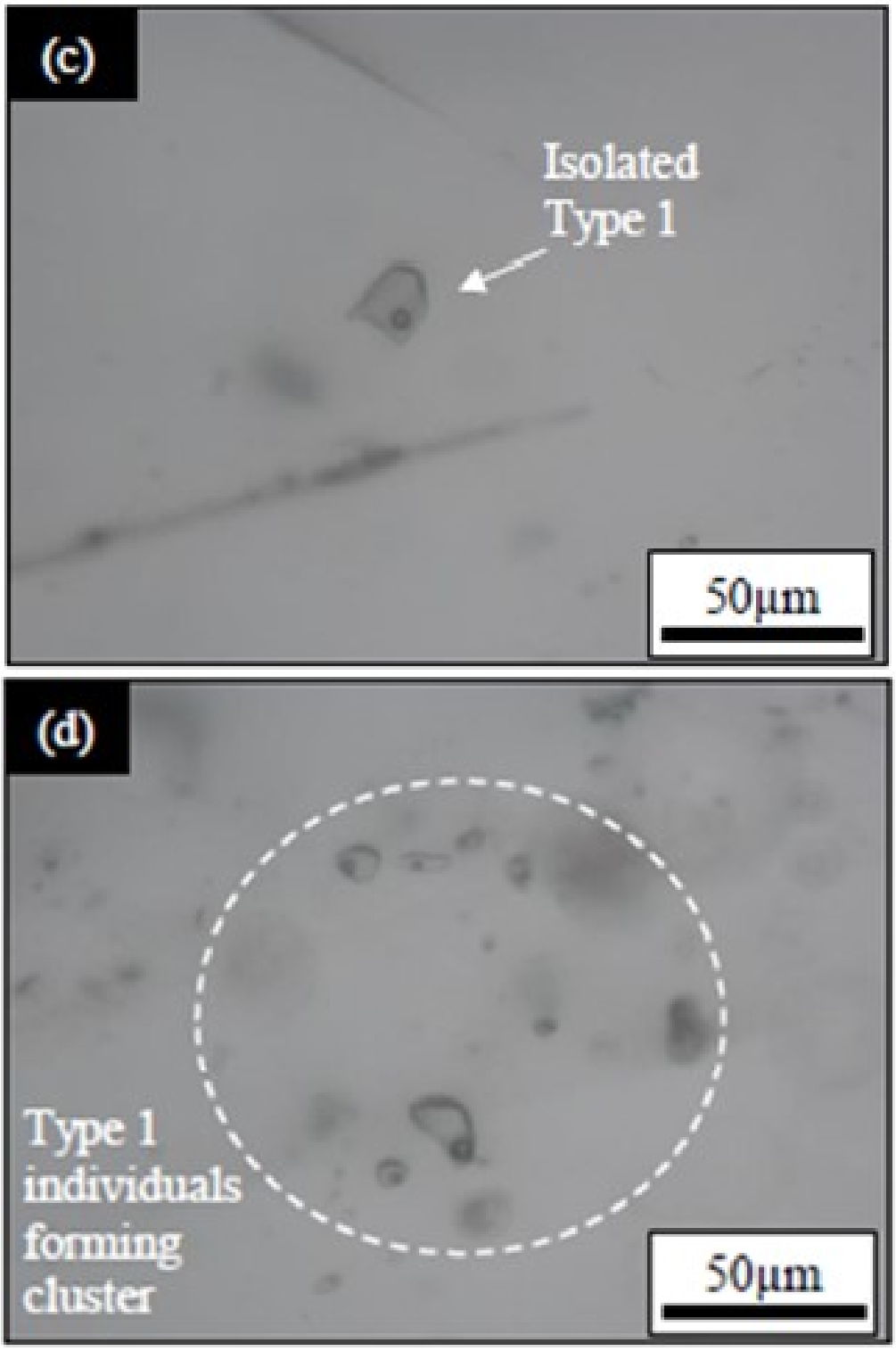

Figure 4.89: Photomicrographs of sample CO 003 (Coco) (c) Isolated Type 1. (d) Multiple Type 1 individuals forming cluster.

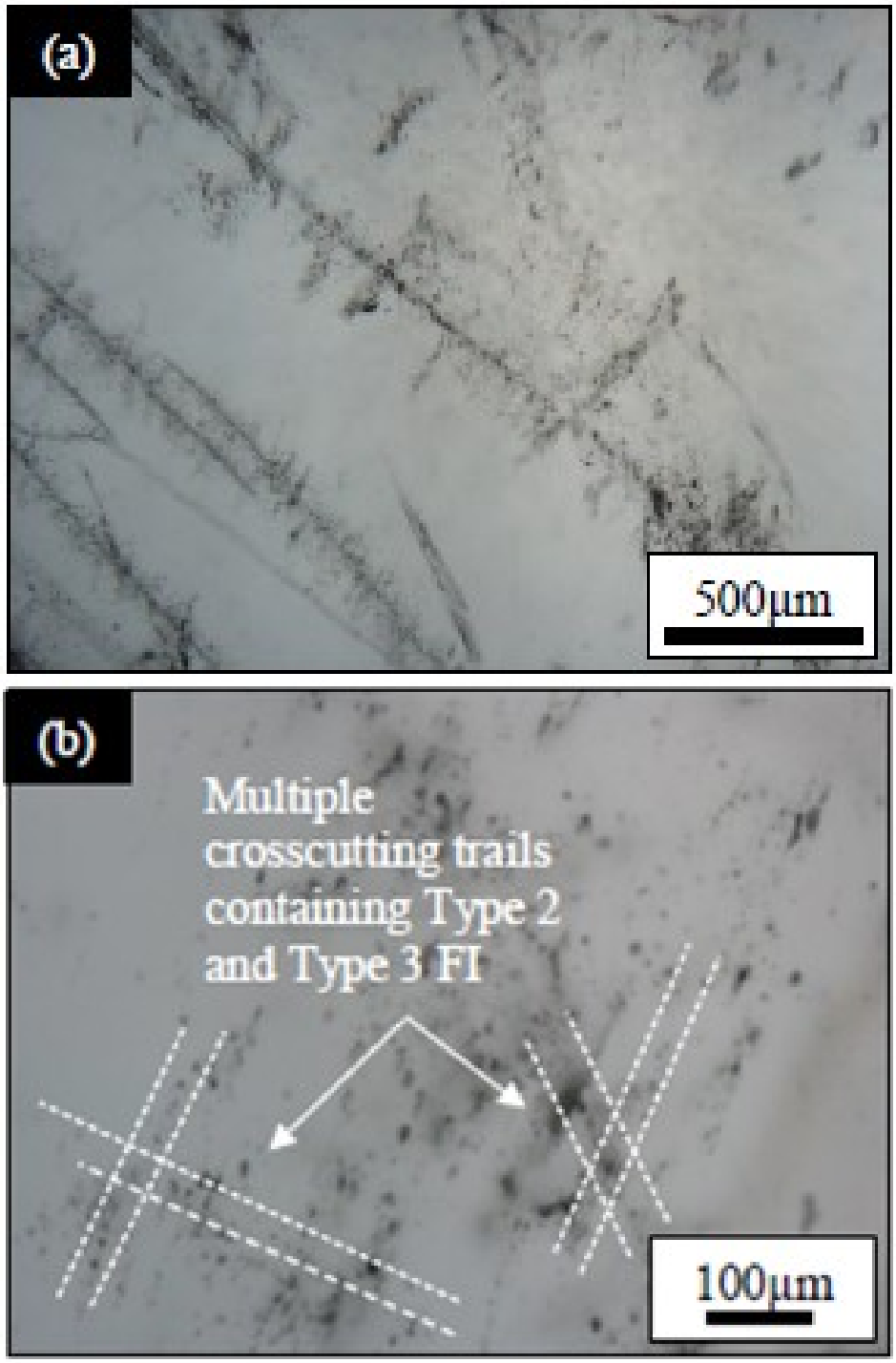

Figure 4.90: Photomicrographs of sample CO 005 (Coco). (a) General view of typical quartz grain under low magnification. (b) Multiple crosscutting trails containing Type 1and Type 3 FI

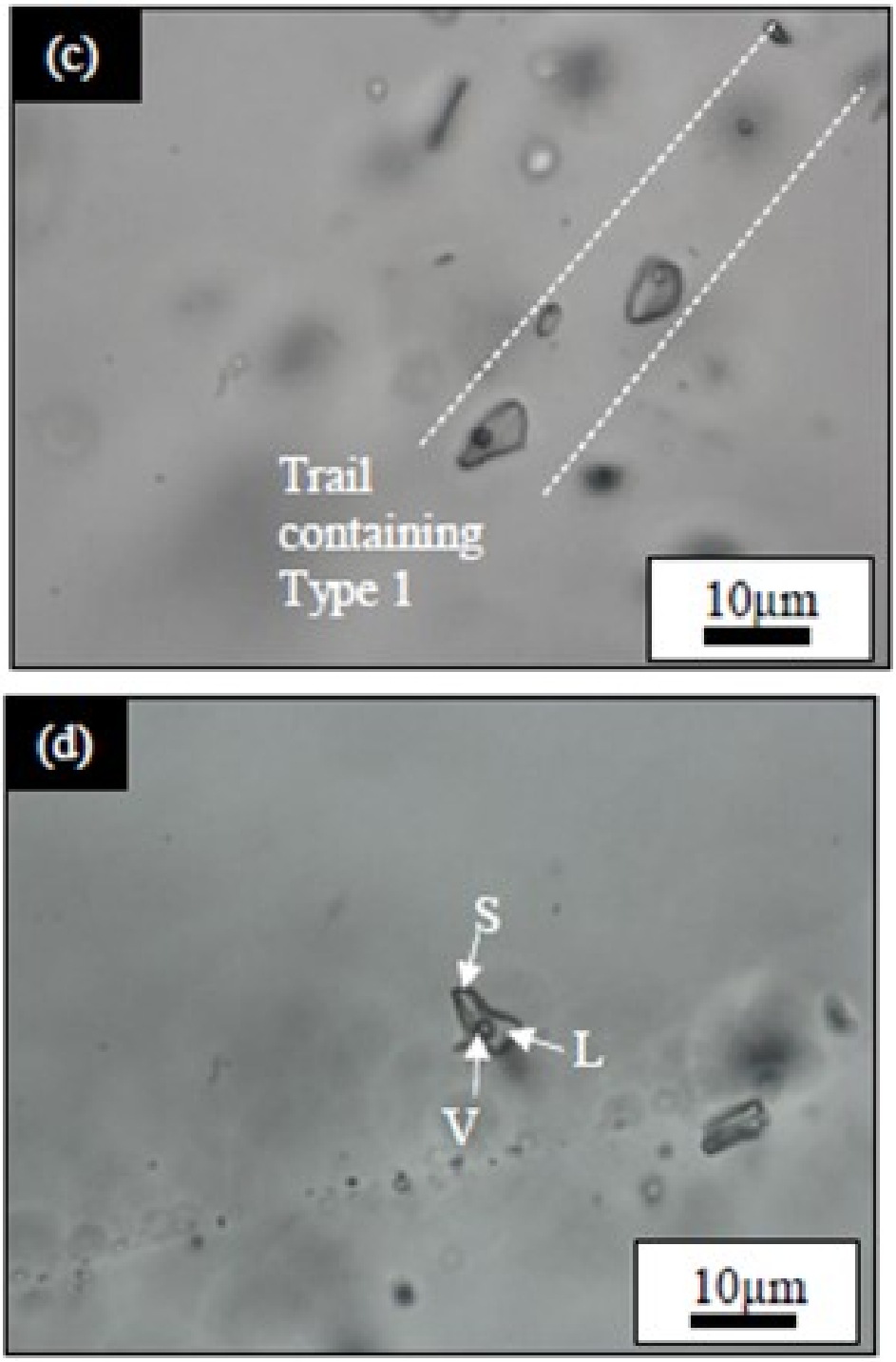

Figure 4.91: Photomicrographs of sample CO 005 (Coco) (c) Trail containing Type 1. (d) Isolated Type 2 (L=Liquid, V=Vapour, S=Solid).

4.3.3.1: Abuja Leather, Komu

Fluid inclusion microthermometry was carried out on thirteen Type 1 inclusions in sample AB 006 and fifteen Type 1 inclusions in sample AB 007 obtained from Abuja Leather in Komu. The length of inclusions vary from 3.7-9.2μm; type 1 inclusions in sample AB 006 homogenise to the liquid phase between 118°C to 130°C with mean T_H value of 125.3°C (Figure 4.92-4.93, table 4.19-4.20). T_{LM} values ranges from -1.4°C to -4.8°C corresponding to salinity values of 2.4 to 7.6 eq. wt.% NaCl. Type 1 inclusions in sample AB 007 homogenise to the liquid phase between 80°C and 99°C with a mean T_H value of 89.2°C. TLM values ranges from -3.9°C to -8.2°C corresponding to salinity values of 6.3 to 11.9 eq. wt.% NaCl (mean = 9.1 eq. wt.% NaCl).

4.3.3.2: Omoba in Okeho

Fluid inclusion microthermometry was carried out on seven Type 1, six Type 2 inclusions in sample OM 009 and eleven Type 1 inclusions in sample OM 010. The length of inclusions vary from 5.1-20.6μm; type 1 inclusions in sample OM 009 homogenise to the liquid phase at 159°C and 259°C with a mean T_H value of 204°C (Figure 4.94-4.95, table 4.21-4.22). TLM values ranges from -3.2°C to -5.6°C corresponding to salinity of 5.3 to 8.7 eq. wt.% NaCl (mean = 6.7 eq. wt.% NaCl).

Type 2 inclusions in sample OM 009 homogenise to the liquid phase (solid phase does not homogenise) between 318°C and 385°C with mean T_H value of 327.4°C. Type 1 inclusions in sample OM 010 homogenise to the liquid phase at 138°C to214°C with a mean T_H value of 185.2°C. T_{LM} values ranges from -0.4°C to -1.7°C which corresponds to salinity values of 0.7 and 3.1 eq. wt.% NaCl (mean = 1.8 eq. wt.% NaCl).

Table 4.19: Microthermometric result of Abuja Leather samples

Sample AB 006

Number	Sample	Type and Composition	Degree of Fill (F)	Length (µm)	T_{LM} (-°C)	Salinity (eq.wt.% NaCl)	T_H (°C)	To	Setting	Host Mineral
1	Chip 2	Type 1 Aqueous	0.90	4.8	4.8	7.6	125.8	Liquid	Trail	Quartz
2	Chip 2		0.90	5.3	4.2	6.7	126.3	Liquid	Trail	
3	Chip 2		0.90	8.2	2.5	4.2	130.3	Liquid	Trail	
4	Chip 2		0.90	4.6	4.5	7.2	118.2	Liquid	Trail	
5	Chip 1		0.90	8.1	2.0	3.4	124.3	Liquid	Trail	
6	Chip 1		0.85	3.7	1.8	3.1	128.2	Liquid	Trail	
7	Chip 1		0.90	5.4	1.5	2.6	126.5	Liquid	Trail	
8	Chip 1		0.90	4.6	1.6	2.7	130.2	Liquid	Trail	
9	Chip 1		0.90	6.2	1.4	2.4	122.4	Liquid	Trail	
10	Chip 1		0.90	6.8	1.8	3.1	128.4	Liquid	Trail	
11	Chip 1		0.90	7.4	2.4	4.0	124.9	Liquid	Trail	
12	Chip 1		0.90	8.6	2.5	4.2	120.3	Liquid	Trail	
13	Chip 1		0.90	9.2	2.2	3.7	123.7	Liquid	Trail	
				Minimum	1.4	2.4	118.2			
				Maximum	4.8	7.6	130.3			
				Average	2.6	4.2	125.3			

Table 4.20: Microthermometric result of Abuja Leather samples

Sample AB 007

Number	Sample	Type and Composition	Degree of Fill (F)	Length (μm)	T_{LM} (-°C)	Salinity (eq.wt.% NaCl)	T_H (°C)	To	Setting	Host Mineral
1	Chip 1	Type 1 Aqueous	0.90	7.0	8.2	11.9	93.6	Liquid	Trail	Quartz
2	Chip 1		0.90	6.5	7.6	11.2	94.2	Liquid	Trail	
3	Chip 1		0.90	4.4	4.5	7.2	99.1	Liquid	Trail	
4	Chip 1		0.90	4.6	4.8	7.6	84.3	Liquid	Trail	
5	Chip 1		0.90	4.8	7.2	10.7	86.4	Liquid	Trail	
6	Chip 1		0.90	6.6	6.2	9.5	80.1	Liquid	Trail	
7	Chip 1		0.90	6.9	4.3	6.9	82.6	Liquid	Trail	
8	Chip 1		0.90	5.9	3.9	6.3	98.3	Liquid	Trail	
9	Chip 1		0.90	4.7	4.2	6.7	94.2	Liquid	Trail	
10	Chip 1		0.90	4.8	4.2	6.7	93.6	Liquid	Trail	
11	Chip 1		0.90	6.5	4.6	7.3	85.3	Liquid	Trail	
12	Chip 1		0.90	6.1	5.8	8.9	85.0	Liquid	Trail	
13	Chip 1		0.90	6.7	8.1	11.8	87.8	Liquid	Trail	
14	Chip 1		0.90	8.2	7.7	11.3	91.4	Liquid	Trail	
15	Chip 1		0.90	3.9	7.9	11.6	81.9	Liquid	Trail	
				Minimum	3.9	6.3	80.1			
				Maximum	8.2	11.9	99.1			
				Average	5.9	9.0	89.2			

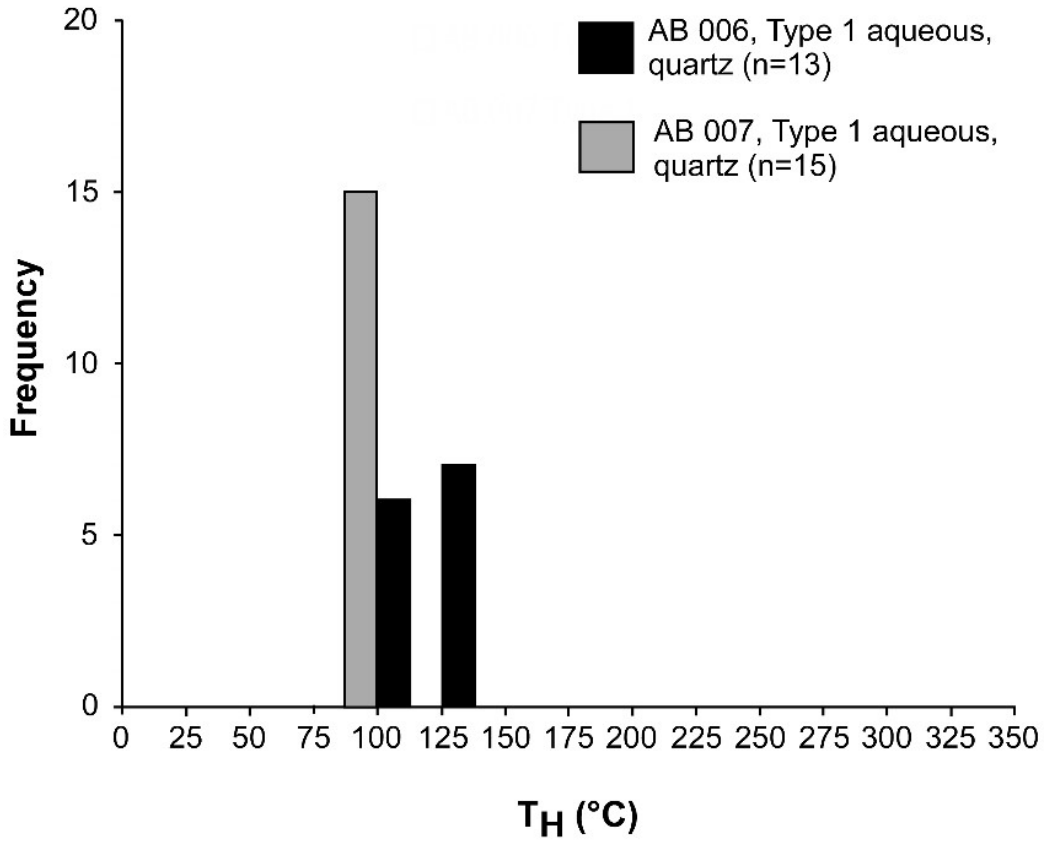

Figure 4.92: T_H frequency distribution histogram for Type 1 (n=28) FIs in Abuja leather samples

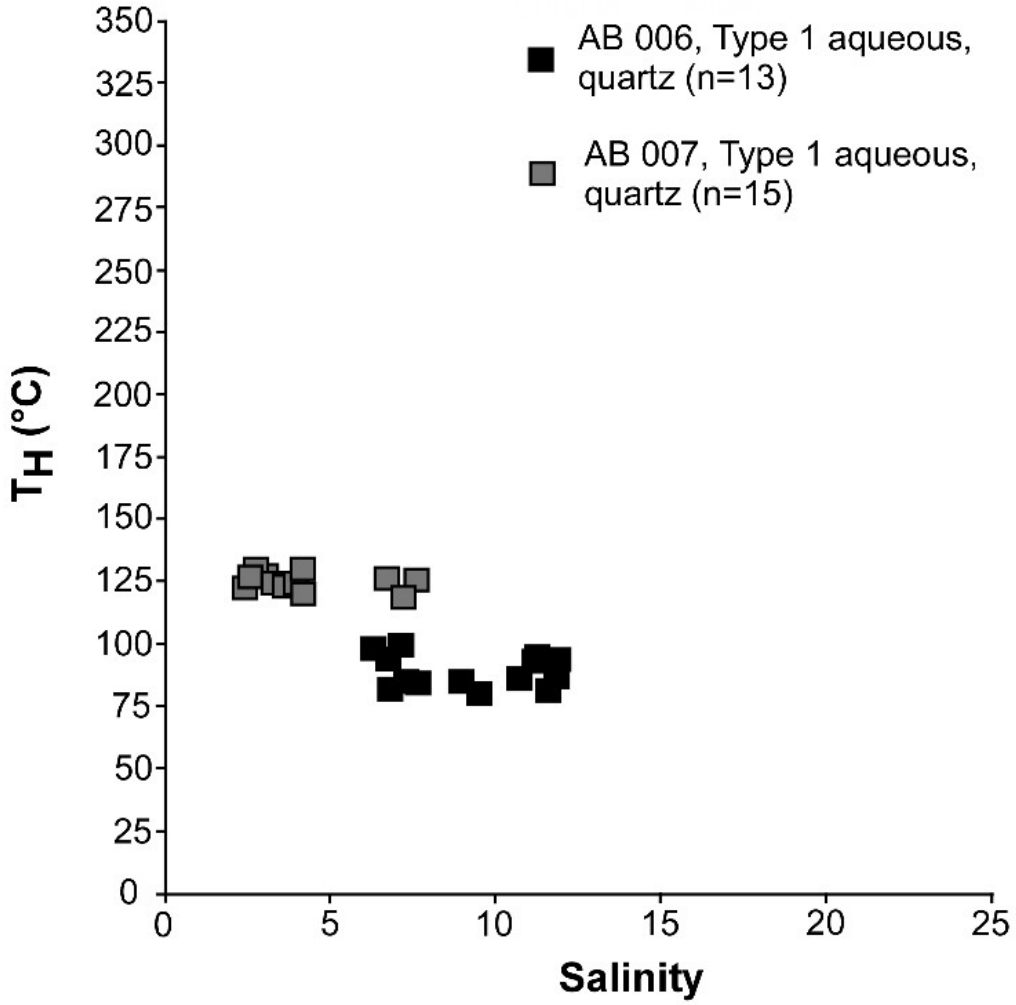

Figure 4.93: T_H versus salinity plot for Abuja leather samples.

Table 4.21: Microthermometric result of Omoba samples

Sample OM 009

Number	Sample	Type and Composition	Degree of Fill (F)	Length (µm)	T_{LM} (-°C)	Salinity (eq.wt.% NaCl)	T_H (°C)	To	Setting	Host Mineral
1	Chip 1	Type 1 Aqueous	0.80	14.6	5.1	8.0	227.5	Liquid	Trail	Quartz
2	Chip 1		0.80	6.3	5.6	8.7	259.1	Liquid	Trail	
3	Chip 1		0.80	9.0	4.2	6.7	254.3	Liquid	Trail	
4	Chip 2	Type 3	0.80	14.3	-	-	329.6	Liquid + solid	Cluster	
5	Chip 2	Type 3	0.90	9.9	-	-	326.5	Liquid + solid	Cluster	
6	Chip 2	Type 3	0.85	6.5	-	-	335.1	Liquid + solid	Cluster	
7	Chip 2	Type 3	0.85	9.6	-	-	329.8	Liquid + solid	Cluster	
8	Chip 3	Type 3	0.90	16.4	-	-	318.5	Liquid + solid	Trail	
9	Chip 3	Type 3	0.90	20.6	-	-	324.7	Liquid + solid	Trail	
10	Chip 4	Type 1 Aqueous	0.85	8.4	3.4	5.6	161.3	Liquid	Trail	
11	Chip 4		0.85	9.4	3.2	5.3	160.5	Liquid	Trail	
12	Chip 4		0.90	13.2	3.5	5.7	159.2	Liquid	Trail	
13	Chip 4		0.85	9.2	3.4	5.6	162.8	Liquid	Trail	
			Type 1	*Minimum*	3.2	5.3	159.2			
				Maximum	5.6	8.7	259.1			
				Average	5.0	7.8	247.0			
			Type 3	*Minimum*	0.0	0.0	318.5			
				Maximum	0.0	0.0	335.1			
				Average	0.0	0.0	327.4			

Table 4.22: Microthermometric result of Omoba samples

Sample OM 010

Number	Sample	Type and Composition	Degree of Fill (F)	Length (μm)	T_{LM} (-°C)	Salinity (eq.wt.% NaCl)	T_H (°C)	To	Setting	Host Mineral
1	Chip 1	Type 1 Aqueous	0.90	17.2	1.3	2.2	212.4	Liquid	Trail	Quartz
2	Chip 1		0.90	8.2	1.5	2.6	210.5	Liquid	Trail	
3	Chip 1		0.90	8.1	1.8	3.1	168.5	Liquid	Trail	
4	Chip 1		0.80	11.9	1.0	1.7	164.2	Liquid	Trail	
5	Chip 1		0.90	5.1	1.1	1.9	214.6	Liquid	Trail	
6	Chip 1		0.90	6.5	0.5	0.9	141.2	Liquid	Trail	
7	Chip 1		0.90	5.6	0.8	1.4	145.7	Liquid	Trail	
8	Chip 1		0.90	6.9	0.4	0.7	138.3	Liquid	Trail	
9	Chip 1		0.85	7.6	1.2	2.1	167.3	Liquid	Trail	
10	Chip 1		0.85	5.1	0.4	0.7	172.4	Liquid	Trail	
11	Chip 1		0.90	8.4	0.6	1.1	166.3	Liquid	Trail	
				Minimum	0.4	0.7	138.3			
			Type 1	*Maximum*	1.8	3.1	214.6			
				Average	1.0	1.7	172.9			

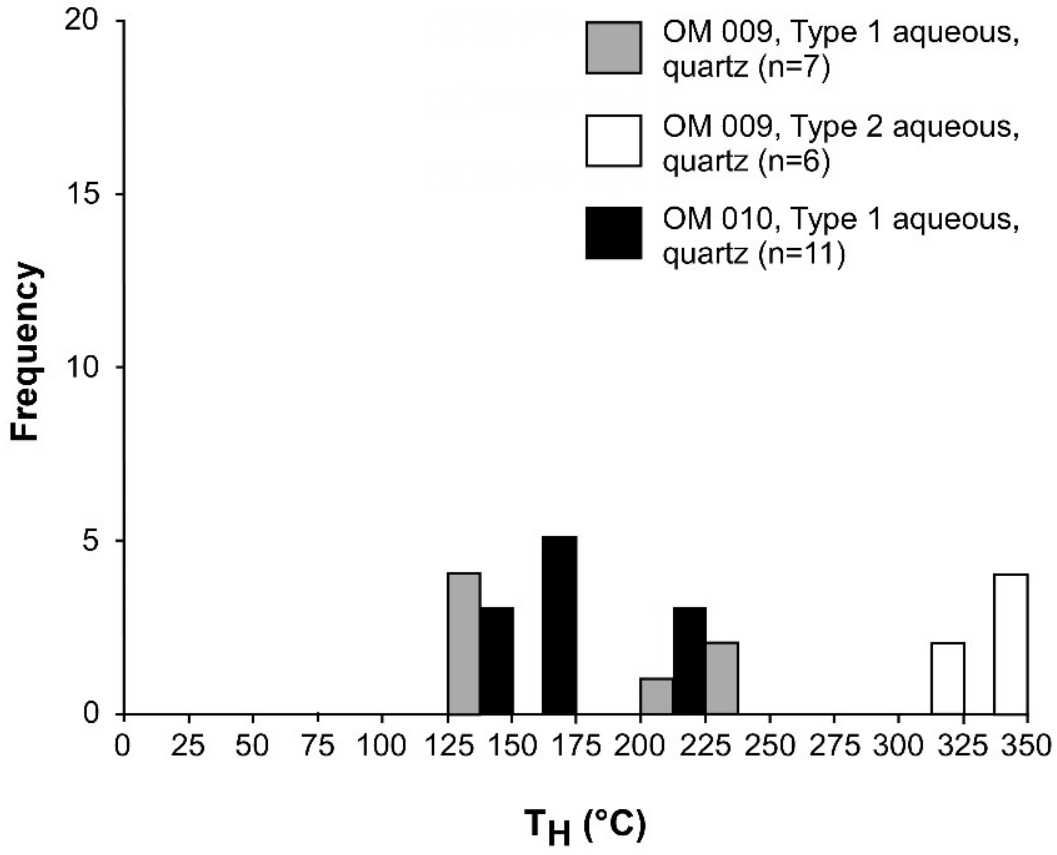

Figure 4.94: T_H frequency distribution histogram for Type 1 (n=18) and Type 2 (n=6) FIs in Omoba samples.

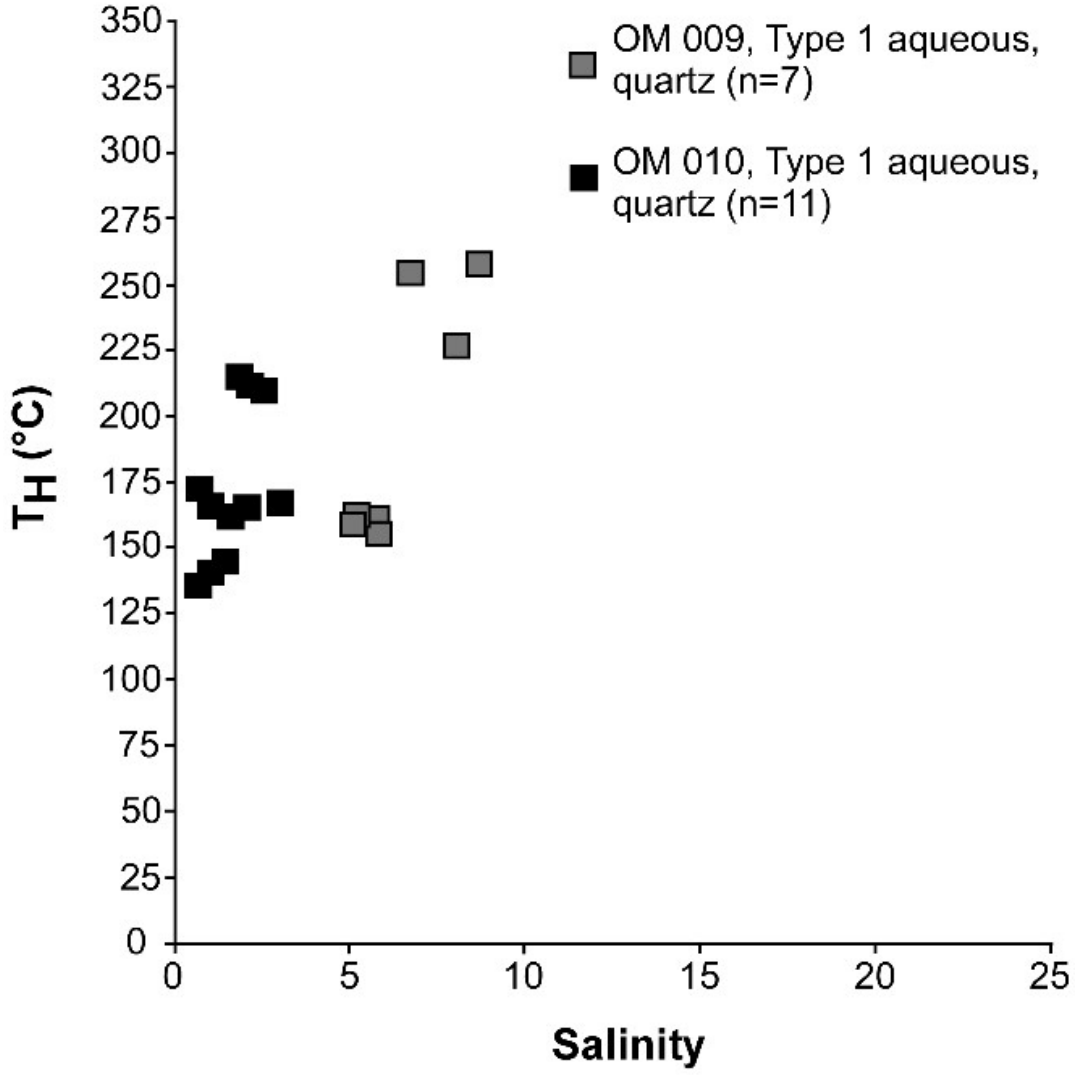

Figure 4.95: T_H versus salinity plot for Omoba samples.

4.3.3.3: Owode, Ibarapa

Microthermometry was carried out on eleven Type 1 inclusions and two Type 2 inclusions in sample OW 003. It was also carried out on eleven Type 1 inclusions and one Type 2 inclusion in sample OW 005. The length of inclusions vary from 2.9-20.1µm; type 1 inclusions in sample OW 003 homogenise into the liquid phase between 109°C and 229°C with mean T_H value of 167°C (Figure 4.96-4.97, table 4.23-4.24). T_{LM} occurs between -0.2°C and -8.6°C corresponding to salinity values of 0.4 and 12.4 eq. wt.% NaCl (mean = 6.9 eq. wt.% NaCl). Type 2 inclusions in sample OW 003 homogenise to the liquid phase (solid phase does not homogenise) at 142.5°C to 146.3°C with a mean T_H value of 144.4°C. Type 1 inclusions in sample OW 005 homogenise to the liquid phase between 152°C and 172°C with mean T_H value of 161.2°C. T_{LM} occurs between -0.1°C and -1.5°C corresponding to salinity values of 0.2 to 2.6 eq. wt.% NaCl (mean = 1.2 eq. wt.% NaCl). The Type 2 inclusion in sample OW 005 homogenises to the liquid phase (solid phase does not homogenise) at 162.5°C.

Table 4.23: Microthermometric results of Owode, Ibarapa samples

Sample OW 003

Number	Sample	Type and Composition	Degree of Fill (F)	Length (μm)	T_{LM} (-°C)	Salinity (eq.wt.% NaCl)	T_H (°C)	To	Setting	Host Mineral
1	Chip 1	Type 1 Aqueous	0.85	8.6	8.1	11.8	229.7	Liquid	Trail	Quartz
2			0.95	5.2	6.4	9.7	211.7	Liquid	Trail	
3			0.90	4.0	6.7	10.1	-	Liquid	Trail	
4			0.80	4.2	-	-	-	Liquid	Trail	
5			8.00	8.2	-	-	-	Liquid	Trail	
6			0.90	8.9	1.2	2.1	112.5	Liquid	Trail	
7			0.90	4.5	8.0	11.7	110.1	Liquid	Trail	
8			0.95	2.9	8.6	12.4	109.4	Liquid	Trail	
9	Chip 2	Type 3	0.80	5.3	-	-	142.5	Liquid + solid	Trail	
10			0.80	4.3	-	-	146.3	Liquid + solid	Trail	
11			0.85	5.7	-	-	-	Liquid + solid	Trail	
12		Type 1 Aqueous	0.85	5.6	1.2	2.1	175.3	Liquid	Trail	
13			0.90	6.1	1.5	2.6	163.5	Liquid	Trail	
14			0.80	6.1	0.5	0.9	169.5	Liquid	Trail	
15			0.85	3.2	0.2	0.4	173.2	Liquid	Trail	
16			0.80	4.1	0.6	1.1	164.5	Liquid	Trail	
17			0.90	5.1	0.2	0.4	166.3	Liquid	Trail	

Type 1	*Minimum*	0.2	0.4	109.4
	Maximum	8.6	12.4	229.7
	Average	3.3	5.0	162.3
Type 3	*Minimum*	0.0	0.0	142.5
	Maximum	0.0	0.0	146.3
	Average	0.0	0.0	144.4

Table 4.24: Microthermometric results of Owode, Ibarapa samples

Sample OW 005

Number	Sample	Type and Composition	Degree of Fill (F)	Length (μm)	T_{LM} (-°C)	Salinity (eq.wt.% NaCl)	T_H (°C)	To	Setting	Host Mineral
1	Chip 1	Type 3	0.85	8.6	-	-	162.1	Liquid + solid	Trail	Quartz
2	Chip 1	Type 3	0.85	7.0	-	-			Trail	
3	Chip 2	Type 1	0.80	20.1	1.3	2.2	152.3	Liquid	Trail	
4	Chip 2	Type 3	0.90	12.9	-	-	-		Trail	
5	Chip 2	Type 1 Aqueous	0.85	3.1	1.1	1.9	172.4	Liquid	Trail	
6	Chip 2		0.90	3.3	0.5	0.9	166.2	Liquid	Trail	
7	Chip 3		0.90	7.2	0.2	0.4	166.5	Liquid	Trail	
8	Chip 3		0.85	5.8	0.1	0.2	160.2	Liquid	Trail	
9	Chip 3		0.80	6.2	1.2	2.1	158.4	Liquid	Trail	
10	Chip 3		0.80	7.1	1.5	2.6	159.4	Liquid	Trail	
11	Chip 3		0.90	7.6	1.1	1.9	163.2	Liquid	Trail	
12	Chip 3		0.90	8.1	0.5	0.9	155.7	Liquid	Trail	
13	Chip 3		0.90	5.6	0.2	0.4	158.6	Liquid	Trail	
14	Chip 3		0.85	6.4	0.1	0.2	159.9	Liquid	Trail	

Type 1	*Minimum*	0.1	0.2	152.3
	Maximum	1.5	2.6	172.4
	Average	0.7	1.2	161.2
Type 3	*Minimum*	0.0	0.0	162.1
	Maximum	0.0	0.0	162.1
	Average	0.0	0.0	162.1

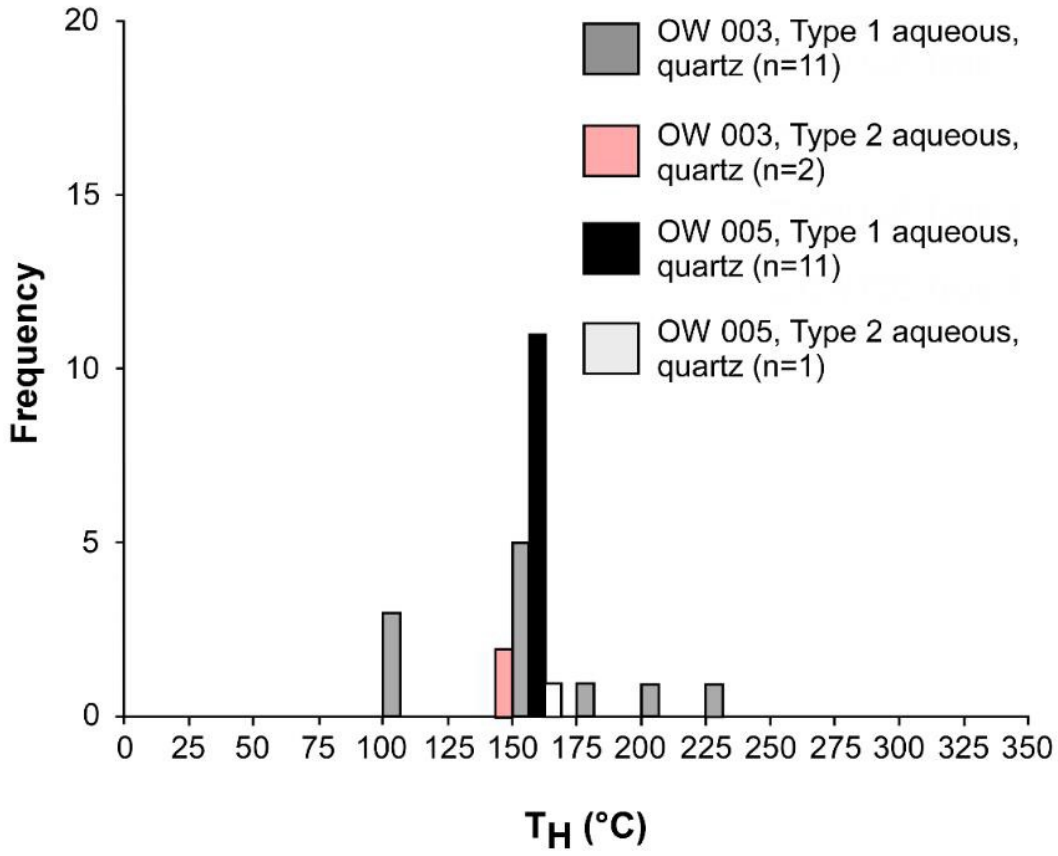

Figure 4.96: T_H frequency distribution histogram for Type 1 (n=22) and Type 2 (n=3) FIs in Owode, Ibarapa samples.

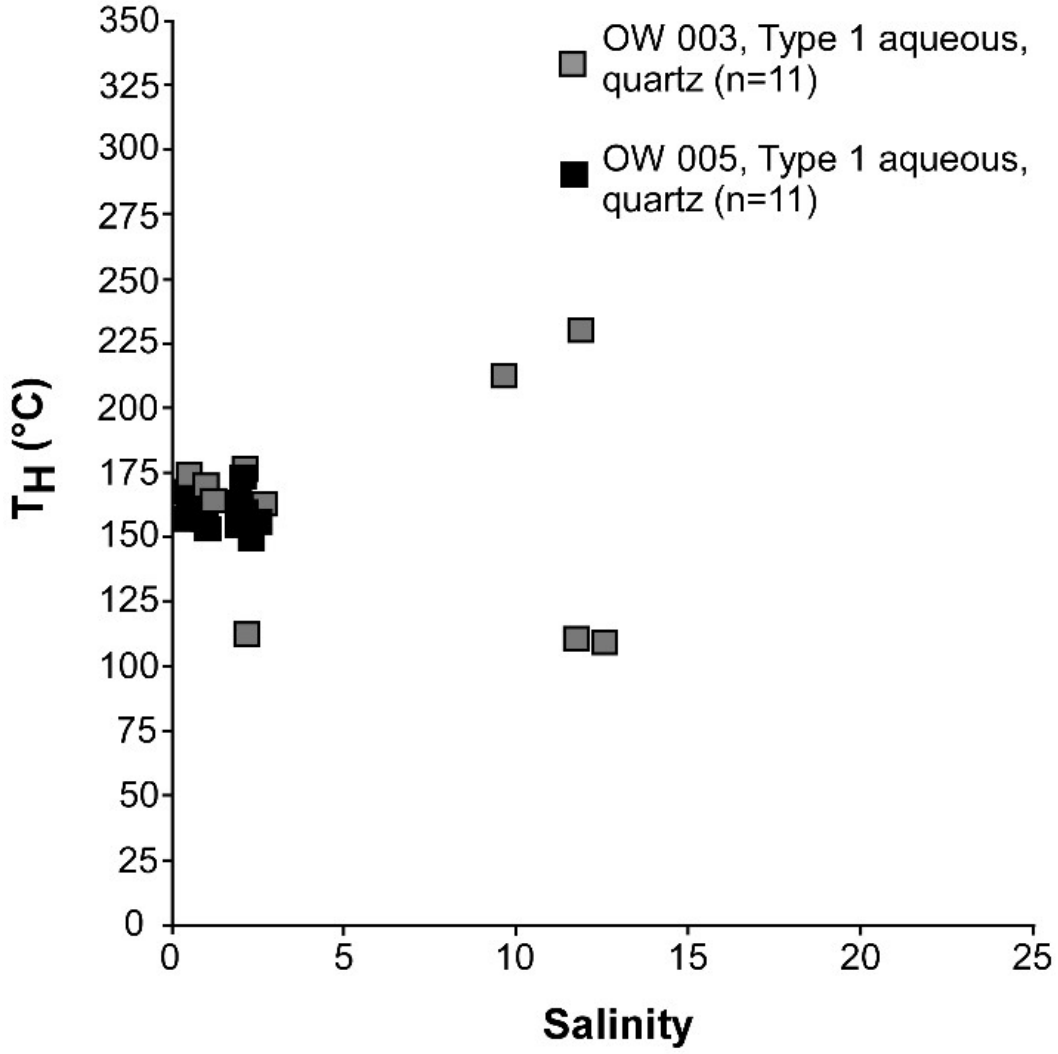

Figure 4.97: T_H versus salinity plot for Owode, Ibarapa samples

4.3.3.4: Gbayo, Olode

Fluid inclusion microthermometry was carried out on twenty-one Type 1 aqueous-rich inclusions in sample GB 001 and twelve Type 1 aqueous-rich inclusions and four Type 2 inclusions in sample GB 002. Type 1 inclusions in sample GB 001 homogenise to the liquid phase between 145°C and 156°C with a mean T_H value of 151°C (Figure 4.98-4.99, table 4.25-2.26). T_{LM} occurs between -17.2°C and -19.4°C corresponding to salinity values of 20.4 to 22 eq. wt.% NaCl (mean = 21.3 eq. wt.% NaCl). Type 1 inclusions in sample GB 002 homogenise to the liquid phase between 162°C and 175°C with a mean T_H of 169°C. T_{LM} occurs between -4.1°C and -6.2°C corresponding to salinity values of 6.6 to 9.5 eq. wt.% NaCl (mean = 7.8 eq. wt.% NaCl). Type 2 inclusions in sample GB 002 homogenise to the liquid phase between 146°C and 158°C. The solid phase homogenises to the liquid phase at 175°C.

Table 4.25: Microthermometric results of Gbayo samples

Sample GB 001

Number	Sample	Type and Composition	Degree of Fill (F)	Length (μm)	T_{LM} (-°C)	Salinity (eq.wt.% NaCl)	T_H (°C)	To	Setting	Host Mineral
1	Chip 1	Type 1 Aqueous	0.85	10.8	19.2	21.8	156.3	Liquid	Trail	Quartz
2	Chip 1		0.90	8.4	18.5	21.3	155.2	Liquid	Trail	
3	Chip 1		0.85	9.9	17.6	20.7	145.1	Liquid	Trail	
4	Chip 1		0.80	19.5	18.2	21.1	146.3	Liquid	Trail	
5	Chip 1		0.95	25.2	19.1	21.8	146.7	Liquid	Trail	
6	Chip 1		0.90	7.0	19.2	21.8	148.2	Liquid	Trail	
7	Chip 1		0.90	8.1	18.6	21.4	147.5	Liquid	Trail	
8	Chip 1		0.90	4.6	18.3	21.2	146.8	Liquid	Trail	
9	Chip 1		0.85	3.1	17.3	20.4	145.3	Liquid	Trail	
10	Chip 1		0.85	5.8	17.4	20.5	149.6	Liquid	Trail	
11	Chip 1		0.95	12.0	18.6	21.4	151.2	Liquid	Trail	
12	Chip 1		0.90	4.8	19.4	22.0	154.3	Liquid	Trail	
13	Chip 1		0.90	9.5	19.1	21.8	155.3	Liquid	Trail	
14	Chip 1		0.90	12.4	19.3	21.9	145.8	Liquid	Trail	
15	Chip 1		0.80	18.1	18.5	21.3	149.2	Liquid	Trail	
16	Chip 1		0.85	10.0	18.3	21.2	152.7	Liquid	Trail	
17	Chip 1		0.85	13.2	18.4	21.3	156.3	Liquid	Trail	
18	Chip 1		0.80	8.3	17.2	20.4	155.4	Liquid	Trail	
19	Chip 1		0.85	7.3	17.6	20.7	153.8	Liquid	Trail	
20	Chip 1		0.90	9.4	18.4	21.3	149.9	Liquid	Trail	
21	Chip 1		0.90	9.6	18.3	21.2	151.1	Liquid	Trail	
				Minimum	17.2	20.4	145.1			
				Maximum	19.4	22.0	156.3			
				Average	18.4	21.3	150.6			

Table 4.26: Microthermometric results of Gbayo samples

Sample GB 002

Sample	Type and Composition	Degree of Fill (F)	Length (μm)	T_{LM} (-°C)	Salinity (eq.wt.% NaCl)	T_H (°C)	To	Setting	Host Mineral
Chip1	Type 3	0.75	5.2	-	-	146.2	Liquid + solid	Trail	Quartz
Chip 1	Type 3	0.75	7.9	-	-	152.3	Liquid + solid	Trail	
Chip 1	Type 3	0.80	5.6	-	-	158.3	Liquid + solid	Trail	
Chip 1	Type 3	0.80	17.2	-	-	158.1	Liquid + solid	Trail	
Chip 2	Type 1 Aqueous	0.80	11.9	4.4	7.0	165.2	Liquid	Trail	
Chip 2		0.85	16.3	4.9	7.7	175.0	Liquid	Trail	
Chip 2		0.80	8.5	5.2	8.1	168.3	Liquid	Trail	
Chip 2		0.90	14.6	5.7	8.8	164.1	Liquid	Trail	
Chip 2		0.90	8.5	5.1	8.0	169.6	Liquid	Trail	
Chip 2		0.80	4.9	4.3	6.9	169.4	Liquid	Trail	
Chip 2		0.85	5.4	4.1	6.6	165.5	Liquid	Trail	
Chip 2		0.80	4.4	4.2	6.7	172.8	Liquid	Trail	
Chip 2		0.90	12.7	4.2	6.7	172.1	Liquid	Trail	
Chip 2		0.80	8.2	5.8	8.9	174.4	Liquid	Trail	
Chip 2		0.85	7.9	5.7	8.8	162.4	Liquid	Trail	
Chip 2		0.85	6.9	6.2	9.5	164.7	Liquid	Trail	

Type 1	*Minimum*	4.1	6.6	162.4
	Maximum	6.2	9.5	175.0
	Average	5.0	7.8	168.6
Type 3	*Minimum*	0.0	0.0	146.2
	Maximum	0.0	0.0	158.3
	Average	0.0	0.0	153.7

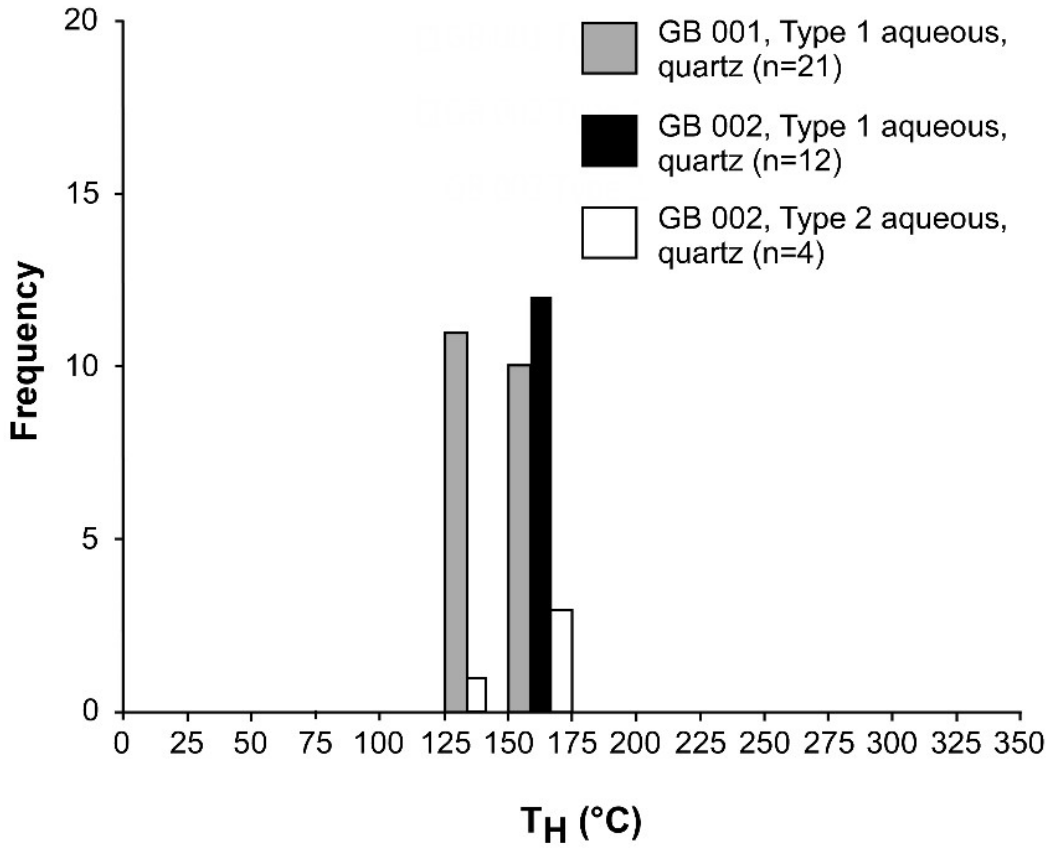

Figure 4.98: T_H frequency distribution histogram for Type 1 (n=33) and Type 2 (n=4) FIs in Gbayo, Olode samples.

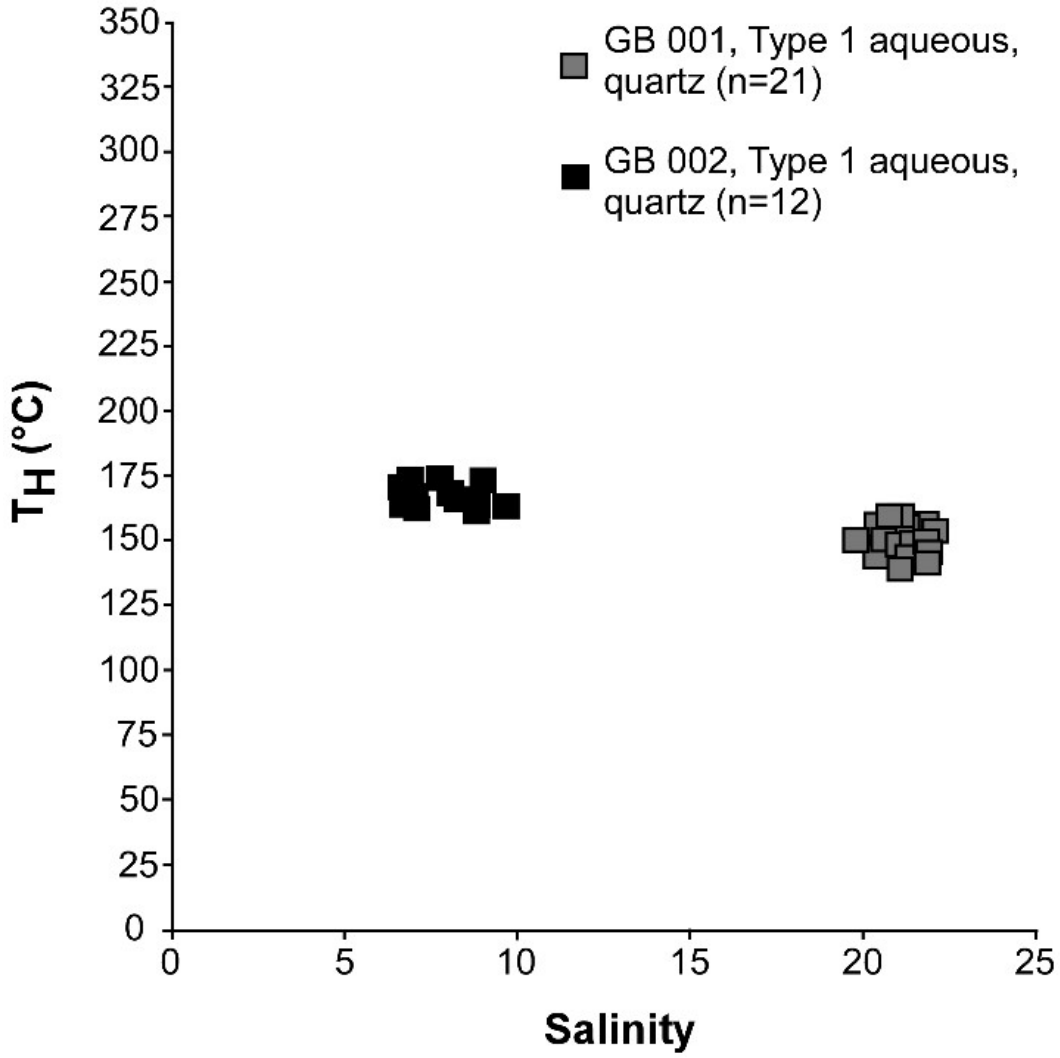

Figure 4.99: T_H versus salinity plot for Gbayo, Olode samples.

4.3.3.5: Coco, Olode

Fluid inclusion microthermometry was carried out on fourteen one Type 1 aqueous-rich inclusions in sample CO 003 and ten Type 1 inclusions and five Type 2 inclusions from sample CO 005. Type 1 inclusions in sample CO 003 homogenise to the liquid phase between 122°C and 142°C with a mean T_H value of 132°C (Figure 4.100-4.101, table 4.27-4.28). T_{LM} values ranges from -0.6°C to -2.1°C corresponding to salinity values of 1.1 to 3.5 eq. wt.% NaCl (mean = 2.2 eq. wt.% NaCl). Type 1 inclusions in sample CO 005 define two fluid populations (Population A and Population B).

Population A (n=3) which homogenise to the liquid phase between 150°C and 156°C with a mean T_H value of 153°C. T_{LM} occurs between -1.5°C and -3.4°C which corresponds to salinity values of 2.6 to 5.6 eq. wt.% NaCl (mean = 4.1 eq. wt.% NaCl). **Population B** (n = 7) homogenise to the liquid phase between 238°C and 261°C with a mean T_H value of 248°C. T_{LM} occurs between -2.8°C and -3.4°C corresponding to salinity values of 4.6 to 5.6 eq. wt.% NaCl (mean = 5.2 eq. wt.% NaCl/). Type 2 inclusions in sample CO 005 homogenise to the liquid phase (solid phase does not homogenise) between 305°C and 312°C.

A summary of the homogenisation properties of the inclusions is also in table 4.29-4.30

Table 4.27: Microthermometric results of Coco samples.

Sample CO 003

Number	Sample	Type and Composition	Degree of Fill (F)	Length (μm)	T_{LM} (-°C)	Salinity (eq.wt.% NaCl)	T_H (°C)	To	Setting	Host Mineral
1	Chip 1	Type 1 Aqueous	0.85	14.2	1.3	2.2	122.5	Liquid	Trail	Quartz
2	Chip 1		0.90	5.3	1.1	1.9	135.6	Liquid	Trail	
3	Chip 1		0.90	13.6	0.8	1.4	124.6	Liquid	Trail	
4	Chip 1		0.85	11.8	0.6	1.1	136.6	Liquid	Trail	
5	Chip 1		0.80	22.0	1.5	2.6	142.2	Liquid	Trail	
6	Chip 2		0.80	10.5	1.2	2.1	140.5	Liquid	Trail	
7	Chip 2		0.90	8.6	1.6	2.7	128.5	Liquid	Trail	
8	Chip 2		0.90	11.3	0.8	1.4	131.4	Liquid	Trail	
9	Chip 2		0.90	10.3	0.6	1.1	134.8	Liquid	Trail	
10	Chip 2		0.80	8.9	1.8	3.1	136.2	Liquid	Trail	
11	Chip 2		0.85	7.4	1.5	2.6	122.3	Liquid	Trail	
12	Chip 2		0.80	8.6	2.1	3.5	126.5	Liquid	Trail	
13	Chip 2		0.80	7.4	1.5	2.6	130.4	Liquid	Trail	
14	Chip 2		0.90	6.2	1.6	2.7	131.2	Liquid	Trail	
				Minimum	0.6	1.1	122.3			
				Maximum	2.1	3.5	142.2			
				Average	1.3	2.2	131.7			

Table 4.28: Microthermometric results of Coco samples.

Sample CO 005

Number	Sample	Type and Composition	Degree of Fill (F)	Length (μm)	T_{LM} (-°C)	Salinity (eq.wt.% NaCl)	T_H (°C)	To	Setting	Host Mineral
1	Chip 1	Type 1 Aqueous	0.85	7.1	3.2	5.3	156.2	Liquid	Trail	Quartz
2	Chip 1		0.90	7.7	3.4	5.6	150.3	Liquid	Trail	
3	Chip 1		0.90	12.0	2.8	4.6	152.8	Liquid	Trail	
4	Chip 1	Type 3	0.85	8.2	-	-	305.2	Liquid + solid	Trail	
5	Chip 1	Type 3	0.90	9.6	-	-	310.6	Liquid + solid	Trail	
6	Chip 1	Type 3	0.90	8.2	-	-	312.2	Liquid + solid	Trail	
7	Chip 2	Type 3	0.90	10.4	-	-	310.8	Liquid + solid	Trail	
8	Chip 2	Type 3	0.90	10.5	-	-	305.4	Liquid + solid	Trail	
9	Chip 2	Type 1 Aqueous	0.85	8.1	1.5	2.6	241.3	Liquid	Trail	
10	Chip 2		0.80	13.4	2.1	3.5	238.6	Liquid	Trail	
11	Chip 2		0.90	12.2	3.2	5.3	250.2	Liquid	Trail	
12	Chip 2		0.90	6.0	2.5	4.2	261.3	Liquid	Trail	
13	Chip 2		0.85	8.1	2.8	4.6	248.3	Liquid	Trail	
14	Chip 2		0.90	9.6	1.7	2.9	245.7	Liquid	Trail	
15	Chip 2		0.90	6.4	3.4	5.6	253.4	Liquid	Trail	
			Type 1	*Minimum*	1.5	2.6	150.3			
				Maximum	3.4	5.6	261.3			
				Average	2.7	4.4	219.8			
			Type 3	*Minimum*	0.0	0.0	305.2			
				Maximum	0.0	0.0	312.2			
				Average	0.0	0.0	308.8			

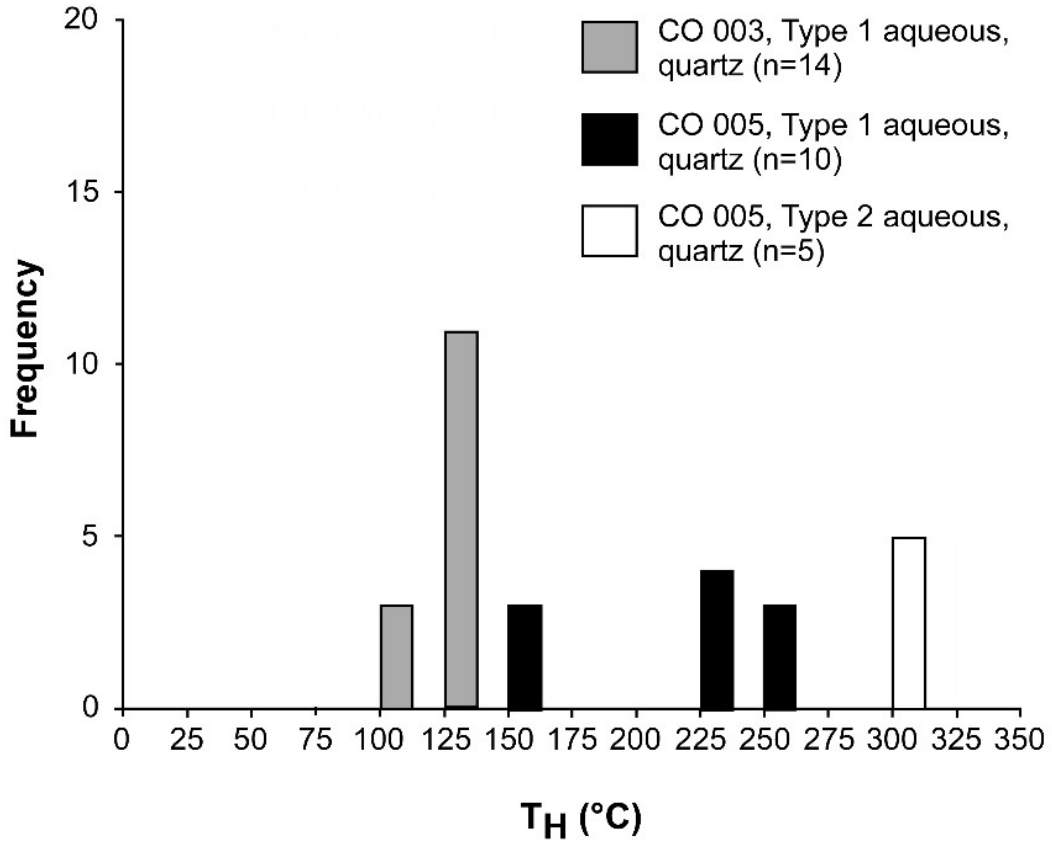

Figure 4.100: T_H frequency distribution histogram for Type 1 (n=24) and Type 2 (n=4) FIs in Coco samples.

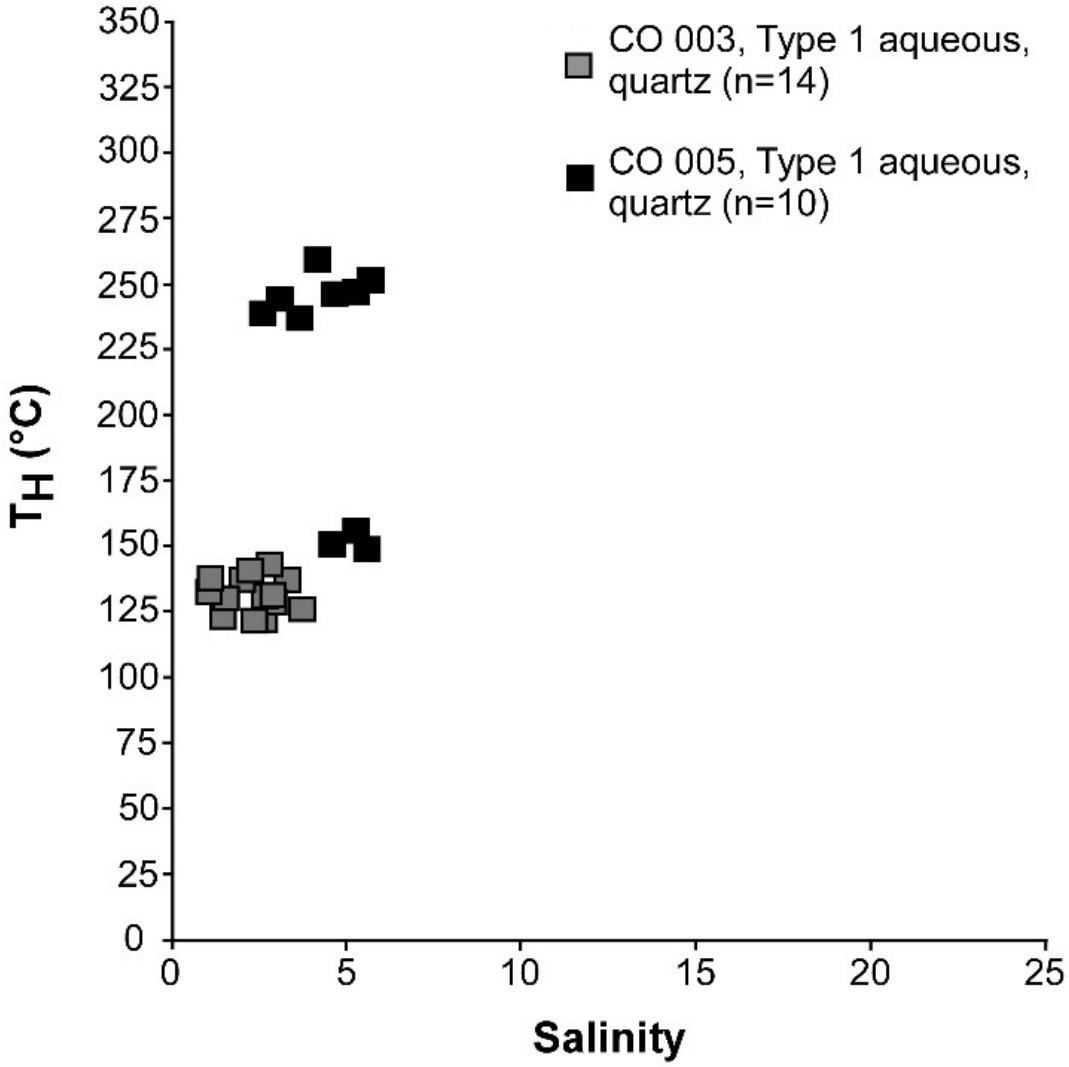

Figure 4.101: T_H versus salinity plot for Coco samples.

Table 4.29: Salinity and homogenisation measurements of inclusion wafers

Sample	Salinity (eq. wt. % NaCl)			T_H (°C)		
	Minimum	Maximum	Average	Minimum	Maximum	Average
AB 006	2.4	7.8	4.2	118	130	125
AB 007	6.3	12	9.1	80	99	89
OM 009	5.3	8.7	6.7	159	260	201
OM 010	0.7	3.1	1.9	138	215	186
OW 003	0.4	12.4	6.9	109	230	167
OW 005	0.2	2.6	1.2	152	172	162
GB 001	20.4	22	21.3	145	156	151
GB 002	6.6	9.5	7.8	162	175	169
CO 003	1.1	3.6	2.2	122	142	132
CO 005 Pop. A	4.6	5.6	5.2	150	156	153
CO 005 Pop. B	2.6	5.6	4.1	238	261	248

Table 4.30: Range and average of homogenisation temperature per location

Sample	T_H (°C)		
	Minimum	Maximum	Average
OM 009	319	335	327
OW 003	143	146	144
OW 005	152	172	161
GB 002	146	158	154
CO 005 Pop. B	305	312	309

4.3.4: Discussion: Modelling Trapping Pressure and Temperature (P-T) of Aqueous Fluids

Isochores were constructed to constrain trapping temperature and pressure of fluids using the PVT (Pressure, Volume, Temperature) modelling software FLUIDS. Temperature of homogenisation (T_H), calculated salinity (eq. wt% NaCl), for Type 1 aqueous inclusions, were used to generate an isochore for each sample. To model fluid trapping temperatures, a maximum trapping pressure was estimated based upon crystallisation depth for granitoid magmas (1.5 kilobar ≈ 5.1km; Hunt et al., 2005).

4.3.4.1: Abuja Leather, Komu

The microthermometric data used are as follows: sample AB 006, T_H = 89.2°C, F = 0.9, T_{LM} = -6.0°C and for sample AB 007, T_H = 125.3°C, F = 0.9, T_{LM}= -2.6°C.

Both temperatures are considered to be low and therefore unrelated to higher temperature magmatic fluids. Assuming a maximum lithostatic pressure of ~1.5kbar (~5 km) this equates to corrected minimum trapping temperatures of ~190°C. These modelled temperatures show a temperature correction of about 65°C for the fluids modelled in this pegmatite (Figure 4.102). The differing TH and salinity values between the fluids in AB 006 and AB 007 may represent a dilution trend that indicates an interaction of two fluids, one of which may be of meteoric origin.

4.3.4.2: Omoba, Okeho

The microthermometric data used for Omoba samples was T_H = 165.5°C, F = 0.9 and T_{LM} = -2.1°C. This temperature is considered to be moderate to high and is therefore likely to be related to higher temperature magmatic fluids. Assuming a minimum lithostatic pressure of ~1.5kbar (~5km) this equates to corrected maximum trapping temperatures of ~250°C. This modelled temperature shows a temperature correction of about 85°C for the fluids modelled in this pegmatite (Figure 4.103).

4.3.4.3: Owode, Ibarapa

The microthermometric data used for Owode samples was T_H = 164.9°C, F = 0.85 and T_{LM} = -0.7°C. This temperature is considered to be moderate to high and is therefore likely to be related to higher temperature magmatic fluids. Assuming a maximum lithostatic pressure of ~1.5 kbar (~5km) this equates to corrected minimum

trapping temperatures of ~250°C. This modelled temperature shows a temperature correction of about 85°C for the fluids modelled in this pegmatite (Figure 4.104).

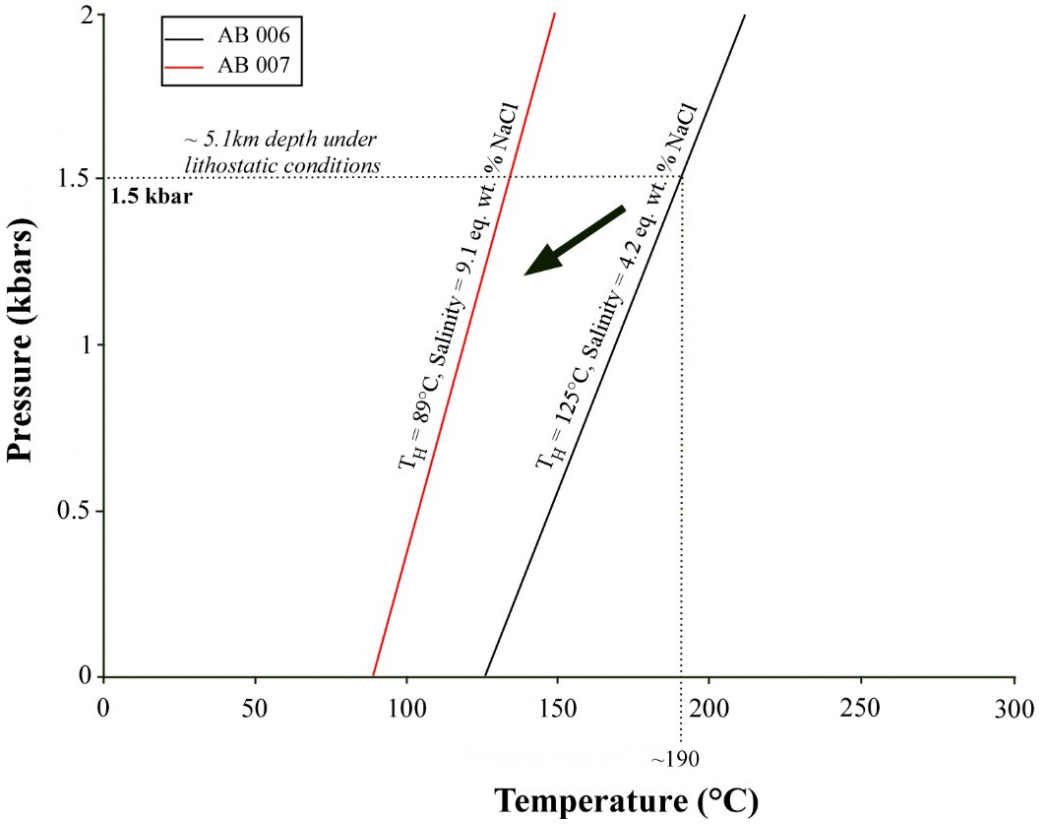

Figure 4.102: Isochores calculated for Type 1 aqueous FIs in Abuja leather sample. Arrow indicates possible dilution trend.

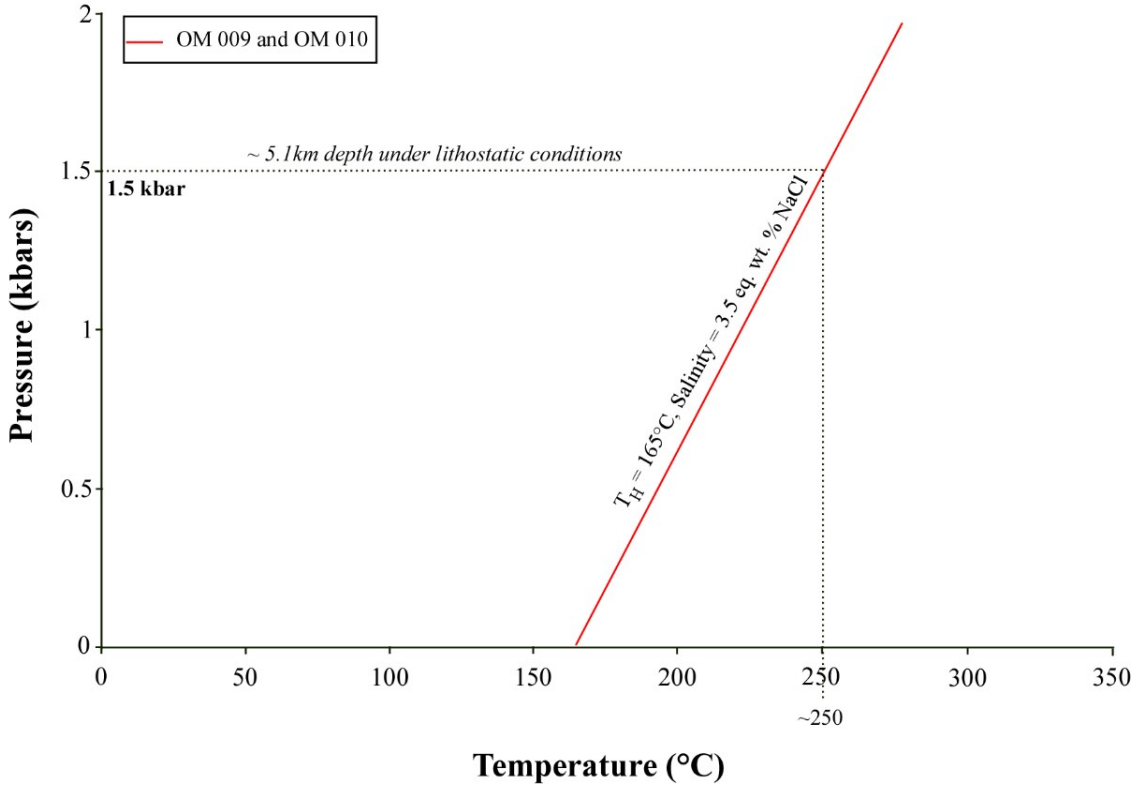

Figure 4.103: Isochore calculated for Type 1 aqueous FIs in samples from Omoba area.

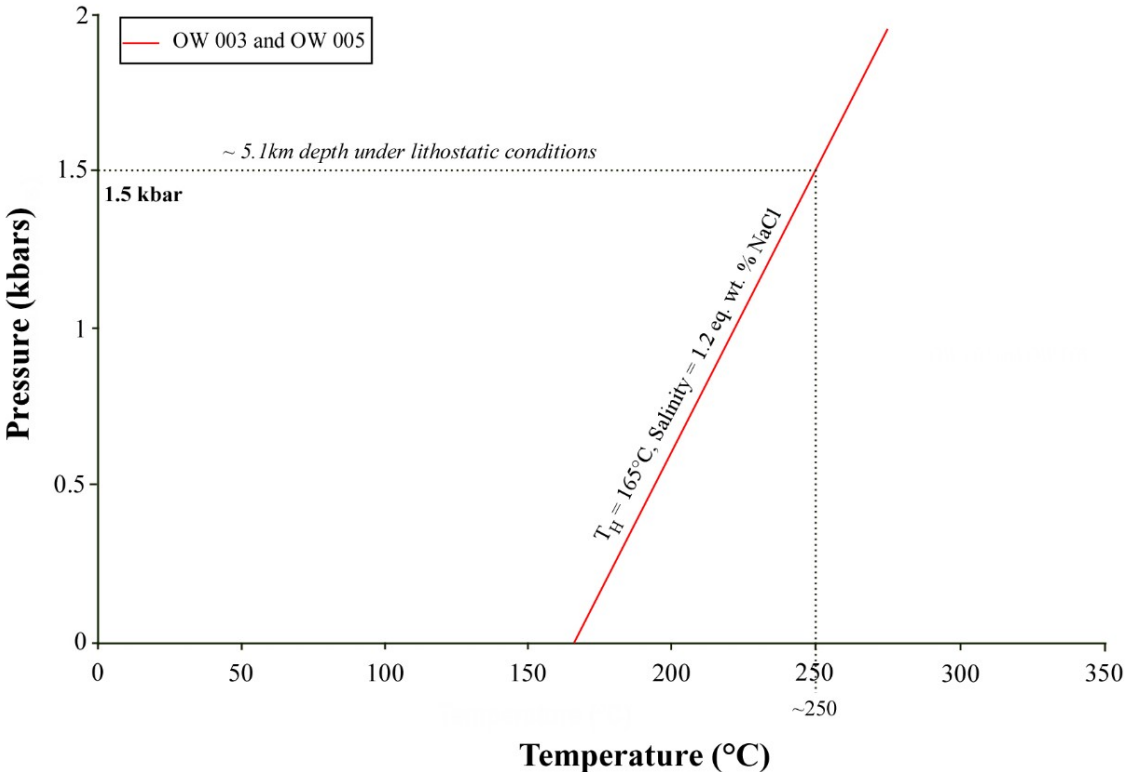

Figure 4.104: Isochore calculated for Type 1 aqueous FIs in Owode samples.

4.3.4.4: Gbayo, Olode

The microthermometric data used are as follows:

sample GB 001, T_H = 150.6°C, F = 0.9, T_{LM} = -18.4°C;

sample GB 002, T_H = 168.6°C, F = 0.9, T_{LM}= -5°C.

These temperatures are considered to be moderate to high and are therefore likely to be related to higher temperature magmatic fluids. Assuming a maximum lithostatic pressure of ~1.5kbar (~5km) this equates to a corrected minimum trapping temperature of ~250°C. These modelled temperatures show a temperature correction of about 80°C for the fluids modelled in this pegmatite (Figure 4.105). The differing T_H and salinity values between the fluids in AB 006 and AB 007 may represent a dilution trend that indicates an interaction of two fluids, one of which may be of meteoric origin.

4.3.4.5: Olode

The microthermometric data used are as follows:

Sample CO 003, T_H = 131°C, F = 0.85, T_{LM} = -1.3°C;

Sample CO 005, T_H = 248.4°C, F = 0.9, T_{LM}= -2.5°C.

Temperatures for CO 003 are considered to be low to moderate and therefore unrelated to higher temperature magmatic fluids. Temperatures for sample CO 005 are considered to be high and therefore the fluids are associated with magmatic activity. Assuming a maximum lithostatic pressure of 1.5kbar (~5km) this equates to a corrected minimum trapping temperature of ~ 325°C. These modelled temperatures show a temperature correction of about 75°C for the fluids modelled in this pegmatite (Figure 4.106). The differing T_H and salinity values between the fluids in AB 006 and AB 007 may represent a dilution trend that indicates an interaction of two fluids, one of which may be of meteoric origin.

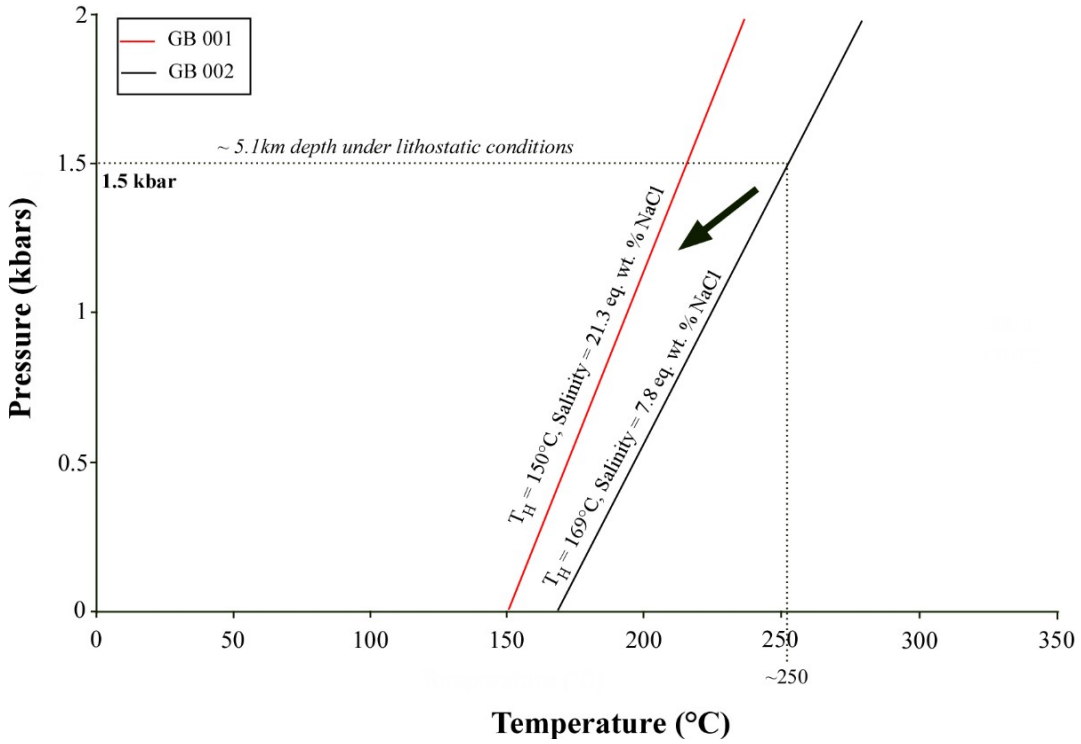

Figure 4.105**:** Isochores calculated for Type 1 aqueous FIs in samples from Gbayo. Arrow indicates possible dilution trend.

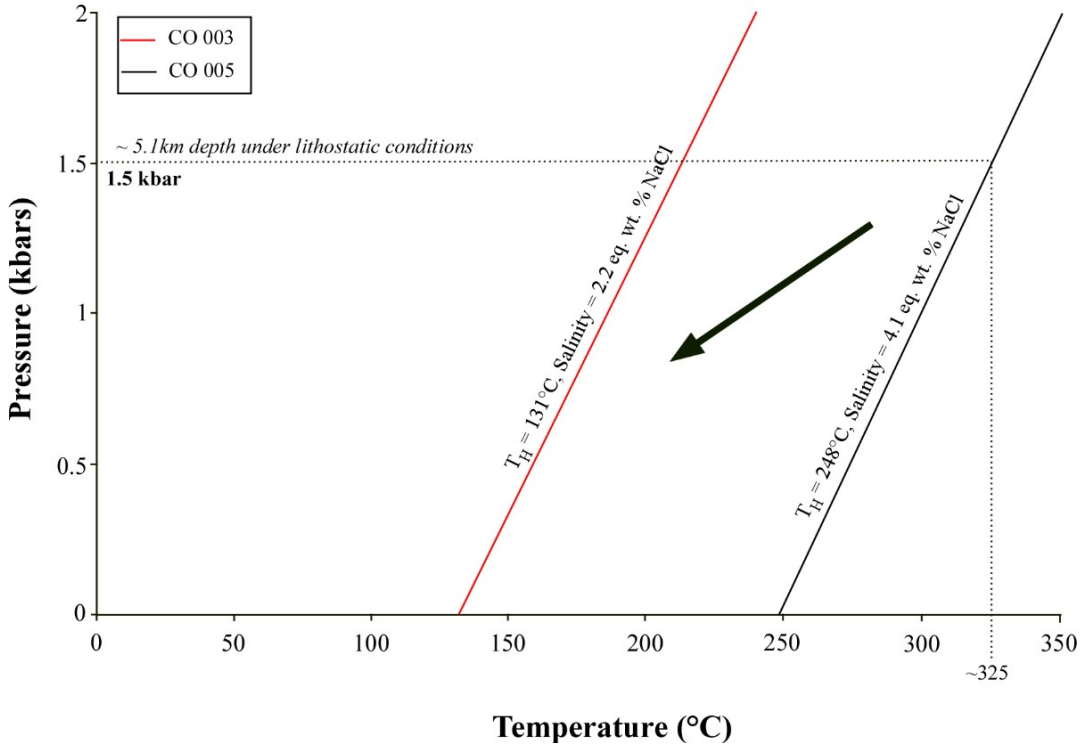

Figure 4.106: Isochores calculated for Type 1 aqueous FIs in Coco samples. Arrow indicates possible dilution trend.

Based on the data presented above, a qualitative model is generated that shows a pressure-temperature-time (PTt) path of fluid trapping for the pegmatites (Figure 4.107). The fluids trapped initially at Time 1 (Type 2 FI) have relatively high minimum trapping temperatures (i.e. homogenisation T~350°C). These may then be the earliest fluids trapped and may be associated with late magmatic-hydrothermal fluids. The trapping of Type 2 fluids is then followed by the trapping of Type 1 fluids (Time 2 and Time 3). Higher (~250°C) and lower (~160°C) T_H values for Type 1 FI may indicate a dilution trend suggesting interaction between at least two fluids suggesting interaction between very late magmatic and meteoric fluids. Finally, the presence of Type 3 FI indicate a much lower temperature and pressure regime at Time 4 (<50°C).

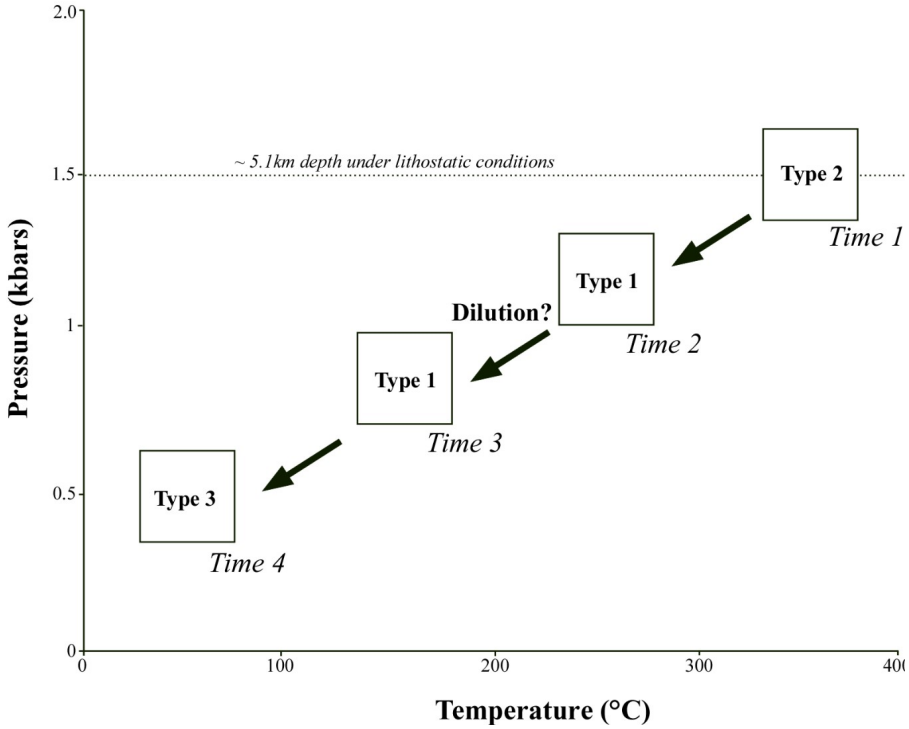

Figure 4.107: A qualitative pressure-temperature-time (PTt) model for fluid trapping.

CHAPTER FIVE

SUMMARY, CONCLUSION ANDRECOMMENDATIONS

5.1: Summary

Geochemistry, mineralisation potential and fluid characteristics of pegmatites in selected areas of southwestern Nigeria has been studied. The areas were systematically mapped and mapping revealed pegmatites are associated with different lithological units in the selected areas; these lithologies include: granite gneisses, sillimanite quartzite, pellitic schists, amphibolites and quartz mica schists.

Pegmatites occur as intrusions associated with the different lithologies and are composed of quartz + microcline + muscovite $\pm$ biotite. Geochemical analysis reveals silica concentration for whole rock pegmatites while other mineral extracts had lower silica content while alumina concentration varies across the extracts. Across all samples, SiO_2 ranged 35.22-82.17%, CaO ranged 0.01-2.61%, Na_2O ranged 0.09-10.16%, and P_2O_5 ranged 0.01-0.23%. Al_2O_3 ranged 9.84-34.81%, Fe_2O_3 ranged 0.10-19.70%, MnO ranged 0.01-1.69%, MgO ranged 0.02-8.55% and K_2O 0.08-12.66% with highest concentration of Al_2O_3, TiO_2, MnO, MgO and Fe_2O_3 in biotite extracts.

Geochemical analysis revealed low concentration of rare metals. Ta, Nb, Ta, Cs and W had values (in ppm) ranging 0.54-76.00, 0.60-73.00, 0.70-50.00 and 97.00-933.00 in whole rock pegmatites; 0.32-69.00, 0.60-61.00, 0.90-351.00 and118.00-600.00 in feldspar extracts; 33.00-107.00, 237.00-330.00, 40.00-252.00 and 17.00-214.00 in muscovite extracts; 1.00-69.00, 4.80-312.00, 0.70-475.00 and 28.00-699.00 in biotite extracts while $\sum$REE (in ppm) in whole rock pegmatites and extracts vary from low to moderate with values ranging 0.39-555.77, 0.19-58.36, 0.16-3.4 and 12.79-486.83 in whole rock, feldspar extracts, muscovite extracts and biotite extracts respectively.

Plots of K/Rb versus Cs, Ta versus Ga, Ta vs Cs, Ta vs Cs + Rb, Ta vs K/Cs as well as the Th/u vs K/Cs revealed low level of Ta-Nb mineralisation the pegmatites and extracts. Nb/Ta and Ta/W ranged from 0.41-7.74 and 0.01-0.80 in whole rock

pegmatites, 0.85-6.02 and 0.01-0.25 in feldspar extracts, 2.35-7.29 in muscovite extracts and 3.54-12.73 and 0.01-0.92 in biotite extracts.

Fluid characterisation using microthermometry on pegmatitic quartz revealed three types of aqueous inclusions. Type 1 are two-phase LV (L>V) inclusions (~2 - 100 μm) occurring as isolated individuals, in clusters and in trails in quartz. They are primary to pseudosecondary in origin. Microthermometric analyses yield final temperature of melting of ice which ranged -19.5 ^{o}C to -0.1 ^{o}C which is equivalent to salinity of 0.18 to 22 eq. wt. % NaCl while T_H values ranged from 80°C to 261°C.

Type 2 inclusions are three-phase (L+V+S) inclusions (~2-15μm) occurring in isolation and in trails. They are primary to pseudosecondary in origin. Microthermometric analyses yield T_H values of 143°C to ~335°C with higher T_H values inferred to be magmatic in origin. Two distinct solid phases were being observed in samples obtained from Omoba, Owode and Coco, both types are <3μm in longest dimension and may indicate the presence of sylvite (KCl).

Type 3 are monophase (liquid) aqueous inclusions at room temperature and occur as isolated individuals, as clusters and in trails that also contain Type 1 and Type 2 in quartz. Type 3 is primary to pseudosecondary in origin and is indicative of trapping temperatures of below 50°C; and they record migration of low temperature aqueous fluids.

5.2: Conclusion

Based on geochemical analytical results and geochemical variation plots, pegmatites in the studied locations have low level of Ta mineralisation and moderate levels of Nb and W mineralisation in muscovite extracts compared to other extracts. Fluid characterisation revealed pegmatites are magmatic in origin but meteoric fluids were involved in pegmatite genesis in some of the areas.

5.3: Recommendations

1. Fluid inclusion analyses on additional samples should be carried out to consolidate results for each pegmatite.
2. Identification of the solid phases in Type II fluid inclusions should be done using Laser and Raman Microspectroscopy.

REFERENCES

Abaa, S. I. 1983. The structure and petrography of alkaline rocks of the Mada Younger Granite Complex, Nigeria. *Journal of African Earth Sciences* 3:107–113.

Ackerman, J., Zacharia, J., Pudilova, M. 2007. P–T and fluid evolution of barren and lithium pegmatites from Vlasteˇjovice, Bohemian Massif, Czech Republic. *International Journal of Earth Science* 96:623–638

Ajibade, A. C., Fitches, W. R., Wright, J. B. 1979. The Zungeru mylonites, Nigeria: recognition of a major unit. *Rev de Geol Geog Phys* 21:359–363.

Akçay, M., Moon C.J., and Scott B.C. 1995. Fluid Inclusions and Chemistry of Tourmalines from the Gümüþler Sb-Hg ± W Deposits of the Niðde Massif, Central Turkey. Chem. Erde 55: 225-236.

Akintola, A. I., Omosanya, K. O., Ajibade O. M., Okunlola, O. A and Kehinde-Philips, O. O. 2011. Petrographic and geochemical evaluations of Rare – Metal (Ta-Nb) potentials of Precambrian pegmatities of Awo Area Southwestern, Nigeria. *International Journal of Basic and Applied Sciences* 11.4: 57 – 70.

Arribas, A., Cunningham, C.G., Rytuba, J.J., Rye, R.O., Kelly, W.C., Podwysocki, M.H., McKee, E.H., Tosdal, R.M. 1995. Geology, Geochronology, fluid inclusions, and isotopes geochemistry of the Rodalquilar gold alunite deposit, Spain. *Economic geology.* 90.4:795-822

Ashworth, L. 2014. Mineralised pegmatite of the Damara Belt, Namibia: Fluid inclusion and geochemical characteristics with implications for post collisional mineralisation. Ph.D Thesis. University of the Witwatersrand.

Bakker, R. J., 2003. Clathrates: computer programs to calculate fluid inclusion V-X properties using clathrate melting temperatures. *Computers and Geosciences* 23.1:1-18.

Bailey, S.W. 1984. Structures, classification and crystal chemistry of micas. *The Micas* S.W. Bailey. Ed. Mineralogical Society of America, Reviews in Mineralogy 13: 1–57.

Belyankina, Y.D. and Petrov, V.P. 1983. Geochemical role of micas in mineral associations: classification, chemistry and genesis of micas. *International Geology Review* 25: 993–1003.

Beurlen, H., Rainer, T., Rodrigues da Silva, M.R., Müller, A., Rhede, D and, Soares, D.R. (2014): Perspectives for Li- and Ta-Mineralization in the Borborema Pegmatite Province, NE-Brazil: A review. *Journal of South American Earth Sciences* 56 (2014)

Beurlen, H., Da Silva, R. R., Thomas, R., Soares, D. R. and Olivier, P., 2008. Nb-Ta-(Ti-Sn)-oxide mineral chemistry as tracers of rare -element granitic pegmatite fractionation in the Borborema Province, Northeast Brazil. *Mineralium Deposita*,. 43: 207-228.

Beus, A. A. 1966. Distribution of tantalum and niobium in muscovites of granitic pegmatites. *Geokhimiy*, 10:1216 – 1220.

Burke, K. C. and Dewey, J. F., 1972. African Geology *Orogeny in Africa*.. A.J. Dessauragie, T.F.J. Whiteman Eds, University of Ibadan Press, Nigeria. 583-608.

Cameron, E.N., Jahns, R.H., McNair, A.H. and Page, L.R. 1949. Internal structure of granitic pegmatite. *Economic Geology* Monograph 2.

Cempirek, J. and Novak, M. 2006. Mineralogy of dumortierite-bearing abyssal pegmatites at Starkoc and Bestvina, Kutna Hora Crystalline Complex. I. *C'zech Geological. Society.* 51:259-270.

Černý, P. 1991b. Rare-element granitic pegmatite. Part II: regional to global environments and petrogenesis. *Geoscience Canada* 18:49 - 62.

Černý, P., London, D. and Novák, M. 2012. Granitic Pegmatite as reflections of their Sources. Elements: *An International Magazine of Mineralogy, Geochemistry, and Petrology* 8.4:289 - 294.

Černý, P., Trueman, D.L., Ziehlke, D.V., Goad, B,E, and Paul, B.J. 1981. The Cat Lake - Winnipeg River and the Wekusko Lake pegmatite fields, Manitoba. *Manitoba Department of Energy and Mines Mineral Resources Division, Economic Geology Report* ER80-1.

Cerny, P. and Ercit, T. S., 2005. The classification of granitic pegmatite revisited. *Canadian Mineralogist* 43:2005-2026.

Černý, P. 1991a. Rare-element granitic pegmatite. Part I: Anatomy and Internal Evolution of Pegmatite deposits. *Geoscience Canada* 18: 29 - 46.

Cerny, P. 1986. Exploration strategy and methods for pegmatite deposits of tantalum. *Lanthanides, Tantalum, and Niobium.* P. Mbller, P. CernS' and F. Saupe, (Eds.). Special Publication of the Society for Geology Applied to Mineral Deposits,.Springer. 274-302.

Dada, S.S. 2006. Proterozoic Evolution of Nigeria. *The Basement Complex of Nigeria and its Mineral Resources (A Tribute to Prof. M. A. O. Rahaman)*. O. Oshi. Ed. Ibadan: Akin Jinad and Co. 29–44.

Deveaud, S., Millot, R., Villaros, A. 2015. The genesis of LCT-type granitic pegmatites, as illustrated by lithium isotopes in micas, *Chemical Geology.* 411:97-111

Ekwueme, B. N. and Matheis, G., 1995. Geochemistry and economic value of pegmatites in the Precambrian basement of southeast Nigeria. *Magmatism in relation to diverse tectonic settings.* R. K. Srivastava and R. Chandra (Eds.), and IBH Publishing Co. 375 - 392.

Ekwueme, B. N. and Schlag, C., 1989. Compositions of monazites in pegmatites and related rocks of Oban Massif, southeast Nigeria: Implications for economic mineral exploration. *International Geological Correlation Programme.* 255.2:15-20.

Esmail, E and Moharem, A. 2009. Fluid Inclusion Studies of Radioactive Mineralized Pegmatites at Gabal Abu Furad Area, Central Eastern Desert, Egypt. JKAU: Earth Sci., Vol. 20, No. 2, pp: 11-26

Falconer, J. D., 1911. The geology and geography of Northern Nigeria. Macmillan, London, 135pp.

Fersman, A.E. 1924. Ueber die Natur der Pegmatitbildungen. Compt. Rend. Acad. Sci. in Russian, 89-92.

Fredriksson, J. R., 2017. Fluid inclusion and trace-element analysis of the rare element pegmatite bodies Altim and Tamanduá from the Borborema Province, Brazil. MSc. Thesis, University of Helsinki.

Gagnon, J.E., Samson, I.M., Fryer, B.J., and Williams-Jones, A.E. 2004. The composition and origin of hydrothermal fluids in a NYF-type granitic pegmatite, South Platte District, Colorado: Evidence from LA-ICPMS analysis of fluorite and quartz-hosted fluid inclusions. *The Canadian Mineralogist* 42:1331-1355

Gandu, A. H., Ojo, S. B. and Ajakaiye, D. E. 1986. A gravity study of the Precambrian rocks in the Malumfashi area of Kaduna State, Nigeria. *Tectonophysics* 126:181–194.

Garba, I. 2002. Late Pan African tectonics and origin of Gold mineralisation and rare metal pegmatite in the Kushaka schist belt, north western Nigeria. *Journal of Mining and Geology* Vol 38.1:1-12

Garba, I. 2003. Geochemical discrimination of newly discovered rare metal bearing and barren Pegmatite in the Pan-African (600 + 150 Ma) basement of northern Nigeria. *Applied Earth Science Transaction Institute Of Mining and Metallurgy* 13:287-291.

Garba, I. and Akande, S.O. 1992. Origin and significance of non-aqueous CO_2 fluid inclusions in auriferous veins of Bin Yauri, Northwestern Nigeria. *Mineralium deposita* 27.3:249-255

Gaupp, R., Moller, P. and Morteani, G., 1984. Tantalum pegmatite: geologische, petrologische und geochemische unterschungen. Monograph series min dep 23. Borntreger Berlin Struttggart

Goldstein, R. H., Reynolds, T. J., 1994. Systematics of fluid inclusions in diagenetic minerals. *SEPM Short Course* 31, 199pp.

Gordiyenko, V. V. 1971. Concentration of Li, Rb and Cs in potash feldspar and muscovite as criteria for assessing the rare metal mineralisation in granite pegmatites. *International Geology Review* 13:134-142.

Grant, N. K., 1970. Geochronology of Precambrian basement rocks from Ibadan, South-Western Nigeria. *Earth Planet Science Letters* 10:19–38.

Grant, N. K., 1978. Structural distinction between a metasedimentary cover and an underlying basement in the 600 Ma old Pan-African domain of Northwestern Nigeria. *Geological Society of America Bulletin* 89:50–58.

Grew, E.S. 2002. Beryllium in metamorphic environments (emphasis on aluminous compositions). Beryllium: Mineralogy, Petrology and Geochemistry. Grew, E.S. (Eds.): Reviews in Mineralogy, 50, 487-549.

Hunt, J., Baker, T., and Thorkelson, D., 2005. Regional-scale Proterozoic IOCG-mineralized breccias systems: examples from the Wernecke Mountains, Yukon, Canada. *Mineralium Deposita* 40:492- 514

Holt, R.W. 1982. The Geotectonic evolution of the Anka Belt in the Precambrian Basement Complex of Northwestern Nigeria. Ph.D. Thesis. The Open University, Milton Keynes, England. 264.

Jacobson, R., and Webb, J. S., 1946. The pegmatites of Central Nigeria. *Geol. Surv. Nig. Bull.* 17, 61 p.

Jahns, R.H. and Burnham, C.W. 1969. Experimental studies of pegmatite genesis: A model for the derivation and crystallization of granitic pegmatites. *Econ. Geol.* 64:843-864.

Jahns, R.H. 1953. The Genesis of Pegmatites. Occurrence and origin of giant crystals. *Am. Mineral*. 38:563-598.

Jiang, S. 1998. Stable and radiogenic isotope studies of tourmaline: An overview. *Journal of the Czech Geological Society*, 43:75-90.

Küster, D. 1990. Rare-metal pegmatites of Wamba, central Nigeria - their formation in relationship to late Pan-African granites. *Mineral Deposita* 25:25 - 33.

Larsen, R.B., 2002. The distribution of rare earth elements in K-feldspar as an indicator of petrogenetic process in granitic pegmatites. Examples from two pegmatite fields in southern Norway. *Can. Miner.* 40, 137-151.

Landes, K.K. 1933. Origin and classification of pegmatites. *American Mineral*. 18:33-56.

Leeder, O., Thomas, R., Klemm, W., 1987: *Einschlüsse in Mineralien*. VEB Deutscher Verlag für Grundstoffenindustrie, Leipzig, 180 pp.

Levasseur, R. 1997. Fluid inclusion studies of rare element pegmatites, south platte district, Colorado. MSc. Thesis, University of Windsor. 123.

London, D., and Morgan, GB. 2012: The pegmatite puzzle. *Elements* 8:263-268.

London, D., 2008. Granitic pegmatites: An assessment of current concepts and directions for the future. *Lithos*. 8:281–303.

London, D., Morgan G. B., and Hervig, R. L. 1989. Vapor-under saturated experiments with Macusani glass + H_2O at 200 MPa, and the internal differentiation of granitic pegmatites. Contributions to Mineralogy and Petrology. 102.1:1-17

Maniar, P. D. and Piccoli, P. M., 1989. Tectonic discriminations of granitoids. *Geological Society of America Bulletin* 101:635–643.

Martin, R.F. and De Vito, C 2005. The patterns of enrichment in felsic pegmatites ultimately depend on tectonic setting. Canadian Mineralogist 43:2027-2048.

Matheis, G. and Caen-Vachette, M. 1983. Rb-Sr isotopic study of rare-metal-bearing and barren pegmatites in the Pan-African reactivation zone of Nigeria. *Journal of African Earth Science* 1:35–40

Matheis, G. 1987. Nigerian rare-metal pegmatites and their lithological framework. *Geol. J.* 22:271–291.

McCurry, P. 1976. Geology of degree sheet 21, Zaria, Nigeria. *Overseas Geol Mineral Res* 45:1–30**.**

Moller, P. and Morteani, G., 1987. Geochemical exploration guide for tantalum pegmatite. *Economic Geology*. 42:1388 – 1597.

Morgan, GB, and London, D. 1999. Crystallization of the Little Three layered pegmatite-aplite dike, Rarnona District, California. *Contrib. Mineral. Petrol.* 136:310- 330.

Nigerian Geological Survey Agency. 2004: Geological map of Nigeria (1:2,000,000 scale). Geological Survey of Nigeria, Abuja.

Obaje N.G. 2009. *Geology and Mineral Resources of Nigeria. Lecture notes in Earth Sciences.* Springer.

Ogezi, A.E.O. 1977. Geochemistry and Geochronology of basement rocks from Northwestern Nigeria. *Paper presented at the Precambrian Geology of Nigeria symposium, of the Geological Survey of Nigeria.* Kaduna, October 14-17.

Okunlola, O.A. 2017. Riches beneath our feet: mineral endowment and sustainable development of Nigeria. Inaugural Lecture, University of Ibadan, Ibadan, Nigeria.

Okunlola, O.A. and Ocan, O.O. 2009. Rare metal (Ta-Sn-Li-Be) distribution in Precambrian pegmatite of Keffi area, Central Nigeria. *Nature and Science* 7.7: 90-99.

Okunlola, O. A. 2005: Metallogeny of Ta-Nb mineralisation of Precambrian pegmatite of Nigeria. *Mineral Wealth* 137:38–50.

Okunlola, O.A. and Ogedengbe. E 2003. Investment Potentials of Gemstone Occurrences in Southwestern Nigeria. *Prospects for investment in Mineral Resources of Southwestern Nigeria*. A.A. Elueze. Eds. 41-45.

Okunlola O.A and Omitogun A. 2014. Inventory and environmental effects of active and abandoned artisanal mining sites of rare metals and gold mineralization in parts of Southwestern Nigeria. Proceedings of the closing workshop of the IGCP /SIDA projects 594 and 606 Prague, Czech Republic. 155-159.

Olade, M. A. and Elueze, A. A. 1979. Petrochemistry of the Ilesha amphibolites and Precambrian crustal evolution in the Pan – African domain of southwest Nigeria. *Precambrian Research* 8: 303 – 318.

Olayinka, A.I. 1992. Geophysical siting of boreholes in crystalline basement areas of Africa. *Journal of African Earth Sciences* 14:197–207.

Ollila, J.T. 1987. Genetic aspects of Sn, Li, Be, Nb-Ta pegmatites and Sn-W vein deposits of the Damaran orogeny, Namibia. *Bull. Geol. Soc. Finland* 59.1:21-34

Online Nigeria, 2003. Retrieved from https://www.onlinenigeria.com/oyo-state/?blurb=355

Oyawoye, M.O. 1972. *Basement Complex of Nigeria in African Geology*. Ibadan University Press. 62-98.

Oyebamiji, A.O. 2013. Petrography and petrochemical characteristics of rare metal pegmatites around Oro, Southwestern Nigeria. M.Sc Thesis. Dept. of Geology. University of Ibadan. 147.

Quéméneur, J. and Lagache M. 1999. Comparative Study of Two Pegmatitic Fields From Minas Gerais, Brazil, Using The Rb And Cs Contents of Micas and Feldspars. *Revista Brasileira De Geociências* 29:27-32.

Raeburn, C., 1927. Tinstone in the Calabar District. *Geological. Survey of Nigeria Bulletin* 11: 72–88.

Rahaman, M.A. 1981. Recent advances in the study of the Basement Complex of Nigeria. *Abstract in First Symposium on the Precambrian Geology of Nigeria. Obafemi Awolowo University.*

Rahaman, M.A. 1988. Recent advances in the study of the Basement Complex of Nigeria. *Precambrian Geology of Nigeria*. P.O. Oluyide, W.C. Mbonu, A.E.O. Ogezi, I.G. Egbuniwe, A.C. Ajibade and A.C. Umeji. Eds. Kaduna: Nigerian Geological Survey. 11–43.

Rahaman, M.A. 1976 Review of the basement geology of southwestern Nigeria. In: *Geology of Nigeria* C.A Kogbe. Eds. Lagos. Elizabethean Publishing Company, 41-58.

Rahaman, M. A., Lancelot, J. R., 1984. Continental crust evolution in SW Nigeria:

constraints from U/Pb dating of pre-Pan-African gneisses. *Rapport d'activite 1980–1984 – Documents et Travaux du Centre Geologique et Geophysique de Montpellier 4*: 41

Rahaman, M. A. and Ocan, O., 1978. On relationships in the Precambrian Migmatite-gneisses of Nigeria. *Niger J Min Geol* 15:23–32

Raslan, M. F. and Ali, M. A., 2011. Mineralogy and mineral chemistry of rare-metal pegmatites at Abu Rusheid granitic gneisses, South Eastern Desert, Egypt. *Geologija* 54.2:205–222.

Roedder, E. 1981. Problems in the use of fluid inclusions to investigate fluid-rock interaction in igneous and metamorphic processes. *Fortschr. Mineral*., 59:267 - 302

Roedder, E. 1984. Fluid Inclusions: *Mineralogical Society of America, Reviews in Mineralogy* 12: 644.

Sasmaz A. and Yavuz F .2007. REE geochemistry and fluid-inclusion studies of fluorite deposits from the Yaylagözü area (Yıldızeli-Sivas) in Central Turkey. *N. Jb. Miner. Abh*. 183.2:215–226.

Shand, S.J. 1947. *Eruptive Rocks*. London: Thomas Murby and Co. 488.

Shepherd, T.J., Rankin, A.H. and Alderton, D.H.M. 1985. *A Practical Guide to Fluid Inclusion Studies.* Glasgow: Blackie and Son. 239.

Sirbescu, M.L.C. and Nabelek, P.I. 2003. Crustal melts below 400°C. *Geology* 31: 685-688.

Simmons, W.B. 2007. Gem-bearing pegmatite. Geology of Gem Deposits. L.A. Groat. Ed. *Mineralogical Association of Canada Short Course* 37: 169-206.

Simmons, W.B., Foord, E.E. and Falster, A. U. 1996. Anatectic origin of granitic

pegmatites, Western Maine, USA. Geol. Assoc. Can. — Mineral. Assoc. Can. Program Abstr. A87.

Simmons, W.B., Foord, E.E., Falster, A.U. and Krng, V.T. 1995. Evidence for an anatectic origin of granitic pegmatites, western Maine, USA. Geol. Soc. Am. Annual Meeting., Abstract Programs 27.6: A4l 1.

Simmons, W.B., Lee, M.T. and Brewster, R.H. 1987. Geochemistry and evolution of the South Platte granite-pegmatite system, Jefferson County, Colorado. Geochim. Cosmochim. Acta 51:455-472.

Simmons, W.B., Webber, K.L. and Falster, AU. 1999a: NYF pegmatites of the South Platte District, Colorado. *Can, Mineral*. 37:836-838.

Shafaroudi, A.M. and Karimpour, M.H. 2015. Mineralogical, fluid inclusion and sulphur isotope evidence for the genesis of Sechangi Lead-Zinc (- Copper) deposit, Eastern Iran. *Journal of African Earth Science.* 107:1-14

Sorby, H.C., 1858: On the microscopic structure of crystals, indicating the origin of minerals and rocks *Geological Society of London Quarterly Journal* 14:453-500

Straurov, O. D., Stolyarov, I. S., and Iocheva, E. I., 1966. Geochemistry and origin of Verkh-Iset granitoid massif in Central Ural. *Geochem. Intern*. 6:1138 – 1146.

Sun S.S and McDonough W.F 1989. Chemical and isotopic systematics of oceanic basalts: implications for mantle composition and processes. Magmatism in the Ocean Basins. A.D. Saunders and M. Norry. Eds. Geological Society of London Special Publications 42: 313-345.

Swanson, S. E., and Veal, W. B., 2010. Mineralogy and *petrogenesis of pegmatites in the Spruce Pine District, North Carolina, USA. Journal* of Geosciences, 55:27–42

Taylor, B. E. and Friedrichsen, H. 1983. Oxygen and hydrogen isotope disequilibria in the Landsverk l pegmatite, Evje, southern Norway: Evidence for anomalous hydrothermal fluids. *Norsk Geologik Tidskrf.* 63:192-209

Taylor, S.R. and McLennan, S.M. 1985. The continental crust: its composition and evolution. Carlton: Blackwell Scientific Publication. 312.

Taylor S.R., Rudnick R.L., Mc Lennan S.C., and Eriksson K.A. 1986. Rare earth element patterns in Archean high-grade metasediments and their tectonic significance. *Geochimica et Cosmochimica Acta* 50:2267–2279.

Tischendorf, G. 1977. Geochemical and petrographic characteristics of silicic magmatic rocks associated with rare metal mineralisation. Mineralisation Associated with Acid Magmatism. M. Stemprok, L. Burnol, G. Tischendorf. Eds. *Geological Survey* 2: 41-98.

Touret, J.L.R. 2001. Fluid inclusions in metamorphic rocks. *Lithos*, v.55:1-25**.**

Turner, D. C., 1983. Upper Proterozoic schist belts in the Nigerian sector of the Pan-African Province of West Africa. *Precambrian Reserach* 21:55–79

Van den Kerkhof, A.M. and Hein, U.F. 2001. Fluid inclusion petrography. In: T. Andersen, M.L., Frezzoti, E.A.J. Burke (Eds) Fluid inclusions: phase relationships – methods applications (special issue). Lithos 55.1-4. 320.

Vapnik, Y and Moroz, I: 2000. The Fluid inclusions in emerald from the Jos complex (Central Nigeria). *Schweiz. Mineral. Petrogr. Mitt* 80:117-129.

Whitworth, M.P. and Rankin, A.H. 1989. Evolution of Fluid Phases associated with lithium pegmatites from Southeast Ireland. *Mineralogical magazine* 53.371: 271-284.

Woakes, M., Rahaman, M. A., Ajibade, A. C., 1987. Some metallogenetic features of the Nigerian basement. *Journal of African Earth Science* 6:54–64

Wright, J. B., 1970. Controls of mineralisation in the Older and Younger Tin Fields of

Nigeria. *Econ. Geol*. 65: 945 - 951.

Wright, J. B., 1985. *Geology and mineral resources of West Africa*. George Allen and Unwin, 187.

Zarasvandi A., Zaheri N., Pourkaseb H. Chrachi A., Bagheri H 2014. Geochemistry and fluid-inclusion microthermometry of the Farsesh barite deposit, Iran. *Geology.*